Studies on Gloss of Printed Surfaces

vom Fachbereich Maschinenbau

der Technischen Universität Darmstadt

zur Erlangung des Grades

Doktor-Ingenieur

(Dr.-Ing.)

Dissertation

von

Carl Fridolin Weber

Erstgutachter: Prof. Dr.-Ing. Edgar Dörsam

Zweitgutacher: Prof. Dr.-Ing. habil. Tran Quoc Khanh

Darmstadt 2024

Weber, Carl Fridolin: „Studies on Gloss of Printed Surfaces“
Darmstadt, Technische Universität Darmstadt
Jahr der Veröffentlichung der Dissertation auf TUprints: 2024
URN: urn:nbn:de:tuda-tuprints-267415
URL: http://tuprints.ulb.tu-darmstadt.de/26741
Tag der Einreichung: 04.12.2023
Tag der mündlichen Prüfung: 28.02.2024

Kurzfassung

Diese wissenschaftliche Arbeit untersucht den Glanz von durch Drucken metallisierten Oberflächen. Im ersten Teil der Arbeit werden drei verschiedene Glanzmessgeräte - das micro-TRI-gloss von Byk Gardner, das IQ-S von Rhopoint und der Surface Reflectance Analyzer von Canon - auf ihre Eignung zur Glanzmessung von gedruckten metallisierten Proben hin untersucht und verglichen. Die Vor- und Nachteile dieser verschiedenen Glanzmessgeräte werden beleuchtet, und ihre Tauglichkeit für die Durchführung von Glanzmessungen im Kontext dieser Dissertation wird bewertet.

Die Arbeit setzt sich auch mit dem Druck von Aluminiumpigmenten auseinander und untersucht, wie verschiedene Druckparameter den Glanz beeinflussen. Im Fokus steht der Flexodruck mit UV-Druckfarben, die Aluminiumpigmente enthalten. Dabei wird die Auswirkung der Zeitspanne zwischen dem Drucken der UV-Farben und deren Aushärtung auf den Glanz analysiert. Diese Untersuchung vom dynamischen Glanz betrachtet die Veränderung des Glanzes pro Zeiteinheit. Die Änderungsrate hängt von den verwendeten Druckfarbentypen, Pigmenten und Substraten ab. Des Weiteren erfolgt die Analyse der Topographie der Pigmentschicht von metallisierten Proben, bei denen die gedruckten UV-Farben nach verschiedenen Zeitabständen gehärtet wurden. Diese Erkenntnisse werden anschließend auf eine industrielle Druckmaschine übertragen, wobei auch der Einfluss der Zeitspanne zwischen dem Drucken und dem Härten der UV-Farben sowie der Einsatz von Heißluft auf den Glanz untersucht wird. Zudem wird der Einfluss des Primer Andrucks auf den Glanz analysiert.

Abschließend werden die Ergebnisse eines psychophysikalischen Experiments vorgestellt, das sich mit der Wahrnehmung von Glanz von gedruckten metallischen Proben befasst. Hierbei wurden zwei verschiedene Probensets von Laien und Experten der Druckindustrie hinsichtlich ihres Glanzes, metallischen Charakters, wahrgenommenen Rauheit, Bildschärfe der Spiegelung und Helligkeit bewertet. Die erhaltenen Ranglisten wurden miteinander verglichen, und mit den Messwerten eines Glanzmessgeräts korreliert.

Abstract

This scientific work investigates the gloss of printed metallized surfaces. In the first part of the study, three different gloss meters - the micro-TRI-gloss by Byk Gardner, the IQ-S by Rhopoint, and the Surface Reflectance Analyzer by Canon - are examined and compared regarding their suitability in measuring the gloss of printed metallized samples. The advantages and disadvantages of these different gloss meters are highlighted, and their suitability for conducting gloss measurements in this context of this dissertation is evaluated.

The work also delves into the printing of aluminum pigments and explores how different print parameters affect gloss. The focus is primarily on flexo printing using UV-printing inks containing aluminum pigments. The impact of the time interval between printing of the UV-inks and curing on gloss is analyzed. This investigation of dynamic gloss considers the change in gloss per time unit. The change rate depends on the ink types, pigment varieties, and substrates used. Furthermore, an analysis of the topography of pigment layers on metallized samples, with varying time intervals between the printing and curing of UV-inks, is conducted. These findings are then transferred to an industrial printing press, examining the influence of the time gap between printing and curing the UV-inks and the use of hot air on gloss. Additionally, the effect of primer application on gloss is analyzed.

Finally, the results of a psychophysical experiment dealing with the perception of gloss of printed metallic samples are discussed. Two different sets of samples were evaluated by amateurs and experts from the printing industry with regard to their gloss, metallic character, perceived roughness, image sharpness of the reflection and brightness. The obtained rankings were compared with each other and correlated with the measured values of a gloss meter.

Acknowledgement

The present work was written within the time I worked at the Institute of Printing Science and Technology (IDD) at the Technical University (TU) of Darmstadt. Especially towards Prof. Dr.-Ing. E. Dörsam, I would like to express thanks for the many valuable discussions and support provided during this time, as well as the opportunities I have been able to pursue. Both professionally and personally, I have learned a lot. I thank Prof. Dr.-Ing. habil. T.Q. Khanh, head of the Institute of Adaptive Lighting Systems and Visual Processing at the TU Darmstadt, for taking the co-lecture of this dissertation and showing interest in this work. Thanks go to Heidelberger Druckmaschinen AG, and especially to Dr. rer. nat. M. Schmitt-Lewen, for the financial support, the trust that was placed in me, the interesting technical discussions, and the good cooperation within the scope of this bilateral project. For providing the inks used in this work and sharing information about aluminum pigments, I would like to express my gratitude towards Schlenk Metallic Pigments GmbH and especially B. Krietsch. I would also like to sincerely thank all students who supported me in the course of my scientific work and the industrial project I worked for. I would like to special mention L.A. Solangi for the conscientious execution of the psychophysical experiment. Additionally, I want to express my gratitude towards the IDD team for the mutual support. I am glad that I could be a part of the team. I would like to thank Dr. rer. nat. H.M. Sauer for the weekly project discussions and all advice given to me. In addition, special thanks is given to T. Euler for informative conversations and support of the printing experiments. Furthermore, I would like to express my gratitude to the numerous individuals working in the field of gloss, appearance, or printing science, who shared knowledge with me and gave me inspiration for my research. I especially thank the members of the Deutsche farbwissenschaftliche Gesellschaft e.V. for exchange and insightful discussions on the topic. I would also like to thank all those who have supported me in other ways, especially my girlfriend, family, and friends.

Contents

Kurzfassung **3**

Abstract **4**

Acknowledgement **5**

Notations **9**

1 Introduction **13**

2 Fundamentals and state of the science **17**

2.1 Concept of appearance 17
2.2 Concept of gloss 18
2.3 Physical gloss measurement 20
2.3.1 Specular gloss 20
2.3.2 Distinctness of image 26
2.3.3 Haze 28
2.3.4 Bidirectional reflectance distribution function 29
2.4 Visual perception studies on gloss 31
2.5 Printing aluminum pigments 33
2.5.1 Aluminum pigments 34
2.5.2 Flexo printing of UV-inks with aluminum pigments 35
2.6 Dynamic gloss of printing inks 37
2.7 Orientation of metal effect pigments in coatings 40

3 Instrumental measurement of gloss **44**

3.1 Criteria for selecting gloss meters 44
3.2 General comparison and measurement procedure 44
3.3 Continuous gloss measurement 54
3.4 Gloss on samples from an industrial print test 55
3.5 Decision on gloss meters for further experiments 62

4 Printing experiments **65**

4.1 Gloss influencing factors in printing 65
4.2 Experiments on dynamic gloss – materials and method 66
4.2.1 Flexo print proofer 66
4.2.2 Gloss meter 69
4.2.3 Printing inks 70
4.2.4 Substrates 72
4.3 Experiments on dynamic gloss – results and interpretation 75

4.3.1 Chromolux paper and Chromolux cardboard 79
4.3.2 Influence of UV-primer 81
4.3.3 Further considerations 82
4.3.4 Modelling of dynamic gloss curves 84
4.4 Influence of dwell time and hot air – materials and method 87
4.4.1 Experimental setup 88
4.4.2 Confocal microscopy and evaluated topography parameters 91
4.4.3 Experimental procedure and measurement scheme 93
4.5 Influence of dwell time and hot air – results and interpretation 95
4.5.1 Influence of dwell time and hot air on gloss 95
4.5.2 Evaluation of the topography data 102
4.6 Transfer to an industrial printing machine 110
4.6.1 Experimental setup 110
4.6.2 Impact of post-printing web speed on gloss 114
4.6.3 Influence of hot air after printing on gloss 117
4.6.4 Influence of UV-primer application on gloss 120
4.6.5 Evaluation of the topography data 125
4.6.6 Outcomes 130

5 Psychophysical experiment 132

5.1 Research questions and points for consideration 132
5.2 Choice of the method 133
5.3 Samples for the experiment 134
5.4 Experimental setup 138
5.5 Observers 141
5.6 Experimental procedure 142
5.7 Results and analysis 146
5.7.1 General evaluations and observations 146
5.7.2 Evaluation of data obtained with Series A 149
5.7.3 Evaluation of data obtained with Series B 156
5.7.4 Evaluation of additional data 157
5.8 Comparison to a similar study 158

6 Discussion 163

6.1 Comparison of three gloss meters 163
6.2 Printing experiments using metallic inks 165
6.2.1 General procedure 165
6.2.2 Experiments on dynamic gloss 166
6.2.3 Pigment layer topography 169

6.2.4 Transfer to an industrial printing machine 171
6.3 Psychophysical ranking experiment 172
6.3.1 Brightness and lightness 176
7 Summary and outlook 177
Bibliography 180
Own and contributed publications 202
Supervised student works 204
Appendix 206
Appendix 1 206
Appendix 2 207
Appendix 3 208
Appendix 4 211
Appendix 5 212

Notations

Symbols

Symbol	Unit	Designation
α	°	*Angle that describes the span of a measuring field along the polar angle (see Section 2.3.1 and Section 2.3.4)*
β	°	*Angle that describes the span of a measuring field along the azimuth angle (see Section 2.3.1 and Section 2.3.4)*
η	$N\,s/m^2$	*Dynamic viscosity*
θ	°	*Angle of incidence and angle of reflection (see Section 2.3.1)*
θ_1	°	*Angle of incidence, equals θ_2 (see Section 2.3.1)*
θ_2	°	*Angle of reflection, equals θ_1 (see Section 2.3.1)*
λ	nm	*Wavelength*
λ_S	μm	*Wavelength at which a long-pass filter transmits wavelength of a measured topography (see Section 4.4.2)*
λ_L	μm	*Wavelength to which a short-pass filter transmits wavelength of a measured topography (see Section 4.4.2)*
σ	N/m	*Surface tension*
τ	-	*Kendall's correlation coefficient*
A	mm^2	*Area (see Section 4.4.2)*
a	-	*Non-negative fit parameter (see Section 4.3.4)*
a^*	-	*Green-red component of the CIE LAB color space*
b	-	*Non-negative fit parameter (see Section 4.3.4)*
b^*	-	*Blue-yellow component of the CIE LAB color space*
b'	-	*Non-negative fit parameter (see Section 4.3.4)*
c	-	*Non-negative fit parameter (see Section 4.3.4)*
d	-	*Stretching exponent (see Section 4.3.4)*
d_{XX}	μm	*Measure of the size distribution of pigments (see Section 2.5.1)*
h	mm	*Ink profile height (see Section 2.6)*
cor	-	*Correction factor (see Section 2.3.1)*
k	-	*Imaginary extinction coefficient*
n	-	*Refractive index*
$\hat{\boldsymbol{n}}$	-	*Complex refractive index*
R	-	*Ratio of reflection of a boundary surface, quotient of the reflected light flux to the incident light intensity, depending on the angle of incidence of the light*
R_p	-	*p-polarized share of R*

Symbol	Unit	Designation
R_S	-	*s-polarized share of R*
r	-	*Pearson's correlation coefficient*
r^2	-	*Coefficient of determination*
Sa	μm	*Arithmetical mean height (see Section 4.4.2)*
Sz	μm	*Maximum heights and depths (see Section 4.4.2)*
Sq	μm	*Root mean square height deviation (see Section 4.4.2)*
Sdq	-	*Root mean square gradient (see Section 4.4.2)*
Sdr	%	*Developed interfacial ratio (see Section 4.4.2)*
SPI	%	*Specular Reflection Index (see Section 5.8)*
t	s	*Time*
Y	-	*Luminance in CIE Yxy color space*
$Yspin$	-	*Luminance in CIE Yxy color space measured with the specular component included*
$Yspex$	-	*Luminance in CIE Yxy color space measured with the specular component excluded*
z	μm	*Height of single points of a topography measurement (see Section 4.4.2)*
$\overline{z}$	μm	*Mean height (see Section 4.4.2)*
$\% \, w/w$	-	*Mass percentage*
$\varnothing$	mm	*Diameter*

Abbreviations

Abbreviation	Explanation
ASME	*American Society of Mechanical Engineers*
ASTM	*American Society for Testing and Materials*
BRDF	*Bidirectional Reflectance Distribution Function*
Brightness ranking A	*Data of the ranking of samples in Series A according to brightness (see Section 5.6)*
ChromC/ChromP/LumiArt_ (Prim)_VMP/Corn	*Refers to substrate-ink combinations used for the experiments on dynamic gloss (see Table 4.5)*
ChromP_VMP/corn_ha/nha	*Refers to substrate-ink combinations and print settings such as hot air and dwell time (see Table 4.6)*
CIE	*International Commission on Illumination (French: Commission Internationale de l'Eclairage)*
CSV	*Comma-separated values*
D65	*CIE standard illuminant D65*
DIN	*German Insitute for Standardisation (German: Deutsches Institut für Normung)*

Abbreviation	Explanation
DOI	*Distinctness of image*
et al.	*Latin: et alii, and others.*
FFT	*Fast Fourier Transformation*
FOGRA	*Fogra Forschungsinstitut für Medientechnologien (Munich, Germany)*
F_XX_N/Y	*Metallic samples printed on film with the Gallus RCS330-HD. XX denotes the web speed after printing. N means that no hot air was used, Y means that hot air was used (see Table 4.6)*
GlossXX	*Specular gloss measured at an angle of XX*
Gloss ranking A1/A2/B	*Data of the ranking of samples in Series A for the first (1) or the second (2) time or of samples in Series B according to gloss (see Section 5.6)*
HDR	*High dynamic range*
IC	*Image clarity*
IDD	*Institute of Printing Science and Technology (German: Institut für Druckmaschinen und Druckverfahren)*
IR	*Infrared*
ISO	*International Organization for Standardization*
LED	*Light emitting diode*
Matlab	*Matrix laboratory software (Math Works)*
Metallicity ranking A	*Data of the ranking of samples in Series A according to metallicity (see Section 5.6)*
n.d.	*No date*
NIR	*Near-infrared*
obs.	*Observers*
PCC	*Precipitated calcium carbonate*
P_XX	*Paper primed in a specific way using the Gallus RCS330-HD (see Table 4.6)*
P_YY_XX_N/Y	*Metallic samples printed on paper or primed paper using the Gallus RCS330-HD. YY stands for the way primer was applied on the paper, XX stands for the speed of the web after printing metallic ink. N means that no hot air was used, Y means that hot air was used (see Table 4.6)*
rel. std.	*Relative standard deviation*
RIQ	*Reflected image quality*
Roughness ranking A	*Data of the ranking of samples in Series A according to roughness (see Section 5.6)*
Sharpness ranking A	*Data of the ranking of samples in Series A according to the sharpness of the reflected image (see Section 5.6)*
SRA	*RA-532H Surface Reflectance Analyzer*
TU	*Technical University*
UV	*Ultraviolet*

Abbreviation	Explanation
UV-ink-corn/VMP	*Specific flexo printing UV-inks with cornflake pigments or vacuum metallized pigments (see Section 4.2.3)*
VMP	*Vacuum metallized pigment*
VIS	*Visible*

1 Introduction

Print products such as packaging and labels with metallic surfaces can be encountered in various aspects of everyday life. For example, they can be found on perfume packaging, chocolate wrapping, book covers, and beer or wine bottles. The recognition of the appeal of metallic embellishments is not new. Throughout history, humans have cherished the aesthetic appeal of glossy surfaces and the outstanding visual effects that a metallization can bestow upon products. The attracting effect of metallization found use in many civilizations across ages. For instance, ancient Egyptians worked gold into thin sheets and applied it on art objects. Gold was also used for books that were meant for religious purposes. For instance, from the 3rd century AD starting, the Manichaeism spread widely in Asia not mainly due to its ideas but mostly due to the extraordinary allure of its books (Monro 2014). In Germany, the early pioneers of applying metallic embellishments to non-religious products emerged in the 19th century, notably among brewers and winemakers. They introduced the use of golden, silver, and bronze effects on bottle labels (MAN Roland Druckmaschinen 2002). Nowadays, using modern printing methods, metallic embellishments are more applied on labels or packaging of consumer products than ever before. Due to the increased noteworthiness and the outstanding gloss of such kind of products, consumers are more likely to be drawn to purchase them (Clement 2007; Meert et al. 2014; Hartmann and Haupt 2019). Examples for packaging with applied metallization by various printing methods can be seen in Figure 1.1. Recent developments in the field of printing metallic embellishments demonstrate high interest of the industry in this field (Label Pack 2019a, 2019b; Lohmann 2020; Podieh 2021; Kurz 2021; Print.de 2023).

Figure 1.1: Examples for packaging of consumer products with metallization applied by using different printing methods - hot foil stamping (left), foil fusing (middle), and gravure printing of inks containing aluminum pigments (right).

The increased attractiveness and noteworthiness of packaging with metallization can be attributed to the high gloss of the metallized surfaces that makes them stand out. However, unlike color, gloss is a phenomenon that is not understood well yet. Remarkably, until today it is not possible to measure gloss in a way that makes its exact communication and description feasible. This can complicate communication between customers and manufacturers and the verification of the desired quality of a product. In addition, the way how humans perceive gloss is not well understood yet. Especially the field of gloss of metallic surfaces lacks research. Gloss meters are measurement instruments utilized by manufacturers in the printing industry, as well as in various other industrial sectors, to assess the gloss of consumer products. However, there is still a lack of knowledge in how to interpret gloss measurements.

Many different printing methods that can be employed for the metallization of labels or packaging are available. One of method that could be chosen by a printer is printing inks that contain aluminum pigments (also called 'metallic inks' in the following). For the reason that these printing inks can have high prices of up to several hundred euro per kilogram, it is in interest of the printer to exploit their full potential. However, there is a limited amount of research available on how aluminum pigments behave in the inks after the printing process and how their behavior impacts gloss of the print products. While there has been substantial research in this area concerning printing inks with conventional pigments, there is a need for more knowledge in topics such as the interaction of metallic inks with different substrates and the influence of key factors in the print process on the resulting gloss.

This work aims at broaden the scientific understanding of the issues raised. First, the measurement of gloss of printed metallized surfaces is addressed. Different gloss meters are compared and comparisons are drawn between gloss measurement values captured on metallized print samples. Second, the topic of printing metallic inks is covered. The change of gloss of these inks after printing is measured and described, the influence of hot air after printing and the impact of primer application on gloss is analyzed and an analysis of the aluminum pigment layer topographies is made. Third, the perception of gloss of printed metallized samples is dealt with through a psychophysiological experiment. Doing so, conclusions can be drawn in what extend measurement values of gloss meters reflect human perception when dealing with metallized print products. This dissertation is structured into the following chapters to cover the three different topics:

Chapter 2 provides the fundamentals and the state of the science in this field. Gloss is categorized under the umbrella term appearance and it is described how gloss can be divided into different characteristics or aspects. Next, the principles of gloss measurement are explained and the different aspects of gloss that can be measured and are important in context of this dissertation are dealt with individually. In addition, important studies on the visual perception of gloss are discussed, with particular emphasis on recent studies dealing with gloss of metallic surfaces. Further, printing techniques for the production of metallic embellishments are introduced. Particular attention is given to the different sorts of aluminum pigments, UV-inks, and flexo printing. Last, relevant studies are addressed, in which the gloss of freshly printed inks has been measured over time after printing, as well as studies characterizing the topography of aluminum pigments inside of coating layers.

In Chapter 3, first criteria for choosing a suitable gloss meter for studies on gloss conducted for this dissertation are stated. Further, the question what kind of measurement uncertainties should be expected when measuring the gloss of printed metallized samples is followed. The performance of three different gloss meters is assessed and the comparability of measurements using these three different gloss meters is addressed by examining gloss measurements on samples metallized on industrial printing machines. This is followed by a discussion why differences between gloss meters exist. Further, the important gloss measurement values used for this work are identified and a decision is made regarding which gloss meters are most suitable for the investigations conducted in this work.

The first part of Chapter 4 deals with the changing gloss of printing inks immediately after printing, which is also called dynamic gloss. Continuous gloss measurements were carried out on freshly printed UV-inks containing aluminum pigments on different paper substrates. It is addressed why dynamic gloss measured at different angles can behave differently or in an opposing way and how the substrate and the type of ink influences dynamic gloss. Further, a mathematical model is established that describes different trends of dynamic gloss. In the second part of this chapter, a closer examination is made on the topography of the aluminum pigment layers in the UV-inks that are cured after different time intervals, along with the associated gloss. In addition, the relationship between two relevant topography parameters and measured gloss is examined. This is

done by investigating samples printed using a laboratory flexo printing machine and by investigating samples printed with an industrial printing machine.

In Chapter 5, the results of a psychophysical experiment on the appearance of samples metallized by printed metallic inks are covered. Both experts from the printing industry, who regularly evaluate the appearance of print products, and observers with little to no experience in judging print products, participated in the experiment. It is shown how the judgements of observers on gloss correlate to instrumental gloss measurements depending on the sort of printed metallized samples and how the observers differ from each other in their judgement of gloss. Further, findings of this study are compared to a former study in this field.

At the end of this dissertation, the findings are discussed. Further, a summary of the most important results is provided and an outlook on future research activities in the field of printed metallic surfaces is given.

2 Fundamentals and state of the science

The first part of this chapter deals with gloss. Gloss can be categorized in the broader topic appearance for which a short explanation is given. Then, an overview of the measurement of gloss using gloss meters is provided. The measurement principles of different aspects of gloss such as specular gloss, distinctness of image (DOI) and haze are explained. At the end of the first part, visual perception studies that have been conducted to investigate gloss perception and studies on the perception of gloss of metallic surfaces are addressed.

The second part of this chapter deals with metallization methods of substrates using printing inks that contain aluminum pigments. Aluminum pigments are categorized and different properties that such pigments can have, are explained. Further, flexo printing, the relevant printing method of this thesis, as well as UV-inks are introduced. The last two sections of the second part of this chapter refer to previous scientific studies investigating dynamic gloss of freshly printed ink layers as well as studies investigating the topography and gloss of metallic pigment layers in coatings.

2.1 Concept of appearance

According to the standard CIE S 017/E:2020 (reapproved 2020), appearance is defined as the "aspect of visual perception through which an object is perceived to have attributes such as size, shape, color, texture, gloss, transparency, and opacity." According to Hunter and Harold (1987), the appearance of objects is evaluated in terms of color properties and spatial properties related to geometric attributes, such as gloss, translucency, and texture. Geometric attributes, unlike color, are related to the spatial distribution of light from an object. As stated by Sève (1993), three different aspects have to be considered when speaking of appearance. These are the physical aspect, the physiological, as well as the psychological aspect. The physical aspect describes the distribution of light from an object. The physiological aspect describes the stimulation of the visual system. These stimuli are then interpreted by the cerebral cortex and are recognized as objects and features of an object, which is described by the psychological aspect. The perception of the attributes of appearance of an object such as gloss, color, translucency, and texture is determined by the set of illumination-object-observer. As shown in several studies, the different attributes of appearance can influence each other and are not necessarily independent (Judd and Wyszecki 1952; Dalal and Natale-Hoffman 1999; Ferwerda et al. 2001; Simonot

and Elias 2003; Obein et al. 2004; Briones et al. 2006; Ho et al. 2007; Ho et al. 2008; Gigilashvili et al. 2019).

Quantifying the appearance of an object is a complicated issue due to the difficulty that appearance is linked to subjective perception and thus implies a judgement (Hutchings 1999). In case of packaging, issues to be judged could be: Has the surface the kind of gloss that is preferable for the product? Does chocolate box x with color y has the same gloss as chocolate box w with color z? A psychometric approach to numerically characterize the visual perception and to find answers to such kind of questions is sensory testing. It is used to quantify sensory attributes in order to assess the relationship between a given physical stimulus and the perceptual response of a subject (Meilgaard et al. 2015). However, such kind of psychophysical assessments are usually very time consuming, cost intensive, and not always possible to conduct. Hence, pertinent measurements of optical properties with instrumental analysis that correlate with sensory properties must help (Eugene 2008; Meilgaard et al. 2015). Such kind of measurement techniques as well as mathematical models that enable the objective measurement of parameters that, either singly or in combination, correlate with attributes of human response, are summarized under the term 'soft metrology' (Pointer 2003; Eugene 2008; Leloup et al. 2014). In order to obtain an objective quantification of appearance parameters, as for instance the quantification of the gloss of an object, a measurement scale has to be generated that allows the human subjective response to be predicted from a physical, objective measurement (Eugene 2008; Kingdom and Prins 2016).

2.2 Concept of gloss

The standard CIE S 017/E:2020 (reapproved 2020) defines gloss as the "mode of appearance by which reflected highlights of objects are perceived as superimposed on the surface due to the directionally selective properties of that surface." This means that gloss is generally associated with surface light reflection of an object in the specular angle, opposite to the angle of incidence (Ignell et al. 2009). As stated by Hanson (2006), this definition also includes the dual nature of gloss that relates both to the perception of (reflected) images and highlights. Results of experiments dating back until 1951 by Harrison and Poulter show that gloss is not a physical property but a physiological Gestalt (Harrison and Poulter 1951). This means that it cannot be directly encoded on biological sensors but is constructed from the global scene on the field of view of an observer and is

hence referred to as a second-order attribute of appearance (Obein et al. 2003). It was also shown that some observers judge gloss more with reference to the total amount of reflected light and others more with reference to the sharpness of images seen via the reflection of objects on a surface (Harrison and Poulter 1951).

Further, gloss cannot be described or communicated through a single number. As one of the first noticing this, Pfund (1930) pointed out, that the glossy appearance of a surface relates both to the contrast between the specular shininess and the brightness of the surrounding surface area as well as the specular reflection. Therefore, black surfaces with the same specular shininess than white ones will appear glossier, as the contrast of the specular highlight to the background is more distinct (Leloup et al. 2014).

In 1937, Hunter concluded from his experience on gloss that gloss is made up of at least six visual criteria (Hunter 1937). Hunter called these six criteria specular gloss, sheen, contrast gloss or luster, absence-of-bloom gloss (which is the same as absence of haze), distinctness of image gloss and surface-uniformity gloss (Hunter 1937). Specular gloss is perceived as the brightness of reflected highlights and sheen is very similar to specular gloss but describes the shininess at grazing angles. Contrast gloss describes the contrast between specularly reflecting areas and other areas. Haze is the milky appearance adjacent to reflected specular highlights. The term DOI stands for the distinctness and sharpness of mirror images and a high surface uniformity gloss describes the freedom of a surface from visible nonuniformities such as texture. O'Donnell and Billmeyer (1968) and Billmeyer (1968) showed that humans are not able to distinguish between these six different gloss dimensions defined by Hunter. However, the findings by Hunter have had significant impact on the development of gloss meters.

Physical quantities that were expected to correlate with the visual criteria established by Hunter have been developed and adopted into gloss measurement standards. Experiments showed that no linear relationship between measured instrumental data and visual perception can be expected (Harrison 1945; Billmeyer and O'Donnell 1987; Obein et al. 2004; Gruber et al. 2012; Leloup et al. 2010; Leloup 2012). The aspiration to measure a combination of physical quantities that correspond well with human gloss perception is an ultimate goal of ongoing research on physical gloss measurement (Leloup 2012; Beuckels et al. 2023).

2.3 Physical gloss measurement

The standard CIE S 017/E:2020 (reapproved 2020) defines the term 'gloss meter' as "instrument for measuring the various photometric properties of a surface giving rise to gloss." Most measureable aspects of gloss are derived from the visual criteria of gloss that were established by Hunter (1937) and have the same name. Today, there are still differences between existing instrumental gloss scaling methods, and what humans perceive as gloss. Originally, gloss meters were meant to at least give results on the glossiness of a surface that make it possible to instrumentally distinguish surfaces of different glossiness and to describe the difference with numerically (Hanson 2006). For reliable measurements, commercially available gloss meters are restricted to the measurement of gloss on flat surfaces (Silvennoinen et al. 2008b). Sometimes in industry, commercial gloss meters are also used to measure gloss on slightly curved surfaces. In this case, only gloss measurement results obtained from objects with the same curvature can be compared. Since the development of gloss meters started, many different standards for different industries and gloss meter designs were developed that were expected to correlate with visual gloss. A good overview over the historical background of gloss meters and their development over time is given by Hunter and Harold (1987) and Leloup (2012).

Most gloss meters that can be found in the printing industry as well as in many other industries with a need for the characterization of gloss are based on the measurement of specular gloss. It is the most often measured aspect of gloss to evaluate the optical quality of surfaces of products (Silvennoinen et al. 2008b). However, also gloss meters for the measurement of haze and the DOI can be found. Currently, gloss meters which enable the characterization of an even larger set of gloss nuances such as contrast gloss are under development (Beuckels et al. 2022a; Beuckels et al. 2022b). In the following subchapters, the measurement of specular gloss, DOI and haze is described. Further, the Bidirectional-Reflectance-Distribution-Function is briefly explained.

2.3.1 Specular gloss

Specular gloss is defined in the standard CIE S 017/E:2020 (reapproved 2020) as "perceived surface brightness associated with the luminous (specular) reflection of a surface", which is a definition in terms of visual perception. Specular gloss is related to light reflection of objects that can be partly transparent or opaque (Silvennoinen et al. 2008b). Using specular gloss meters, physical measurements of specular gloss can be

made. For a typical gloss meter, the measurement principle is as described in the standard ASTM D523 − 14 (reapproved 2014): A light source (nowadays LED) flashes light at an oblique angle of incidence (θ_1) through a light source aperture and a source lens as a parallel beam onto a specimen. On the measuring spot, the light is partially specularly reflected, scattered and absorbed. Reflected light passes a receptor lens at an angle of θ_2 and a receiver aperture and is further collimated onto a photodiode. The angle of incidence and the angle of reflection is always the same. Hence, when further referring to the angle θ, this means both θ_1 and θ_2. The intensity or intensity distribution of the reflected light is then measured with the use of a photodiode or a sensor matrix. In gloss meter design it is differentiated between parallel-beam gloss meters, which are used in this dissertation, and converging-beam gloss meters that are mainly used for the assessment of paper gloss. Measurements of converging-beam gloss meters are also classified as TAPPI-method (Zwinkels et al. 2018).

The angle θ depends on the standard that the construction of a gloss meter is guided by. Leloup (2012) provides an overview of gloss measurement standards used in industry. They can be divided into those made for a specific industry such as the paint, plastics, ceramics or fabrics industry, and general ones. Important general ones are ASTM D523 − 14 (reapproved 2014), ASTM D5767 − 95 (reapproved 2012) and ASTM E430 - 11 (reapproved 2011). Most gloss meters used in the printing industry measure specular gloss at an angle of $\theta = 60°$. This is a standard gloss measurement angle, adopted in 1939 by the ASTM as ASTM method D523 (Leloup 2012; Kigle-Boeckler 1995). This resulted from Hunter's research, where visual evaluations were conducted on painted panels. It was discovered that the 60° geometry yielded the best overall correlation with visual rankings. The 60° geometry of specular gloss measurement is still the most widely used geometry today. In 1951, the 20° geometry test method for the evaluation of high gloss finishes and the 85° geometry test method for the evaluation of low gloss surfaces was incorporated into ASTM D523. Other standards specify the measurement of specular gloss at 45° for the ceramics and plastic industry and for the measurement at 75° for the paper industry.

Table 2.1 shows the aperture sizes of the light source apertures and the receiver apertures for the measurement of specular gloss at 20°, 60° and 85° as specified in ASTM D523 − 14 (reapproved 2014). Figure 2.1 provides a corresponding schematic for a better understanding of the aperture angles. Most specular gloss meters in the printing industry are based on this standard. It can be seen that the light receiver apertures, especially the

20° and 60° receiver apertures, differ in size. This in return means that a greater portion of the distribution of the reflected light flux enters the photodiode at 60° compared to the photodiode at 20°.

Table 2.1: Angles of the light source aperture and receptor aperture for the measurement of specular gloss at 20°, 60° and 85° stated in ASTM D523 − 14 (reapproved 2014). The angles α and β are the aperture opening angles as depicted in Figure 2.1. The plane of measurement spans between the angle of incidence and the angle of reflection of the light.

	In plane of measurement (α)	Perpendicular to plane of measurement (β)
Light source aperture (for all angels)	0.75° ± 0.25°	2.5° ± 0.5°
20° receiver aperture	1.8° ± 0.05°	3.6° ± 0.1°
60° receiver aperture	4.4° ± 0.1°	11.7° ± 0.2°
85° receiver aperture	4.0° ± 0.3°	6.0° ± 0.3°

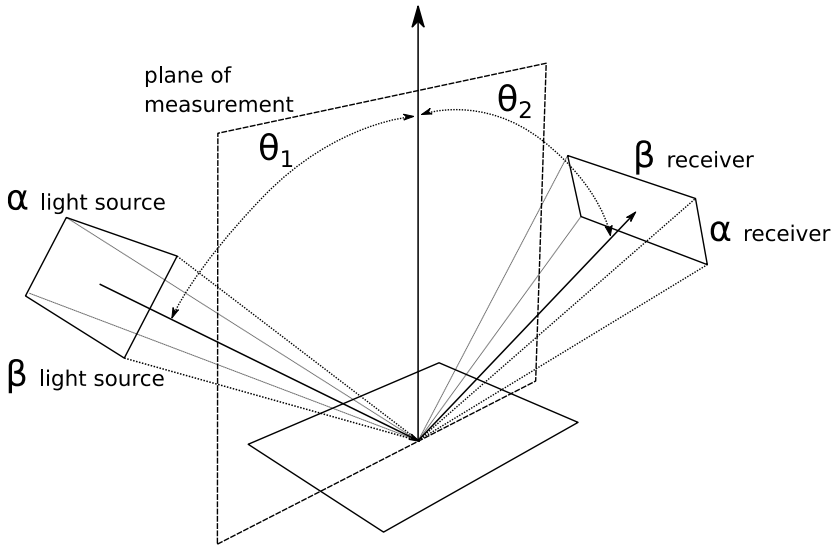

Figure 2.1: Schematic of the specular and aperture opening angles of specular gloss meters after (Hunter and Harold 1987). The angles α and β correspond with the angles in Table 2.1. θ_1 is the angle of incident light and θ_2 is the angle of reflection and they are equal.

In the standard ASTM D523 − 14 (reapproved 2014), specular gloss is defined as the ratio of the luminous flux of light, reflected from a specimen in the specular direction at specified source and receptor angles, to the luminous flux of light reflected from an ideally flat black glass standard. This standard has a refractive index of n = 1.567 for the sodium D line. The sodium D lines, of which there are actually two characteristic ones, are part of the Fraunhofer absorption lines. The sodium D lines are in the yellow region of the spectrum (Jenkins and White 1981). The standard for specular gloss meters ASTM D523

− 14 (reapproved 2014) is based on the sodium D_1 line at 589.3 nm while DIN EN ISO 2813:2014 (reapproved 2014), another very similar standard for specular gloss meters, is based on the d line for helium at 587.6 nm (Frankhuizen, Industrial Physics 2023). For the black glass standard, a specular gloss value of 100 gloss units (GU) is assigned for every specular angle θ (ASTM D523 − 14 reapproved 2014; DIN EN ISO 2813:2014 reapproved 2014). BaK50, an optical quality barium crown glass has a refraction index of n=1.567 for the sodium D line (Hanson 2006; Nadal et al. 2006). However, a calibration standard out of this material would be expensive. The actually used black glass standards of gloss meters do not have a refractive index of n = 1.567, which has to be made up for by using a correction factor *cor* (Nadal et al. 2006). The actual calculation of the specular gloss value is as shown in Equation 2.1. R_{sample} is the reflected luminous flux from a sample and $R_{standard}$ is the luminous flux of light reflected from the black glass standard for a specified source and receptor angle. Both R_{sample} and $R_{standard}$ are measured under the same geometric conditions.

$$gloss_{\theta}(in\ GU) = cor\ \cdot 100\ \cdot \frac{R_{sample}}{R_{standard}} \qquad 2.1$$

Hunter and Harold (1987) describe the specular gloss measurement at 20° as suitable for high gloss surfaces, 60° for mid-range gloss surfaces and 85° for low gloss surfaces. The standard method for measuring specular gloss ASTM D523 − 14 (reapproved 2014) states more specific that the 20° geometry is advantageous over the 60° geometry for comparing specimens having specular gloss 70 GU or higher measured with the 60° geometry. The 85° geometry is used for comparing very matte specimen with specular gloss lower than 10 GU measured at 60°.

The reason why the different angles are used for specular gloss measurement is a consequence of the Fresnel equations. For dielectric materials whose extinction coefficient k is negligible small. The quotient of the reflected light to the incident light intensity R, can be calculated according to Equation 2.2, 2.3 and 2.4. It depends on the specular angle θ and the refractive index n of the material as explained in further detail by Hébert (2013) and Silvennoinen et al. (2008b). R_p is the p-polarized (parallel) share of R, R_S is the s-polarized (senkrecht – perpendicular) share of R. The refractive index n as well as the extinction coefficient k vary with the wavelength of light λ.

$$R_p(\theta,\lambda) = \left(\frac{n(\lambda)^2\cdot\cos(\theta)-\sqrt{n(\lambda)^2-\sin^2(\theta)}}{n(\lambda)^2\cdot\cos(\theta)+\sqrt{n(\lambda)^2-\sin^2(\theta)}}\right)^2 \qquad 2.2$$

$$R_s(\theta,\lambda) = \left(\frac{\cos(\theta)-\sqrt{n(\lambda)^2-\sin^2(\theta)}}{\cos(\theta)+\sqrt{n(\lambda)^2-\sin^2(\theta)}}\right)^2 \quad 2.3$$

$$R(\theta,\lambda) = \frac{1}{2}\Big(R_p(\theta,\lambda) + R_s(\theta,\lambda)\Big) \quad 2.4$$

Metals however have a high, non-negligible imaginary extinction coefficient *k*. This is due to the delocalized nature of the valence electrons with their ability of freely moving in a piece of metal (Nassau 2001). For that reason, only little or no electric field can be set up in metal. Therefore, very little light penetrates the surface of metals and is reflected instead (Christie 1969). This in return is the reason for the high reflectivity of metals. Due to the non-negligible extinction coefficient of metals, the refractive index becomes the complex refractive index $\hat{n}$ as shown in Equation 2.5 (Hébert 2013).

$$\hat{n}(\lambda) = n(\lambda) + ik(\lambda) \quad 2.5$$

Due to the complex refractive index, Equation 2.4 becomes more complicated, which is explained in detail by Hébert (2013). The reflection of glass with a refractive index of n = 1.567 and the reflectance of aluminum with a refractive index of n = 1.205 and an extinction coefficient of k = 7.064 at a wavelength of 589.3 nm, a sodium D line, with dependence on θ can be seen in Figure 2.2. This is under the condition of an ideal flat surface that is surrounded by air.

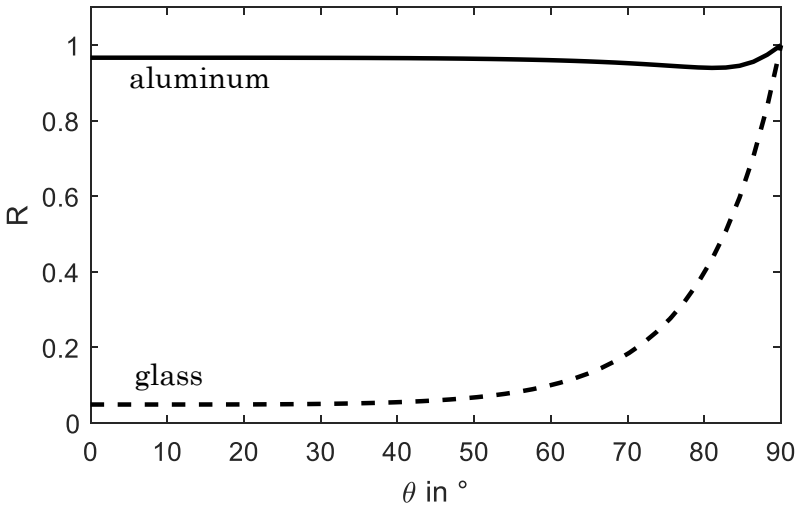

Figure 2.2: Angular reflectance as a function of the incident angle of glass (n = 1.567) and aluminum ($\hat{n} = 1.205 + i7.064$) for light with a wavelength of 589.3 nm under the condition of a flat surface that is surrounded by air. Figure plotted by the author. Data of n and k were obtained from Polyanskiy (2023). R is the quotient of the reflected light to the incident light intensity.

It can be observed that the relative reflected luminous flux of glass increases as the angle of reflection becomes higher. In contrast, for aluminum, the dependence of reflectivity on the angle is much smaller than that for glass, resulting in higher relative reflectivity over the angular range. Table 2.2 provides the relative reflective luminous flux values for glass and aluminum at angles θ = 20°, 60°, and 85°.

Table 2.2: Quotient of the reflected light to the incident light intensity R for a flat surface of glass (n = 1.567) and aluminum ($\hat{n}$ = 1.205 + i7.064) surrounded by air for a wavelength of light of 589.3 nm at the specular angles of 20°, 60° and 85°, corresponding to Figure 2.2. Values calculated by the author.

Angle θ	Glass: R(θ, λ)	Aluminum: R (θ, λ)
20°	0.0491	0.9669
60°	0.1001	0.9604
85°	0.6191	0.9473

Figure 2.2 indicates that matte dielectric materials can be differentiated better at grazing angles because here the reflected light flux is higher. For high gloss dielectric materials however, a smaller angle is preferable. The measurement resolution of gloss meters are not the same for the measurement at the three angles. A popular gloss meter, which is often used in the industry, has a measurement range for specular gloss of 0-2000 GU for measurements at θ = 20°, 0-1000 GU for measurements at θ = 60° and 0-160 GU for measurements at θ = 85° (Byk-Gardner n.d.b). For every range, a value of 0 GU would be obtained for a perfect light absorbent material. The highest value would be obtained on surfaces without any absorbance or scattering.

If the refractive index of two compared samples is the same, the measured gloss difference is solely a function of the roughness of the substrates (Desjumaux et al. 1998). Arney et al. (2006) showed that specular gloss measurements on rough materials behave in a different way as it would be expected if the angular reflection would be only governed by the Fresnel equations due to shadowing effects. Further, as explained by Ignell et al. (2009), for flat surfaces, gloss measurement is only associated with the specular reflection. For rough surfaces however, beneath this coherent contribution to specular gloss, also a diffuse component contributes to the measured value. The diffuse component can be modeled using the angle of incidence θ, the wavelength of the light and the surface roughness, e.g. the root mean square roughness Sq as well as the correlation length as a

measure of the lateral size of the surface irregularities (Alexander-Katz and Barrera 1998; Ariño et al. 2005).

2.3.2 Distinctness of image

DOI is defined in the standard CIE S 017/E:2020 (reapproved 2020) as the "aspect of appearance characterized by the sharpness of images of objects produced by reflection at a surface." The definition in ASTM E284 −17 (reapproved 2017) is very similar. The definition suggests that speaking of the DOI of surfaces only makes sense if they have a high gloss and can reflect images of objects (Silvennoinen et al. 2008b). As for specular gloss, the definition focuses on the visual perception of DOI. In order to physically measure DOI, the spread of light reflected at the specular angle is quantified to give an indication of how sharp a surface reflection is likely to appear (Gruber et al. 2008). Different methods have been developed for the measurement of DOI which are summarized by Gruber et al. (2008). For measurement instruments used in this work, test methods A and B, described in ASTM D5767 − 95 (reapproved 2012), are relevant.

According to Test method A, measurements of the reflected luminous flux are made on the sample in a region very close to the specular angle as well as 0.2° to 0.4° off the specular viewing angle of 20° or 30° as indicated in Figure 2.3. Most instruments however work with the specular angle of 20°.

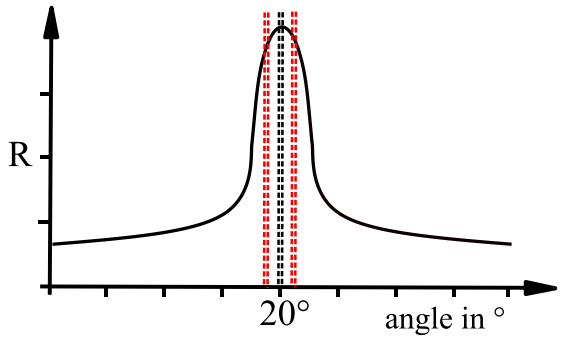

Figure 2.3: For the measurement of DOI according to Test method A, measurements very close to the specular angle (region indicated with black dotted lines) are compared to measurements at 0.2° to 0.4° off the specular angle (regions indicated with red dotted lines).

The calculation of the DOI is then as shown in Equation 2.6. The dashes between the angles indicate the angle intervals where the luminous flux is measured. A DOI of 100 % indicates a very high sharpness of the reflected image. Values close to 0 % indicate a very

low sharpness of the reflected image. R_{sample} is measured under the condition, that the angle of the incident and reflected light is not necessarily the same.

$$DOI[\%] = 100\ \% \cdot \left(1 - \frac{R_{sample(19.6°-19.8°)} + R_{sample(20.2°-20.4°)}}{R_{sample(19.95°-20.05°)}}\right) \quad 2.6$$

In Test method B, which is very similar to a measurement method described in JIS K 7374:2007 (2007), light passes from a light source through a slit and is irradiated onto a surface. Rectangular to the optical axis, an optical comb is placed that moves rectangular to the axis of the reflected light. Behind the optical comb, the reflected light is measured. Due to the movement of the optical comb, a wave form of received light is measured. The highest measured value of this wave is M, the lowest m. The ratio between (M-m) and (M+m) results in a value called image clarity (IC) as shown in Equation 2.7 (Inoue et al. 2012a).

$$IC[\%] = 100\ \% \cdot \left(\frac{M-m}{M+m}\right) \quad 2.7$$

An IC of 100 % indicates a very high sharpness of the reflected image. A value close to 0 % indicates a very low sharpness of the reflected image. The angle of illumination and measurement of this method is 60°. Four different gratings of the optical comb lead to four IC values, which are reported together with the regarding grating. The measurement principle of Test method B and an optical comb with four different gratings is shown in Figure 2.4.

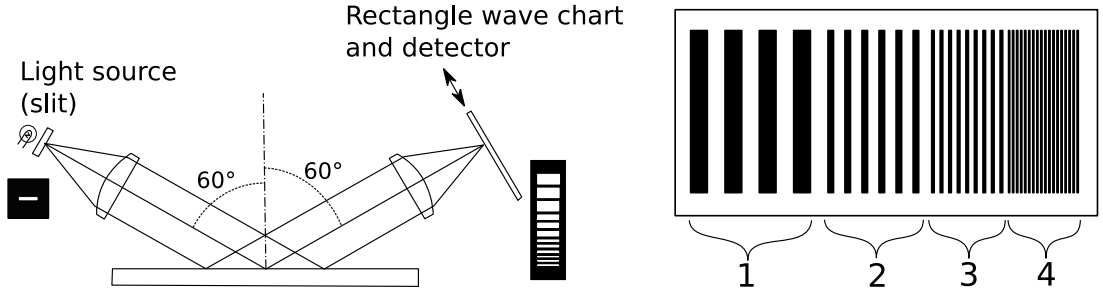

Figure 2.4: In the left image the measurement setup for IC is shown after Inoue et al. (2012b). Light passes through a slit is reflected on a sample and passes through an optical comb. The light that passes through the optical comb is recorded and from those measurements the IC is calculated. The right image shows an optical comb having four different widths of opaque and translucent regions after ASTM D5767 − 95 (reapproved 2012).

2.3.3 Haze

There are two types of haze. One is reflection haze and one transmission haze. For the reason that transmission haze is of no importance for the research of this dissertation, the further use of the term 'haze' solely refers to reflection haze. The standard ASTM E284 −17 (reapproved 2017) provides three definitions for haze. First, "scattering of light at the glossy surface of a specimen responsible for the apparent reduction in contrast of objects viewed by reflection at the surface." Second, "percent of reflected light scattered by a specimen having a glossy surface so that its direction deviates more than a specified angle from the direction of specular reflection." Third "cloudy appearance attributable to light scattering". Definitions given in CIE S 017/E:2020 (reapproved 2020) are very similar. As stated by Beuckels et al. (2023), the first and the third definition describe perceptual haziness, while the second definition describes the standardized instrumental evaluation method of haze. Beuckels et al. (2023) and Vangorp et al. (2017) suggest that a good perceptual DOI is required before one can consider haze.

Several methods can be found for the measurement of haze (Silvennoinen et al. 2008b). ASTM D4039 − 09 (reapproved 2015) describes a haze measurement method that makes use of the size differences of the receptor apertures for the specular gloss measurement at 60° (larger receptor aperture) and 20° (smaller receptor aperture) as shown in Table 2.1. By subtracting the specular gloss measured at 20° from the specular gloss measured at 60° in gloss units (GU), a haze value can be computed. However, a precondition for this method is that the specular gloss measured at 60° is higher than the specular gloss measured at 20°. For metallic specimens with a small roughness, this condition is often not met.

The haze measurement method described in the standard ASTM E430 - 11 (reapproved 2011) method B, which is similar to a method described in DIN EN ISO 13803:2014 (reapproved 2014) is relevant for the measurement instruments used in this work. Here the ratio of reflected flux measured beneath the region where specular gloss is measured at 20° to the specular gloss measured at 20° in GU (*Gloss20*) on the calibration standard is calculated as shown in Equation 2.8. R_{sample} is measured under the condition, that the angle of the incident and reflected light is not necessarily the same.

$$haze[HU] = 100 \cdot \frac{R_{sample(DHaze\ 18.1°)} + R_{sample(DHaze\ 21.9°)}}{Gloss20_{standard}} \qquad 2.8$$

DHaze is the size of the haze apertures beneath the aperture for specular gloss and it is spanned by the opening anlges $\alpha_{receiver\ haze}$ and $\beta_{receiver\ haze}$. There is one haze aperture at 18.1° and one at 21.9°. The aperture sizes for the haze according to ASTM E430 - 11 (reapproved 2011) method B are 1.8° ± 0.05° for $\alpha_{receiver\ haze}$ and 5.5° ± 0.25° for $\beta_{receiver\ haze}$ and they are shown in Figure 2.5. Haze is reported in haze units (HU).

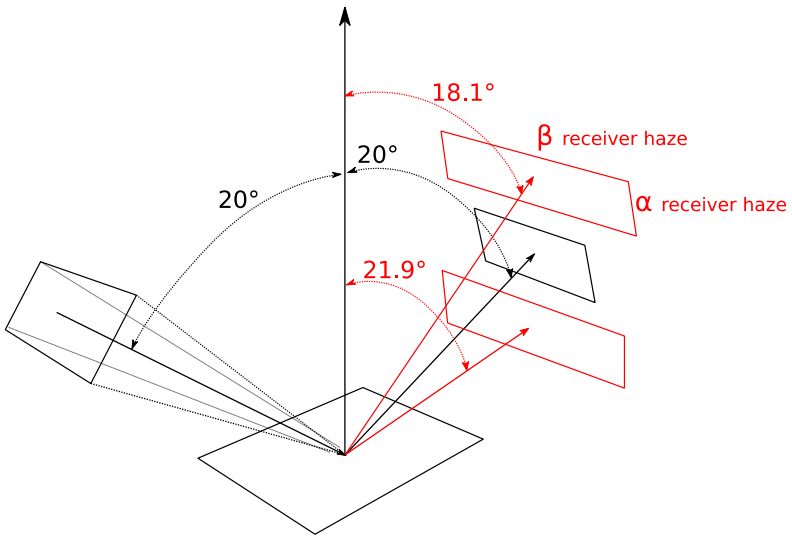

Figure 2.5: Schematic of the opening angles that are additionally needed for the measurement of haze as stated in ASTM E430 - 11 (reapproved 2011) method B. All lines in black correspond to Figure 2.1. DHaze, which is shown in Equation 2.8 is spanned by the haze aperture opening angles $\alpha_{receiver\ haze}$ *and* $\beta_{receiver\ haze}$.

The standard ASTM E430 - 11 (reapproved 2011) also describes the measurement of logarithmic haze. According to Fensterseifer, Byk Gardner (2021) it corresponds better to human perception for dielectric materials. However, for metallic materials, logarithmic haze is not preferred in the industry. Further, ASTM E430 - 11 (reapproved 2011) also describes the measurement of compensated haze. This metric allows a better comparison of the haze of surfaces with different colors (Konica Minolta n.d.b). It is usually not used to examine the haze of metallic surfaces. Compared to specular gloss and DOI, haze is a rarely studied aspect of gloss (Beuckels et al. 2023).

2.3.4 Bidirectional reflectance distribution function

The bidirectional reflectance distribution function (BRDF) describes and specifies the (geometrical) reflecting properties of most opaque surfaces (Nicodemus 1965; Nicodemus

et al. 1977). It tells how bright a surface element seen from a viewing direction appears when light from a given incident direction is reflected on a surface (Gruber et al. 2012). There is no direct correlation of the BRDF to the human perception of surface gloss (Gruber et al. 2012).

Multiple techniques for the measurement of the BRDF have been developed. A good summary of these techniques is provided by Herranz (2014). Normally, to measure a full BRDF, a goniophotometer is used that enables the positioning of the illuminant and the detector in any angular value (Eugene 2008; Inoue et al. 2022). However, this measurement is a difficult and time-consuming task (Obein et al. 2004).

Some gloss meters on the market are equipped not only with single photodiodes that measure one value but also with linear diode arrays or sensor matrices, enabling the measurement of a partial BRDF (Smith 1999). Partial BRDF, often also called simplified BRDF, means that there is only one angle of incidence and the viewing direction is limited to an interval of angles. Gloss meters that measure a partial BRDF and which are used in this work can either only make measurements along the angle α or along α and ß. In this dissertation, the former is called 1D-BRDF, the latter is called 2D-BRDF. The angles are shown in Figure 2.6. Using the data from the light distribution, the specular gloss, DOI, and haze and more values can be calculated internally by gloss meters. This way of obtaining these aspects of gloss is not yet taken into account by the standards for the measurement of specular gloss, DOI, or haze. For the BRDF measurement principle diagramed in Figure 2.6, θ_1 and θ_2 are not necessarily the same.

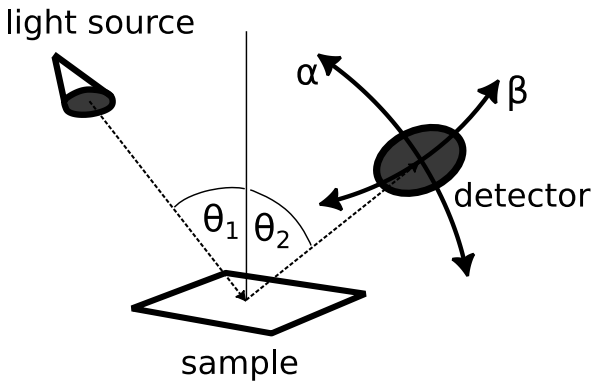

Figure 2.6: Principle of simplified BRDF measurement. If the measurement of the distribution of the reflected light takes place along the angle α, it is referred to as 1D-BRDF. If the distribution of the reflected light is measured along α and β, it is referred to as 2D-BRDF.

2.4 Visual perception studies on gloss

Many different approaches for visual experiments have been developed. Thorough explanations and classifications of different types of visual experiments are provided by Engeldrum (2000) and Kehren (2013). Visual perception studies on gloss can be broadly divided into studies that use computer rendered images and studies that use real world samples. In recent years, many experiments on gloss using dielectric materials were conducted to answer a wide range of research questions. Some influential studies in gloss science that were conducted using non-metallic samples are briefly outlined:

Obein et al. (2004) conducted a study to obtain gloss scales using coated paper samples that had a range of specular gloss measured at 60° from 1 GU to 91 GU. It was found that for this gloss range, there is a nonlinear relation between the gloss percept and instrumental specular gloss values. It was also concluded exclusively for high gloss that for binocular vision, the gloss sensitivity is higher than in monocular vision. The independence of the geometrical variation of the luminous flux for gloss ratings by observers was shown. Analogous to 'color constancy', this property was named 'gloss constancy'. Further, from the results of the experiment it was concluded that for very glossy samples with smooth surfaces, the gloss judgement is based exclusively on the DOI.

Ji et al. (2006) investigated the relationship between visual-scaled data of samples with differing gloss and color and the measured gloss values. As samples, gloss scales of the Natural Color System (NCS, Sweden) were used that had a maximum specular gloss of 90 GU measured at 60°. It was shown that color did not appear to significantly influence gloss ratings. Leloup et al. (2010) used samples out of flat glass to examine the influence of both the geometry of illumination and luminance contrast on gloss perception. The light sources used could be individually varied. As a result, it was found that not only the sample surface characteristics determine gloss perception but also the illumination geometry. Leloup et al. (2012) investigated the multidimensionality of gloss perception and the interaction between several visual aspects of gloss (specular gloss, contrast gloss, and DOI). Flat glass samples that were used differed regarding multiple visual gloss criteria. From the results of this psychophysical experiment, it could be concluded that both differences in DOI and differences in luminance affect gloss perception. Analysis of the data showed that one group of observers used mainly DOI to judge glossiness. The second group evaluated gloss primarily from differences in luminance of the specular highlight and the diffuse background. Ged et al. (2020) measured the effect of environment

complexity over perception of gloss of samples. In this experiment both a standard black light booth and a realistic office cubicle were used as test environments. The results showed that the environment affects gloss perception of very matte samples.

In comparison to research conducted on gloss of non-metallic surfaces, research employing psychophysical experiments for the investigation of gloss of metallic surfaces is still scarce. Experiments using virtual and real world samples are briefly outlined in the following:

Todd and Norman (2018) investigated how the presence or absence of ambient light influences the appearance of computer rendered metal objects of which the metallic appearance and shininess was rated by observers. Under simulated ambient illumination, surfaces with the lowest roughness were rated highest regarding metallicity and shininess. As the simulated roughness was increased, these ratings dropped systematically. When illuminated by point or area lights, objects with the lowest roughness were judged less metallic and shiny. However, objects with intermediate levels of roughness were judged more metallic and shiny than under ambient illumination.

The following studies report on experiments using real world metallic samples: Dekker et al. (2011) investigated how texture and color combines when assessing the appearance of special effect coatings. A set of metallic samples, pearlescent samples, and samples containing both metallic and pearlescent materials were used as representative for car finish coatings. Both instrumental and visual data was analyzed and compared. A visual appearance score was created that correlates with the measurements of color and texture differences. Using this data, a calculation procedure was developed yielding predictions on visual acceptability of coatings using measured data.

Mirjalili et al. (2014) used samples of automotive coatings to find correlations between visually perceived and instrumentally measured appearance. This was done to improve the consistent control of the appearance of achromatic automotive finishes. Good correlations between instrumentally measured specular gloss, DOI, waviness and visual judgement were reported. A psychophysical study was carried out by Wu et al. (2016) to assess the gloss of metallic coatings from the automotive industry with different colors and textures. The visual data were compared with spectrophotometric measurements and instrumental specular gloss values under the geometries of 20°, 60°, and 85°. A model was proposed to link these measurements to be continuous monotonically and to improve the

accuracy of estimating visual gloss. These studies show that it is possible to link visual percepts of metallic surfaces with instrumentally measured scales.

Rich et al. (2017) used samples metallized by printing to conduct a study on the agreement between visual assessment and the measurement of the reflectivity. It could be shown that for these samples a reliable scale for visual metallic brilliance could be developed. Gemeinhardt (2020) reported on studies on the metallicity of metallic printed samples, and compared metallicity with brightness of the samples. It was found that there is a link between measured brightness and perceived metallicity.

2.5 Printing aluminum pigments

In general sense, graphical printing is mostly the reproduction of originals (or print masters). In two-dimensional graphic printing, the focus is on the correct reproduction of color information as well as text and image information on a substrate (DFTA 1999; Hupp 2008). In the broader sense, graphic printing is not only about the reproduction of color information, but about the reproduction of appearance, which includes gloss (Weber et al. 2022d). A categorization of the different printing methods, which can be used for metallization in a printing process, is shown in Figure 2.7. The methods can be categorized into two groups: those for which pre-metallized film plays a direct role in the printing process, such as foil fusing, cold foil transfer, and hot foil stamping, and those where metal effect pigments are used. The latter category can be further divided into methods where the pigments are incorporated into the printing ink during the printing process and methods where pigments are applied to a sticky preprint, as seen in processes like bronzing or the EcoLeaf technology. The printing methods that utilize metal effect pigments in printing inks can be further classified into form-bound printing methods, including offset printing, gravure printing, flexo printing, and screen printing, as well as digital printing methods, such as inkjet printing and electrophotography. In this dissertation, most of the samples investigated were metallized using printing inks containing aluminum pigments, which were applied through flexo or offset printing. The printing method employed for the printing experiments in this dissertation is flexo printing.

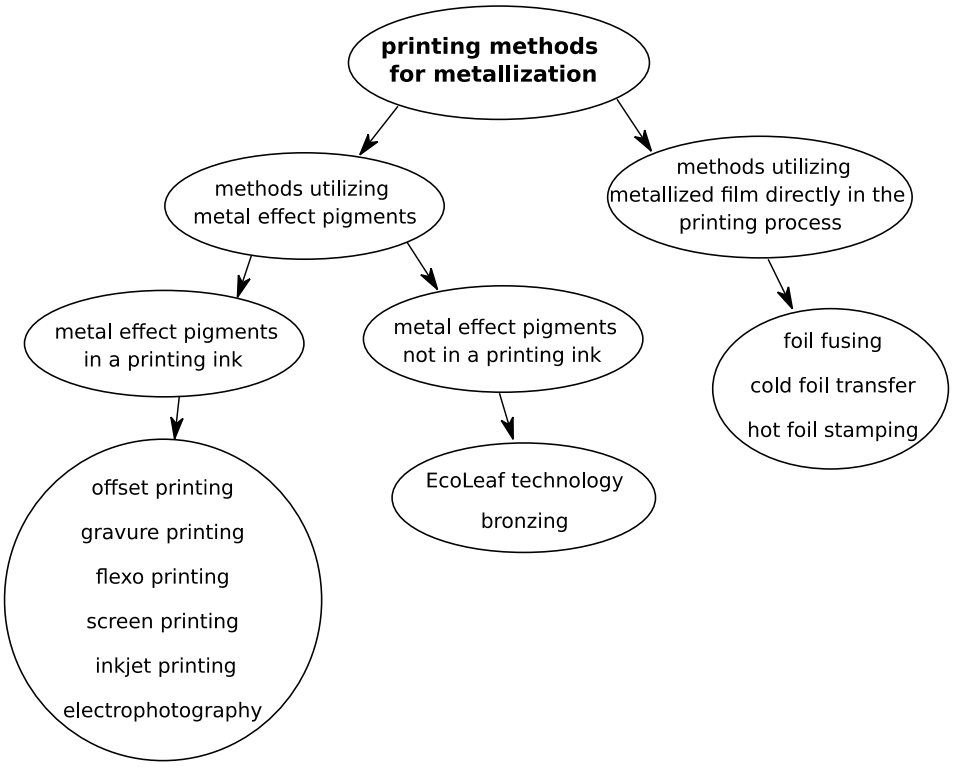

Figure 2.7: Classification of methods used for the production of metallic embellishments in the label and package printing industry (Weber et al. 2022d).

2.5.1 Aluminum pigments

There is a huge variety of metal effect pigments. In the field of graphic printing, mostly aluminum or bronze pigments are used. Bronze pigments come into play if it is desired to produce a bright gold tone (Krietsch, Schlenk Metallic Pigments 2021). One reason why pigments out of aluminum are more often used in the graphical printing industry is that they have negligibly small chroma themselves. By overprinting, polychromatic metallic effects can be obtained (Pfaff 2017). Furthermore, the material is easy to process and comparatively inexpensive (Wheeler 1999). Aluminum pigments can be classified into three different types. These are cornflake pigments, silverdollar pigments, and vacuum metallized pigments (VMPs) (Wheeler 1999; Maile et al. 2005; Wißling 2013).

Cornflake pigments, which have irregularly frayed edges, and silverdollar pigments with round fringes are both produced in a wet milling process out of aluminum grit (Wheeler 1999; Wißling 2013). In this process, a lubricant, in form of an oleic acid or stearic acid is added to prevent cold fusion. VMPs achieve the highest gloss of the three types of pigments. As described by Levine et al. (1982) and Wheeler (1999), for the production of these, layers of 40-60 nm of aluminum are applied in the gas phase under high vacuum on

a polymer film that is previously coated with a release layer. Then, the aluminum layers are released in a solvent bath under ambient pressure. In the next step, the released aluminum is reduced to smaller flakes until the desired size distribution is reached. Before incorporating the pigments into UV-inks, VMPs are then treated with phosphorous organic compounds (Krietsch, Schlenk Metallic Pigments 2021).

As explained by Brock et al. (2000) and Eckart GmbH (n.d.), the choice of the acid used in the production of cornflake and silverdollar pigments decides about relevant properties of the pigments produced because it decides about the polarity of the pigments surface. If the binder and the pigment surface have the same polarity, the pigments show a favorable wetting behavior and do not have a leafing property. In this case they orient themselves predominantly parallel to the substrate and rather on the bottom of the wet ink film (Pfaff 2017). If the pigment surface and the binder have an opposing polarity, the pigments do not have good wetting properties. In this case, the pigments with leafing properties move towards the surface of a wet film and orient parallel to the ink film surface (Pfaff 2017). There, the leafing pigments form a dense layer. However, due to the low surface tension of ink systems with leafing pigments, the adhesion properties are decreased, which can make overprinting more difficult (Eckart GmbH n.d.). Due to the float-up of leafing pigments and overlap close to the ink film surface, leafing pigments lead to a more bright surface and higher gloss, compared to non-leafing pigments (Smith 1983).

The size of pigments in inks is mostly communicated as a size distribution for which d_{XX} is the measure. For instance, if the d_{50} size is 10 µm, the diameter of 50 % of the pigments in the ink is larger and 50 % of the pigments diameter is smaller than the given value. if the d_{90} size is 10 µm, the diameter of 90 % of all pigments is smaller than 10 µm and 10 % are larger (Wißling 2013). The thickness of the platelet shaped pigments is usually not provided in datasheets. However, the shape factor of the metallic pigments that describes the ratio of thickness to diameter is between 1:50 and 1:500 (Brock et al. 2000).

2.5.2 Flexo printing of UV-inks with aluminum pigments

As explained in detail by DFTA (1999), Kipphan (2000) and Teschner (2017), in flexo printing, ink is taken up from an ink tank by an anilox roller that also serves for dosing the printing ink. A doctor blade, removes surplus ink that is not in the cells of the anilox roller. Hereafter, the ink is transferred to a flexible polymer printing plate on a printing cylinder. In flexo printing, the image is formed by small elevations on the printing plate.

The ink is transferred onto the substrate, which moves between the printing cylinder and the impression cylinder. The principle is depicted in Figure 2.8 for a flexo printing unit in a sheet-fed printing machine with a chambered doctor blade. The transferred ink volume and thus the transferred ink film thickness is essentially determined by the selected anilox roller (Hupp 2008). The scoop volume (in ml/m² or g/m²) characterizes the amount of ink transported by an anilox roller to the printing plate. Flexo printing allows to print with a high printing speed. As outlined by Haas (2012), in industry, flexo printing units can be found in row construction in the narrow-web printing sector which is predominantly used for label printing. Often flexo printing units are used for the finishing process in graphical printing and are mostly installed subsequent to the offset printing units. A significant proportion of flexographic printing units in the printing industry can be found in central cylinder printing machines, which are advantageous for flexible package printing (Kipphan 2000).

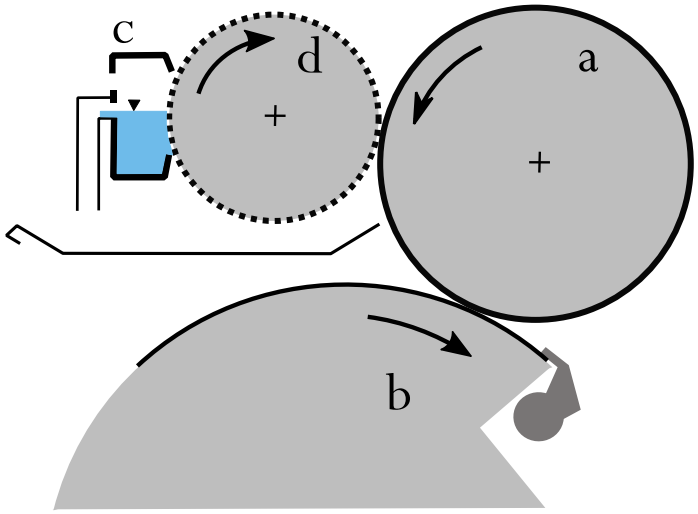

Figure 2.8: Schematic of a possible flexo printing unit with a chambered doctor blade in a sheet-fed printing machine after Neumann (2009): Coating unit with chambered doctor blade, a) plate cylinder with printing plate, b) impression cylinder with engaged substrate, c) ink fountain and d) anilox roller.

According to Krietsch, Schlenk Metallic Pigments (2021) and Kehren (2013) it is possible to use inks with platelet-shaped pigments with a size of up to 200 µm in flexo printing. Before printing inks containing metal effect pigments onto a paper, sometimes a primer is printed. Its function is to smoothen the surface and reduce the water absorptivity or the ink holdout of the substrate which in return can increase gloss (Eckart GmbH n.d.).

In flexo printing, solvent-based, water-based and UV-curing inks are commonly used (Haas 2012). Inks that undergo physical drying, such as solvent-based or water-based inks, evaporate at either room temperatures or elevated temperatures after the printing process. UV-inks only cure due to the activation of UV-light sensitive components (UV-initiators) in the ink that start a polymerization of film-forming components (Radiation curing 2008). The curing of UV-inks takes place without any evaporation of solvent (Radiation curing 2008). UV-curing inks consist of oligomers (often also called binder) and monomers that polymerize with each other. This reaction is started by UV-initiators. Besides that, pigments and fillers are present in the ink. Additionally, additives, used in small quantities, aim to enhance properties such as substrate wetting, leveling, slip, scratch resistance, as well as defoaming and deaeration (Tego Journal 2007 cited in Radiation curing 2008). For UV-inks with aluminum pigments, there are inks with leafing and non-leafing pigments available on the market. However, commercially non-leafing types only can be found for cornflake and silverdollar pigments. In the case of VMPs in UV-curing inks, there are only leafing types commercially available. A reason for this is the treatment of VMPs used for UV-inks with organic phosphorus compounds that makes them float (Krietsch, Schlenk Metallic Pigments 2021). The purpose of this treatment is to prevent a chemical reaction between the aluminum and the photo initiators in the ink, which could result in the ink hardening while it is still in the ink container.

2.6 Dynamic gloss of printing inks

After printing ink on a substrate, the gloss of the ink film changes over time until the ink is dried in the case of water-based and solvent-based inks or cured in the case of UV-inks. This change of gloss with time is called ‘dynamic gloss’. Many experiments have been carried out on the investigation of the dynamic gloss of printing ink after the printing process. These investigations give insight into the substrate-ink-pigment interaction after the application of the ink onto the substrate in the printing process.

The dynamic gloss of inks without metal effect pigments is mainly based on two different processes that happen after printing (Fetsko and Zettlemoyer 1962). First, the leveling of ink filaments takes place. These filaments form at the exit of the printing nip as indicated in Figure 2.9 and as explained by Desjumaux et al. (1998).

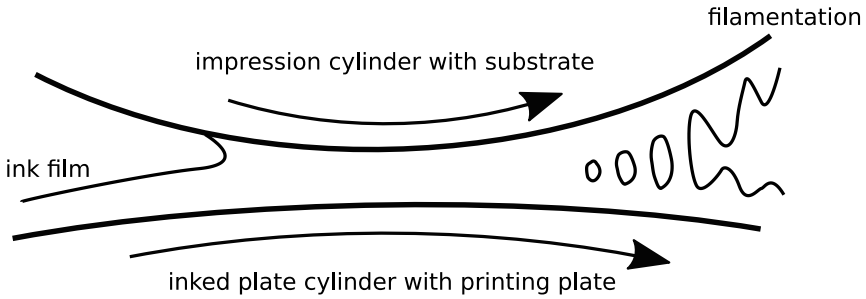

Figure 2.9: Forming of ink filaments in the printing process in the printing nip after Fetsko and Zettlemoyer (1962). The dimensions in the illustration are exaggerated.

The ink filaments break at some point and recoil in the direction of the printed surface and in the direction of the non-transferred ink. Filaments that recoil in substrate direction form small bumps on the ink film which level due to surface tension forces. Sauer et al. (2021) showed that the speed of ink film levelling for a solvent-free ink on a non-absorptive surface is abundant of the height h of the surface profile at a specific time t, the surface tension σ of the ink film as well as the ink viscosity η as shown in Equation 2.9. The second driving process of dynamic gloss is the ink-paper interaction after the printing process, which is especially the absorption of binder into the paper.

$$\frac{\partial h}{\partial t} = -\frac{h^3 \sigma}{3\eta} \Delta^2 h \qquad 2.9$$

Some of the earliest investigations on dynamic gloss have been reported by Glatter and Bousfield (1996) and Glatter and Bousfield (1997) who set up a model to predict the leveling of an offset ink film on a substrate. The predictions of the model were compared to experiments using a laser beam detector system, which continuously monitored the specular gloss at 75° directly after printing offset ink with a laboratory print tester onto coated papers. With the use of a video microscope, the gloss measurement results could additionally be compared to the topography of the ink film surface. The results show that there is an influence of the printing speed on the ink film thickness and dynamic gloss. Desjumaux et al. (1998) reported on the development of ink gloss for the first time under 20 s after printing. The impact of pigment size on dynamic gloss reveals that, in offset inks, as pigment sizes decrease, specular gloss measured at 20° also decreases. It was inferred that finer pigments lead to a more rapid migration of the binder into the substrate, thereby slowing down the leveling process of the ink.

Desjumaux et al. (2000) used a novel gloss meter that measured gloss at the specular angle of 75° to measure the dynamic gloss of wet inks with different pigment concentrations on

latex coatings. It was shown that the pigment concentration is one of the key parameters that controls the ink gloss. In a study by Enomae et al. (2000), a video microscope was used to observe the wet ink on the substrate after printing and a confocal laser scanning microscope to investigate the three-dimensional shape of the dried ink films. Specular gloss measurement were made at an angle of 75°. Offset inks were printed with a laboratory printability tester. Both calendered and uncalendered paper sorts were used as substrate. It was found that for uncalendered papers the gloss reaches a maximum 50 s after printing and then decreases gradually. For calendered papers, no decrease of gloss could be measured. Further, it was shown that higher ink volumes lead to a slower initial rising speed of gloss after printing. Using a freeze drying technique, the topography of the ink could be investigated after certain time intervals after printing. Jeon (2002) investigated roles and significances of different factors on print gloss development of offset inks. Gloss measurements were made to measure the initial gloss development on a variety of paper samples with differences in roughness, porosity, and pore size. Main outcomes of the study were data about the impact of roughness, porosity, and pore size of the paper substrate on dynamic gloss. It was shown that there are inconsistencies between the dynamic gloss measurements measured at the angles 60° and 75°.

Preston et al. (2003a) assessed the influence of ink film thickness on the final print gloss. The change of gloss after printing was discussed in terms of changes in roughness and refractive index after printing. For their experiments, a laboratory offset test printer was used. The dynamic gloss measurement system measured gloss at 75°. It was found that the majority of total gloss change occurs within the first two seconds after printing and that thicker ink films have a slower rise of gloss towards the maximum gloss. It was concluded that the application of a thicker ink film onto a substrate did not lead to a higher final print gloss. Preston et al. (2003b) investigated the influence of the substrate in the gloss development after printing. Paper samples were characterized in terms of roughness, porosity, and ink setting rate. It was shown that fast ink setting papers lead to poor print gloss. Also increasing the amount of ink applied did not compensate for this.

Preston et al. (2006) reported on the influence of coated paper porosity on the print quality using UV-offset inks. The experimental set up used resembles the set up used by Preston et al. (2003a). Beneath the measurement of the dynamic gloss, also measurements of the dynamic refractive index were made. The mineral particles used to produce two different paper coatings for the experiment were kaolin and precipitated calcium carbonate (PCC).

The measurements showed that the 100 % kaolin coated paper had superior ink hold out properties. This led to a higher print gloss and a smoother surface. Measurements on short time scales of up to ten seconds revealed that the gloss measured on PCC-coated paper decreased after an initial rise. In contrast, the dynamic gloss measured on kaolin-coated paper rose abruptly after printing and then continued to steadily increase. Measurements on longer time scales of up to 120 minutes, however, revealed that the gloss measured on kaolin-coated paper once again decreased within the first ten minutes after the initial short rise and then increased again. The decrease in gloss during the first ten minutes was attributed to an increase in micro-roughness, which can be linked to the pigments getting closer to the ink film surface. The subsequent increase was attributed to a reduction in macro-roughness within the ink film due to the filling of macro-roughness features and the leveling of ink filaments.

Silvennoinen et al. (2008a) presented a novel system for dynamic print gloss measurement on papers based on the use of a diffractive optical element based gloss meter that also made online gloss measurement on a moving substrate possible. The dynamic gloss was studied using papers with a differing pore size and a non-absorbing film. Koivula et al. (2009) compared three dynamic gloss measurement techniques, which are a dynamic gloss meter, a diffractive-optical-element-based gloss meter, and a polarized-light reflectometer. They showed that the three instruments produced similar results while the differences could be attributed partially to practical aspects of the specific measurements. Despite the numerous extensive investigations on the dynamic gloss of ink films after printing, to the best of the author's knowledge, no research on the dynamic gloss of ink films containing aluminum pigments has been conducted.

2.7 Orientation of metal effect pigments in coatings

In the field of surface analysis the terms topography, morphology and topology can be found. The meanings of these terms overlap partially. Topography describes the surface properties or the geometric-spatial shape of technical surfaces, but also of microstructures, which are recorded, for example, with atomic force microscopy, confocal microscopy, or profilometers (Martin 2022). It stems from the Greek words topos – place and graphia – writing. Morphology describes form-giving aspects in space in many disciplines and focusses on the shape of surfaces. The term morphe means shape in greek and – logia some branch of learning. Topology describes the way how parts of bodies (as for example

pigments) are arranged and related to each other (Oxford Learner's Dictionary n.d.). All three terms can be encountered in research related to aluminum pigments within ink films applied to surfaces. However, in the context of the studies conducted for this dissertation, only the term 'topography' is used as it encompasses all the relevant aspects of the pigment layer that are the primary focus of this research. In the subsequent listing of recent research on the topic, the terminology employed mirrors that which was used in the studies.

In addition to the type of pigments used and the ink system, the optical properties of a coating containing metallic effect pigments are also influenced by the orientation and distribution of the metallic effect pigments. For automotive coatings, intensive studies have been carried out on the relationship between appearance and microstructure. Automotive coatings have a much greater thickness than printed ink layers. In the automotive coatings industry, it is important to control the surface structure, i.e. the structure formed by the pigments in the coating. Various techniques can be used to investigate the alignment and distribution of metallic effect pigments.

As described by Kirchner and Houweling (2009) and Seubert et al. (2015), cross-cuts through the substrate and the ink film can be carried out for the analysis of the metal effect pigments. However, this technique has the drawback that it is not possible to capture the orientation of the pigments in all three spatial dimensions and that it is very time consuming. With the development and more broad use of confocal microscopy, more investigations on pigment topographies were carried out using this technique.

Kettler and Richter (1997) used various methodological approaches for the characterization of the topology of platelet-like effect pigments in automotive basecoats. These are goniospectrophotometry, confocal laser-scanning microscopy, and microscopic image analysis techniques of basecoat cross-cuts to examine the relation between the orientation of platelet-like effect pigments in surface coatings and the coloristic properties of the surfaces. In order to influence the orientation of the aluminum pigments, different amounts of an organic extender was added to the coatings as disorientation agent. It was shown how the measured lightness measured at different angles as well as the roughness of the coating surface varied with the amount of disorientation agent added. Sung et al. (2000) present preliminary studies on coatings with aluminum pigments that were investigated with the use of laser scanning confocal microscopy and the measurement of BRDF data. It was shown that using Fast Fourier Transformation (FFT) image analysis,

microscopic image data can be related to scattering measurements. Further it was found that coatings with rather coarse pigments lead to higher off-specular lightness than coatings with finer flakes.

Sung et al. (2002) used a set of automotive aluminum-flake pigmented coatings produced using varying spraying conditions to influence the flake surface topography as well as the orientation of the pigments. The samples were investigated using goniospectrophotometry and confocal laser-scanning microscopy. With the obtained data a model was created that could be used to compute the angular-resolved reflectance from topographic data of the confocal microscope. Kirchner and Houweling (2009) made investigations on a set of 117 metallic coatings applied with a spray gun on panels with varying concentrations of aluminum pigments and disorientation agent and varying size and type of aluminum pigments. The coatings used were solvent- and water-based systems. With the use of laser scanning confocal microscopy data it was shown that silverdollar pigments orient better than cornflake pigments and that coarse metallic flakes orient better than fine flakes. Furthermore, it was shown that larger flakes generally orient better than small flakes. Kirchner (2009) employed the data from this study to investigate whether the film shrinkage mechanism of solvent- and water-based coatings remains the dominant factor influencing flake orientation. It was found that although film shrinkage plays a role in the orientation of the flakes, there must also be other mechanisms that are important. Seubert et al. (2015) made investigations on samples coated with automotive paints to explore microstructural parameters of platelet-coating systems that control the appearance. Laser-scanning confocal microscopy data was compared with the measured lightness. It was concluded that the orientation of the flakes is a major parameter that influences the lightness. It was also shown that the size of the height, or in other words, the gap between the flakes in different layers (gap factor) strongly affects the scattering behavior of the system. Later, the data of this study was used by Seubert et al. (2018) to create an accurate model to predict the scattering behavior of aluminum pigment paint systems and to predict how the microstructure and surface roughness of the pigments affects the appearance of the system.

Despite the numerous investigations conducted on the orientation of metal effect pigments in automotive coatings and the resulting visual properties, the author was unable to find any published research on the orientation and distribution of these pigments in printed ink films. One distinction between metallic automotive coatings and printed metallic ink films is that the majority of automotive coatings only exhibit sub-surface texture, formed

by the pigments. The top layer, coated with clear coat, is typically very smooth. Further, the automotive coatings have a thickness of 25 µm or more (Rich et al. 2017). In contrast, printed ink films often showcase both sub-surface texture and surface texture, and have a thickness of only 2-3 µm for flexo printing (Rich et al. 2017).

3 Instrumental measurement of gloss

In this chapter, first, four criteria for gloss meters for studies in this work are stated. Subsequently, a comparison is made between three gloss meters, assessing their measurement values and peculiarities such as measurement consistency over time and the time required per measurement. Following this, gloss measurement results from a set of printed metallic samples produced with an industrial printing machine are presented. The differences in measurement results among the gloss meters are explored, and the reasons behind these deviations are discussed. This analysis aims at providing insights into the differences of the gloss meters in capturing gloss measurements. Parts of the results of the investigations in this chapter have previously been published by Weber et al. (2021a), Weber and Dörsam (2021) and Weber et al. (2021b).

3.1 Criteria for selecting gloss meters

There are four general criteria for gloss meters used for the research conducted in this thesis. They were established on basis of the literature review in Chapter 2 and general experience by the author. Firstly, the gloss meter should be portable to allow for easy use, whether it is near a printing press for quickly checking printed samples or in the laboratory. Secondly, it should be possible to differentiate samples with a very high reflectance factor. A black glass calibration tile with a near-normal reflectance factor of about 4 % in the visible spectrum results in measured gloss values of about 100 GU. An aluminum mirror however has a near-normal reflectance factor of about 95 % in the visible spectrum. This would result in a specular gloss value of about 1935 GU at the angle of 20° (Rich et al. 2017). However, many gloss meters cannot report such high gloss values, which especially accounts for low-priced gloss meters. Thirdly, the gloss meter should have the capability to measure not only specular gloss but also provide values that account for DOI and haze. The reported values should be easily understandable. Fourthly, the preferred gloss meter should either already be accepted within the industry or have potential for acceptance in the near future.

3.2 General comparison and measurement procedure

The three gloss meters which were available and which are compared in the following are the micro-TRI-gloss model 4446 (Byk-Gardner, Germany), the IQ-S (Rhopoint

Instruments, UK), and the RA-532H Surface Reflectance Analyzer (SRA) (Canon, Japan). The gloss meters as well as their calibration tiles are shown in Figure 3.1.

Figure 3.1: Left image: three available gloss meters used for the research. From left to right: micro-TRI-gloss, IQ-S, SRA. Right image: calibration tiles. a) black glass calibration tile of the micro-TRI-gloss, b) black glass calibration tile of the IQ-S, c) high gloss calibration tile of the IQ-S, d) black glass calibration tile of the SRA. To show their mirroring capabilities, they were placed in front of a checkerboard pattern that is reflected by the tiles.

Among the three gloss meters, the IQ-S stands out as the sole instrument capable of calibration not only on a black glass calibration tile but also on a high gloss calibration tile. Using it, the instrument is calibrated at 1938 GU for specular gloss measured at 20°, 930 GU for specular gloss measured at 60° and 147.7 GU for specular gloss measured at 85°. During pretests, it was observed that when using the IQ-S, measured specular gloss values measured at 60° on metallized surfaces, exceeding 150 GU, often exhibited significant discrepancies when the calibration on the black glass tile was employed as the reference. When calibrated with the high gloss calibration tile, measured specular values at 60° compared well with measurement results of the other gloss meters. When calibrated with the black glass calibration tile however, specular gloss values measured at 60° were not comparable with data obtained with the other gloss meters. As a result, the decision was made to use the high gloss calibration tile as the standard for the IQ-S when conducting measurements on metallized surfaces. The sizes of the measurement spots of the micro-Tri-gloss, obtained from Byk Gardner (n.d.a) and the IQ-S, obtained from Konica Minolta (n.d.a) can be seen in Table 3.1. Data regarding the measurement spot size of the SRA were not available in a datasheet and were also not available upon request at Canon.

Table 3.1: Measurement spot sizes of the micro-TRI-gloss and the IQ-S depending on the angle of measurement. For the SRA, no information on the measurement spot sizes was available.

Angle θ	micro-TRI-gloss	IQ-S	SRA
20°	10 mm x 10 mm	6 mm x 6.4 mm	?
60°	9 mm x 15 mm	9 mm x 13.5 mm	?
85°	5 mm x 38 mm	4.4 mm x 44 mm	?

All of the three instruments can measure specular gloss at the angles of 20°, 60° and 85°. At these angles, the micro-TRI-gloss utilizes photodiodes on the receptor side, enabling it to measure a single specular gloss value for each angle as explained in Section 2.3.1. For the IQ-S, photodiodes are only installed at the receptor angles of 60° and 85°. At 20° the IQ-S is equipped with a 512-element linear diode array that measures the light distribution. The linear diode array is in the plane of measurement. At the angles of 20° and 60° on the receptor side, the SRA is equipped with area sensors rather than photodiodes. These also measure the light distribution around the specular angles. That means that for gloss measurements at 20°, the IQ-S outputs in a 1D-BRDF (explained in Section 2.3.4), while the measurement of the SRA at the angles of 20° and 60° outputs 2D-BRDF data. Based on these BRDF data, gloss values such as specular gloss, DOI, or haze can be internally calculated by the instruments.

The measurement range for specular gloss of the micro-TRI-gloss is specified as 0-2000 GU for measurements at 20°, 0-1000 GU for the measurement at 60° and 0-160 GU for the measurement at 85°. The measurement range for specular gloss of the IQ-S is specified as 0-2000 GU for the measurement at 20°, 0-1000 GU for the measurement at 60° and 0-199 GU for the measurement at 85°. The measurement range of the SRA is 0-2000 GU for measurements at 20°. More specifications on the range of specular gloss measured at 60° and 85° could not be found.

Before conducting measurements for this study, it was necessary to decide on a number of measurements per sample. Most publications in which the measurement of gloss plays a role mention up to five measurements per sample. With these five measurements, average values are calculated (Leloup et al. 2016; Bertholdt and Müller 2014; Mirjalili et al. 2014; Mirjalili et al. 2016). In studies that utilize the highest number of measurements on samples, ten gloss measurements are made per sample (Wang et al. 2017; Yong et al. 2020). In many studies in which gloss measurement plays a role, the number of

measurements is not reported. As will be demonstrated later in this section, deviations in measurements can be high, particularly for printed metallized specimens with high gloss. This influenced the decision to conduct ten measurements on each sample. The procedure used for carrying out these ten gloss measurements, unless specified otherwise, is depicted in Figure 3.2. For all gloss measurements, a sheet of maxi offset paper with a gramature of 80 g/m² (IGEPA, Germany) was placed between the specimen and the table.

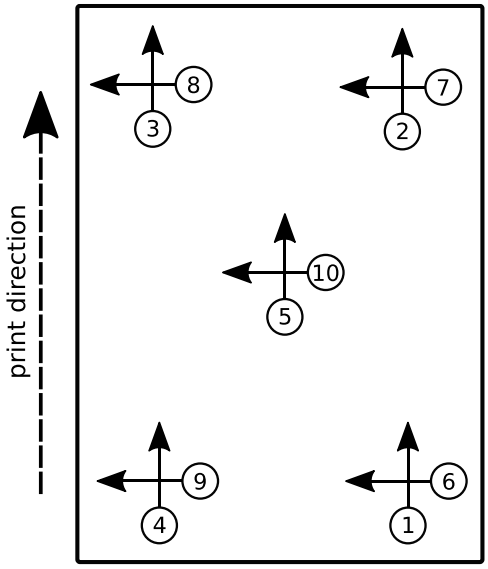

Figure 3.2: Scheme of the ten measurements made on each print sample if not described differently. Five measurements were made in print direction. One of them on each corner of the print sample and one in the middle. Then five measurements at the same position were made across print direction.

Measurements were taken on four printed metallized samples, which are shown in Figure 3.3. Based on these measurements it is exemplary shown what kind of measurement values can be obtained using the three gloss meters. The four samples were metallized using four different printing methods. Sample 1 (provided by Heidelberger Druckmaschinen, Germany) was metallized by foil fusing. Small ripples on the surface can be seen by looking at the small distortions of the reflected checkerboard pattern. Sample 2 (provided by H. C. Moog, Germany) was metallized by gravure printing. Sample 3 (provided by Heidelberger Druckmaschinen, Germany) was metallized by flexo printing and Sample 4 (provided by Heidelberger Druckmaschinen, Germany) was metallized by offset printing.

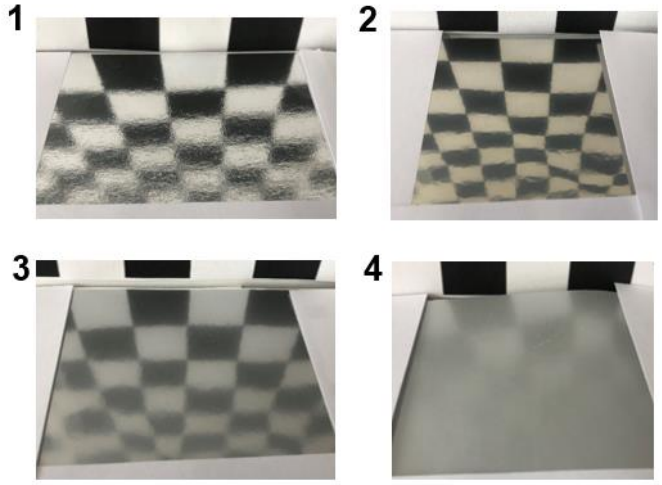

Figure 3.3: Used printed metallic samples. Sample 1 was made by foil fusing, Sample 2 by gravure printing, Sample 3 by flexo printing and Sample 4 by offset printing. The pictures were taken in front of a checkerboard pattern with fields of 27 x 27 mm² to convey an impression of the reflectiveness and texture of the samples.

Table 3.2 shows the specular gloss values measured with the micro-Tri-gloss on the samples shown in Figure 3.3. The specular gloss measurements at 20° and 60° show a clear ranking. The measured specular gloss at these angles of Sample 1 is the highest, Sample 2 follows, Sample 3 is on penultimate specular gloss level, while Sample 4 has the lowest specular gloss. Even if specular gloss measured at 85° is not very relevant for comparing samples of high gloss, it is interesting to note that the ranking according to this measurement value is different. It is likely that the texture of Sample 1 results in a high degree of shadowing and scattering when measured at this low angle, leading to a lower specular gloss value at 85° compared to Sample 2.

Table 3.2: Measured specular gloss of the four samples at the angles of 20°, 60° and 85° using the micro-TRI-gloss and standard deviation (ten measurements). GlossXX denotes specular gloss measured at an angle of XX. The sample numbers 1 to 4 correspond to the samples depicted in Figure 3.3.

Sample number	1	2	3	4
Gloss20 in GU	570 ± 49	525 ± 16	185 ± 8	12 ± 1
Gloss60 in GU	515 ± 32	495 ± 3	258 ± 4	53 ± 2
Gloss85 in GU	93 ± 1	134 ± 1	92 ± 1	67 ± 1

Gloss measurement results obtained on the four samples using the IQ-S are shown in Table 3.3. The specular gloss values differ from those measured with the micro-TRI-gloss.

Especially the specular gloss values measured at 20° are higher. The haze was determined according to the standard ASTM E430 - 11 (reapproved 2011).

It stands out that Sample 2 and Sample 3 almost have the same measured haze, although their appearance in terms of 'milky-ness' differs clearly as can be seen in Figure 3.3. A reason for this is that haze, differently to DOI, is not independent of the total amount of reflected light flux or specular gloss, respectively. This means that samples of higher specular gloss tend to have a higher haze. It stands out, that the haze value of Sample 1 is extremely high. This high haze value is measured because Sample 1 both has a high specular gloss and is more textured, what leads to high light scattering. It is questionable whether haze is applicable for Sample 4 since it has a very low visible and measureable DOI. When having a closer look on DOI, it is noticeable that Sample 2 reaches the highest DOI value what corresponds well to the comparably clear reflection of the checkerboard pattern shown in Figure 3.3.

Table 3.3: Different aspects of gloss of the four samples at the angles of 20°, 60° and 85° using the IQ-S gloss meter and the respective standard deviations. The values and standard deviations were derived by taken the average of ten measurements at different point in machine and across machine direction. GlossXX denotes specular gloss measured at an angle of XX. The sample numbers 1 to 4 correspond to the samples depicted in Figure 3.3.

Sample number	1	2	3	4
Gloss20 in GU	687 ± 89	627 ± 28	233 ± 24	17 ± 1
Gloss60 in GU	563 ± 38	535 ± 5	261 ± 9	53 ± 2
Gloss85 in GU	83 ± 4	122 ± 2	77 ± 5	57 ± 2
haze in HU	522 ± 51	162 ± 5	159 ± 10	22 ± 2
DOI in %	21 ± 2	51 ± 9	21 ± 1	1 ± 1
RIQ in %	4 ± 1	29 ± 8	4 ± 1	1 ± 1
Rspec in GU	109 ± 17	176 ± 35	37 ± 4	3 ± 0

The value Reflected Image Quality (RIQ) is a proprietary value specific to Rhopoint Instruments. Its calculation method has not been made publicly available. Rhopoint Instruments describes it as an updated version of DOI and a new parameter that gives higher resolution results than the DOI (Rhopoint Instruments n.d.). As the DOI, the RIQ also has the range of 0-100 %. Even if this value is interesting for car manufacturers who deal with surfaces with very sharp reflectance, it is not a very good measure for printed samples because for those it predominantly reports low values that lack differentiation.

Furthermore, pretests showed that the relative standard deviation of RIQ values measured on metallized printed samples can be high.

The Rspec value, ranging from 0-2000 GU, corresponds to the pixel of the linear diode array at 20° that registers the highest value. This corresponds to the peak of the reflection curve of the 1D-BRDF obtained with the IQ-S. If using high gloss samples and smooth surfaces, the deviation of the Rspec from specular gloss measured at 20° can indicate texture or give an indication of microstructures in the material. However, as shown by Rich et al. (2017) and Radermacher (2016), the correlation between Rspec and specular gloss measured at 20° is high and does not necessarily give an added value. The Pearson correlation of the specular gloss measured at 20° with the IQ-S and the Rspec values is $r = 0.9990$ for measurements on the 48 samples presented in Section 3.4.

A look at the 1D-BRDF curves in Figure 3.4, measured with the IQ-S, shows why the haze of Sample 2 and Sample 3 is very similar. As shown in Equation 2.1, haze calculated following ASTM E430 - 11 (reapproved 2011) depends on the measurement at about 2° away from the specular reflection angle of 20°. Since in this area, the reflectance curves of Sample 2 and Sample 3 are almost on top of each other, the measured haze is also very similar.

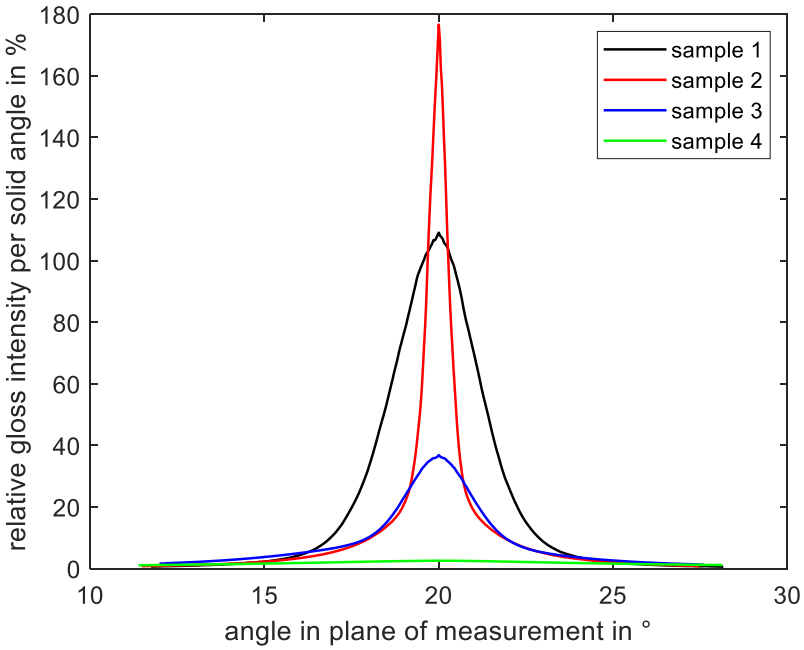

Figure 3.4: 1D-BRDF measured on the four samples using the IQ-S gloss meter. Every curve shows the average of ten measurements. The ten 1D-BRDFs obtained from every sample were offset so that the respective maxima are on top of each other. The maxima of the curves correspond to the Rspec values in Table 2.2. The sample numbers 1 to 4 correspond to the samples depicted in Figure 3.3. The plane of measurement is diagramed in Figure 2.1. The relative gloss intensities are related to the maximum intensity measured on the black glass calibration tile.

Table 3.4 shows the measurement values obtained using the SRA. The order of the samples according to specular gloss is consistent with both the IQ-S and the micro-TRI-gloss measurements. The haze value of Sample 1 is much lower than the one measured with the IQ-S. However, it was realized that no haze values higher than 300 HU are measureable using the SRA. The IC values are derived from the data obtained with the sensor matrix at 20° and 60°, but the manufacturer does not provide specific information about the calculation method. It is conceivable that the digits that belong to IC (0.25 to 2.0) stand for the width of the optical comb that was originally used for IC measurement as described in Section 2.3.2. A higher number stands for a greater width while a smaller number stands for a finer comb. IC 2.0 would be the best to compare the samples because for the other IC values measurements on Sample 4 result in a value of zero. The magnitude of the measured IC 2.0 values are comparable with the DOI values measured with the IQ-S.

Table 3.4: Measured aspects of gloss of the four samples at the angles of 20°, 60° and 85° using the SRA gloss meter. The values and standard deviations were derived by taken the average of ten measurements at different point in machine and across machine direction. GlossXX denotes specular gloss measured at an angle of XX. The sample numbers 1 to 4 correspond to the samples depicted in Figure 3.3.

Sample number	1	2	3	4
Gloss20 in GU	641 ± 63	545 ± 41	199 ± 5	12 ± 0
Gloss60 in GU	542 ± 36	497 ± 10	271 ± 5	58 ± 2
Gloss85 in GU	97 ± 2	133 ± 0	90 ± 1	61 ± 6
haze in HU	300 ± 0	206 ± 20	178 ± 7	30 ± 1
IC 0.25 in %	0.0 ± 0.0	3.1 ± 2.3	0.0 ± 0.0	0.0 ± 0.0
IC 0.5 in %	0.0 ± 0.0	4.6 ± 2.2	0.0 ± 0.0	0.0 ± 0.0
IC 1.0 in %	0.7 ± 0.7	23.8 ± 4.1	3.5 ± 0.3	0.0 ± 0.0
IC 2.0 in %	16.9 ± 3.5	58.5 ± 3.7	28.4 ± 0.7	1.7 ± 0.7
C20	69 ± 16	19 ± 6	65 ± 1	260 ± 9
C60	80 ± 11	14 ± 3	52 ± 1	173 ± 5

C20 and C60 are described as scattering values that encompass the measured of DOI and IC while having a higher sensitivity for finishes with low gloss (Canon n.d.). While C20 is calculated from the 2D-BRDF data captured at 20°, C60 is calculated from the 2D-BRDF data captured at 60°. They have a range from 0 to 1000. Low scattering values represent low scattering of light while high scattering values are measureable on matte samples. No information is given about how these values are obtained. However, they refer to the shape of the measured BRDF. It is described that the C20 value can be a substitute for the standard ASTM D5767 (method A) and C60 can be a substitute for the IC measurement described in ASTM D5767 (method B) and JIS K7374 (Canon n.d.). The 2D-BRDF shapes measured on the four samples using the SRA are shown in Figure 3.5.

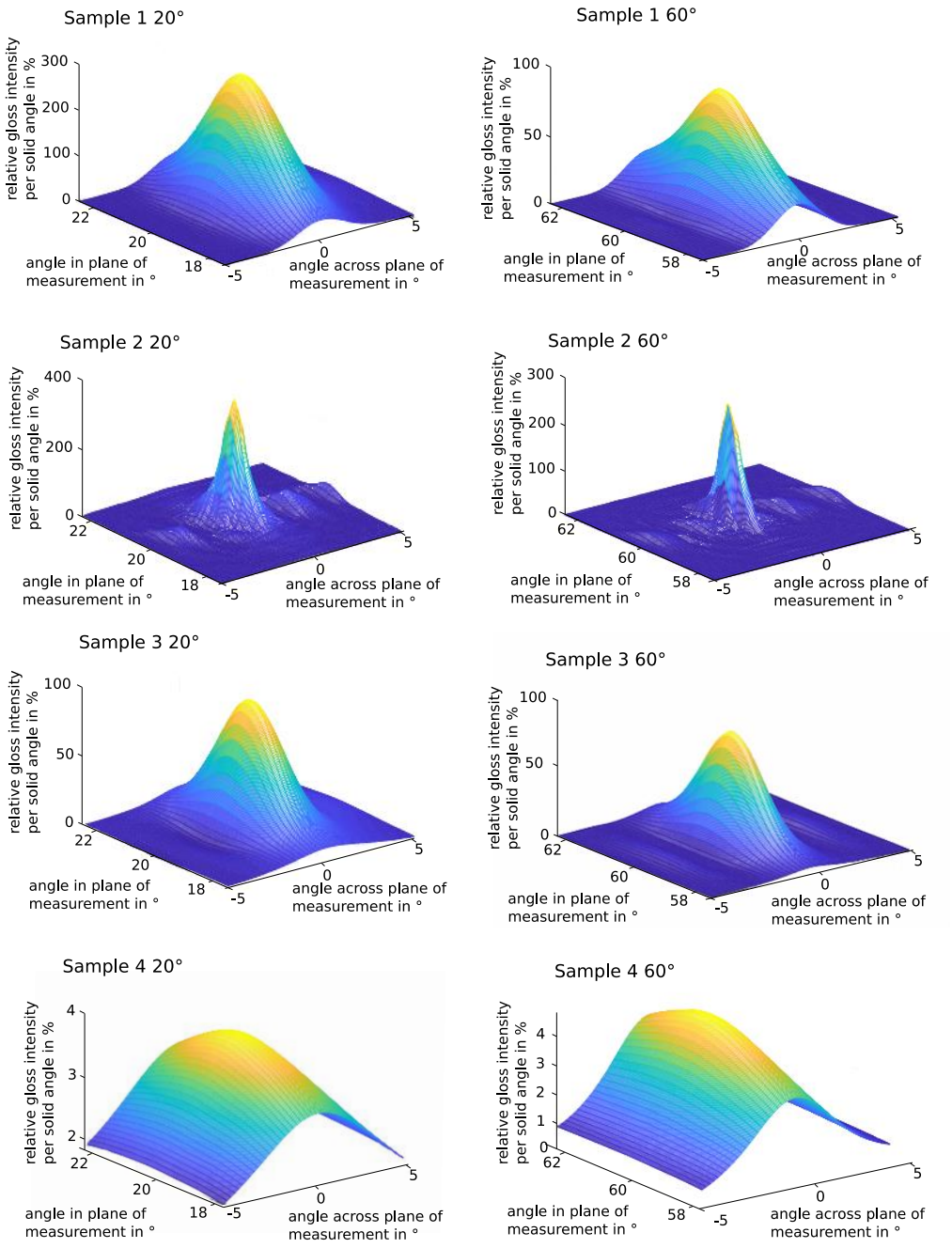

Figure 3.5: 2D-BRDFs measured at the specular angles of 20° and 60° using the SRA gloss meter. Every image shows the average of ten measurements. It can be seen that the more diffuse the reflection the wider the peak. The maximum of the z-axis varies between the plots. The sample numbers 1 to 4 correspond to the samples depicted in Figure 3.3. The plane of measurement is diagramed in Figure 2.1. The relative gloss intensities are related to the maximum intensity of the black glass calibration tile.

As a result of this first comparison of the three gloss meters it can be determined that all three gloss meters measure specular gloss at 20°, 60° and 85°. However, the measurement results seem to differ depending on the gloss meter used. For the reason that the IQ-S and

SRA also acquire the 1D- or 2D-BRDFs, it is possible to obtain more values that give indications on the reflection properties of measured samples. Some of the acquired values are device specific, rendering direct comparisons challenging. The added benefit of these values for the analysis of printed metallic samples is not obvious.

3.3 Continuous gloss measurement

It was determined what measurement deviation could be expected from multiple consecutive measurements. To do so, the three gloss meters were calibrated on their device specific calibration tile (for this test the IQ-S was calibrated on the black glass calibration tile) and the three specular gloss calibration values were recorded. Afterwards, 500 measurements were triggered manually as fast as possible on a sheet of maxi offset paper from IGEPA with a gramature of 80 g/m^2. Every 100th measurement was triggered on the device specific black calibration tile and the deviation from the initial calibration value was recorded. The results shown in Table 3.5 reveal that the micro-TRI-gloss is the gloss meter with the lowest deviation of under 1 GU. Both IQ-S and SRA deviate more than 2 GU from the initial calibration value for measurements of specular gloss at 20°. As mentioned by Hanson (2006), an explanation for these deviations is that components get warm, which causes the measurements to shift. This assumption is supported by the final measurements on the device specific calibration tiles after 24 hours with the micro-TRI-gloss and the IQ-S. These are much closer to the initial calibration values. The final measurement could not be taken with the SRA since this device requires recalibration every time it is turned on.

Table 3.5: After an initial calibration (the calibration values written in bold, given in GU) 500 measurements were triggered as fast as possible using the gloss meters micro-TRI-gloss, IQ-S, and SRA. Every 100th measurement was made on the device specific calibration tiles and the deviation from the initial calibration value was recorded (deviations in GU are written in italics).

Number of measurement	micro-TRI-gloss			IQ-S			SRA		
	20°	60°	85°	20°	60°	85°	20°	60°	85°
1st and calibration value	**92.9**	**95.4**	**99.3**	**104.0**	**101.6**	**99.8**	**86.9**	**93.3**	**99.4**
100th	*-0.1*	*-0.1*	*0.0*	*1.1*	*0.3*	*0.7*	*-0.9*	*-0.4*	*-0.8*
200th	*-0.4*	*-0.2*	*-0.1*	*1.9*	*0.5*	*1.0*	*-1.3*	*-0.7*	*-1.3*
300th	*-0.3*	*-0.2*	*-0.4*	*2.5*	*0.6*	*1.1*	*-1.7*	*-1.0*	*-1.5*
400th	*-0.1*	*-0.1*	*-0.4*	*3.1*	*0.6*	*0.7*	*-1.9*	*-1.1*	*-1.7*
500th	*-0.9*	*-0.1*	*-0.7*	*3.4*	*0.6*	*0.7*	*-2.1*	*-1.4*	*-1.8*
Measurement after 24 h	*-0.3*	*-0.1*	*-0.6*	*-0.2*	*-0.4*	*-0.5*	Not ascertainable		

The time for one measurement using the micro-TRI-gloss took less than one second. Using the IQ-S, one measurement took about 3.5 seconds at the beginning of the measurement series. However, it could be noticed that the time for one measurement took longer as more measurements were made. After 500 measurements, one measurement took about eight seconds. A reason for this could be that the device internally saves the measurements in a CSV file and calculates the statistics of a series of measurements. The time required for measurements with the SRA consistently averaged about 3.5 seconds. Nevertheless, during other measurement trials, it was observed that this gloss meter occasionally encountered periods of unresponsiveness during extended measurement sessions, only resuming normal operation after a few minutes.

3.4 Gloss on samples from an industrial print test

Measurements on a set of 48 printed metallic samples, which were provided by Heidelberger Druckmaschinen, were made using the three gloss meters introduced in Section 3.2. An impression of the kind of samples measured on is given in Figure 3.6. The samples were printed using a Heidelberg XL 75 Anicolor printing machine (Heidelberger Druckmaschinen, Germany). 35 of the samples were metallized using a flexo printing unit of the machine with UV-ink containing aluminum pigments. 13 were metallized through an offset printing unit employing UV-ink with aluminum pigments. 25 samples were printed on LumiArt paper, nine samples were printed on Chromolux paper and 14 on GD2

cardboard. LumiArt paper is a wood-free, multicoated illustration printing paper used, for example, for art books or brochures (PremierPaper 2017). Chromolux paper is a one-side cast coated paper of high gloss. It is, for instance, used to produce packaging of exclusive products (PaperSpecs n.d.). GD2 cardboard is a one-side coated duplex cardboard, which is commonly used for the production of standard packaging (Harder 2023). Information on the exact print settings cannot be published due to confidentiality agreements with Heidelberger Druckmaschinen.

Figure 3.6: Impression of three of the 48 samples. Pictures were taken in front of a checkerboard.

In terms of specular gloss, the IQ-S and SRA were compared to the micro-TRI-gloss, as the latter is the most well-known instrument in the industry among the three. Other gloss values, such as DOI, IC, or haze, were compared by utilizing the measurement results obtained from the IQ-S and SRA.

Comparison of measured specular gloss

Figure 3.7 shows the comparison of specular gloss measurement results between the micro-TRI-gloss and IQ-S. Every data point corresponds to the average of ten measurements on one of the 48 samples. A systematic deviation between the specular gloss measurements is evident when taken at 20° and 85° (Weber et al. 2021a). However, specular gloss measurements at 60° differ only slightly. The statistical deviation between the specular gloss values measured at 20° seems to increase with higher specular gloss values.

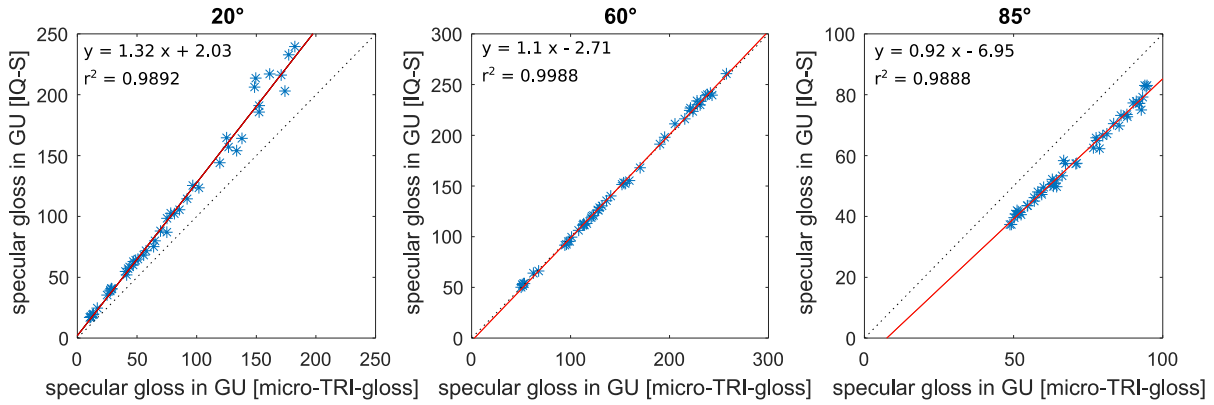

Figure 3.7: Comparison of specular gloss measured with the gloss meters micro-TRI-gloss and IQ-S at 20°, 60°, and 85°. Every data point shows the mean of ten gloss measurements. The red line is the regression line. Its function as well as the coefficient of determination is given. The black dotted line shows the 1st median. Note that the axes differ in scale.

Figure 3.8 shows the comparison of specular gloss measurement results between the micro-TRI-gloss and the SRA. The systematic deviation of the SRA from the micro-TRI-gloss is lower compared to the IQ-S. The statistical deviation of the specular gloss measured at 20° on the individual samples increases as the measured specular gloss values increase. This trend suggests that higher specular gloss values measured at 20° are more prone to exhibit greater variability in the measurements.

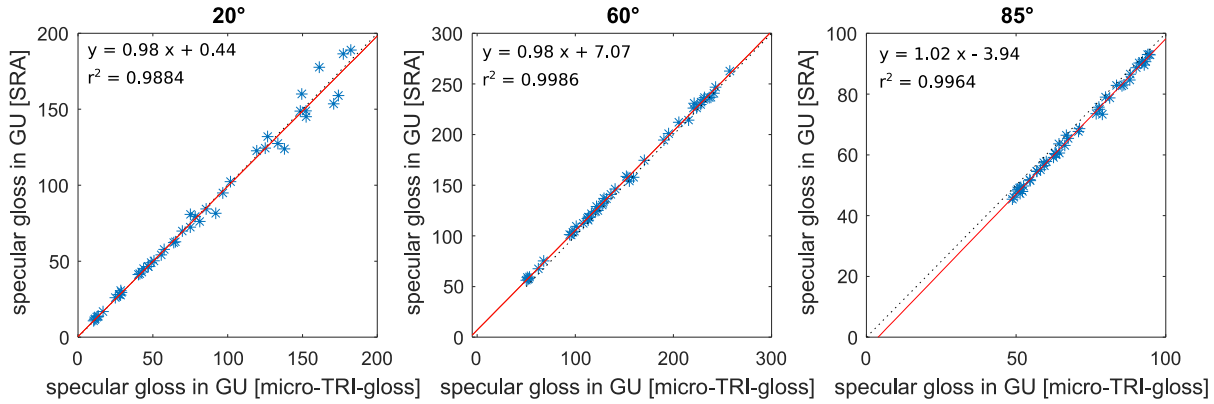

Figure 3.8: Comparison of specular gloss measured with the gloss meters micro-TRI-gloss and SRA at 20°, 60° and 85°. Every data point shows the mean of ten gloss measurements. The red line is the regression line. Its function as well as the coefficient of determination is given. The black dotted line shows the 1st median. Note that the axes differ in scale.

The average of the relative standard deviations calculated from the ten measurements on every sample of all specular gloss values measured at 20°, 60°, and 85° with the micro-TRI-gloss, the IQ-S, and the SRA are shown in Table 3.6. It can be seen that the relative standard deviations of the specular gloss measurements at 20° are generally higher than

those at 60° and 85°. As shown in Figure 3.9, the relative standard deviation for specular gloss measurements at 20° increases with higher average specular gloss values of the samples. This explains why the deviation from the regression line for specular gloss measurements at 20° get higher as the samples have a higher gloss as can be seen in Figure 3.7 and Figure 3.8. This trend of increasing relative standard deviations with increasing gloss values is not applicable to specular gloss measurements at 60° and 85°.

Table 3.6: Relative standard deviations of the measurements of specular gloss at 20°, 60° and 85° obtained with the micro-TRI-gloss, IQ-S and SRA. Measurements were taken on 48 offset and flexo printed metallic samples.

Measurement angle	20°	60°	85°
micro-TRI-gloss average of all relative standard deviations	6.2 %	3.3 %	2.6 %
IQ-S average of all relative standard deviations	7.4 %	3.8 %	3.7 %
SRA average of all relative standard deviations	6.7 %	3.7 %	3.4 %

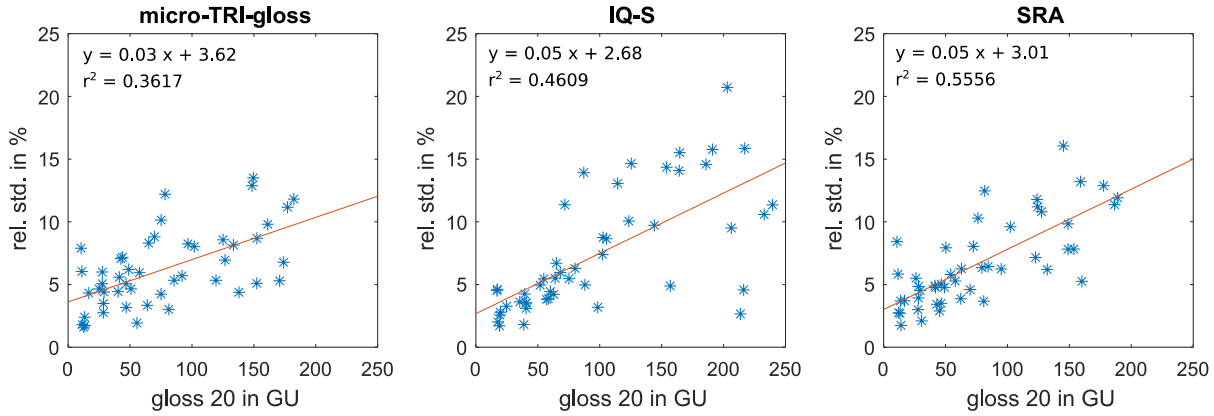

Figure 3.9: Relative standard deviations of the measurements with the three gloss meters vs. the mean gloss value of the respective ten measurements on every sample. The specular gloss values on the x-axis show the mean of ten measurements. The relative standard deviations were calculated from these ten measurements. The red line is the regression line. Its function as well as the coefficient of determination is given.

The higher relative standard deviations for measurements of specular gloss at 20° can be ascribed to the small receiver aperture at this angle. This smaller aperture makes gloss measurements more sensitive to minor unevenness on the measured surface. This effect is pronounced when the measured surface exhibits high gloss and when surface irregularities increase light scattering, either allowing reflected light to reach the sensor or preventing its reach. As the small deviations in gloss measurements on the calibration tiles shown in Table 2.3 indicate, the primary source of deviations in specular gloss

measurements can be attributed to the unevenness of the paper surface and variations in gloss resulting from an uneven distribution of the ink through the print process.

Research on specular gloss of galvanized chrome surfaces using a micro-TRI-gloss by Heinzler (2020) suggests that the high relative standard deviations for printed paper surfaces is higher due to surface unevenness and deviations in the printing process. For the galvanized chrome surfaces, an average relative standard deviation of only 0.4 % for specular gloss measurements at 20° using a micro-TRI-gloss were reported.

Systematic deviations of specular gloss measurements have been subject of research in earlier studies. Arney et al. (2006) reported on different aperture sizes of gloss meters from different companies. According to Frankhuizen (2015), variations of aperture sizes of up to 30 % between gloss meters from different manufacturers can be observed. Systematic deviations between the gloss meters could also have their root in differences between the calibration tiles. Black glass standards can differ in roughness and in the distribution of black pigments on the glass (Fensterseifer, Byk Gardner 2021; Frankhuizen 2015). The calibration on the black glass standard of the SRA and the micro-TRI-gloss and the calibration on the high gloss calibration tile of the IQ-S adds a further deviation. Especially the high systematic differences between specular gloss values measured at 20° and 85° with IQ-S and the micro-TRI-gloss stand out. In order to exclude a malfunction of the IQ-S, measurements were compared with an IQ-S from FOGRA (Germany); it was checked by the customer support of Konica Minolta and compared with an IQ gloss meter at KU Leuven (Belgium). These examinations did not provide any evidence of a malfunction of the IQ-S.

A further difference between the gloss meters could be the LEDs. If the spectra of different gloss meters do not match, also gloss measurement results can differ between the instruments (Burrows 2021). Due to the only very short light flash of the gloss meters it was not possible to measure the spectra of the IQ-S and micro-TRI-gloss. Only the spectrum of the SRA could be recorded using a CAS140CT spectrometer (Instrument Systems, Germany) at the Institute of Adaptive Lighting Systems and Visual Processing at the TU Darmstadt. It is shown in Appendix 1. A further difference between the gloss meters is that the IQ-S and the SRA are equipped with sensor matrices at the receiver for measurements at 20°, while the micro-TRI-gloss uses a photodiode. These distinct sensor types can potentially lead to different measurement results. However, the exact influence of these different sensors on the measurement results is not known to the author. Last,

the differences in the size of the measurement spots can influence gloss measurement results and are likely one of the reasons for the differences of relative standard deviation in the measurements between the gloss meters.

Comparison of measured haze and DOI with C20

A comparison of haze values and DOI with C20 values was conducted using data obtained with the IQ-S and SRA. Figure 3.10 (left) shows the comparison of haze measurements between the IQ-S and SRA. Interestingly, the haze measurements of these two gloss meters match well, even though the specular gloss values measured at 20° show systematic deviations. For both gloss meters, no dependencies between the height of the measured haze value and the relative standard deviation of the measured haze values of a sample could be found. For the IQ-S, the average relative standard deviation of the measured haze values is 4.7 %. The maximum relative standard deviation for one sample is 8.1 %. For the SRA the average relative standard deviation of the measured haze values is 4.4 %. The maximum relative standard deviation for one sample is 9.1 %.

Figure 3.10 (right) shows the comparison of DOI measured with the IQ-S and the scattering value C20 measured with the SRA. It is noticeable that the DOI values can be differentiated into three regimes. One that includes all DOI values under a DOI of 2 %, one that includes all DOI values from 8 % to 15 %, and one that includes DOI values above 15 %. When analyzing these three regimes, it was found that all samples with an average DOI of under 2 % were printed in the offset printing unit. While the DOI does not provide a clear differentiation for these matte samples, the C20 value offers better distinguishability. All samples with a DOI of over 8 % to 15 % were printed in the flexo printing unit on GD2 or on LumiArt with a rasterized printing plate. Those above 15 % were printed in the flexo printing unit on LumiArt or GD2 without rasterization of the printing plate. For the C20 value, such kind of segmentation is not visible in the plotted data. DOI and the C20 value are therefore influenced differentially by the choice of the printing method and substrate sort.

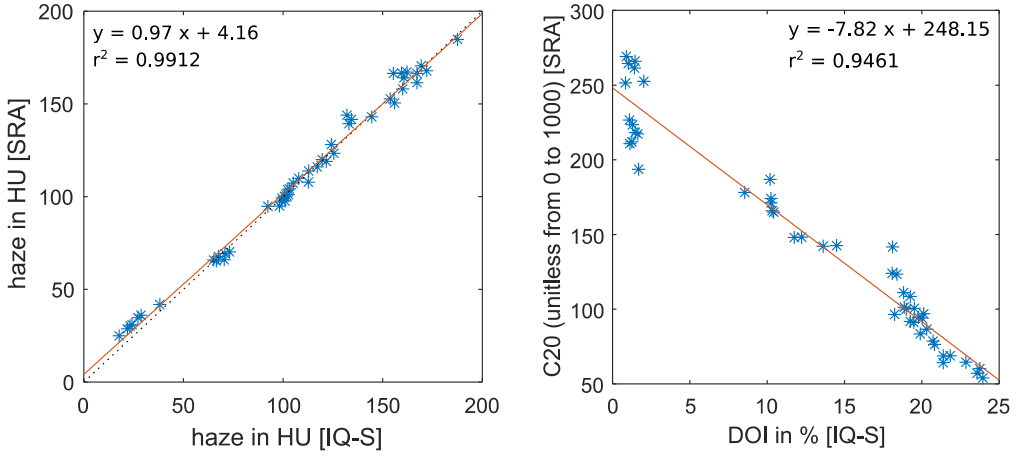

Figure 3.10: Left: Comparison of haze measured with the gloss meters IQ-S and SRA. Right: Comparison of the DOI measured with the IQ-S and the scattering value C20 measured with the SRA. Every data point shows the mean of ten gloss measurements. The red line is the regression line. Its function as well as the coefficient of determination is given.

Further, standard deviations of DOI measurements obtained with the IQ-S and C20 measurements obtained with the SRA were compared. In the left plot of Figure 3.11, it can be seen that measurements on samples with a low DOI (low sharpness of the reflected image) tend to result in a higher relative standard deviation. In the right image it can be seen that measurements on samples with a low C20 (higher sharpness of the reflected image) by tendency result in a higher relative standard deviation. This means that for the evaluation of DOI of surfaces with high gloss and a high sharpness of the reflected image, the IQ-S seems to be preferable over the SRA.

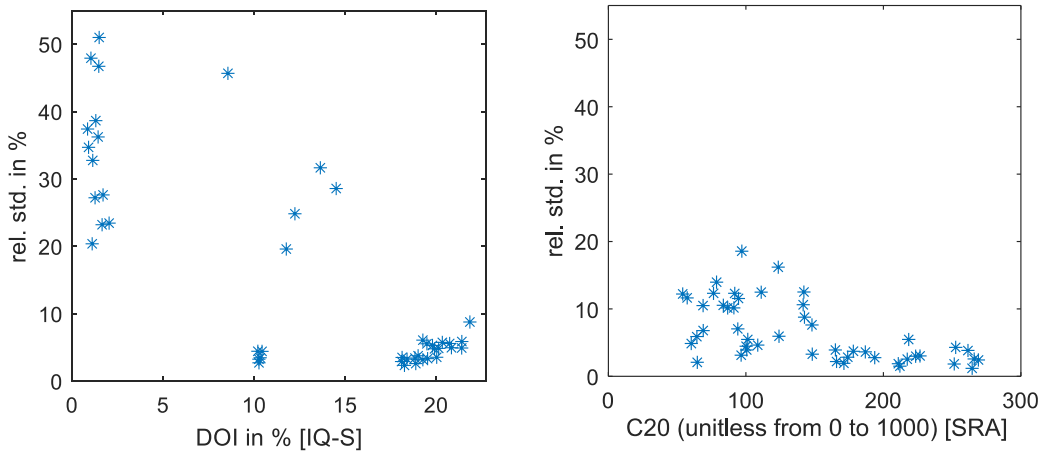

Figure 3.11: DOI measured with the IQ-S and C20 measured with the SRA vs. the relative standard deviations of the measurements. The higher the mirroring capability of a surface, the higher the DOI, and the lower the C20 value. The DOI or C20 values on the x-axis show the mean of ten measurements. The relative standard deviations were calculated from these ten measurements.

In conclusion, it can be stated that especially specular gloss measurements at 20° differ between the IQ-S and the micro-TRI-gloss. The high deviations of the measurements on metallized printed samples are not caused by inaccuracies of the gloss meters but by the texture of the substrates and an uneven distribution of the ink through the print process.

3.5 Decision on gloss meters for further experiments

In Section 3.1, four criteria for gloss meters used in research on printed metallic surfaces in this dissertation were stated. All of the three gloss meters meet the criteria of portability. None of the three gloss meters demonstrated restrictions in their specular gloss measurement range. However, it was found that the SRA has a limitation in terms of the haze measurement range, which is capped at 300 HU. The IQ-S and the SRA report more gloss values than only specular gloss due to their capability to measure a partial BRDF. Some of these values could provide valuable insights into surface properties and may offer additional information on how the surface gloss is perceived. The fourth criteria, which is the acceptance of the gloss meters in science and industry is discussed in the following.

The micro-TRI-gloss or the micro-gloss 60° (Byk-Gardner, Germany), which only measures specular gloss at 60°, is a standard gloss meter used in the printing industry or in many other industries that have a need for the characterization of surface gloss. In scientific research dealing with gloss measurements, the micro-TRI-gloss or the micro-gloss 60° that only measures specular gloss at 60° has been frequently used (Briones et al. 2006; Heinzler et al. 2020; Brumm et al. 2017; Samadzadegan et al. 2015; Aydemir et al. 2018; Ozcan et al. 2022). The IQ-S has been used in many industries including automotive and the paint industry. The main area of application of the IQ gloss meter series from Rhopoint is in the field of paints and coatings, with the automotive and yachting industries being the leading sectors (Dietz, Rhopoint Instruments 2023). The IQ gloss meters from Rhopoint, which are comparable to the IQ-S were used in several studies for different purposes. Rich et al. (2017) used the Rhopoint IQ to use the measured specular gloss measured at 20°, haze as well as the Rspec value to compare them with the visual assessment of gloss of printed metallic samples. Yang et al. (2022) used a Rhopoint IQ 20/60 gloss meter to assess the specular gloss and DOI of powder coatings. Mirjalili et al. (2014) used a Novo-Gloss IQ to measure specular gloss and DOI of automotive coatings. Radermacher (2016) used a Rhopoint IQ to evaluate and compare gloss of UV-lacquered and foil laminated cardboard. In this study, specular gloss measured at 20°, haze, DOI and the Rspec value were used

for the evaluation of the print samples. Beuckels et al. (2023) utilized measurements acquired with the Rhopoint IQ to compare DOI and haze data with visual assessments, and to compare the data with measurements obtained from an image-based gloss meter.

Studies could be found that evaluate gloss measurements in depth or compare them with gloss measurement results obtained with different gloss meters. Leloup et al. (2016) report on inter-instrument agreement between the specular gloss measurements of six gloss meters. Among them, a micro-TRI-gloss and a micro-TRI-gloss-S (Byk Gardner, Germany), an IQ Flex 20, and an IQ Trigloss (Rhopoint, UK) with which measurements on 25 samples with specular gloss values ranging between 2 GU and 110 GU (60° geometry) were conducted. It was shown that the average of five measurements of specular gloss of the different instruments varied considerably, while the best inter-instrumental agreements could be obtained for gloss meters developed by the same manufacturer. Herranz (2014) compared BRDF measurements obtained with the IQ gloss meter with BRDF data obtained with a laboratory Murakami GCMS-10x goniospectrophotometer. It was concluded that it is possible with the IQ gloss meter to correctly approximate the measurements of the high accuracy goniospectrophotometer. However, precision and accuracy limitations could be noticed for measurements on matte materials.

Compared to the micro-TRI-gloss and the IQ-S or similar gloss meters from the same manufacturers, published experimental data obtained with the SRA are scarce. Inoshita et al. (2018) showed measurement results of the SRA on print samples. Šarić et al. (2021) used the SRA to measure printed paper samples of different color and glossiness. The scattering values C20 and C60 were compared to perceived visual gloss. However, no convincing results could be found. Vazquez et al. (2021) utilized specular gloss data (20°, 60°, 85°) obtained using the SRA to evaluate the gloss of patches with UV-curable ink application. Golhin and Strandlie (2023) used the BRDF data obtained at 20° and 60° using the SRA to show the directionality of 3D-printed patches. Further, they used specular gloss values, haze as well as the scattering values C20 and C60 to show the influence of the thickness of 3D-printed layers as well as directionality.

It is noticeable that most gloss measurements of studies using data of the SRA were taken with a SRA from FOGRA, Germany by Šarić et. al. In the authors' experience, acquiring the gloss meter from Canon might not be straightforward, and there may be doubts about a widespread utilization of the SRA in the future. For samples with low gloss, the SRA would still remain a favorable device due to its capability to provide scattering values and

the BRDF. However, samples analyzed in this work have high gloss and the IQ gloss meters are more accepted in industry. Hence, it was decided to perform all non-dynamic measurements on metallic printed samples with the IQ-S. Mainly specular gloss measured at the angles of 20° and 60°, DOI and haze were used for the evaluation of the measurement results.

4 Printing experiments

After introducing key factors affecting gloss in the context of printing metallic inks, the focus is on flexo printing UV-inks containing aluminum pigments. The experiments on dynamic gloss are explained and discussed. Next, the gloss of printed UV-inks containing aluminum pigments, which were cured after different dwell times, is investigated. In the following, 'dwell time' refers to the time between printing and curing of UV-inks. The influence of hot air usage after printing on gloss is examined, and the pigment layer topographies of samples are analyzed and compared. Lastly, it is determined to which extent the results can be transferred to an industrial printing machine. Pretests for the experiments presented in this chapter were carried out in the course of student works by Wang (2021), Polat (2022) and Alhotary (2022), supervised by the author. Parts of the results of experiments on dynamic gloss and on pretests regarding the influence of hot air during dwell time were published previously by Weber et al. (2022a) and Weber et al. (2023).

4.1 Gloss influencing factors in printing

Gloss influencing factors for printing inks with aluminum pigments were determined through preliminary tests on both laboratory and industrial printing machines. Some of them were mentioned in Chapter 2. The gloss influencing factors can be broadly categorized into six groups, with an awareness that factors within these categories exhibit interdependencies.

a. Printing method: The choice of the printing method as for example gravure printing, flexo or offset printing, exerts huge impact on attainable gloss levels. Factors of other categories such as ink viscosity, pigment size, or printing speed are partially dependent on the printing method.
b. Printing machine: Regardless of the printing method, the choice of the printing machine can have impact on gloss. For instance, according to the authors' experience, sheet-fed flexo printing units tend to yield higher gloss than web-fed printing machines.
c. Substrate: Various properties such as smoothness, porosity, or additives affect the print quality and the gloss of the final print products. In addition, the use of a primer can have great influence on the gloss by affecting the roughness and porosity of a paper surface.

d. Pigment type: The choice of pigments used in the printing process influences the attainable gloss. For instance, the application of VMPs normally yields much higher gloss than silverdollar or cornflake pigments. Another critical factor is the behavior of these pigments in the ink layer after printing. Leafing type pigments float up to the top of the ink layer resulting in a higher gloss. If they are a non-leafing type, they stay relatively evenly distributed in the ink. The quantity of pigments in the ink also exerts a notable influence on gloss.
e. Inks system: Apart from UV-inks there are solvent-based, water-based or oil-based inks with aluminum pigments available. The type of ink system influences the ink viscosity and the drying process (curing in case of UV-inks).
f. Process parameters: A multitude of print parameters influence gloss. These parameters encompass factors such as printing speed, the hardness of the printing plate, and the application of heat to the printed ink film. In addition, the amount of ink printed on the substrate is a gloss-influencing factor. When using UV-inks with aluminum pigments, also the duration of the dwell time is a gloss-influencing factor.

4.2 Experiments on dynamic gloss – materials and method

This section describes the flexo print proofer used for the laboratory experiments, the substrates and the gloss meter used for the experiments on dynamic gloss of UV-inks containing aluminum pigments.

4.2.1 Flexo print proofer

The laboratory printing trials were carried out using an IGT F1 flexo print proofer (IGT Testing Systems, Netherlands). The actual machine can be seen in Figure 4.1. Figure 4.2 depicts a schematic of the flexo printing unit of the IGT F1. Compared to an industrial flexo unit, it is simpler.

Figure 4.1: IGT F1 flexo print proofer that was used for the experiments on dynamic gloss and for laboratory experiments on the influence of the duration of dwell time and hot air on gloss.

An interchangeable anilox roller and a doctor blade control the ink dosage. The ink for printing is applied manually onto the anilox roller with a spatula or pipette, depending on the ink viscosity. The doctor blade wipes the surplus ink from it to ensure that only ink is transferred further that is inside the cells of the anilox roller. From there, the ink is transferred to the printing plate and then further onto the substrate. The substrate is taped to a substrate support. Substrate and substrate support are transported through the printing nip. The motion is provided by the plate cylinder.

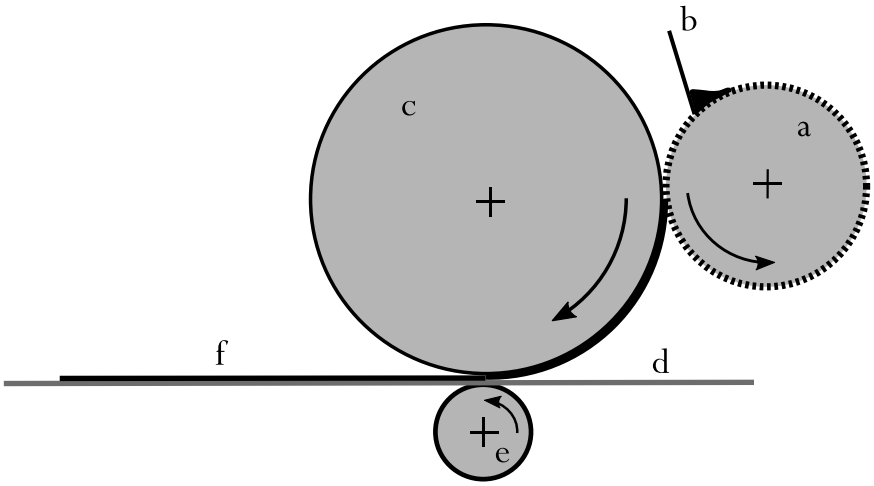

Figure 4.2: Schematic of the IGT F1 flexo print proofer after Ranfeld (2015) with a) anilox roller (⌀ 65 mm), b) doctor blade, c) plate cylinder with printing plate (⌀ 165 mm), d) substrate support, e) impression cylinder and f) printed ink on substrate

In detail, the printing process unfolds as follows: the operator initiates the print procedure by pressing two buttons positioned on both sides of the flexo print proofer. At this point, the plate cylinder rotates into its starting position, provided it is not already in that position. This step ensures consistent alignment of the printing plate for each trial.

Subsequently, the operator releases one of the buttons and then presses the same button again. Then the anilox roller engages with the plate cylinder. In this engaged state, the plate cylinder completes one full rotation, while the anilox roller simultaneously distributes ink onto the printing plate. Both the anilox roller and the plate cylinder come to a halt after this ink distribution. Following this, the impression cylinder ascends and presses firmly against the substrate support, which is clamped between the impression cylinder and the plate cylinder. All three rollers - plate cylinder, anilox roller, and impression cylinder - begin rotating. Consequently, the substrate moves horizontally as the cylinders rotate and ink is applied onto the moving substrate as it traverses along the rotating plate cylinder. The described printing process takes about 15 seconds.

Upon completion of the printing process, it becomes apparent that there are two distinct areas with slightly differing appearance on the printed substrate. On Area 1, spanning a length of 120 mm, only ink is printed that is transferred to the printing plate from the anilox roller during the initial rotation of the anilox roller, before engagement of the impression cylinder. The ink that can be found on Area 2 after printing was both transferred during the first turn of the impression cylinder and during the turning of printing cylinder and anilox roller during the actual printing process. The two different areas are diagramed in Figure 4.3.

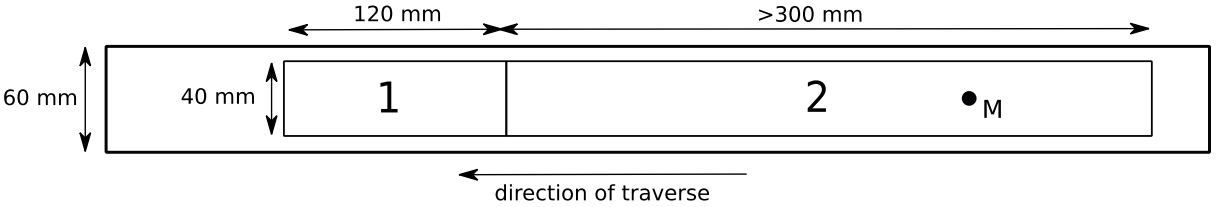

Figure 4.3: Schematic representation of two slightly different areas on the sample printout of the IGT F1. Area 1 and Area 2 are the areas where the ink is applied. Due to the special features of the printing process, Area 1 has a slightly different appearance than Area 2. Both areas have a width of 40 mm. The substrate printed on has a width of 60 mm. The point M indicates approximately the position at which the dynamic gloss measurements were carried out.

Differences between the IGT F1 and an industrial flexo printing unit have to be pointed out previously by Ranfeld (2015). Firstly, the IGT F1 lacks a continuous printing process and ink flow. Hence, especially when using water-based and solvent-based inks, the machine parts have to be cleaned after each printing trial to ensure reproducibility. Since UV-inks do not dry, it is not categorical necessary to clean all machine parts after each trial. However, in order to ensure a high reproducibility of the experiments, it was decided

to wipe the printing plate after each print trial. Secondly, the rollers and the printing cylinder only have single-sided bearings what can lead to a non-uniform distribution of the printing ink. Thirdly, the engagement between anilox roller and printing cylinder as well as between printing cylinder and impression cylinder is adjusted by the force applied between these components. In case of industrial printing machines however, the engagement is adjusted by distance control. Although the IGT F1 has the drawback of only imitating an industrial flexo printing unit, it offers the advantage of easy accessibility and requires only small amounts of ink and substrate for printing experiments. Further, the printed substrate is accessible with a gloss meter immediately after printing.

The print parameters used for the experiments on the IGT F1 are shown in Table 4.1. The anilox force, printing force and printing speed were chosen based on recommendations of the printing engineer at the IDD, TU Darmstadt and preliminary tests, during which small variations of the print parameters were made. The selection of anilox roller volumes was based on a large-scale industrial printing trial for which similar anilox roller volumes for the metallic ink and primer were used.

Table 4.1: Print parameters for printing experiments on the IGT F1 flexo print proofer.

Anilox force	60 N
Printing force	70 N
Printing speed	0.50 m/s
Anilox roller volume and ruling for printing metallic inks	16 ml/m^2, 90 lines/cm
Anilox roller volume and ruling for printing primer	8 ml/m^2, 180 lines/cm

4.2.2 Gloss meter

For the measurements of dynamic gloss, it is important to make continuous measurements. Further, the individual measurements should be initiated without physical contact with the gloss meter, as even small changes of the instrument's position can affect the gloss reading. The micro-TRI-gloss and the IQ-S provide the option of a continuous measurement mode. Both gloss meters were introduced in Chapter 3.

In continuous measurement mode, the micro-TRI-gloss triggers the individual measurements after time intervals that can be customized, ranging from zero to nine seconds in one-second increments. The actual measurement time is much shorter than one second. If the micro-TRI-gloss is used in continuous measurement mode, 100

measurements can be carried out in succession. For another 100 measurements, the device has to be manually triggered again. In continuous measurement mode, the IQ-S provides the option to automatically trigger measurements at time intervals of 2, 5, 10, 30 and 60 seconds between each measurement. However, the actual time required for a single measurement, as explained in Section 3.2, is a minimum of 3.5 seconds, and this duration increases, as more measurements are stored on the device. For that reason, rapid changes in gloss may not be captured using the IQ-S. Additionally, as demonstrated in Section 3.3, measurements obtained with the IQ-S exhibit greater deviations when continuously measured compared to those obtained with the micro-TRI-gloss. Considering these factors, it was decided to use the micro-TRI-gloss for dynamic gloss measurements, despite forgoing the increased depth of information provided with 1D-BRDF measurements and additional captured gloss parameters of the IQ-S. The measurement interval of the micro-TRI-gloss for continuous gloss measurements was set to one second.

To conduct measurements on dynamic gloss, the gloss meter had to be placed on the substrate with the wet ink film. In case of solvent-based or water-based inks, it would be reasonable to anticipate that the confined measuring space within the gloss meter affects the solvent atmosphere surrounding the ink film, and therefore influencing the change of gloss over time. However, using UV-inks, such influence was not expected since UV-inks are solvent-free.

4.2.3 Printing inks

Two UV-inks with different aluminum pigments were used both for the experiments on dynamic gloss and for investigating the influence of dwell time on gloss. Schlenk Metallic Pigments (Germany) provided both of them. The UV-ink containing cornflake pigments is referred to as 'UV-ink-corn' in the following. The UV-ink containing VMPs is referred to as 'UV-ink-VMP'. Both inks were low-migration inks what means that they were specifically designed to prevent ink components from migrating through printed packaging onto a product, such as required for food packaging. According to the datasheet provided by Schlenk Metallic Pigments, the VMPs in UV-ink-VMP have a d_{50} size of 7 µm and a d_{99} size of 10-12 µm and the ink has a metal content of 3 % w/w. The cornflake pigments in UV-ink-corn have a d_{50} size of 6 µm and a d_{99} size 11-12 µm. The metal content of the ink containing cornflake pigments is specified to 15 % w/w. according to Schlenk Metallic Pigments, the binders of UV-ink-corn and UV-ink-VMP differ. For reasons of confidentiality, no information could be provided on the binder formulation. To ensure

even distribution of the pigments in the ink, prior to commencing print trials of a day, the inks were stirred for five minutes.

The shear viscosity of the two inks was measured at shear rates ranging from 0.01 s^{-1} to 100 s^{-1} at temperatures of 25°C, 50°C, and 75°C. The measurements were carried out using a KINEXUX lab+ rheometer (Malvern Panalytical, UK). For the measurement, a plate-plate geometry with a diameter of 25 mm and a gap size of 1 mm was used. The results of the shear viscosity measurements are presented in Figure 4.4. It is evident that both inks have a shear-thinning behavior at all three temperatures tested. For UV-ink-corn, at a low shear rate of 0.1 s^{-1}, the difference in viscosity measured at the three different temperatures is less pronounced than for UV-ink-VMP. At a low shear rate of 0.1 s^{-1}, UV-ink-corn records mean viscosities of 15.0 Pa s at 25°C, 13.4 Pa s at 50°C and 12.1 Pa s at 75°C. UV-ink-VMP has greater variations in shear viscosity across the different temperatures with mean viscosities of 23.8 Pa s at 25°C, 19.9 Pa s at 50°C and 12.0 Pa s at 75°C at a shear rate of 0.1 s^{-1}. Differences in rheology between the two inks can be attributed to variations in the binder and additives as well as differences of the metal content.

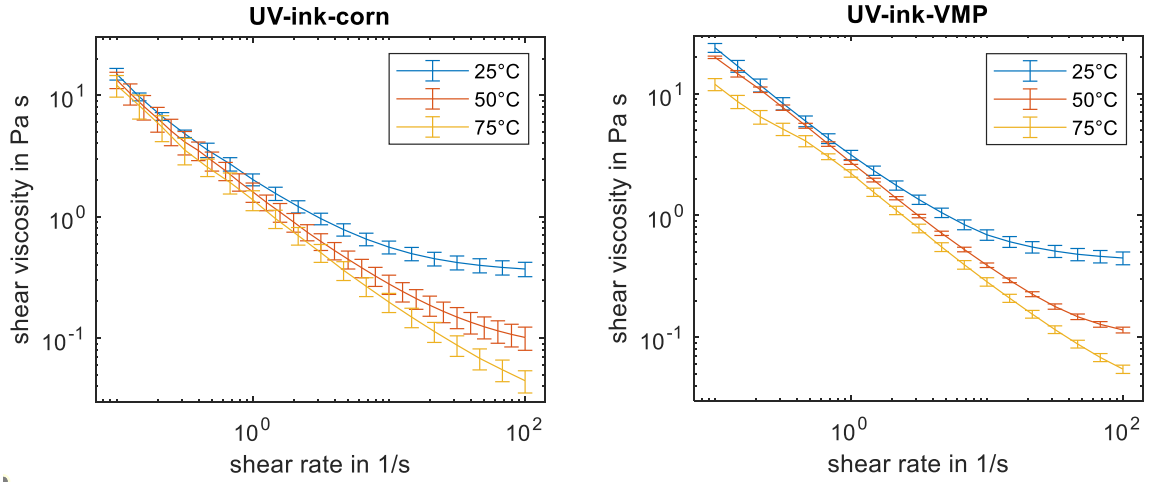

Figure 4.4.: Shear viscosity over shear rates at 25°, 50°, and 75° measured for the UV-ink containing cornflake pigments and VMPs with a KINEXUX lab+ rheometer. The shear viscosities of the inks were measured three times at each temperature. The whiskers on the data points indicate the spread of the standard deviation around the mean.

The primer that was preprinted on paper for the experiments on dynamic gloss was the UV-primer Nutriflex Primer varnish E46 (Siegwerk, Germany), which was recommended by Schlenk Metallic Pigments. It offers printability in a flexo printing unit and has a good over-printability. Further, it is a clear varnish and does not lead to a noticeable color shift.

4.2.4 Substrates

In printing, the word ‘substrate’ describes the material printed on (Kipphan 2000). Normally, this term is associated with paper or film. However, it is important to note that in this dissertation, the inks containing aluminum pigments were also printed on paper that had been primed previously. Therefore, in the following, also primed paper is referred to with the term ‘substrate’.

For the investigation of dynamic gloss, three different paper sorts were used. These were Chromolux paper with a grammage of 100 g/m² (Zanders - no longer in existence due to insolvency, Germany), Chromolux cardboard with a grammage of 400 g/m² (Zanders, Germany) and LumiArt paper with a grammage of 115 g/m² (Stora Enso Oyi, Finland). For one series of the experiment, LumiArt paper was primed and then printed with the metallic inks. Chromolux paper and Chromolux cardboard were not primed since these are very high quality paper substrates, for which primer would not be used in the printing industry, since it would rather impair the high quality of the paper surface. For the print trials, the fiber direction of the papers was across the print direction.

The water absorbency of the Chromolux cardboard, Chromolux paper, LumiArt paper and primed LumiArt paper was determined with the $Cobb_{60}$ test, after DIN EN ISO 535:2014 (reapproved 2014). In this test, a defined area of the paper is wetted with a defined amount of water for a period of 60 seconds. By determining the weight before and after wetting, the proportion of water absorbed can be determined. The test was performed on the side of the substrate that is printed on. That means that both Chromolux paper and Chromolux cardboard were tested on the cast-coated side and the water absorbency of primed LumiArt paper was tested on the primed surface. For unprimed LumiArt paper no differences between the two sides were discernible. This investigation was conducted in the course of the master thesis of Wang (2021), supervised by the author. The determined water absorbency values are shown in Table 4.2. It can be seen that the water absorbency of the LumiArt paper is the highest. Chromolux paper and Chromolux cardboard have a lower water absorbency since they are cast-coated substrates. The UV-primer has a great influence on the water absorbency of LumiArt paper as it reduces it by a factor of more than six. The water absorption capacity of the paper substrates can be used to draw qualitative conclusions about the binder absorption capacity of the paper. The higher the water absorption capacity, the higher the binder absorption capacity is likely to be.

Table 4.2: Results of the Cobb$_{60}$ water absorbency test after DIN EN ISO 535:2014 (reapproved 2014). The results shown are the average values and standard deviations of six measurements obtained from each substrate. (Wang 2021)

Substrate	Water absorbency
Chromolux cardboard	33.9 ± 4.4 g/m2
Chromolux paper	25.6 ± 0.7 g/m2
LumiArt paper	56.9 ± 3.1 g/m2
LumiArt paper with UV-primer	8.7 ± 1.6 g/m2

Using an Ash Content Analyzer (emtec Electronics, Germany) at the Institute for Paper Technology and Mechnical Process Engineering at the TU Darmstadt, the amount, and sort of fillers in the three different paper sorts was determined. This measurement instrument allows for non-destructive measurement of fillers in the top layers of a paper substrate.

Fillers like calcium carbonate ($CaCO_3$), kaolin, or titanium dioxide are commonly used as fillers in paper production. As stated by Blechschmidt (2010), reasons for their usage can be the enhancement of the surface properties for printing or improvement of optical properties (whiteness). Often, fillers are also used to improve the ratio of production cost per paper mass unit, as they are more cost-efficient per mass unit than fibers. For the Chromolux paper and Chromolux cardboard, two measurements were made on the cast coated side and one measurement on the non-coated side. For the LumiArt paper, no clear visual differences between both sides were perceptible. Hence, for LumiArt paper, two measurements on every side were made. The measurement results are shown in Table 4.3. The relative standard deviation of two measurements on one side of a substrate was less than 2 % for all paper sorts. The output data from the Ash Content Analyzer does not distinguish between kaolin and talcum as fillers. However, it is a reasonable assumption that talcum was not used in production of these paper sorts due to its relatively high cost and its rare use as a filler. Unclassifiable fillers are categorized as ‘others’. It can be seen that there are great differences in terms of the amount of kaolin on the coated sides of Chromolux paper and Chromolux cardboard. LumiArt paper has the greatest amount of $CaCO_3$.

Table 4.3: Amount of fillers in the three different paper sorts measured with an Ash Content Analyzer. The coated side of Chromolux paper and cardboard as well as both sides of LumiArt paper was measured twice. The differences in the relative standard deviation of the measurements were less than 2 % and only the mean is displayed. The non-coated side of Chromolux paper and cardboard was only measured once. For the reason that the two sides of LumiArt paper are not distinguishable, they are called Side 1 and Side 2.

Paper sort	Measured side	CaCO3	Kaolin/Talcum	Others
Chromolux cardboard	Coated side	16.95 % w/w	4.25 % w/w	7.60 % w/w
	Non-coated side	11.50 % w/w	20.80 % w/w	0.90 % w/w
Chromolux paper	Coated side	6.65 % w/w	26.35 % w/w	5.10 % w/w
	Non-coated side	18.50 % w/w	1.80s % w/w	0.00 % w/w
LumiArt paper	Side 1	49.10 % w/w	0.00 % w/w	0.00 % w/w
	Side 2	48.95 % w/w	0.00 % w/w	0.00 % w/w

Table 4.4 displays the specular gloss values measured with the micro-TRI-gloss on each substrate. Chromolux cardboard and Chromolux paper have the highest gloss of all four substrates and are comparable. UV-primer printed on LumiArt paper leads to a significant increase in gloss. This is coherent with the visual impression of the substrates. Figure 4.5 shows a picture of them.

Table 4.4: Specular gloss measured at 20°, 60°, and 85° with the micro-TRI-gloss gloss meter on the print sides of the substrates used in the experiments. The average values and standard deviations are calculated from five measurements on each paper sort. GlossXX denotes specular gloss measured at an angle of XX.

Angle of specular gloss measurement	Chromolux cardboard	Chromolux paper	LumiArt paper	LumiArt primed
Gloss20 in GU	57.5 ± 0.4	50.9 ± 1.0	3.4 ± 0.4	15.9 ± 0.9
Gloss60 in GU	77.9 ± 0.2	80.1 ± 0.2	29.9 ± 0.5	58.7 ± 1.6
Gloss85 in GU	97.0 ± 0.1	91.2 ± 0.4	79.9 ± 0.5	85.0 ± 0.8

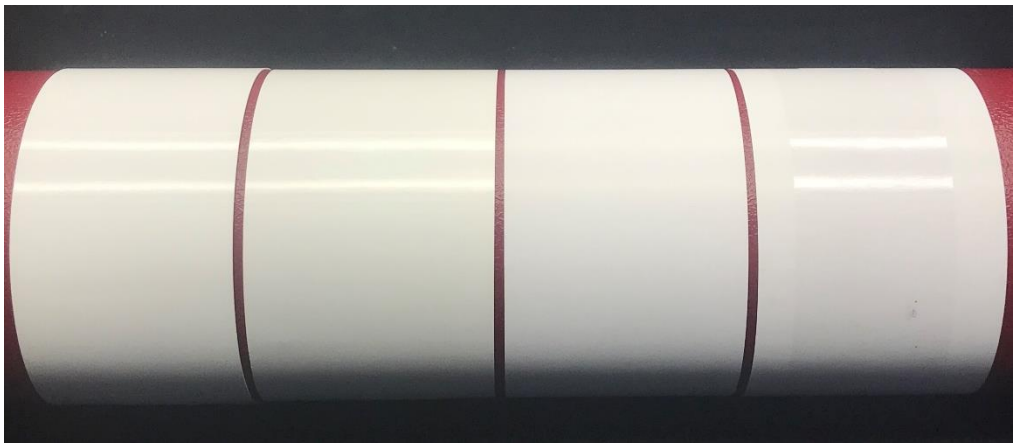

Figure 4.5: Substrates used for the experiments on dynamic gloss. From left to right: Chromolux cardboard, Chromolux paper, LumiArt paper and primed LumiArt paper. The reflections of two light tubes give an impression of the gloss and smoothness of the substrates.

4.3 Experiments on dynamic gloss – results and interpretation

Dynamic gloss was measured on eight different substrate-ink combinations, encompassing the two inks UV-ink-corn and UV-ink-VMP (abbreviations explained in Section 4.2.3), and the four substrates shown in Section 4.2.4. All eight combinations are shown in Table 4.5. In order to communicate these combinations, abbreviations for the substrate-ink combinations are introduced.

Table 4.5: Substrate-ink combinations used in the experiments on dynamic gloss and their respective abbreviations used in the following. Abbreviations of the inks were introduced in Section 4.2.3.

Substrate-ink combination	Abbreviation
Chromolux cardboard + UV-ink-VMP	ChromC_VMP
Chromolux cardboard + UV-ink-VMP	ChromC_Corn
Chromolux Paper + UV-ink-VMP	ChromP_VMP
Chromolux Paper + UV-ink-corn	ChromP_Corn
LumiArt Paper + UV-ink-VMP	LumiArt_VMP
LumiArt Paper + UV-ink-corn	LumiArt_Corn
LumiArt Paper, primed + UV-ink-VMP	LumiArt_Prim_VMP
LumiArt Paper, primed + UV-ink-corn	LumiArt_Prim_Corn

After printing, the micro-TRI-gloss was placed onto the samples and the continuous measurement mode was actuated. The measurements were taken at a position on the

printed substrate close to the printing cylinder of the IGT F1 after the print process. The point M in Area 2, shown in Figure 4.3, roughly indicates this position.

Between printing and the first measurement, a time lag of about two seconds occurred, which was measured repeatedly with a stopwatch. The continuous measurement was stopped when no further noteworthy change of gloss could be noticed. After the dynamic gloss measurement, samples were cured under an UV-unit with a peak irradiance of 4 W/cm² at a wavelength of 395 nm (Phoseon Technology, US). Cured samples of the eight substrate-ink combinations used in the experiment on dynamic gloss can be seen in Figure 4.6. Combinations printed with UV-ink-VMP exhibit a clearer and sharper reflection of the checkerboard compared to combinations printed with UV-ink-corn. In addition, the reflection of printed Chromolux paper and Chromolux cardboard is clearer than that of LumiArt paper and primed LumiArt paper. Further, it is visible that the checkerboard pattern is reflected clearer by the printed primed LumiArt paper than by the printed unprimed LumiArt paper. The imprint that can be seen on some of the samples is a result of the placement of the gloss meter on the uncured ink.

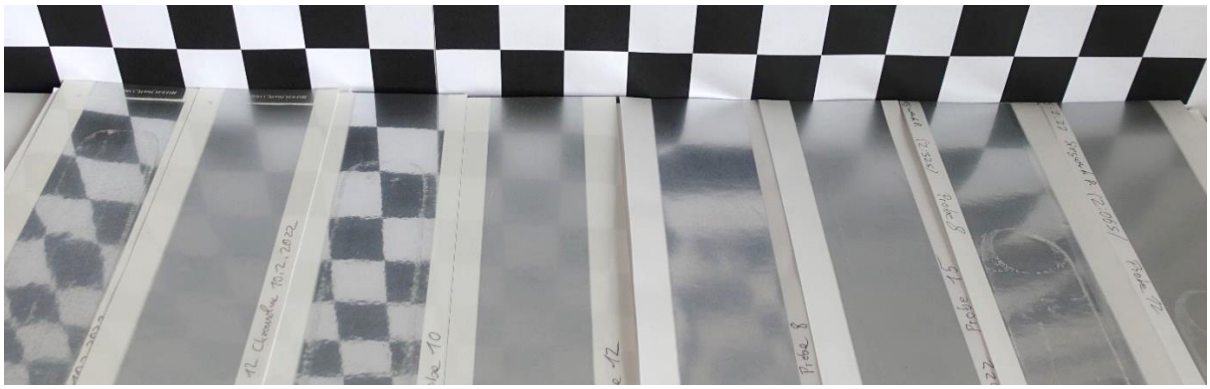

Figure 4.6: Samples printed in the experiments photographed in front of a checkerboard. From left to right: ChromP_VMP, ChromP_Corn, ChromC_VMP, ChromC_Corn, LumiArt_VMP, LumiArt_Corn, LumiArt_Prim_VMP, LumiArt_Prim_Corn. The abbreviations are explained in Table 4.5.

Figure 4.7 shows two microscopic images taken on printed Chromolux cardboard. One printed with UV-ink-VMP and one with UV-ink-corn. The light areas in the images are the pigments. The VMPs appear to align much better to each other and their surface seems to be smoother. The cornflake pigments in comparison seem to have a greater size distribution, a higher roughness, and more edges. These characteristics of the pigments, which were also described in Section 2.5.1, are a main cause for the different appearance of the samples printed with VMPs and cornflake pigments.

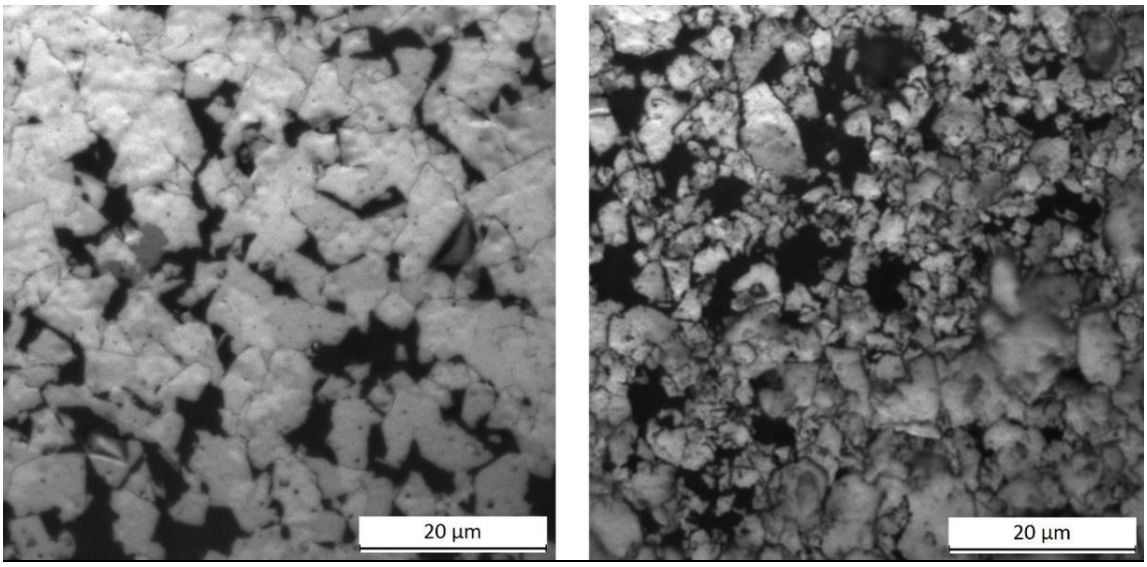

Figure 4.7: Inks containing VMPs (left) and cornflake pigments (right) printed on Chromolux cardboard. Images obtained with a Leica DM4000 microscope with 100x magnification.

The dynamic gloss of each of the eight combinations was measured three times. The three measurement curves for each combination are very similar in shape but differ slightly in gloss level. The measurement results are shown in Figure 4.8.

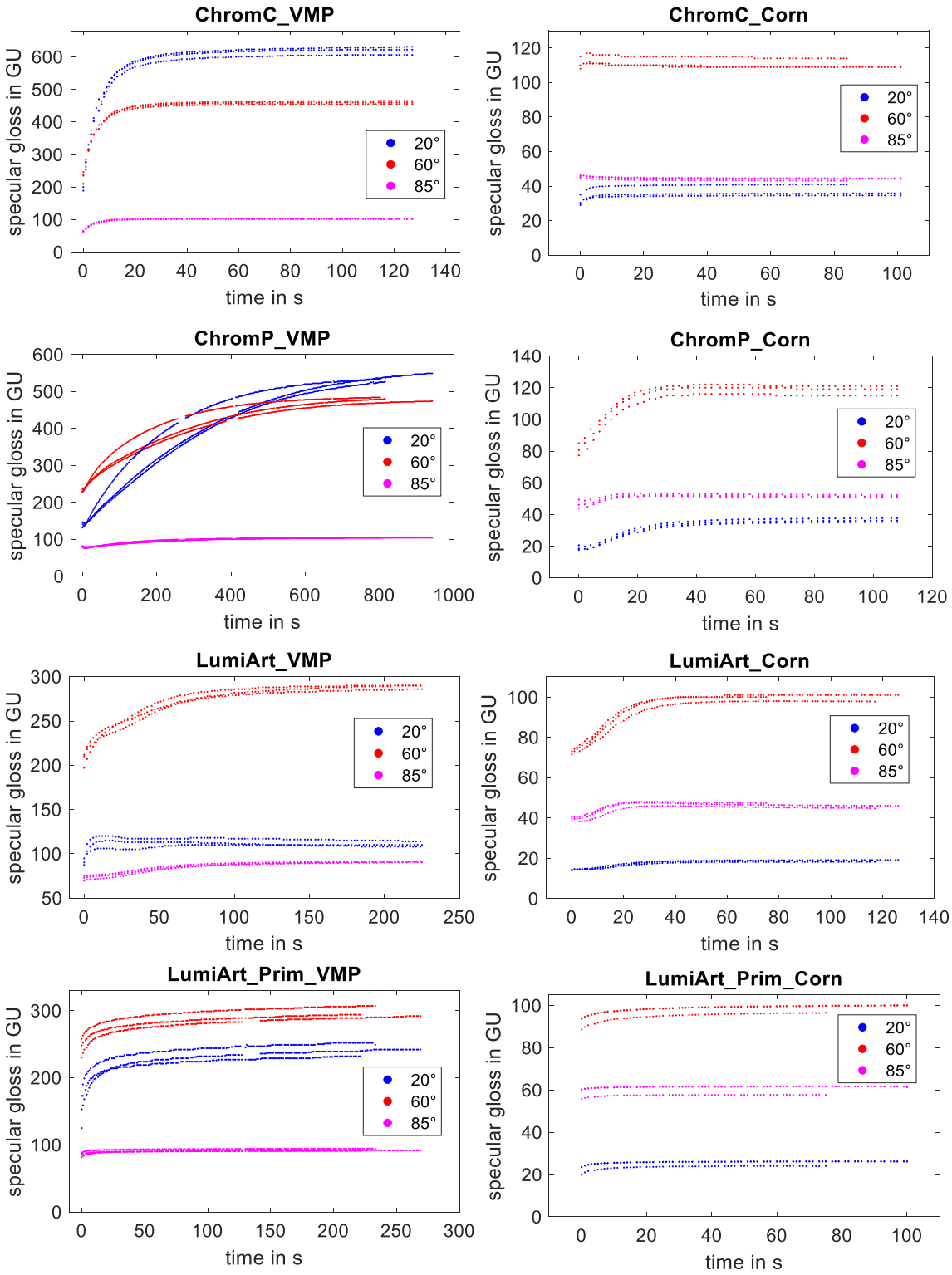

Figure 4.8: Dynamic gloss measured on eight different substrate-ink combinations (abbreviations are explained in Table 4.5.) with a micro-TRI-gloss gloss meter. For each combination, dynamic gloss was measured three times and each measurement series is shown. Specular gloss was measured at the angles of 20°, 60°, and 85°. Note that the scales of the graphs differ.

Figure 4.8 shows that the dynamic gloss is heavily influenced by both the choice of the substrate as well as by the choice of the printing ink. When comparing the substrates, it stands out that the dynamic gloss measured on Chromolux cardboard and Chromolux paper differs greatly.

4.3.1 Chromolux paper and Chromolux cardboard

For the substrate-ink combination ChromC_VMP (abbreviations explained in Table 4.5), specular gloss measured at 20°, 60°, and 85° does not change notably after 30 s. For ChromP_VMP however, the change of gloss per time unit is much smaller and is continuous on a much longer time span. This is also illustrated by the graphs shown in Figure 4.9. Here, the approximate derivative, which is the rate of specular gloss change per second, is shown for a single measurement series for each of the two ink-substrate combinations ChromC_VMP and ChromP_VMP. While for ChromC_VMP, specular gloss measured at 20° rises by more than 50 GU per second after printing, specular gloss measured at 20° and 85° on ChromP_VMP decreases within the first seconds after printing while then increasing. For ChromP_VMP, the shown rate of increase is never higher than 2 GU per second but continues for almost 800 seconds.

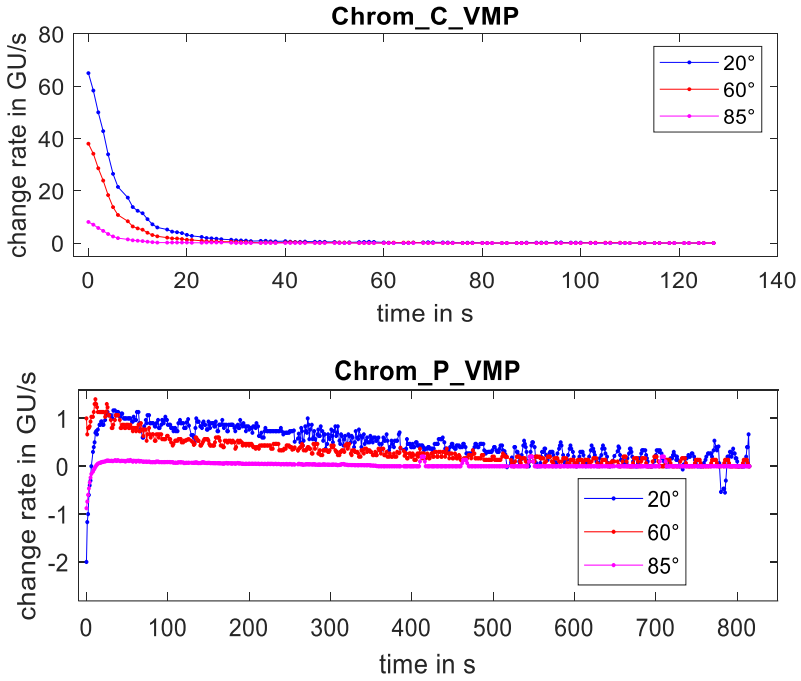

Figure 4.9: Rate of gloss change per second for a single dynamic gloss measurement on the substrate-ink combinations ChromC_VMP and ChromP_VMP (abbreviations explained in Table 4.5). For noise reduction, a moving average filter of five data points was applied to the data. Note that the scales of the graphs differ.

For dynamic gloss measured on the substrate-ink combinations ChromC_Corn and ChromP_Corn the time required to reach steady-state specular gloss is shorter compared to using UV-ink-VMP. For both ChromC_VMP and ChromC_Corn, the maximum observed change rate of specular gloss at 20° and 60° takes place within the first seconds of measurement. Specular gloss measured at 85° forms an exception. For both substrate-ink combinations, 15-20 seconds after printing no significant further changes in specular gloss are measureable. For ChromP_Corn, the time span of specular gloss change is longer than for ChromC_Corn. Specular gloss measured at 20° and 85° decreases slightly within the first second of measurement and increases afterwards. The peak rate of change in specular gloss per second for all three angles is reached a few seconds after the initiation of the dynamic gloss measurement. Figure 4.10 shows the gloss change per second for ChromC_Corn and ChromP_Corn.

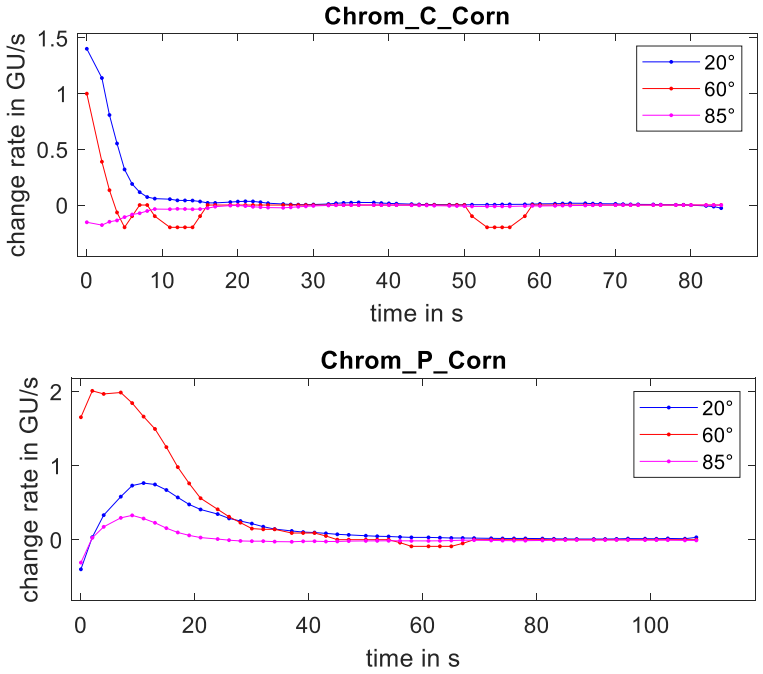

Figure 4.10: Rate of gloss change per second for a single dynamic gloss measurement on the substrate-ink combinations ChromC_Corn and ChromP_Corn (abbreviations explained in Table 4.5). For noise reduction, a moving average filter of five data points was applied to the data. Note that the scales of the graphs differ.

The surprising differences in dynamic gloss measurements between Chromolux cardboard and Chromolux paper, despite their comparable texture and gloss, can most likely be attributed to a disparity in ash content, in terms of $CaCO_3$ and kaolin, present on the coated side of each substrate.

4.3.2 Influence of UV-primer

When comparing LumiArt_VMP and LumiArt_Prim_VMP (abbreviations explained in Table 4.5), it can be seen that specular gloss measured at 60° reaches about 280 GU for both substrate-ink combinations. However, specular gloss measured at 20° is about 100 GU higher for LumiArt_Prim_VMP than for LumiArt_VMP. For both substrate-ink combinations, the highest rate of gloss change can be observed within the first seconds after the start of the measurement as shown in Figure 4.11. However, for LumiArt_Prim_VMP the rate of increasing gloss is more than two times higher at the beginning of the measurement compared to LumiArt_VMP for specular gloss measured at 20°. While no noteworthy changes in specular gloss are observed for LumiArt_Prim_VMP after 30 seconds, it takes considerably longer for a steady state to be reached for LumiArt_VMP. Additionally, it is worth noting that for LumiArt_VMP, a few seconds after the initiation of the measurement, the specular gloss measured at 60° exhibits an increase, while the specular gloss measured at 20° exhibits a slight decrease.

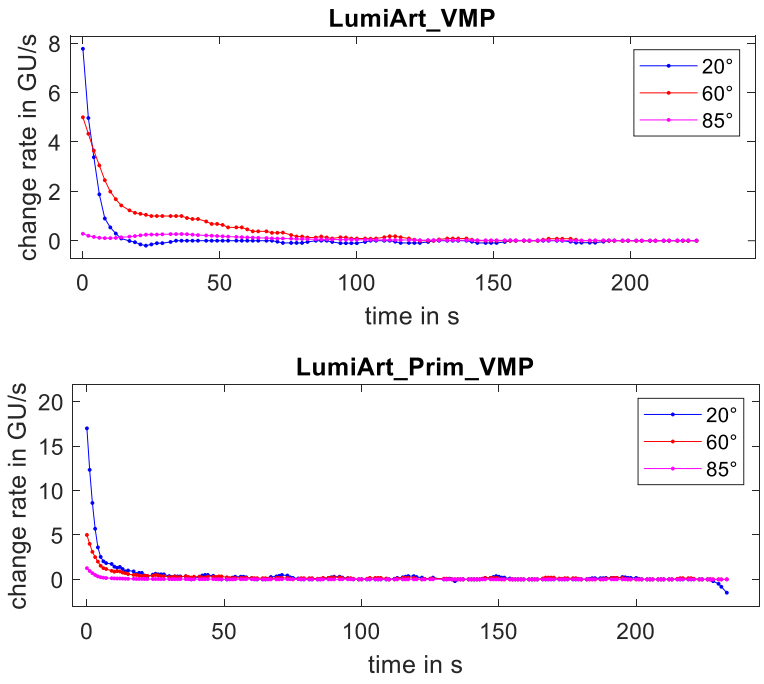

Figure 4.11: Rate of gloss change per second for a single dynamic gloss measurement on the combinations LumiArt_VMP and LumiArt_Prim_VMP (abbreviations explained in Table 4.5). For noise reduction, a moving average filter of five data points was applied to the data. Note that the scales of the graphs differ.

While the absolute specular gloss levels at steady state are comparable between LumiArt_Corn and LumiArt_Prim_Corn, there are variations in the rate of gloss change,

as shown in Figure 4.12. For LumiArt_Corn, the maximum specular gloss at 20° is reached soon after the start of dynamic gloss measurement, whereas at 60° and 85°, the peak gloss increase is observed after approximately 10 seconds. Specular gloss at 85° exhibits a slight initial decrease. In contrast, LumiArt_Prim_Corn shows an increase in specular gloss after the start of the measurement, reaching a steady state earlier.

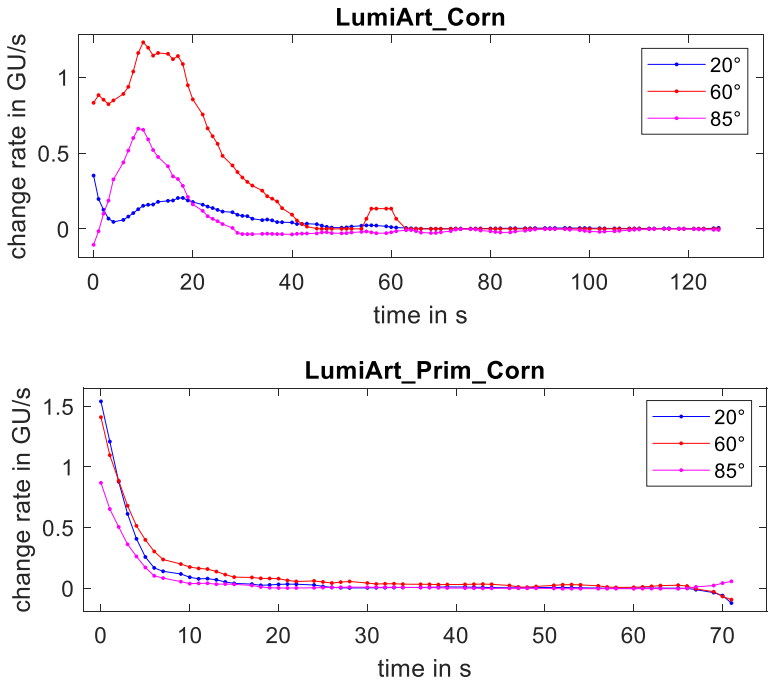

Figure 4.12: Rate of gloss change per seconds for a single dynamic gloss measurement on the combinations LumiArt_Corn and LumiArt_Prim_Corn (abbreviations explained in Table 4.5). For noise reduction, a moving average filter of five data points was applied to the data. Note that the scales of the graphs differ.

4.3.3 Further considerations

It is evident that the UV-primer applied to LumiArt paper exerts an influence on dynamic gloss. For both UV-ink-VMP and UV-ink-corn (abbreviations explained in Section 4.2.3), the maximum specular gloss levels measured at 20°, 60°, and 85° are reached faster when UV-primer is preprinted. This phenomenon could be attributed to the closure of paper pores by the UV-primer, inhibiting ink penetration into the substrate and smoothing the paper surface. Water absorbency tests revealed that primed LumiArt paper exhibits lower water absorbency compared to Chromolux paper and Chromolux cardboard, suggesting slower ink penetration. Nevertheless, the measured gloss values on Chromolux cardboard and paper are higher than on primed LumiArt paper. Probably, an influencing factor

contributing to the lower specular gloss of primed LumiArt paper compared to Chromolux paper is its higher surface roughness.

For all substrates, it can be seen that the specular gloss measured on UV-ink-corn always reaches the maximum specular gloss level faster than specular gloss measured on UV-ink-VMP. A reason for this could be the smaller metal content in UV-ink-VMP compared to UV-ink-corn. This could result in VMPs exhibiting greater agility within the ink film over an extended time range within the printed film.

Some substrate-ink combinations exhibit opposing trends in specular gloss changes at different measurement angles. The increase in specular gloss can be attributed to ink filament leveling, pigment leaving, and pigment alignment. Conversely, decreasing gloss values can be linked to an increasing ink film roughness. Two distinct cases with opposing trends in dynamic gloss, depending on the measurement angle, can be identified. In Case 1, illustrated by measurements on ChromP_VMP, specular gloss measured at 20° and 85° initially decreases and then increases after a few seconds. Specular gloss measured at 60° however, monotonically rises until a steady state is reached. In Case 2, exemplified by measurements on LumiArt_VMP, specular gloss measured at all three angles rises initially, but after a few seconds, specular gloss at 20° decreases slightly.

The data measured in this study do not suggest a possible explanation for Case 1. However, data published in a study by Preston et al. (2006) shows that during a short time after printing UV-offset inks on kaolin coated paper, micro roughness (not further specified in the study) becomes higher while macro roughness (not further specified in the study) decreases at the same time. While the increase in micro roughness after printing leads to a decrease in measured specular gloss, a reduction in macro roughness leads to an increase of specular gloss. Probably, the increase of micro roughness affects the specular gloss measurement at 20° to a greater extent than the specular gloss measurement at 60° due to the differences in aperture sizes at these angles. Due to the larger aperture at 60° (see Section 2.3.1), specular gloss measured at 60° is not affected by light scattering while it increases due to the reduction of macro roughness. Specular gloss measurement at 85° could decrease due to shadowing effects and scattering caused by the increase of micro roughness.

Case 2 could be explained as follows: during the first seconds after printing, the ink filaments level what smoothens the ink film. At the same time, the pigments align to the

ink film surface. Further, the binder of the ink penetrates partly into the substrate and the pigments, which are still present on the substrate surface, align along the paper surface texture. The decreasing gaps between the pigments decrease the multiple reflections between the pigments, which in return increases the amount of totally reflected light. Figure 4.13 diagrams the process of ink filament leveling, pigment leafing and binder penetration. For the reason that the receiver aperture of the gloss meter at 20° is comparatively small, the increased scattering of light results in a decreased fraction of light reaching the photodiode at 20°. Hence, the measured signal decreases. Specular gloss measured at 60° however is not that sensitive to light scattering because the aperture is comparatively large. Hence, the total amount of light reflected to the photodiode at 60° increases over time.

Figure 4.13: Schematic of ink leveling, pigment leafing and ink partly ink imbibition of a rough substrate with a relatively high porosity and roughness. These three processes after printing the ink on a rather rough and ink-absorbent substrate could give and explanation of opposing trends on dynamic gloss measurement, depending on the angle of measurement. (Weber et al. 2022a)

4.3.4 Modelling of dynamic gloss curves

The dynamic gloss curves can be approximated using mathematical functions, which is shown exemplary for specular gloss measured at 20° and 60° for the substrate-ink combinations ChromC_VMP and LumiArt_VMP (abbreviations explained in Table 4.5). The dynamic gloss curves measured on ChromC_VMP can be modelled using the Kohlrausch function (Kohlrausch 1854) shown in Equation 4.1 and as suggested previously by Weber et al. (2022a). This equation originally describes the distribution of attachment energies of electric charges at the dielectric between capacitor plates. *a, b, c* are non-negative fit parameters. The stretching exponent $d = 0…1$ is characteristic for the material and its influence on the capacitor discharge process. The case $d = 1$ corresponds to ordinary exponential relaxation. *t* is the time of measurement.

$$f(t) = -a * exp(-(b * t)^d) + c \qquad 4.1$$

If applied to dynamic gloss, c - a is the gloss delta from the start of the measurement until the steady state gloss value, given by c. b correlates with the time needed to reach the

steady state gloss value, and positively correlates with the initial incline. If applied to dynamic gloss, the stretching exponent d could both describe the feature that pigments float up with size-dependent rates and that the rate of levelling of the ink filaments decreases with time. For the relaxation of the ink of the substrate-ink combination ChromC_VMP (abbreviation explained in Table 4.5), one finds $d = 0.70$ for specular gloss measured at 20° and $d = 0.74$ for specular gloss measured at 60°. This approximation is shown in Figure 4.14.

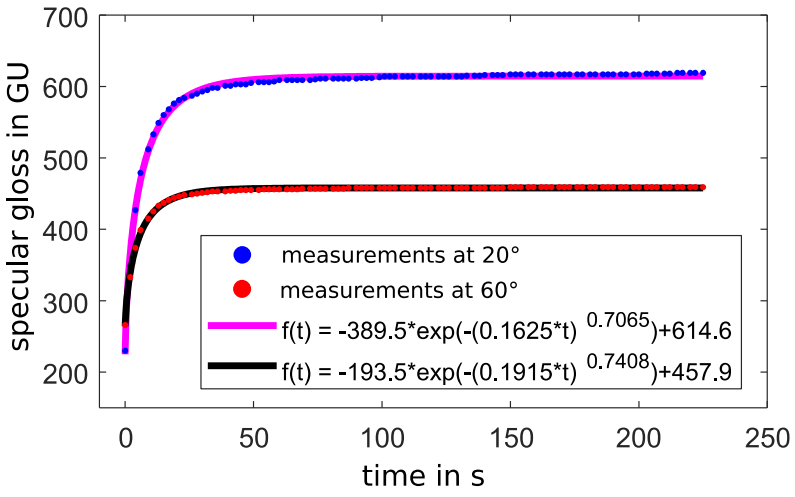

Figure 4.14: Fitting of Equation 4.1 on the dynamic gloss measured on the substrate-ink combination ChromC_VMP (abbreviation explained in Table 4.5) at the angles of 20° and 60°. Measurements were obtained with the micro-TRI-gloss gloss meter.

When applying Equation 4.1 to fit the dynamic gloss trends measured at 20° and 60° on the substrate-ink combination LumiArt_VMP, the Kohlrausch function does not provide a good fit for the trend measured at 20°. However, for the dynamic gloss measured at 60° a Kohlrausch fit with $d = 1$ appears adequate, which is shown in Figure 4.15. Equation 4.2 is a better model of the dynamic gloss measured at 20°. It is the sum of two exponential functions. The first one of them describes the rising, the second one a slow and steady decrease of the specular gloss.

$$f(t) = -a * exp(-b * t) + c * exp(-b' * t) + h \qquad 4.2$$

$h + c$ is the gloss maximum that is reached and a gives the delta between the first measurement and the gloss maximum. b is the rising rate of the initial incline of specular gloss, and $b' << b$ describes the slow decline after the specular gloss maximum has been passed. All of these parameters are non-negative. The description of the dynamic gloss

with the summation of the two exponential functions shows that basically two different processes happen after printing, of which one is responsible for the incline of the curve and one for the decline as explained above. The approximation using Equation 4.2 is shown in Figure 4.15 for the measurement at 20°.

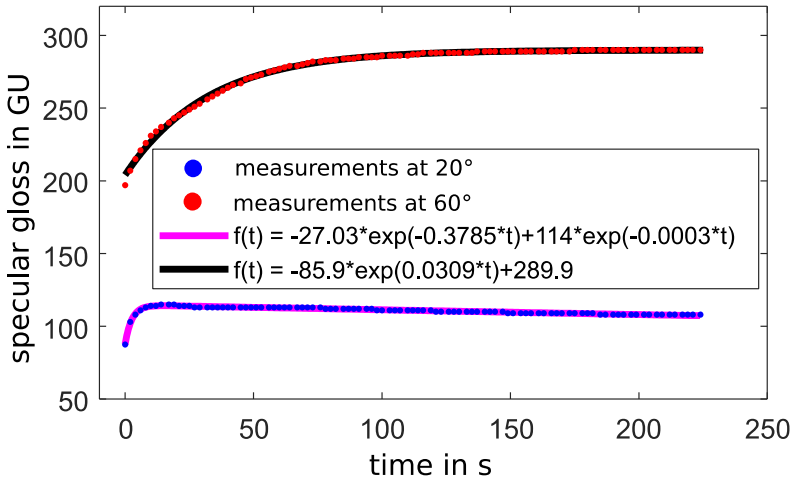

Figure 4.15: Fitting of Equation 4.1 (60° measurement) and Equation 4.2 (20° measurement) on the dynamic gloss measured on the substrate-ink combination LumiArt_VMP (abbreviation explained in Table 4.5). Measurements were obtained with the micro-TRI-gloss gloss meter.

Sauer et al. (2022) goes into more detail in terms of mathematically describing the dynamic gloss measurements shown above. A model was introduced that describes that leafing pigments in an ink film always tend to a state, which is energetically the best or respectively energetically lowest state. The pigments in the ink film are subject to Brownian motion, which is a random motion of particles in a liquid or gas. This motion is abundant from the viscosity of the ink. If the ink has a lower viscosity, pigments move faster and have a greater range of motion. As a result, it is expected that a reduction of ink viscosity fastens pigment leveling by a factor of one. Further, for leafing pigments, the polarity of the pigment surface is different to the polarity of the binder. This means that they repel each other in order to reach a state of a lower energy level. A high polarity of the pigment surface can be reached with for example hydroxyl groups. If a pigment comes close to the ink film surface due to the Brownian motion it stays close to it, because an energetically favorable state is reached. Nevertheless, the pigment surface and the binder maintain adhesion to each other, resulting in a thin layer of binder consistently remaining on top of the pigments. This upward movement of the pigments causes the gaps between

them to diminish, leading to a reduction in scattering within the pigment layer and consequently, an increase in gloss.

The described model only takes the leveling behavior of the pigments into account. In order to adequately predict the dynamic gloss it would have to be connected with more models describing the leveling of the printed ink film. There are numerous studies on the leveling of liquid defects since this is a relevant topic for the paint and printing industry. Orchard (1963) describes the surface-tension-driven leveling of Newtonian fluids on a substrate. However, printing inks are non-Newtonian fluids as they are normally shear-thinning fluids. Iyer and Bousfield (1996) analyzed the leveling of shear-thinning fluids with a one-dimensional model that takes surface tension, gravity, and viscous forces into account. Toivakka et al. (2001) made investigations on the leveling of thin films of pigmented coatings. Shin and Bousfield (2009) characterized the leveling of irregularities in coatings on porous paper media and proposed a model including absorption effects to predict the leveling of ink films. If these findings could be connected to a mathematical model of a gloss meter as described for example by Westlund and Meyer (2001). This could make it possible to predict dynamic gloss in abundance of the substrate and printing ink.

It was demonstrated that dynamic gloss measurements effectively elucidate the impact of the substrate-ink combination on gloss development post-printing. In the methodology employed for dynamic gloss measurement in this dissertation, the influence of hot air post-printing could not be determined, as the measured spot was covered with a gloss meter. Subsequently, in additional experiments covered in the following, the ink was cured after varying time intervals, enabling the assessment of the influence of hot air and the analysis of changing pigment layer topographies.

4.4 Influence of dwell time and hot air – materials and method

In the following, the experimental setup for the laboratory experiments examining the influence of hot air and the duration of the dwell time after printing is outlined. The setup is similar to that used for the investigations on dynamic gloss. Further, the confocal microscope for topography measurement is addressed and the used 3D-surface parameters for the further evaluation of the results are explained.

4.4.1 Experimental setup

Samples were printed on the IGT F1 laboratory flexo printer that was also used for the experiments on dynamic gloss described in Section 4.2. The print settings for the IGT F1 flexo print proofer also remained the same as shown in Table 4.1. After printing, the dwell time was measured using a stopwatch. If no hot air was applied onto the printed samples, these were directly transferred into a UV-curing unit after the expiration of the dwell time. The UV-curing unit (Beltron, Germany), of which the exact specifications are unknown, was equipped with an aperture, which could be opened at a certain time by pressing a button. If hot air was applied onto the sample during the dwell time, the hot air blower was started directly before the actual printing of the samples. After printing, the samples were first transferred to the hot air blower. The time for this transfer lasted three seconds for every sample. After the samples remained under the hot air blower for a specific time, they were transferred to the UV-curing unit. The transfer of the samples from under the hot air blower into the UV-curing unit also lasted three seconds. The experimental setup can be seen in Figure 4.16.

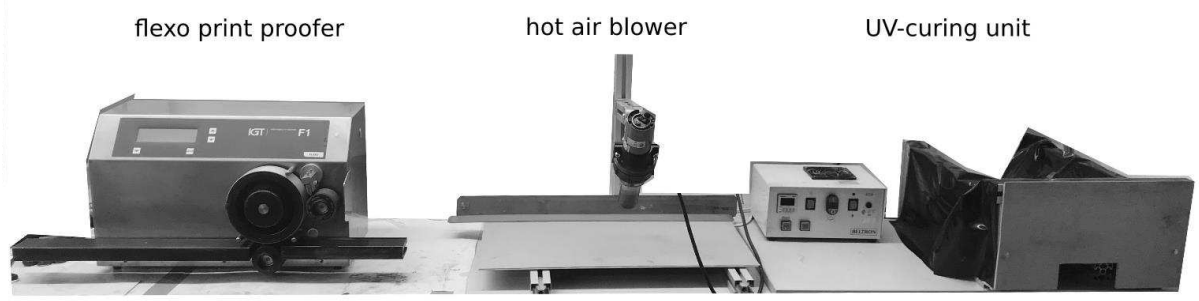

Figure 4.16: Setup of the experiment on the influence of hot air and the duration of the dwell time after printing with IGT F1 flexo print proofer, hot air blower, and UV-curing unit.

Hot air blower

The hot air blower that came to use was an ELECTRON ST hot air blower with a maximum power of 2300 W (Leister, Germany). Pretests showed that a comparable temperature to the hot air blowers in an industrial web-fed printing machine that will be introduced later could be reached by, setting the hot air blower to the device specific temperature level 2.5. In order to find a good position of the hot air blower and the sample, a water basin was placed under the hot air blower. The position of the hot air blower was changed until a spot on the water was found that was both large enough to place the samples and appeared to have a relatively uniform air flow over that area.

A PeakTech 4960 infrared thermometer (PeakTech, Germany) was used to characterize the temperature curve that could be expected on the samples for this positioning of the hot air blower. The temperature could both be measured with an IR-thermometer and a thermocouple integrated in the device. For the characterization of the temperature curve, samples were printed with black UV-ink SICURA Flex 39-8 UV (Siegwerk, Germany) on LumiArt paper described in Section 4.2.4. For this sample the emissivity was estimated to $\varepsilon = 0.94$, based on data provided by novasens Sensortechnik (n.d.) and (Testo n.d.).

As in the actual experiment, the hot air blower was turned on before the print process. After printing, the part of Area 1 (Figure 4.3) was cut out and placed under the hot air blower. Simultaneously, the temperature measurement was started by both using the IR-thermometer and a thermocouple. This procedure was repeated three times. Figure 4.17 shows the procedure of finding a good spot for the placement of the samples under the hot air blower by using a water basin, the positioning, and the placement of a black printed sample under to hot air blower to the characterization of the temperature curves. Figure 4.18 shows the temperature curves obtained for the three temperature measurement series using both the IR-thermometer and the thermocouple. It can be seen that the temperature measurements of the IR-thermometer and thermocouple differ. The IR-measurements were made at an angle that was not recorded. Due to the angle, the emissivity would be slightly reduced. Also, the emissivity changes slightly over time due to the penetration of the ink into the paper. Further, the hot air could create a convective heat transfer process in the wet ink. This influence cannot be captured with the thermocouple. As a result, it can be supposed that the actual temperature of the ink film is somewhere between the IR-thermometer and the thermocouple measurement values.

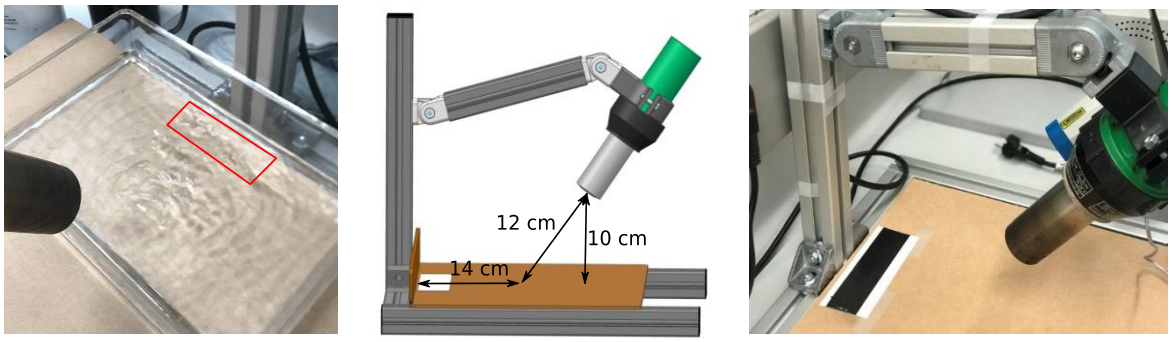

Figure 4.17: Left: Finding a spot under the hot air blower where a uniform air flow could be expected by using a water basin. The red quadrangle shows the area where samples were to be placed. Middle: Positioning of the hot air blower. Right: Placement of a black printed sample under the hot air blower for the characterization of the temperature curves.

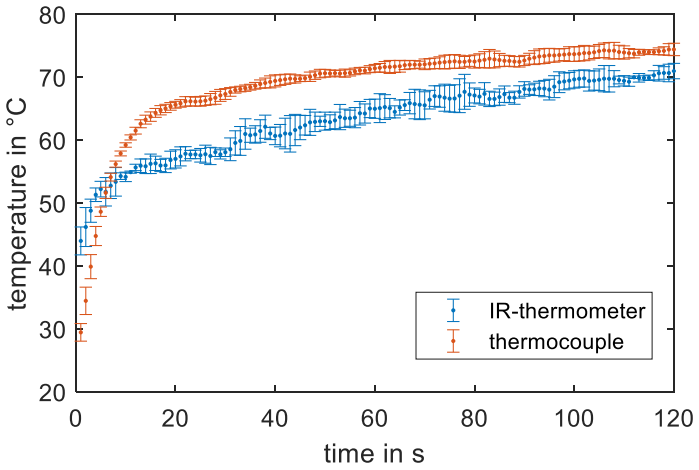

Figure 4.18: Temperature measurement curves obtained from three consecutive measurements using a PeakTech 4960 IR-thermometer and the included thermocouple. The measurement was started shortly after placing the black printed samples under the hot air blower. In total, three measurement series were made. Ten measurements were recorded per second. The data points used for this figure are the average of ten data points recorded each second. The whiskers on the points show the spread of the standard deviation of these ten measurements.

Gloss meter

Gloss measurements conducted on samples printed to study the impact of dwell time and hot air on gloss and pigment layer topography were static. Consequently, the IQ-S gloss meter (introduced in Chapter 3) was used to obtain data on haze and DOI beneath specular gloss.

Substrates

Only Chromolux paper, described in Section 4.2.4, was utilized as substrate. This choice was a result of the dynamic gloss measurements that indicated that gloss changes occur over more extended time intervals on Chromolux paper as compared to the other substrates used.

Printing inks

The same inks UV-ink-VMP and UV-ink-corn (introduced in Section 4.2.3) came to use as for the experiments on dynamic gloss.

4.4.2 Confocal microscopy and evaluated topography parameters

To obtain topographical data of printed samples a confocal microscope Sensofar PLu Neox (Sensofar, Spain) was utilized. The objective used was an EPI (Nikon, Japan) with 50x magnification, a working distance of 0.35 mm, and a numerical aperture of 0.95. Due to its high numerical aperture, it is possible to obtain good 3D-data of surface topographies with high slope angles as they occur between pigments that beneath of each other or overlapping but on a different height level. Images with a size of 340 x 283 μm^2 and a resolution of 0.28 µm/pixel were captured. The depth scanning range was 18 µm with a step size of 0.10 µm. Detailed information about the function of confocal microscopes is given by Leach (2011). The obtained data were processed using the SensoView 1.8 software (Sensofar, Spain) along with Python 3.7 for automatized processing.

Topography parameters

As mentioned by Järnström et al. (2008), surface roughness is an intrinsic property of a surface but the measured roughness is very dependent on the measurement settings. For instance, it depends on the size of the measured area and measurement technique. Further, many different roughness parameters that describe different surface properties can be analyzed and the filtering of the raw data is also important to consider.

Roughness and waviness parameters can be extracted from a measured surface topography by setting filters defined in DIN EN ISO 25178-2 (reapproved 2012). By applying filters to the data, the spatial wavelengths that represent roughness and waviness can be extracted. Changing the settings of a filter also changes the data that represent roughness and waviness. Different short pass/long pass filters are applied when

filtering roughness and waviness. The λ_S filter is a long pass filter. It removes short wavelength components that are not to be considered in the roughness or waviness data. The λ_L filter is a short pass filter. It removes long wavelength components that are not considered in the roughness data. Additionally, a form removal filter removes the primary surface. For instance, if the surface is slightly tilted to the measuring unit, the skewness can be removed. The form removal filter was applied on all measured topography data. Following DIN EN ISO 25178-2 (reapproved 2012), the roughness was filtered by applying the form removal filter, a λ_S filter and a λ_L filter. To filter the waviness, only the form removal filter and a λ_S filter were applied. In this work, roughness data of the topography were obtained using filters with λ_S = 2.50 µm and λ_L = 80 µm to ensure that the pigments size is within this range. To filter the waviness data, λ_S was set to 80 µm, which is above the size of the pigments used.

3D-surface parameters that can be obtained from topography data are divided into different groups following DIN EN ISO 25178-2 (reapproved 2012). These are:

- Functional parameters
- Functional Volume parameters
- Height parameters
- Hybrid parameters
- Spatial parameters

A detailed description of all these groups and the parameters included in them is provided by Leach (2013). Overall, there are 56 3D-roughness parameters defined in the ISO and ASME standards for 3D-topography measurement (Deltombe et al. 2014). This shows that surface topography properties cannot be described by using a single parameter. Some combinations of roughness parameters can describe surface properties efficiently (Czifra and Barányi 2020). Some of the most well-known 3D-roughness height parameters that are often combined are the arithmetic mean height Sa and the parameter for the maximum heights and depths Sz. They are often used for the analysis of functional machined surfaces (Michigan Metrology n.d.; Gayduscheck 2019). The height parameter root mean square height deviation Sq is typically used to specify optical surfaces. It has a high correlation with Sa. Different to Sa, it is directly related to the way light is scattered from a surface (Leach 2014). This parameter was used by Weber et al. (2023) for the comparison of topographic measurements with measured gloss of printed metallized surfaces. Using the scalar Kirchhoff light scattering theory, Alexander-Katz and Barrera (1998) reported on a correlation between Sq and light scattering properties. Yong et al. (2020) used the parameters Sq and Sa to show the linear correlation between these roughness parameters

and specular gloss measurements obtained from matt polyurethane coatings. Sq is evaluated by subtracting the mean height $\overline{z}$ from the height z measured at every point (x,y) in an area A, dividing the sum of the squared results with A and taking the root of that as shown in Equation 4.3. The Sq value is usually reported in µm or nm.

$$Sq = \sqrt{\frac{1}{A}\iint_A [z(x,y) - \overline{z}]^2 dxdy} \quad 4.3$$

For the reason that experience on comparing measured gloss with Sq values of metallized printed surfaces by Weber et al. (2023) showed that the Sq seems to be insufficient to explain differences of the gloss of samples, it was decided to include a further parameter. Based on preliminary investigations, it was decided between the root mean square gradient Sdq or the developed interfacial ratio Sdr, which are both hybrid parameters. As explained by Leach (2013), Sdq is the root mean square of the gradients at all points of a measured area and its value is unit less. Sdr describes the additional area due to slopes in comparison to a flat area in percentage. For both parameters, a flat surface without any slopes would result is a value of 0 (Sdq - unitless) or 0 % (Sdr) respectively. Both parameters were chosen by Rozanski et al. (2014) as parameters that correspond to optical properties of glass and adhesive tapes. Vessot et al. (2015) showed that there is a good correlation between gloss and the Sdq and Sdr parameters for photographic paper. Since there is a high correlation between both parameters as also shown by Czifra and Barányi (2020), only one of the two parameters was selected. For the reason that preliminary studies showed a slightly higher correlation between Sdq and specular gloss measurements than the Sdr, the choice fell on Sdq. The parameter is evaluated as shown in Equation 4.4. ∂z(x,y)/ ∂x is the local gradient at (x,y) along the x axis while ∂z(x,y)/ ∂y is the local gradient at (x,y) along the y axis.

$$Sdq = \sqrt{\frac{1}{A}\iint_A \left[\left(\frac{\partial z(x,y)}{\partial x}\right)^2 + \left(\frac{\partial z(x,y)}{\partial y}\right)^2\right] dxdy} \quad 4.4$$

4.4.3 Experimental procedure and measurement scheme

Four different test series were printed and analyzed. Two of the test series were printed using the UV-ink-VMP (abbreviations explained in Section 4.2.3). For one of them, hot air was applied to the printed ink during the dwell time. Another two series were printed with UV-ink-corn, and for one of them, hot air was applied. Both series printed with UV-ink-VMP consist of six sample sets, each set containing three samples that were printed in

three successive repetitions of the set-specific settings. The time spans of 10 s, 20 s, 30 s, 60 s, 90 s, 120 s were the durations of dwell time for the samples produced without hot air during dwell time. For the samples produced with hot air during dwell time, hot air was applied with the duration of 10 s, 20 s, 30 s, 60 s, 90 s, 120 s. For the total dwell time, additionally six seconds need to be factored in, accounting for the transportation of the samples from the flexo print proofer under the hot air blower and their subsequent transport to the UV-curing station. For the samples printed with the ink containing cornflake pigments applies the same with the difference that only four samples sets with the time spans of 10 s, 20 s, 30 s, 60 s were made. A listing of the settings for sample production and their abbreviations used is shown in Table 4.6. In total, 60 samples were analyzed regarding gloss and 3D-topography.

Table 4.6: Abbreviations for the substrate-ink combinations and settings used in the experiments on the influence on dwell time and hot air.

substrate	pigment type	hot air	dwell times in s	abbreviation
Chromolux paper	VMP	no	10, 20, 30, 60, 90, 120	ChromP_VMP_nha_(10-120)
Chromolux paper	VMP	yes	10, 20, 30, 60, 90, 120 (+6)	ChromP_VMP_ha_(10-120)
Chromolux paper	Cornflake	no	10, 20, 30, 60	ChromP_corn_nha_(10-60)
Chromolux paper	Cornflake	yes	10, 20, 30, 60 (+6)	ChromP_corn_ha_(10-60)

Measurement schemes

For the reason that the printed samples were long and narrow, the scheme for measuring gloss differed from the measurement scheme introduced in Section 3.2. Ten gloss measurements were taken per sample along one row, five of them in print direction, and five across print direction. Performing topography measurements required more time compared to gloss measurements. It took approximately four minutes to complete three topography measurements on one sample. Hence, it was opted to only make three topography measurements on each. The measurement scheme for the gloss measurements and topography measurements is shown in Figure 4.19. All measurements were carried out on Area 1 on the printed samples, described in Figure 4.3. Area 1 was chosen because other substrate-ink combinations were also tested initially. These substrate-ink combinations showed a more even ink distribution in Area 1. To ensure good comparability between the samples, it was decided to use only Area 1 for the measurements. Ultimately, however, only results from samples printed on Chromolux paper were included in this dissertation. Since the length of the measurement spot for specular gloss measurements

at 85° using the IQ-S (shown in Table 3.1) is greater than the width of the printed area, specular gloss measurement at 85° were not considered for the evaluation.

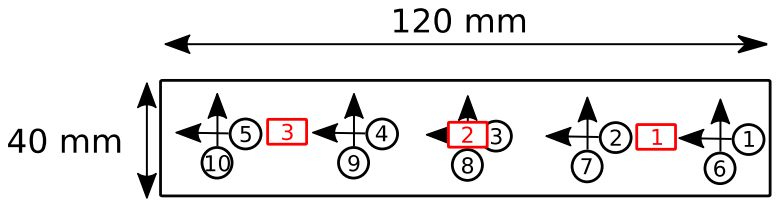

Figure 4.19: Measurement scheme of gloss measurements (black) and 3D-topography measurements (red) on the printed area in Area 1 (shown in Figure 4.3). The size of the red rectangles does not represent the size of the 3D-topography measurements. They only show their positioning on the samples.

4.5 Influence of dwell time and hot air – results and interpretation

The subsequent evaluation first focuses on the measured gloss of the printed samples, considering variations in dwell time and the use of hot air after printing. Then the topography measurements are evaluated and the 3D-surface parameters Sq and Sdq are compared with specular gloss measured at 60°.

4.5.1 Influence of dwell time and hot air on gloss

Figure 4.20 shows samples of all substrate-ink combinations and different spans of dwell time or with hot air during dwell time respectively. For each time interval, one sample was selected for the images. For the samples of ChromP_VMP_nha and ChromP_VMP_ha (abbreviations explained in Table 4.6), it can be seen that with increasing dwell time, the reflection of the checkerboard pattern becomes clearer. The best reflections of the checkerboard pattern can be observed for ChromP_VMP_ha with dwell times of 30 to 120 seconds. Further, it can be seen that for samples of ChromP_corn_nha and ChromP_corn_ha an increasing time interval does not seem have a noticeable impact on the reflectiveness. As can be seen in the following, gloss measurements mirror these visual impressions.

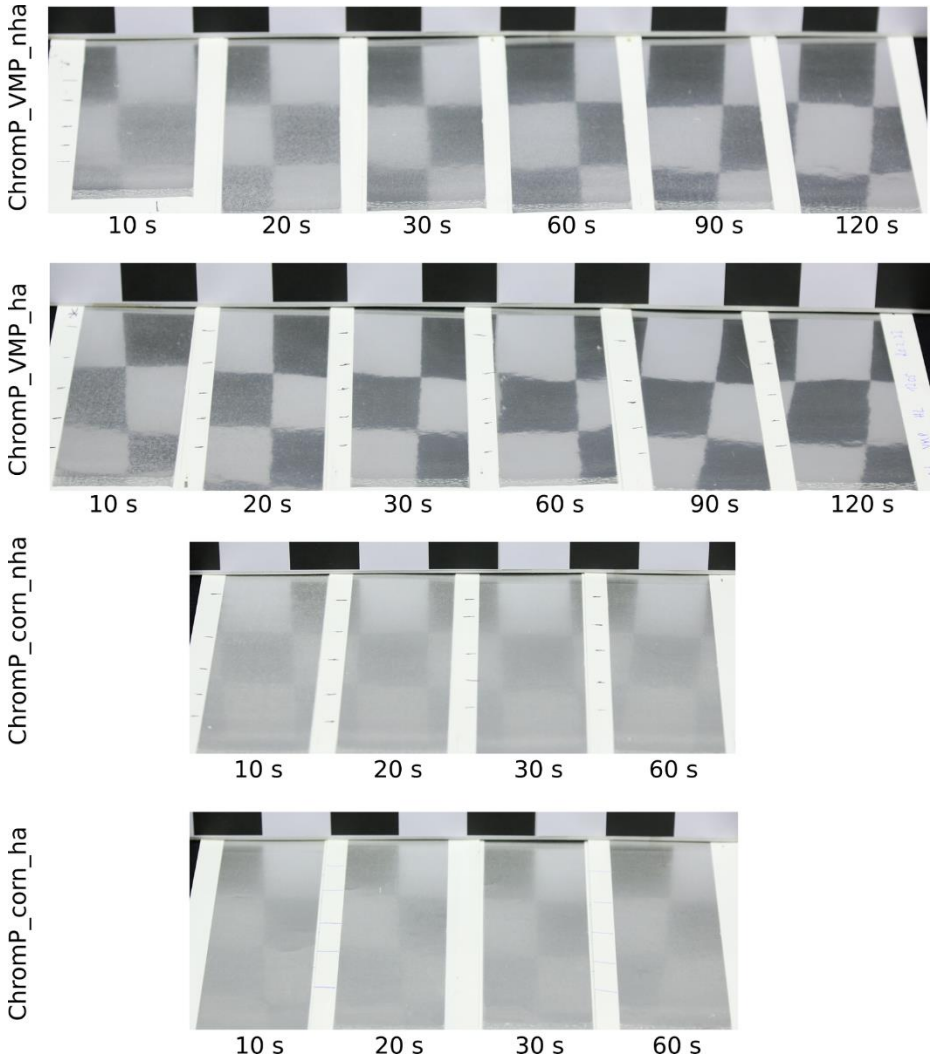

Figure 4.20: Samples printed using inks containing VMPs and cornflake pigments, with and without the application of hot air during the dwell time. The time intervals indicate the duration of dwell time for samples without hot air and the exposure time to hot air for samples where hot air was utilized. The abbreviations are explained in Table 4.6.

Results with inks containing VMPs

The measurement results of specular gloss at 20° and 60° for ChromP_VMP_nha and ChromP_VMP_ha (abbreviations explained in Table 4.6) are shown in Figure 4.21. All further figures with similar violin plots as shown in Figure 4.21 were made using a modified version of a Matlab file by Bechtold (2016). As could already be assumed on basis of the dynamic gloss measurements, longer time intervals lead to higher gloss. It can also be seen that the application of hot air during dwell time has a high influence on gloss. For samples produced without the use of hot air, a dwell time of 120 seconds results in mean specular gloss values of 549 GU (20°) and 454 GU (60°). In contrast, similar gloss values are achieved after applying hot air for only 20 seconds during the dwell time, which results

in mean specular gloss values of 546 GU (20°) and 421 GU (60°). Further, for samples of ChromP_VMP_ha it can be seen, that a maximum mean specular gloss is reached after 30 s with mean specular gloss values of 657 GU (20°) and 473 GU (60°). Notably higher specular gloss values cannot be reached with a longer application of hot air. It can be seen that the deviations of specular gloss values are generally higher for specular gloss measurements at 20° than for specular gloss measurements at 60°. This observation was already discussed in Chapter 3. The deviations of specular gloss measurements at 20° for samples made with hot air during dwell time are higher than for samples made without hot air during dwell time. This is partly due to the fact that the measured values are generally higher. This could also be due to an uneven temperature distribution on the samples. An overview of the mean standard deviations of the gloss measurements measured on the different substrate-ink-hot-air combinations ChromP_VMP_nha, ChromP_VMP_ha, ChromP_corn_nha, and ChromP_corn_ha is given in Appendix 2.

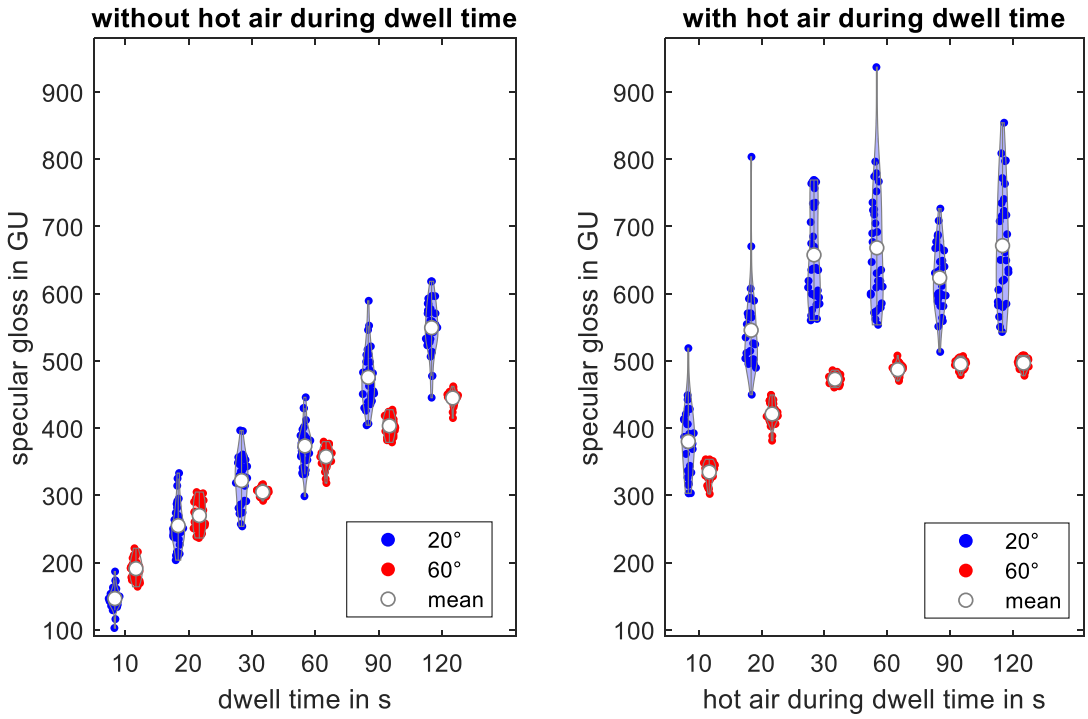

Figure 4.21: Specular gloss (20° and 60°) measured with the IQ-S gloss meter on the series printed on Chromolux paper without and with hot air during dwell time printed with UV-ink containing VMPs. Each colored field consists of 30 data points measured on three samples with the same print settings. The width of the area in the individual violin plots shows the density of the measuring points for a specific measured value range.

DOI values measured on the combinations ChromP_VMP_nha and ChromP_VMP_ha are shown in Figure 4.22. It can be seen that a longer time interval has a positive impact on

the DOI of the samples of ChromP_VMP_nha as it increases from 10 to 90 seconds. Only when increasing dwell time from 90 to 120 seconds, a small decrease is measureable. For the DOI of the samples of ChromP_VMP_ha this tendency is not measureable. Between 10 to 30 seconds of hot air, the mean of the DOI is between 36-37 %. For longer durations of hot air, the DOI drops slightly and is between 30-35 %. As can be seen in the following, this drop of DOI of the values measured on samples with time intervals of 30 and 60 seconds is mirrored by an increasing haze.

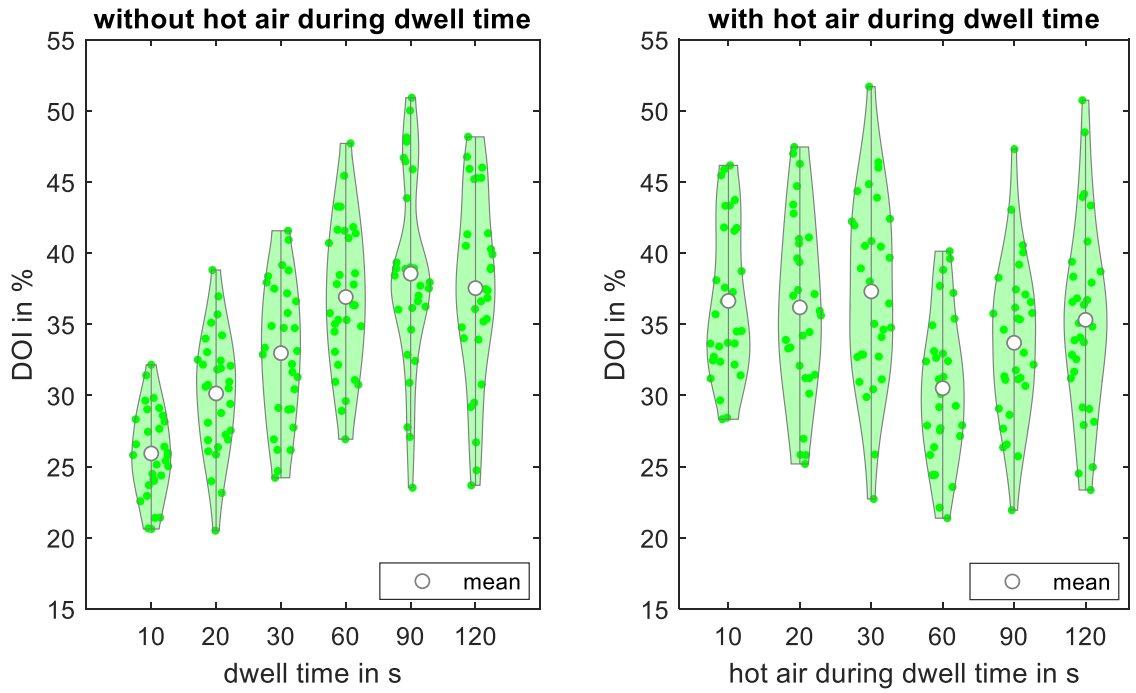

Figure 4.22: DOI measured with the IQ-S gloss meter on the series printed on Chromolux paper without and with hot air during dwell time printed with UV-ink containing VMPs. Each colored field consists of 30 data points measured on three samples with the same print settings. The width of the area in the individual violin plots shows the density of the measuring points for a specific measured value range.

Figure 4.23 shows haze measured on the samples of ChromP_VMP_nha and ChromP_VMP_ha. No clear trend can be seen for the values measured on ChromP_VMP_nha. The mean values fluctuate between 127 HU and 144 HU. Haze values measured on ChromP_VMP_ha however, have an increase from 140 HU (after 30 s) to 176 HU (after 60 s). One possible explanation for this could be that parts of the binder of the ink penetrates into the substrate as its viscosity drops with increasing temperature and as it stays in the substrate longer in an uncured condition. However, this does not seem to have a negative effect on the specular gloss values as could be seen before.

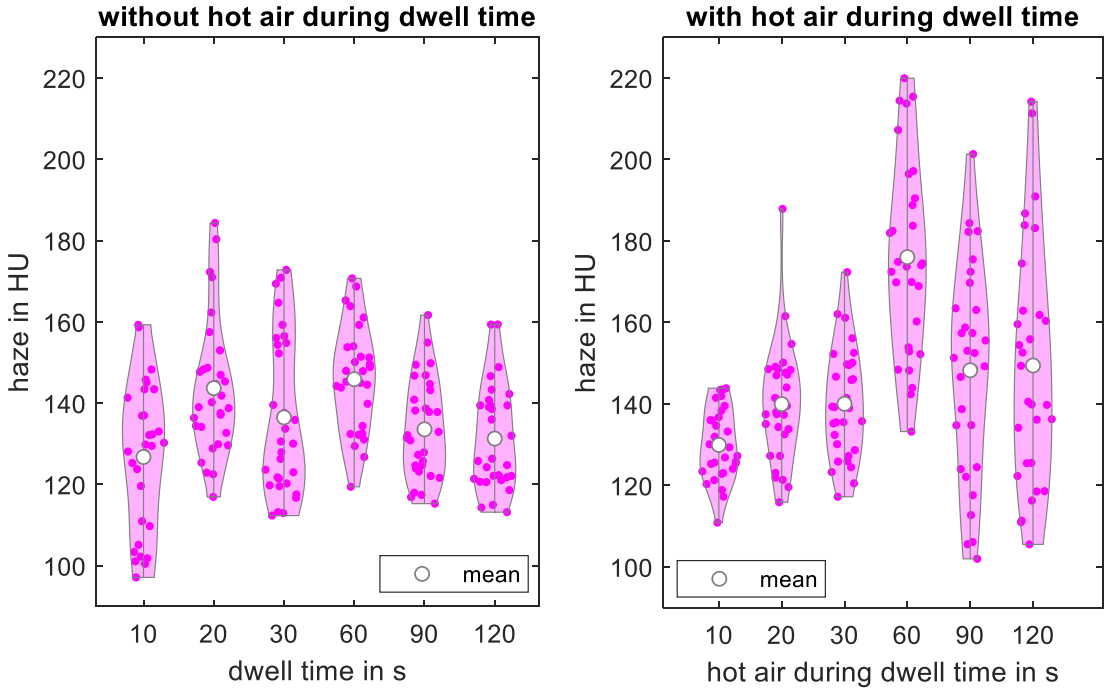

Figure 4.23: Haze measured with the IQ-S gloss meter on the series printed on Chromolux paper without and with hot air during dwell time printed with UV-ink containing VMPs. Each colored field consists of 30 measurements on three samples with the same print settings. The width of the area in the individual violin plots shows the density of the measuring points for a specific measured value range.

Results for inks containing cornflake pigments

The results of specular gloss measurements at 20° and 60° for ChromP_corn_nha and ChromP_corn_ha are shown in Figure 4.24. Based on dynamic gloss measurements, one could assume that for ChromP_corn_nha there should be a difference in specular gloss measured at 60° between dwell times of 10 and 20 seconds. For the combination ChromP_Corn (abbreviation explained in Table 4.5), changes in specular gloss could be observed within the first 20 seconds and the specular gloss level measured at 60° did not exceed 120 GU. It is likely that the cause of these differences is that dwell time was measured on Area 2 of the printed samples. Measurements shown in Figure 4.24 however were made on Area 1. No notable changes in specular gloss occur with longer dwell times. A further assumption for the differences could be that the curing of the UV-ink has influence on the gloss. Measurements carried out by Wang (2021) showed that there can be a slight decrease in specular gloss as a result of UV-curing. This could be due to a small shrinkage of the ink film due to the cross-linking of UV-initiators and polymers that can

result in puckering and wrinkling of the top layer of the ink and results in a lower gloss (Kim et al. 2002).

The use of hot air leads to an only small increase in specular gloss measured at 20°. While for samples made without hot air after 10 seconds of dwell time mean specular gloss values of 60 GU (20°) and 125 GU (60°) are reached, samples made with 10 seconds of hot air reach mean specular gloss values of 69 GU (20°) and 128 GU (60°). Such small differences in gloss are hardly visible to the eye.

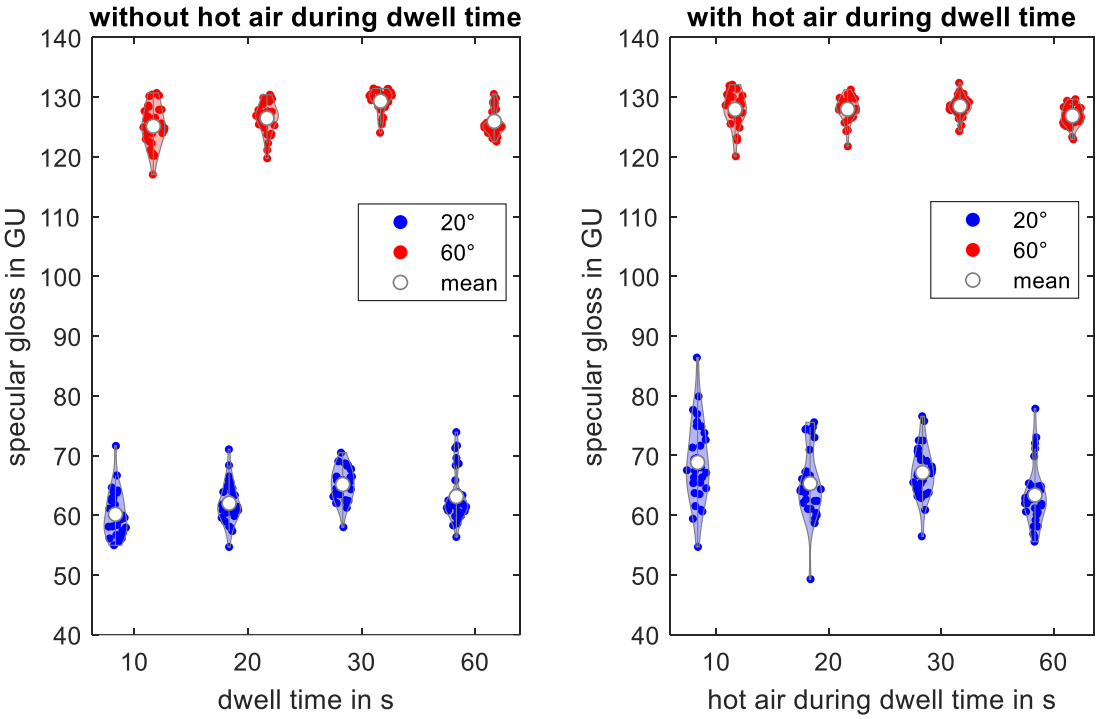

Figure 4.24: Specular gloss (20° and 60°) measured with the IQ-S gloss meter on the series printed on Chromolux paper without and with hot air during dwell time printed with UV-ink containing cornflake pigments. Each colored field consists of 30 data points measured on three samples with the same print settings. The width of the area in the individual violin plots shows the density of the measuring points for a specific measured value range.

The results of DOI and haze measurements on samples of ChromP_corn_nha and ChromP_corn_ha are shown in Figure 4.25 and 4.26. Similar to the specular gloss values, DOI and haze do not exhibit a clear trend. However, it can be observed that for longer dwell times, DOI is slightly lower for ChromP_corn_ha samples than for ChromP_corn_nha, while haze values are higher for ChromP_corn_ha samples. This could be attributed to the penetration of the binder into the substrate due to the ink's low viscosity at high temperatures, coupled with an extended time of the ink on the substrate in an uncured state.

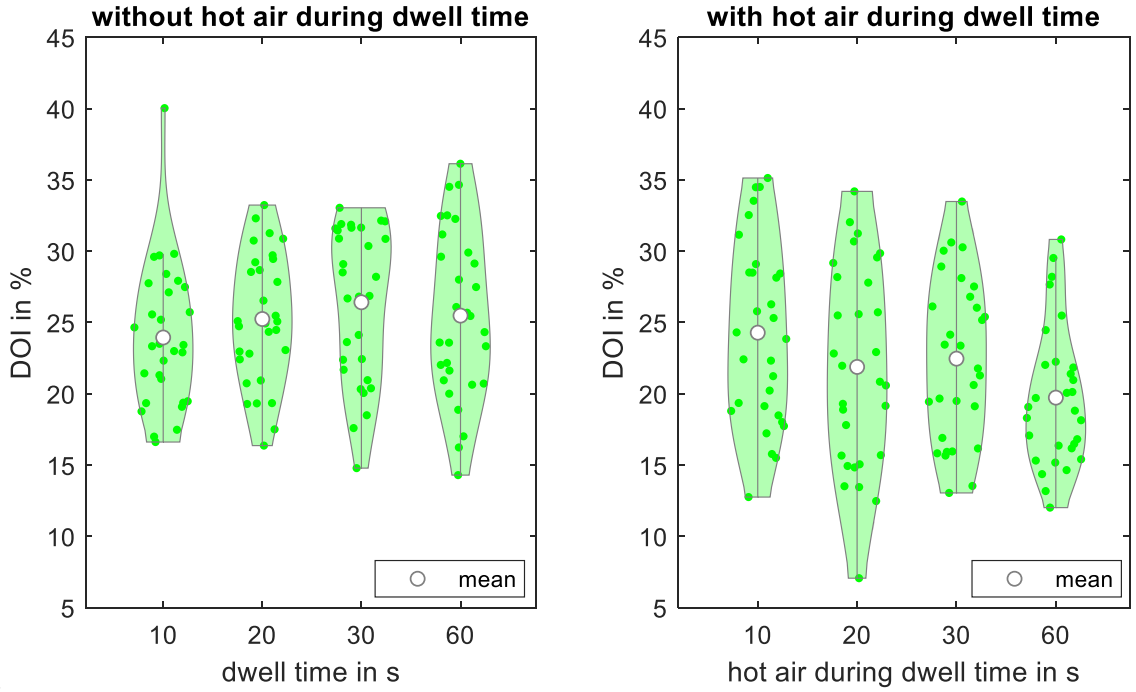

.

Figure 4.25: DOI measured with the IQ-S gloss meter on the series printed on Chromolux paper without and with hot air during dwell time printed with UV-ink containing cornflake pigments. Each colored field consists of 30 data points measured on three samples with the same print settings. The width of the area in the individual violin plots shows the density of the measuring points for a specific measured value range.

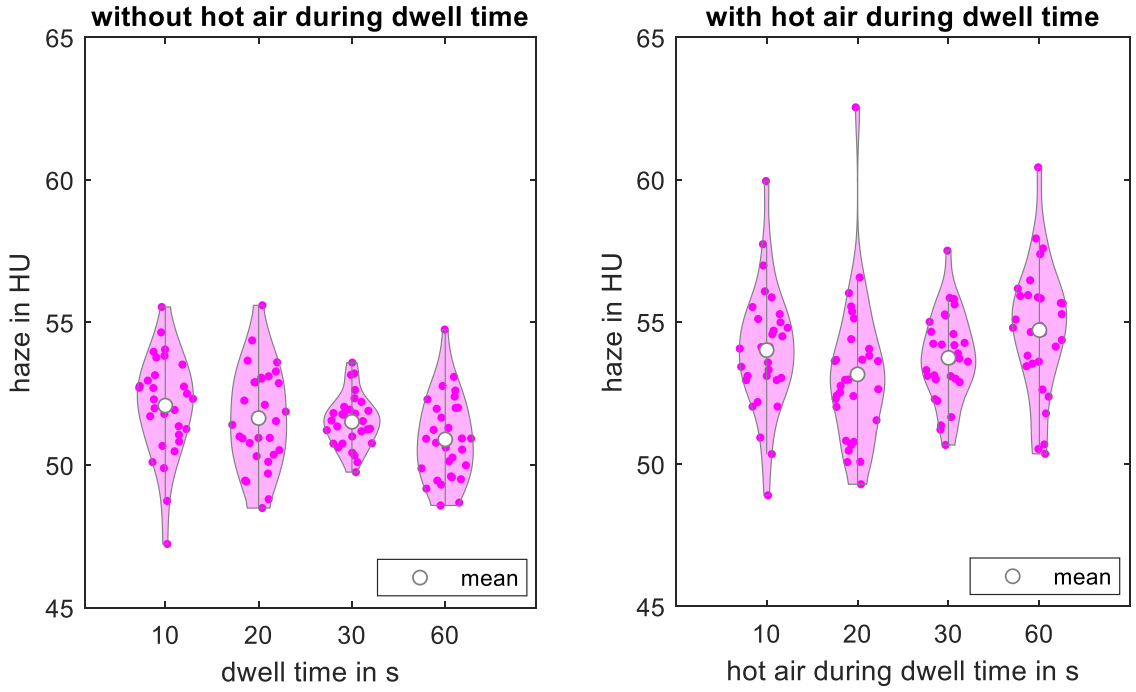

Figure 4.26: Haze measured with the IQ-S gloss meter on the series printed on Chromolux paper without and with hot air during dwell time printed with UV-ink containing cornflake pigments. Each colored field consists of 30 data points measured on three samples with the same print settings. The width of the area in the individual violin plots shows the density of the measuring points for a specific measured value range.

The application of hot air during dwell time caused a faster increase in specular gloss and DOI during when printing UV-ink-VMP on Chromolux paper. This positive influence of hot air on gloss can be attributed to a reduction in ink viscosity due to the increased temperature (see Section 4.2.3). However, this also means that for more ink-absorbent substrates, hot air could have a negative impact on gloss since lower ink viscosity may lead to faster binder absorption. The decision to use hot air depends on the substrate-ink combination, considering whether the benefits in results outweigh the increased energy costs for the production. Applying hot air to the printed ink UV-ink-corn would not be beneficial, as the positive effect on gloss is negligible.

4.5.2 Evaluation of the topography data

As shown in Figure 4.27, confocal images in the following are a merge of the height data that are in false colors with a share of 65 % and black/white light microscopy data with a share of 35 %. Both the pigments and the height data over the whole image are visible. Weber et al. (2023) chose a much lower share of the height data, which resulted in many black spots where there are no pigments. It was concluded that at these black spots no

height data could be obtained at all. However, the amount of points from where no height data could be obtained is smaller than previously assumed. Missing measurement values are generated if the sensor of the confocal microscope does not receive sufficient information from an area to compute the height for a specific pixel (Leach 2013).

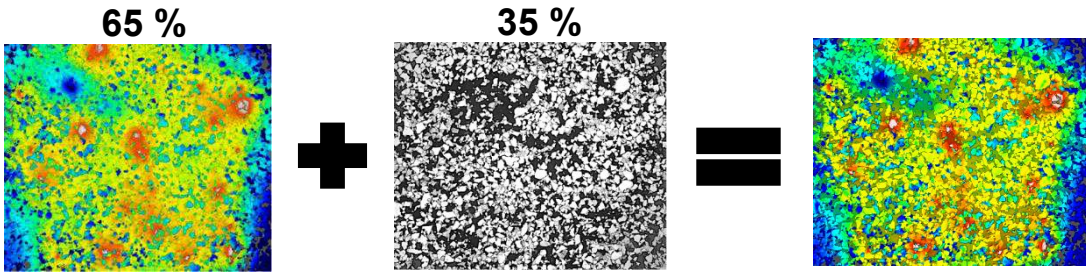

Figure 4.27: Composition of the confocal data shown in this dissertation. They comprise of the height data in false colors with a share of 65 % and the light microscopy image data with a share of 35 %.

Figure 4.28 displays confocal microscopy images captured on samples of ChromP_VMP_nha (abbreviations explained in Table 4.6) with dwell times of 10 s, 30 s, and 120 s. The data has been filtered for roughness and waviness. Due to an automatically applied cutoff on the image data when filtering it for roughness or waviness, the displayed images do not retain their original size of 340 x 284 µm² but were cropped to 260 x 200 µm². It is noticeable that both roughness and waviness decrease with the extension of dwell time, as evident from the growing uniformity of color in the microscope images. The white areas in the images represent heights not covered by the scale.

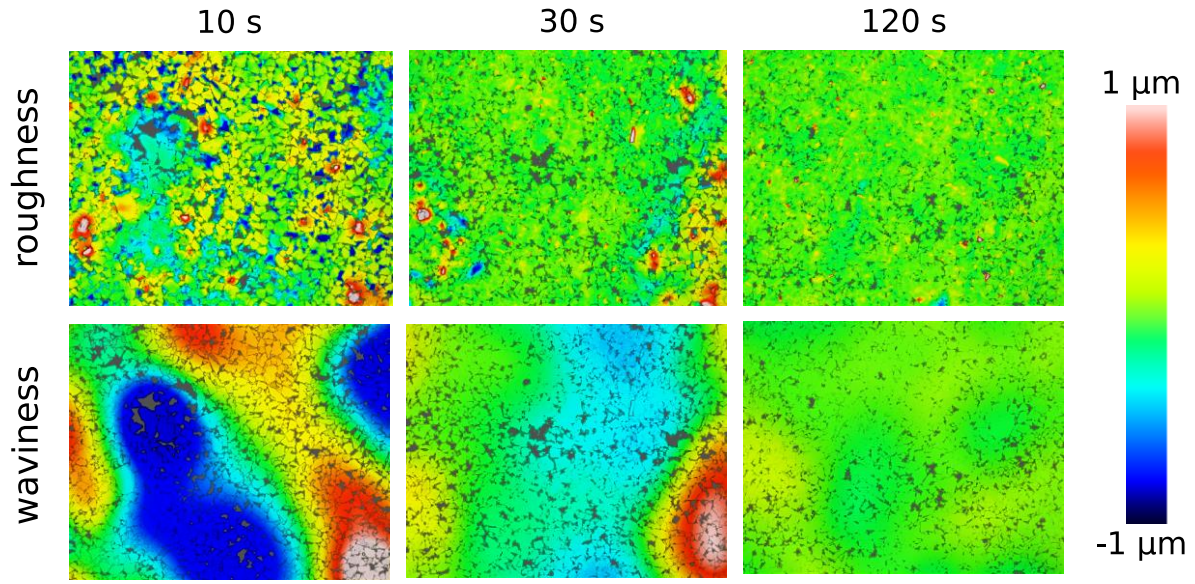

Figure 4.28: Confocal images of samples of ChromP_VMP_nha with dwell times of 10 s, 30 s, and 120 s selectively filtered for roughness and waviness obtained with the PLu neox. Each image has a size of 260 x 200 µm².

Figure 4.29 shows the confocal microscopy images captured on samples of ChromP_corn_nha with dwell times of 10 s, 20 s, and 60 s. Compared to the confocal data obtained from samples of ChromP_VMP_nha, a trend of decreasing roughness or waviness with a longer dwell time cannot be seen. Further, it is visible that the height deviations are higher than those of samples of ChromP_VMP_nha. Despite the enlarged scale for the data filtered for roughness, small white areas still appear which indicate heights that are not covered by the scale.

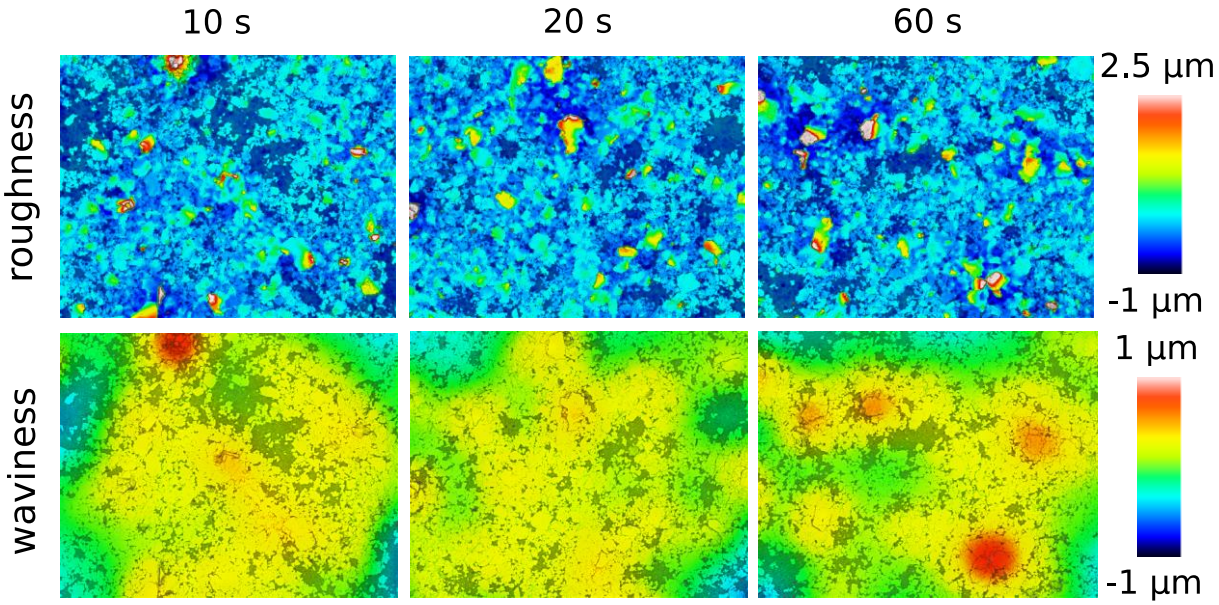

Figure 4.29: Confocal images of samples of ChromP_corn_nha with dwell times of 10 s, 20 s, and 60 s selectively filtered for roughness and waviness obtained with the PLu neox. Each image has a size of 260 x 200 µm².

3D-surface parameters obtained from ChromP_VMP_nha/ha

For the indication of the correlation between data, in the following, beneath Pearson's r, which is a measure for the linear correlation between two sets of data, also a rank correlation coefficient was used. Rank correlation coefficients are a measure of the difference of the ordinal association between two sets of data. The two most well-known rank statistics that were considered for the analysis of the data are Spearman's ρ coefficient and Kendall's τ coefficient (Monjardet 1997). If the order of two data sets is the same, both coefficients yield a value of 1 and if the orders are complete opposite, they yield -1. Spearman's ρ often yields higher values than Kendall's τ. However, large outliers have a greater impact on the Spearman coefficient (Croux and Dehon 2010; Gibbons 1993). There is no intuitive interpretation of Spearmans's ρ. Kendall's τ however can be

interpreted as the probability that a pair of points is concordant minus the probability that a pair of points is discordant (Bergsma and Dassios 2014). For this dissertation it was chosen to use Kendall's τ.

In the course of the evaluation of the 3D-surface parameters Sq and Sdq (explained in Section 4.4.2), it was found that the highest correlations with gloss data can be found for specular gloss measured at 60°. In Figure 4.30, the 3D-surface parameters Sq and Sdq obtained from the sets of ChromP_VMP_nha (abbreviations explained in Table 4.6) are plotted against specular gloss measured at 60°. In the upper row, 3D-surface parameters obtained from topography measurements filtered for roughness are plotted. In the bottom row, 3D-surface parameters obtained from topography measurements filtered for waviness are plotted. It can be seen that there are high negative correlations between specular gloss measured at 60° and the selected 3D-surface parameters. For the range of data represented by this dataset, a linear relationship between specular gloss measured at 60° and Sq and Sdq parameters can be assumed. It can be seen that for the Sq values obtained from the roughness data, there is no clear differentiation between samples with a dwell time of 90-120 seconds, as they all exhibit very small values between 0.005 µm and 0.003 µm. However, the roughness data of the same samples show better differentiation for the Sdq parameter. The scale for the Sq parameter is consistent for both roughness and waviness data, ranging from 0 µm to approximately 0.5 µm. For the Sdq parameter however the scale for waviness data is smaller by a factor of ten compared to the scale for roughness data. The reason for this is that the gradients between the single pigments that are not at the same height level are much higher than the gradients of the waviness.

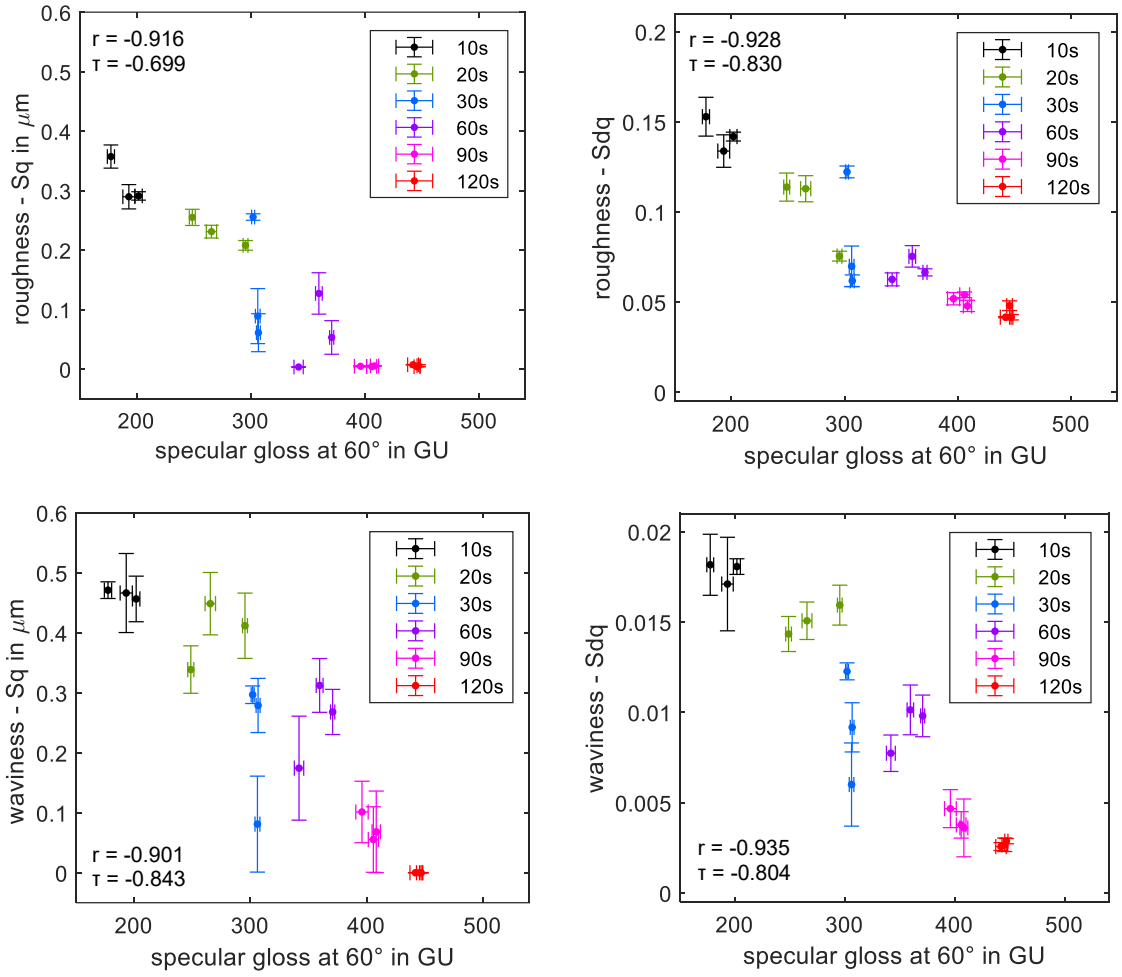

Figure 4.30: ChromP_VMP_nha roughness and waviness data and specular gloss measured at 60° with the IQ-S gloss meter. Each data point represents one sample of which ten gloss measurements and three topography measurements were obtained with a PLu Neox confocal microscope. The whiskers on the points show the standard error of the mean. Pearson's r and Kendal's τ correlation coefficients are given.

In Figure 4.31, specular gloss measured at 60° is plotted against 3D-surface parameters Sq and Sdq obtained from the sets of ChromP_VMP_ha. Here, no linear relationship can be observed. Interestingly, samples on which hot air was applied for 20 seconds or longer do not differ greatly in terms of Sq and Sdq values.

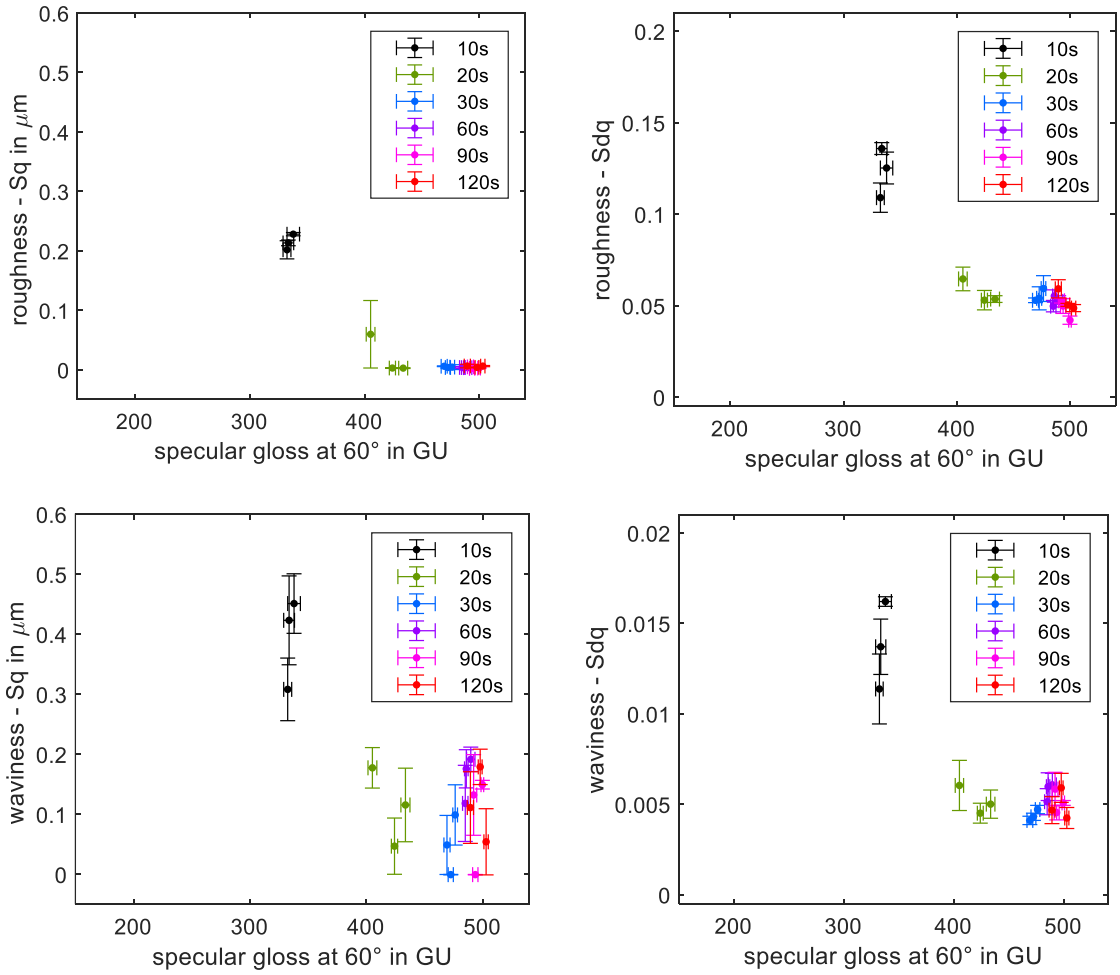

Figure 4.31: ChromP_VMP_ha Sdq roughness and waviness data and gloss 60 with the IQ-S gloss meter. Each data point represents one sample of which ten gloss measurements and three 3D-topography measurements were obtained with a PLu Neox confocal microscope. The whiskers on the points show the standard error of the mean.

3D-surface parameters obtained from ChromP_corn_nha/ha

Measured 3D-surface parameters Sq and Sdq obtained from the sets of ChromP_corn_nha and ChromP_corn_ha (abbreviations explained in Table 4.6) are shown in Figure 4.32. As could be expected on basis of the gloss measurements on these samples, the dwell time or the time of hot air during dwell time respectively does not affect roughness or waviness parameters to a great extent. It can be seen that for time intervals of 10 and 20 seconds, Sq roughness, Sq waviness, and Sdq waviness parameters are smaller for samples produced with hot air during dwell time than samples produced without hot air during dwell time. This corresponds with the higher specular gloss values measured on them.

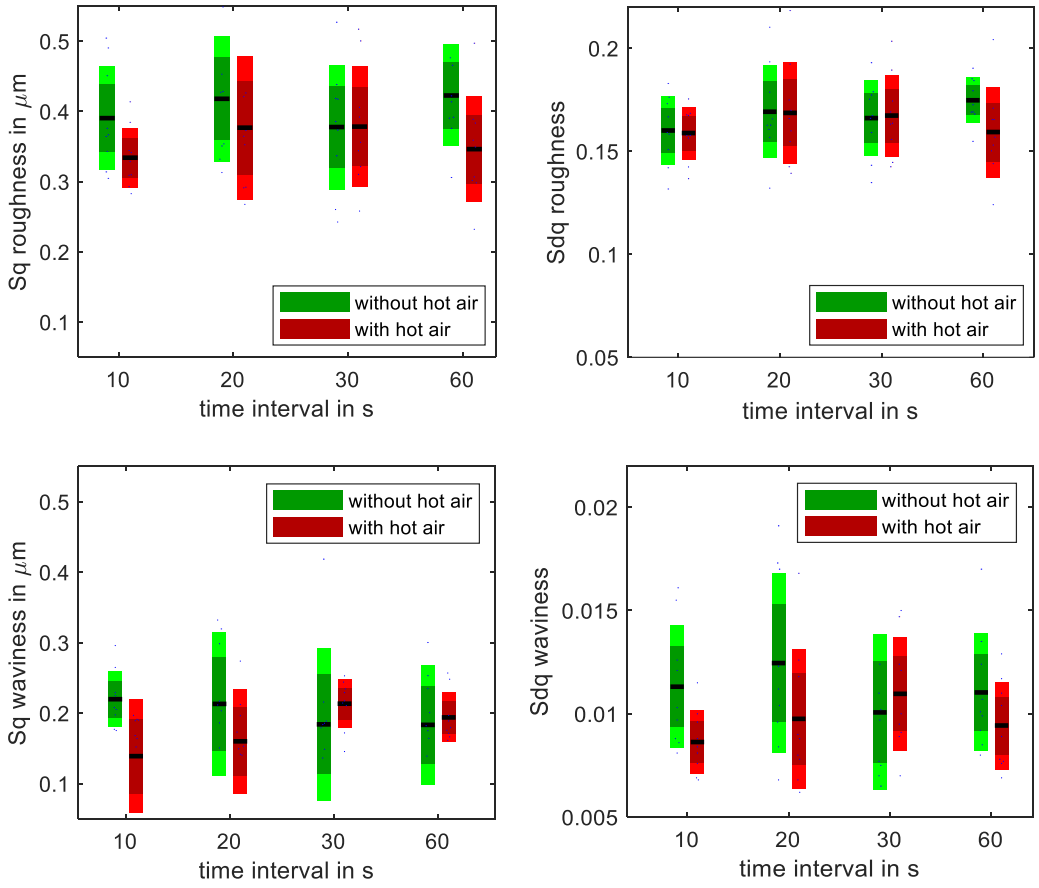

Figure 4.32: 3D-surface parameters obtained from on samples printed with UV-ink containing cornflake pigments on Chromolux paper. Each box comprises nine topography measurements made with a PLu Neox confocal microscope on three different samples that were printed with the same print settings. The black dashes represent the mean values. Darker areas represent the standard error of the mean and lighter areas the standard deviation of the measurements. The graphs were made using a modified version of a Matlab function by Campbell (2023).

Comparision of 3D-surface parameters obtained from ChromP_corn_ha(10) and ChromP_VMP_nha(10)

When comparing the 3D-surface parameters Sq and Sdq measured on samples printed with UV-ink-corn (abbreviation explained in Section 4.3.2) with samples printed with UV-ink-VMP, it is noticeable that the 3D-surface parameters do not differ to a great extent, as the measured gloss values might suggest. Table 4.7 compares mean gloss values and 3D-topography values measured on the set ChromP_VMP_nha(10) (abbreviation see Table 4.6), which includes samples printed with ink containing VMPs with the lowest specular gloss values with the set ChromP_corn_ha(10), which includes samples printed

with ink containing cornflake pigments with some of the highest specular gloss values. While specular gloss values differ by about 80 GU (20°) and 60 GU (60°), roughness values only differ to a small amount. For ChromP_corn_ha(10), the Sq and Sdq parameters obtained from data filtered for waviness are even smaller by more than 50 % when compared to ChromP_VMP_nha(10). This shows that the data extracted from the topography measurements are not suited for the comparison between samples with different pigment types. The decisive difference between the samples of ChromP_corn_ha(10) and ChromP_VMP_nha(10) is the roughness of the pigments themselves that is not part of the extracted roughness data due to the long pass filter of λ_S = 2.50 µm that was applied to the data to filter out noise from the roughness data.

Table 4.7: Mean values of 30 gloss measurements with the IQ-S gloss meter and measured 3D-surface parameters (measured and evaluated as explained in Section 4.4.2) on Area 1 (see Figure 4.3) of the samples of ChromP_corn_ha(10) and ChromP_VMP_nha(10).

	ChromP_corn_ha(10)	ChromP_VMP_nha(10)
Gloss20	69 GU	146 GU
Gloss60	128 GU	191 GU
DOI	24 %	26 %
Haze	54 HU	127 GU
Sq roughness	0.3341 µm	0.3126 µm
Sdq roughness	0.1589	0.1428
Sq waviness	0.1389 µm	0.4644 µm
Sdq waviness	0.0086	0.0178

Only for samples of ChromP_VMP_nha (abbreviation explained in Table 4.6), a strong linear negative correlation between the obtained 3D-surface parameters Sq and Sdq and specular gloss measured at 60° could be observed. The application of hot air disrupts this linear correlation between the 3D-surface parameters and specular gloss measured at 60°. Nevertheless, a negative correlation between the 3D-surface parameters and specular gloss measured at 60° still exists. Meaningful comparisons can only be made among samples with similar print settings and materials, utilizing the 3D-surface parameters Sq and Sdq. However, employing these parameters to compare samples printed with UV-ink-corn and UV-ink-VMP does not explain any differences in gloss.

4.6 Transfer to an industrial printing machine

In addition to the experiments using a flexo print proofer, trials were carried out on an industrial web-fed printing machine to evaluate how the results obtained from the laboratory experiments could potentially be transferred to an industrial printing machine.

4.6.1 Experimental setup

The used narrow-web printing machine was a modular Gallus RCS330-HD (Gallus, Switzerland). This type of machine is used in industrial production, mainly in label printing. As described in more detail by Haas (2012), this specific machine is unique in the world due to its special configuration and modularity. For instance, flexo, gravure, screen, offset printing, and inkjet printing can all be used at the same time and the order of the printing units is interchangeable. Further, it is equipped with a hot air/IR dryer module (IST METZ, Germany) with a maximum power of 24 kW and a length of 0.8 m. In order to reduce blow shadows on the samples, a spacer of 10 cm was inserted on the closing side of the hood of the hot air dryer. The dryer module and pronounced blow shadows caused when no spacer is used are shown in Figure 4.33. This resulted on a slight tilt of the hood and a greater distance between the blower and the web. Irregularities in terms of gloss of the samples due to the tilt could not be determined. During the experiment, a temperature of about 70°C and 75°C was measured on the paper web right at the dryer outlet using a PeakTech 4960 infrared thermometer (PeakTech, Germany). The UV-curing unit of the machine has a maximum power of 200 W/cm. Substrate rolls with a maximum width of up to 330 mm can be printed on. The maximum printing speed of the Gallus RCS330-HD is 160 m/min.

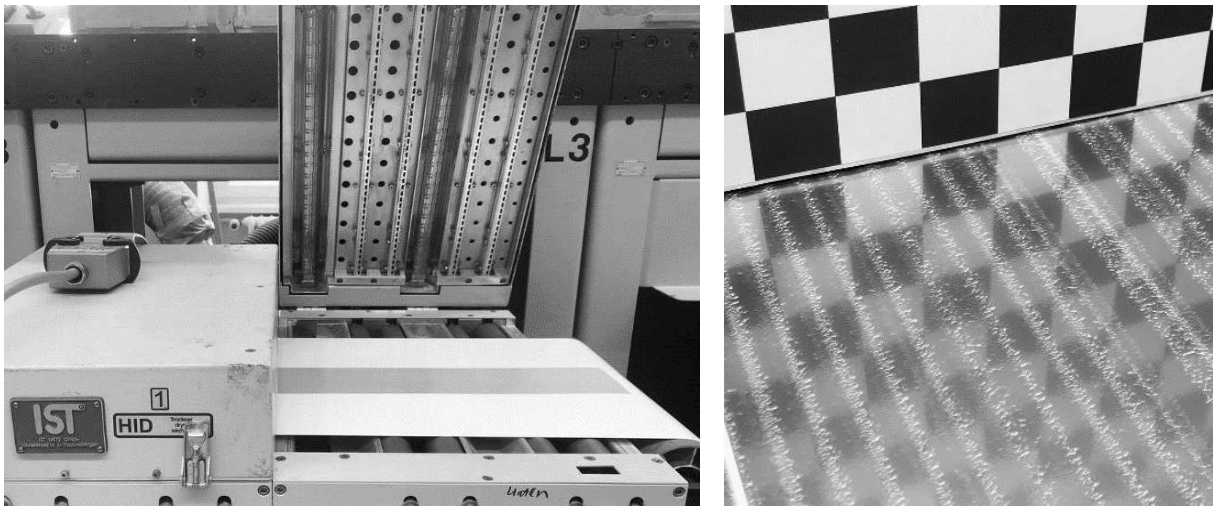

Figure 4.33: Hot air dryer of the Gallus RCS330-HD (left image) with opened hood. The IR-emitters, which were not used in this study, nozzles for hot air supply (elongated) and hot air exhaust (round) can be seen. The blow shadows (right image) that are caused when closing the hood and running the machine at low speed with hot air turned on. To reduce the blow shadows, a spacer of 10 cm was inserted on the closing side of the hood.

The same UV-ink containing VMPs was used as in the experiments on dynamic gloss and dwell time, described in Section 4.2.3. Two different sorts of UV-primer were used on paper. The first, that is referred to as 'Primer 1' in the following was the E46 primer (Siegwerk, Deutschland), which was also used for LumiArt paper in the experiment on dynamic gloss (see Section 4.2.3). The second primer, that is referred to as 'Primer 2' in the following was the unpigmented binder system of the ink containing VMPs and was provided by Schlenk Metallic Pigments (Germany). It appears slightly yellowish. Metallic ink and both types of UV-primer were printed using a flexo printing unit equipped with a chambered doctor blade system (see Figure 2.8) and an anilox roller with a volume of 9.3 ml/m², 200 lines/cm and a 60° cell engraving. The configuration of the Gallus RCS330-HD chosen for the experiment can be seen in Figure 4.34. The flexo printing unit was positioned 4.8 m away from the inlet of the hot air dryer. The curing of the UV-ink was after the hot air dryer.

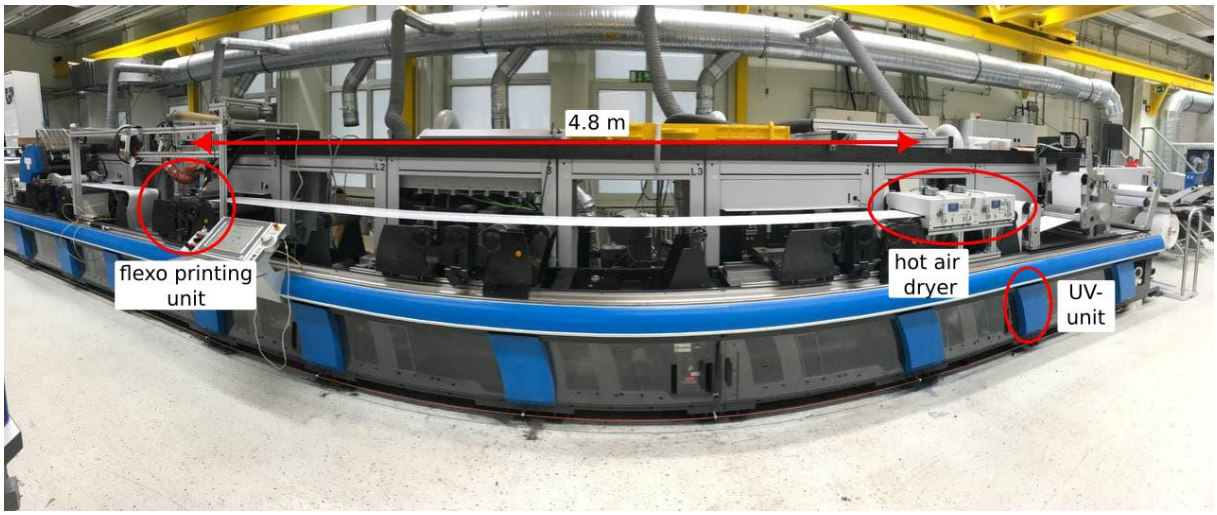

Figure 4.34: Configuration of the Gallus RCS330-HD with flexo printing unit, hot air dryer and UV-unit. The flexo printing unit has a distance of 4.8 m from inlet of the substrate into the hot air dryer module. The web direction is from left to right.

Substrates different to those used in previous experiments had to be used, as LumiArt paper and Chromolux paper were not available in roll form. One substrate used was Digi Finesse paper (UPM, Finland) with a grammage of 135 g/m² (called 'paper' in the following), which is a supercalandered glossy paper and designed for digital printing. However, it is also usable for flexo printing. It was chosen for the reason that no other high quality paper with a smooth surface was available at the time of the experiment. It is commonly used for advertising material, art books or brochures (UPM n.d.). Beneath the paper, also Melinex 339 film with a thickness of 100 µm (DuPont Teijin Films, Luxemburg) was used to study the effect of dwell time on a non-absorbent substrate (called 'film' in the following). It is an opaque film, which is pre-treated on both sides to promote adhesion to most industrial coatings. It is typically used for security and access cards, multiple use tickets or as photographic printing substrate (DuPont Teijin Films n.d.).

Both UV-primer and metallic ink were printed at a speed of 40 m/min. For some of the printed samples, the printing speed, and consequently, the speed of the web, was abruptly reduced after printing. At this reduced speed, the web, along with the area from which the sample was extracted, was moved towards the hot air dryer and UV-curing unit. By doing so, samples could be produced that differed in dwell time and the time in the hot air dryer. Care was always taken to cut out samples that were printed at 40 m/min and had the longest possible path to the hot air inlet. However, it should be noted that this method can have inaccuracies. For some of the samples, hot air during dwell time was used, for other samples the hot air drying unit was switched off. The materials and settings used to print

the individual samples are shown in Table 4.8. For samples printed on primed paper, first the UV-primer was printed. After the UV-primer application, the metallic ink was printed in a separate print run. All samples obtained in the experiment had a size of 260 x 400 mm^2. The gloss measurements were made according to the standard measurement scheme of this work, described in Section 3.2. On each sample, five topography measurements were carried out on each sample. One measurement in each of the four corners of the samples and one in the middle. General information on topography measurements of this dissertation are given in Section 4.4.2.

Table 4.8: Overview of the samples printed on the Gallus RCS330-HD. The rows highlighted in blue show the different settings and materials used for printing UV-primer on the paper. Rows highlighted in red show the settings chosen for printing the metallic ink on film. Rows highlighted in green show the settings and materials chosen for printing the metallic ink onto paper or primed paper. In the right column, the abbreviations are given that are used as denotation of the samples in the following.

Printed sort of UV-primer or metallic UV-ink (VMP)	Substrate	Speed of the web after printing in m/min	Use of hot air unit	Sample name
Primer 1	Paper	40	No	P_1
Primer 1	Paper	1	Yes	P_2
Primer 2	Paper	40	No	P_3
Primer 2	Paper	1	Yes	P_4
Primer 2	Paper	40	Yes	P_5
Metallic ink	Film	40	No	F_40_N
Metallic ink	Film	20	No	F_20_N
Metallic ink	Film	10	No	F_10_N
Metallic ink	Film	5	No	F_5_N
Metallic ink	Film	1	No	F_1_N
Metallic ink	Film	40	Yes	F_40_Y
Metallic ink	Film	1	Yes	F_1_Y
Metallic ink	Primed paper (P_1)	40	No	P_P1_40_N
Metallic ink	Paper (no primer)	40	No	P_40_N
Metallic ink	Primed paper (P_2)	40	No	P_P2_40_N
Metallic ink	Primed paper (P_3)	40	No	P_P3_40_N
Metallic ink	Primed paper (P_4)	40	No	P_P4_40_N
Metallic ink	Primed paper (P_5)	1	No	P_P5_1_N
Metallic ink	Primed paper (P_5)	20	No	P_P5_20_N
Metallic ink	Primed paper (P_5)	40	No	P_P5_40_N
Metallic ink	Primed paper (P_5)	1	Yes	P_P5_1_Y
Metallic ink	Primed paper (P_5)	40	Yes	P_P5_40_Y

4.6.2 Impact of post-printing web speed on gloss

In order to analyze the impact of the post-printing web speed that influences the dwell time, gloss of five different samples using film as substrate and three samples using paper

that was primed under the same conditions for the three samples was analyzed. The samples with primed paper as substrate are P_P5_40_N, P_P5_20_N and P_P5_1_N. Samples printed on film are F_40_N, F_20_N, F_10_N, F_5_N and F_1_N (abbreviations explained in Table 4.8). The speed of the web after printing varied between 40 m/min and 1 m/min. All of these samples were printed without the use of hot air during dwell time. A picture of the samples is shown in Figure 4.35. For the samples printed on primed paper, it cannot be seen that the checkerboard pattern is reflected clearer or sharper as the speed of the web decreases. For samples printed on film however, a slight increase in sharpness can be seen from F_40_N to F_5_N. The reflection of F_1_N is again a bit more blurry. It has to be noted that printing errors recognizable as small bright dots can be seen on sample F_1_N as shown in the upper right image of Figure 4.35.

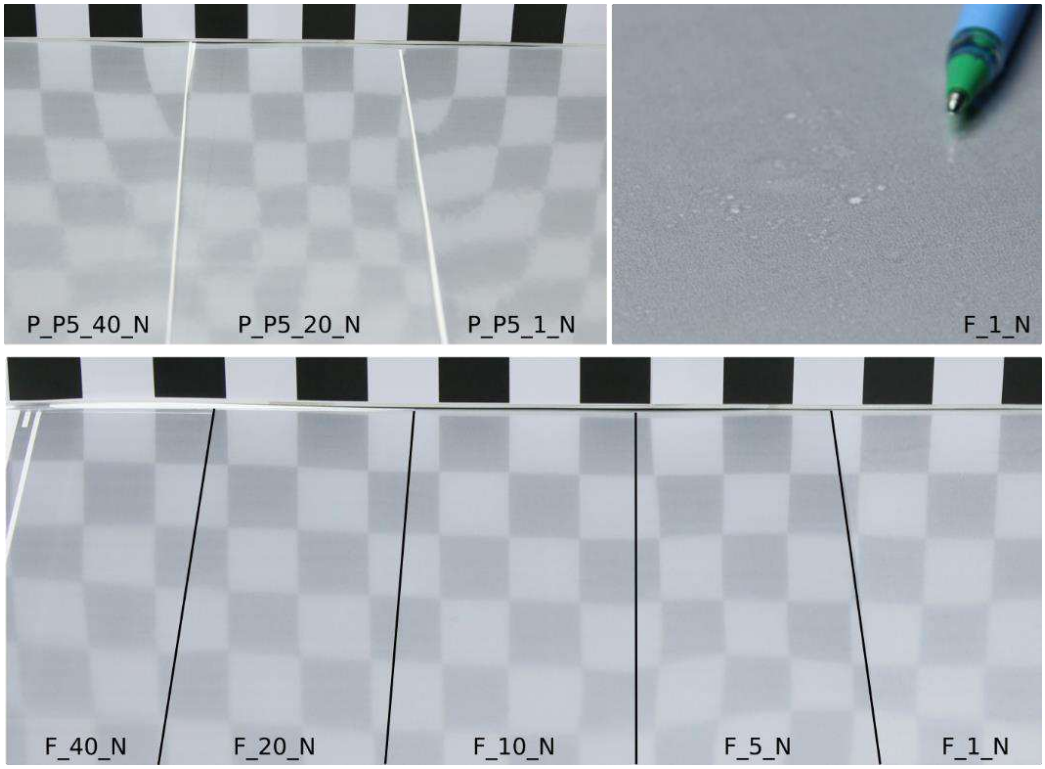

Figure 4.35: Samples printed without hot air on primed paper (upper left) or film (bottom image) with different web speeds after printing the metallic ink. Abbreviations and corresponding print parameters are given in Table 4.8. The single number (1, 5, 10, 20, 40) in the sample names stands for the speed of the web after printing. The upper right image shows print errors on the sample F_1_N.

Figure 4.36 shows the specular gloss data measured at 20° and 60° on these samples. For the samples printed on paper it can be seen that a slower web speed after printing has a slightly positive impact on specular gloss values measured at 20°. Specular gloss measured

at 60° however does not rise much as the web speed is reduced from 40 m/min to 20 m/min. If the web speed is reduced to 1 m/min, specular gloss measured at 60° decreases slightly while specular gloss measured at 20° increases. A similar observation can be made for the specular gloss values measured on samples that have film as substrate. As the web speed is reduced from 40 m/min to 5 m/min, the mean of specular gloss measured at 20° and 60° increases from 219 GU to 263 GU (20°) and from 201 GU to 216 GU (60°). However, as the web speed is further reduced, specular gloss measured at 20° drops sharply to 213 GU while at the same time specular gloss measured at 60° increases to 223 GU. No good explanation for the sharp drop of specular gloss measured at 20° can be given. It cannot be excluded that it could be attributed to incorrect sampling. It is possible that a portion of the web cut out as a sample was printed with a reduced web speed, rather than the intended web speed of 40 m/min. To get a clear answer, the experiment would have to be repeated.

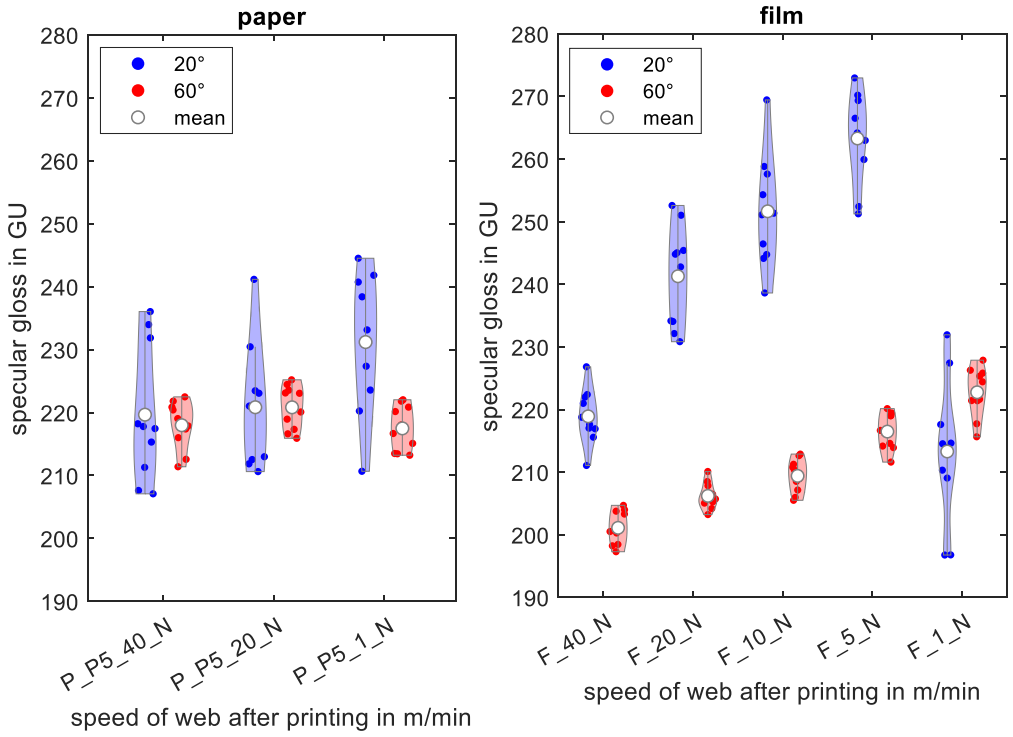

Figure 4.36: Specular gloss (20° and 60°) measured with the IQ-S gloss meter on samples (sample names on the x-axes) with primed paper as substrate (left) and film as substrate (right) differing in the speed of the web after printing. Each colored field includes ten specular gloss values. The width of the area in the individual violin plots shows the density of the measuring points for a specific measured value range. Abbreviations and corresponding print parameters are given in Table 4.8. The single number (1, 5, 10, 20, 40) in the sample names stands for the speed of the web after printing.

Figure 4.37 shows the DOI and haze data measured on these samples. For the samples printed on primed paper, only a very small increase in DOI can be seen which is from 25 % to 27 %. DOI values measured on samples printed on film are generally higher as the mean DOI values range from 40-60 % with the highest values measured for the sample with 10 m/min of web speed after printing and the lowest for the samples with 1 m/min of web speed after printing. While for the samples printed on primed paper the haze decreases as the web speed is decreased, for samples printed on film, there is only one sharp increase of haze for sample F_1_N.

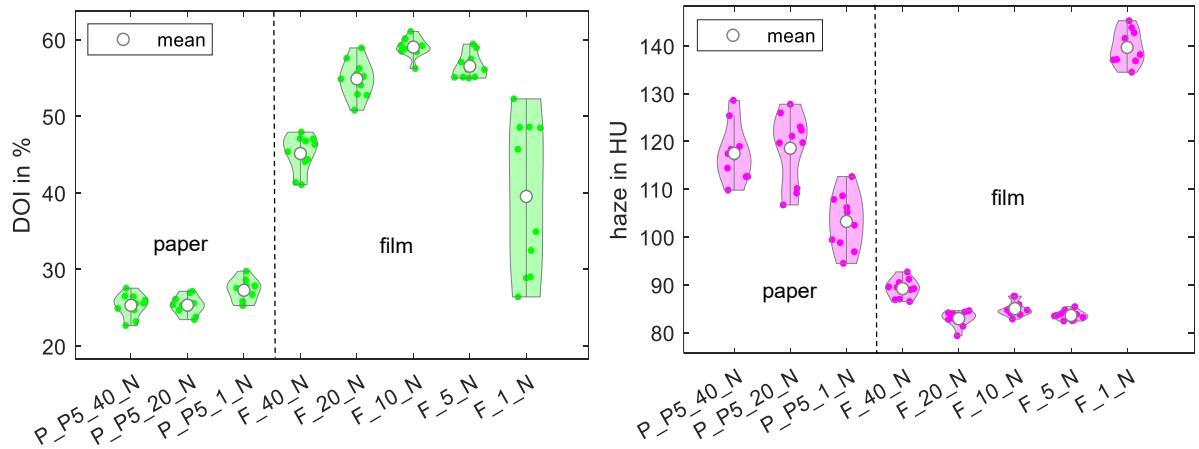

Figure 4.37: DOI (left) and haze (right) measured with the IQ-S gloss meter on samples with primed paper as substrate (left) and film as substrate (right) differing the speed of the web after printing (sample names on the x-axes). Each colored field includes ten DOI or haze values. The width of the area in the individual violin plots shows the density of the measuring points for a specific measured value range. Abbreviations and corresponding print parameters are given in Table 4.8. The single number (1, 5, 10, 20, 40) in the sample names stands for the speed of the web after printing.

As for the laboratory experiments using Chromolux paper as substrate and UV-ink-VMP, also for printing on the industrial printing machine a mostly positive impact on specular gloss for a longer dwell time that comes with a slower web speed after printing could be observed.

4.6.3 Influence of hot air after printing on gloss

For the analysis of the influence the hot air after printing, selected sample pairs printed on primed paper are P_P5_40_N/ P_P5_40_Y and P_P5_1_N/ P_P5_1_Y (abbreviations explained in Table 4.8). Selected sample pairs printed on film are F_40_N/ F_40Y and F_1_N/ F_1_Y. Pictures of these samples are shown in Figure 4.38. The light blow shadows

on the sample printed on film with a low web speed of 1 m/min after printing and with hot air turned on are also shown.

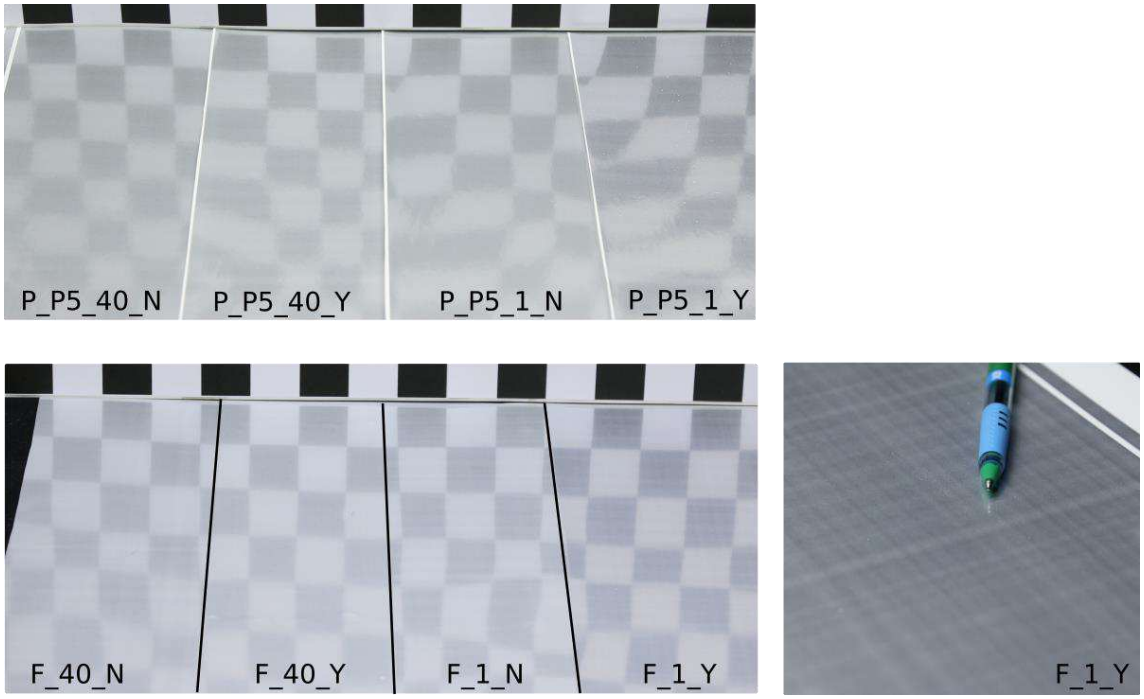

Figure 4.38: Sample pairs printed on primed paper (upper left) and film (bottom left). For each substrate, two pairs were selected that only differ in the use of hot air after printing. Abbreviations and corresponding print parameters are given in Table 4.8. The single number in the sample names stands for the speed of the web after printing. Light blow shadows on sample F_1_Y can be seen in the bottom right image.

Specular gloss values measured at 20° and 60° on these samples are shown in Figure 4.39. For all four pairs it can be seen that the use of hot air has a positive influence on specular gloss. This is especially true for the pair P_P5_1_N/ P_P5_1_Y. Interestingly, for the pair F_1_N/ F_1_Y, specular gloss measured at 60° is always higher than specular gloss measured at 20°. This means that on their surface a greater light scattering takes place, what is also reflected in the haze values shown in Figure 4.40. While the haze values measured on the samples printed on primed paper are more affected by hot air, the effect on haze measured on samples with film as substrate is negligible. It can also be seen that the use of hot air on samples printed on both primed paper and film only has a small impact on DOI.

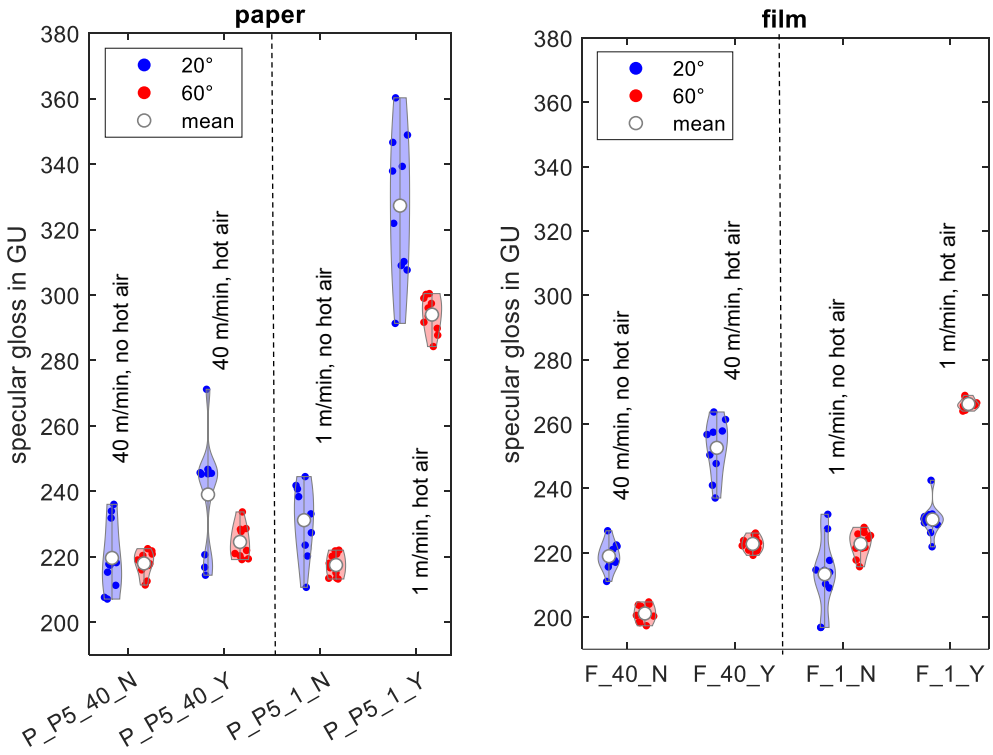

Figure 4.39: Specular gloss (20° and 60°) measured with the IQ-S gloss meter on samples (sample names on the x-axes) with primed paper as substrate (left) and film as substrate (right) differing the use of hot air after printing. Each colored field includes ten measured specular gloss values. The width of the area in the individual violin plots shows the density of the measuring points for a specific measured value range. Abbreviations and corresponding print parameters are given in Table 4.8.

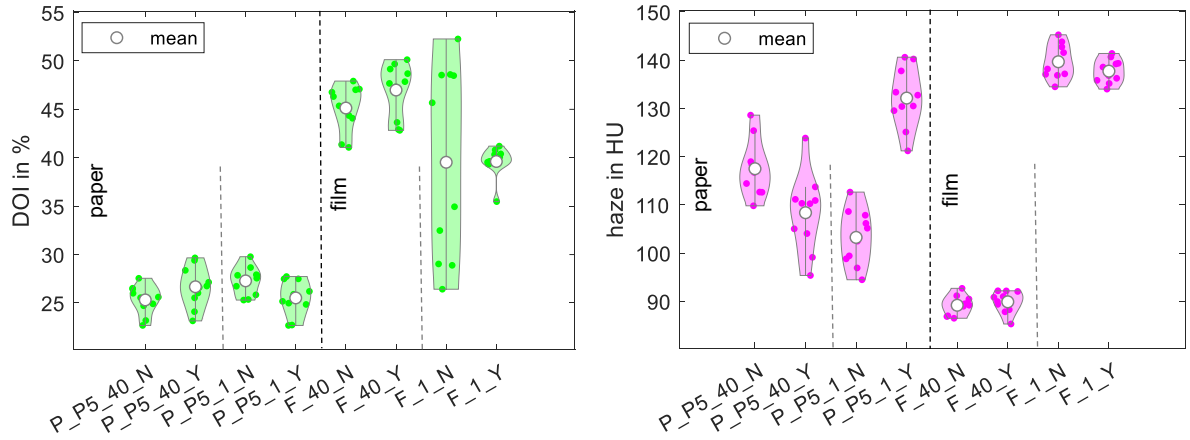

Figure 4.40: DOI (left) and haze (right) measured with the IQ-S gloss meter on samples (sample names on the x-axes) with primed paper as substrate (left) and film as substrate (right) differing the use of hot air after printing. Each colored field includes ten DOI or haze values. The width of the area in the individual violin plots shows the density of the measuring points for a specific measured value range. Abbreviations and corresponding print parameters are given in Table 4.8.

As for the laboratory experiments using Chromolux paper as substrate and UV-ink-VMP (see Section 4.3), also for samples printed on the industrial printing machine a positive impact on specular gloss through the application of hot air could be observed.

4.6.4 Influence of UV-primer application on gloss

Using the samples printed on paper and primed paper, the influence of the application of UV-primer was investigated. Samples, which were produced with no reduction of the web speed after printing the metallic ink and for which no hot air was used, were selected. A picture of the respective samples is shown in Figure 4.41. For sample P_40_N, no UV-primer was applied prior to printing. For samples P_P1_40_N and P_P2_40_N, Primer 1 was preprinted. For the primer application on sample P_P1_40_N, the speed of the web was not reduced after printing and no hot air was applied. For the primer application on sample P_P2_40_N, the speed of the web was reduced to 1 m/min after printing UV-primer and hot air was applied.

For the samples P_P3_40_N, P_P4_40_N and P_P5_40_N, Primer 2 was used. For P_P3_40_N, no reduction of the web speed after primer application was made and the hot air was not turned on. For P_P5_40_N, also no reduction of the web speed took place but hot air was turned on. For P_P4_40_N, both a reduction in web speed to 1 m/min took place and hot air was turned on.

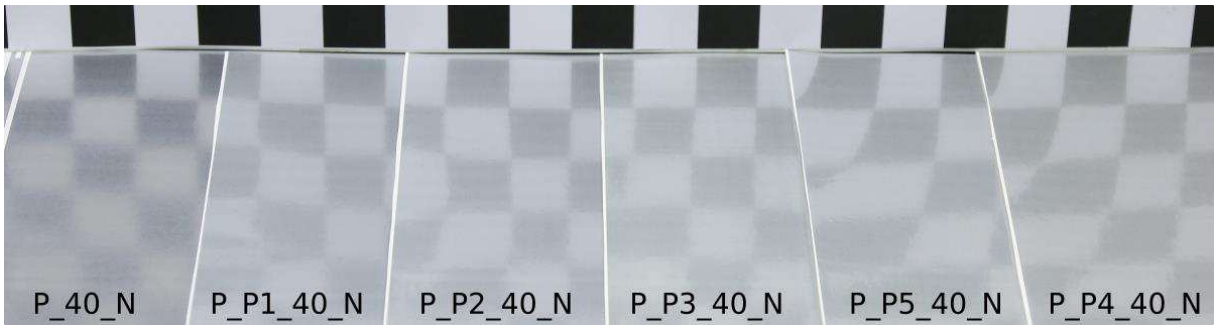

Figure 4.41: Samples only differing in the application of UV-primer onto the paper but with the same speed of the web after printing and no usage of hot air after printing. Abbreviations and corresponding print parameters are explained in Table 4.8.

Figure 4.42 shows specular gloss data measured on these samples. From the comparison of the sample P_40_N, printed on unprimed paper, to all the other samples printed on primed paper it can be seen that the application of UV-primer has a great impact on specular gloss measured at 20°. The mean specular gloss measured at 20° is at least 90 GU higher for samples with primer preprint. Specular gloss measured at 60° is affected less, as this value measured on the samples with primer preprint deviates by a maximum of only 17 GU from sample P_40_N.

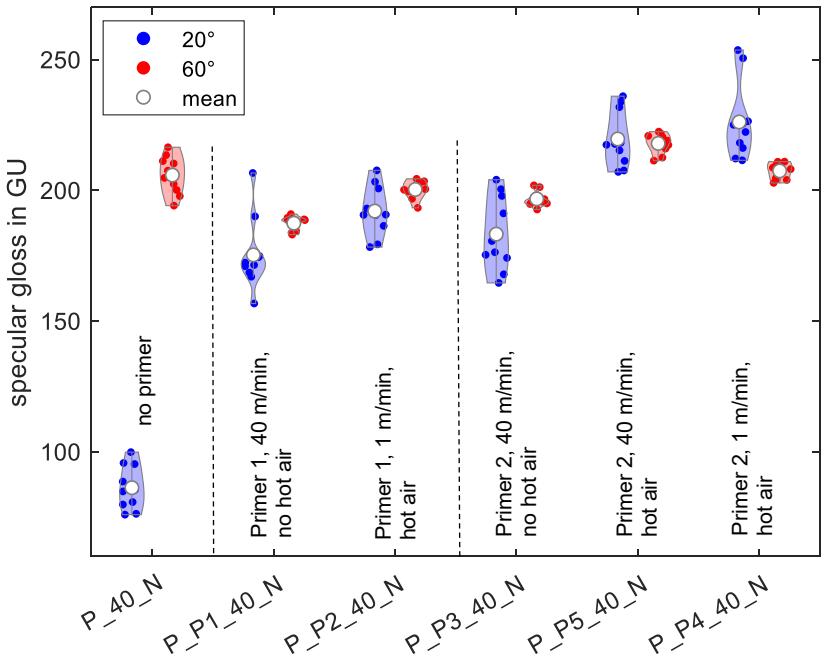

Figure 4.42: Specular gloss (20° and 60°) measured with the IQ-S gloss meter on samples printed on paper or primed paper (sample names on the x-axes). The way of primer application differed between the samples and important settings for the primer application are given in the figure. Each colored field includes ten measured specular gloss values. The width of the area in the individual violin plots shows the density of the measuring points for a specific measured value range. Abbreviations and corresponding print parameters are given in Table 4.8.

The influence of the UV-primer type can be seen when comparing sample P_P1_40_N with P_P3_40_N, and P_P2_40_N with P_P4_40_N. The print parameters of the two samples in each pair only differ in the sort of UV-primer. For both pairs, the sample with Primer 2 yields higher mean specular gloss values measured at 20° and 60°. This is more apparent for the samples of the latter pair for which the web speed was reduced to 1 m/min after primer application and hot air was applied. While the mean specular gloss measured on P_P2_40_N is 192 GU (20°) and 200 GU (60°), the mean specular gloss measured on P_P4_40_N is 226 GU (20°) and 207 GU (60°).

For an assessment of the influence of the reduction of the web speed after printing the UV-primer and the increased dwell time of the UV-primer, only a comparison of the samples P_P5_40_N and P_P4_40_N can be made. While the increased dwell time of the UV-primer leads to an increase of the mean specular gloss measured at 20° by 7 GU, mean specular gloss measured at 60° is reduced by 10 GU. In terms of specular gloss, applying

hot air on the printed UV-primer seems to have a greater and more positive impact on the gloss of the overprinted metallic ink.

When looking at the DOI and haze data shown in Figure 4.43, it is noticeable that the primer preprint increases the mean DOI values by at least 6 % and decreases haze. While the two different primer print settings used for the application of Primer 1 do not seem to have influence on DOI or haze, the three different print settings for the application of Primer 2 do have influence on DOI and haze. When comparing P_P3_40_N and P_P5_40_N, it can be observed that hot air results in a slight increase of the mean DOI value by only 1 % and a 10 HU increase in haze. Additionally, reducing the web speed, as done for sample P_P4_40_N, further increases the mean DOI by 2 % and decreases haze by 15 HU.

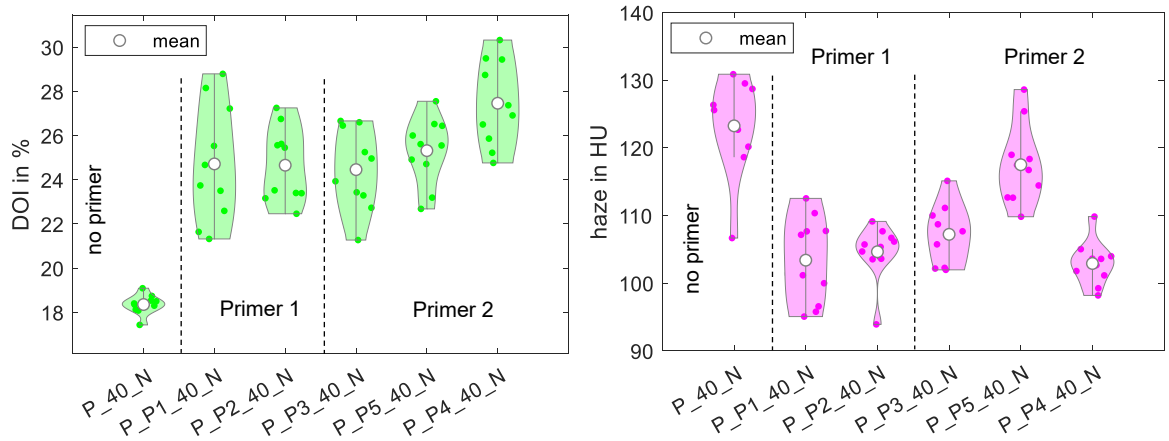

Figure 4.43: DOI and haze measured with the IQ-S gloss meter on samples printed on paper or primed paper (sample names on the x-axes). The way of primer application differed between the samples. Each colored field includes ten DOI or haze values. The width of the area in the individual violin plots shows the density of the measuring points for a specific measured value range. Abbreviations and corresponding print parameters are given in Table 4.8.

The positive impact of primer application on dynamic gloss is elucidated in Section 4.3.2 and is easily comprehensible. However, explaining why the UV-primer has a more positive impact on the gloss of the overprinted metallic ink if applied with a longer dwell time and hot air is not straightforward. Increased gloss is measurable if UV-primer has sufficient time or lower viscosity, facilitated by applied hot air, to penetrate deep into the paper after application. In normal industrial production, the paper web would run much faster with at least 100 m/min and the applied UV-primer would be cured immediately after its application on paper. This would leave only little time for penetration of the UV-primer into the paper. In this experiment however, the paper web is run at only 40 m/min and the

distance between the flexo printing unit and the UV-unit is much larger than it normally would be. This could cause the UV-primer to partially penetrate the paper when printed at this speed, causing a more uneven surface with a probably irregular surface energy. If the UV-primer can penetrate deeply into the substrate, the surface could become more regular. Deep penetration could also seal microscopic pores in the paper. In order to give a more decisive answer, further investigations on the primed paper surface have to be made.

When visually comparing the print samples, it stands out that samples preprinted with Primer 2 appear a bit more yellowish than samples preprinted with Primer 1. To confirm this impression by measurement, color measurements were carried out on the six samples. These were made with a Ci64 sphere spectrophotometer (X-Rite, US). Measurement results of the a* and b* color values measured with the specular reflection included (SPIN) in the color measurement can be seen in Table 4.8. a* is the green-red component of the CIE LAB color space. The more negative its value, the more greenish does a sample appear. The more positive its value, the more reddish does a sample appear. b* is the blue-yellow component of the CIE LAB color space. The more negative its value, the more blueish does a sample appear. The more positive its value, the more yellowish does a sample appear.

*Table 4.8: a*b* color measurement results on the six samples shown in Figure 4.41 printed on paper measured with a Ci64 sphere spectrophotometer with the specular reflection included (SPIN) in the color measurement. Δa*b* is the Euclidean distance between the color measurement results of sample P_40_N and the other samples.*

Sample	Primer	a*	b*	Δa*b*
P_40_N	no primer	-0.3397	-0.0855	0
P_P1_40_N	Primer 1	-0.5005	-0.4545	0.4025
P_P2_40_N	Primer 1	-0.5831	-0.2064	0.2718
P_P3_40_N	Primer 2	-0.9319	0.5087	0.8389
P_P5_40_N	Primer 2	-0.8705	0.5730	0.8458
P_P4_40_N	Primer 2	-0.9298	0.7112	0.9914

It can be seen that samples primed with Primer 2 have more negative a* values which indicates a shift to a more greenish chroma and b* values are higher which indicates a shift to a more yellowish chroma. This shows that the yellowish appearance of Primer 2 is visible even when overprinted with metallic ink. The shift from a more neutral hue to a

slight yellow/green hue would make color management more difficult when overprinting the metallic ink film with an offset color.

4.6.5 Evaluation of the topography data

Topography data were obtained from the samples F_40_N, F_20_N, F_10_N, F_5_N and F_1_N (abbreviations explained in Table 4.8). These samples were all printed on film, with velocities of the film after printing ranging from 40 m/min to 1 m/min. An analysis of the gloss of these five samples is shown in Section 4.6.2.

Further, topography data were obtained from the samples P_40_N, P_P3_40_N, P_P4_40_N, P_P5_40_N and P_P5_1_Y (abbreviations explained in Table 4.8) to get insight into the influence of primer application on the pigment layer topography. Gloss measurements on the four samples P_40_N, P_P3_40_N, P_P4_40_N, and P_P5_40_N were analyzed in Section 4.6.4. For the first four samples, metallic ink was printed on paper or primed paper. After printing the metallic ink, the web speed was not reduced, and no hot air was applied to the metallic ink. Sample P_P5_1_Y differs from these four samples in that, after printing the metallic ink on primed paper, the web speed was reduced to 1 m/min, and hot air was applied.

For a comparison of specular gloss and topography data, specular gloss measured at 60° as well as Sq and Sdq parameters of data filtered for roughness and waviness were intercorrelated.

Topography data from samples with film substrate

Confocal images filtered for roughness and waviness are shown in Figure 4.44. These images are shown only for the samples F_40_N, F_10_N, and F_1_N. Despite the gloss changes documented in Section 4.6.2 with increased dwell time, no significant disparities can be observed in the confocal images. In the confocal images filtered for roughness, dark blue areas indicate the absence of pigments. Notably, for F_1_N, areas without pigments are larger compared to F_40_N and F_10_N. The waviness of the topographies does not seem to vary to a great extent between the samples.

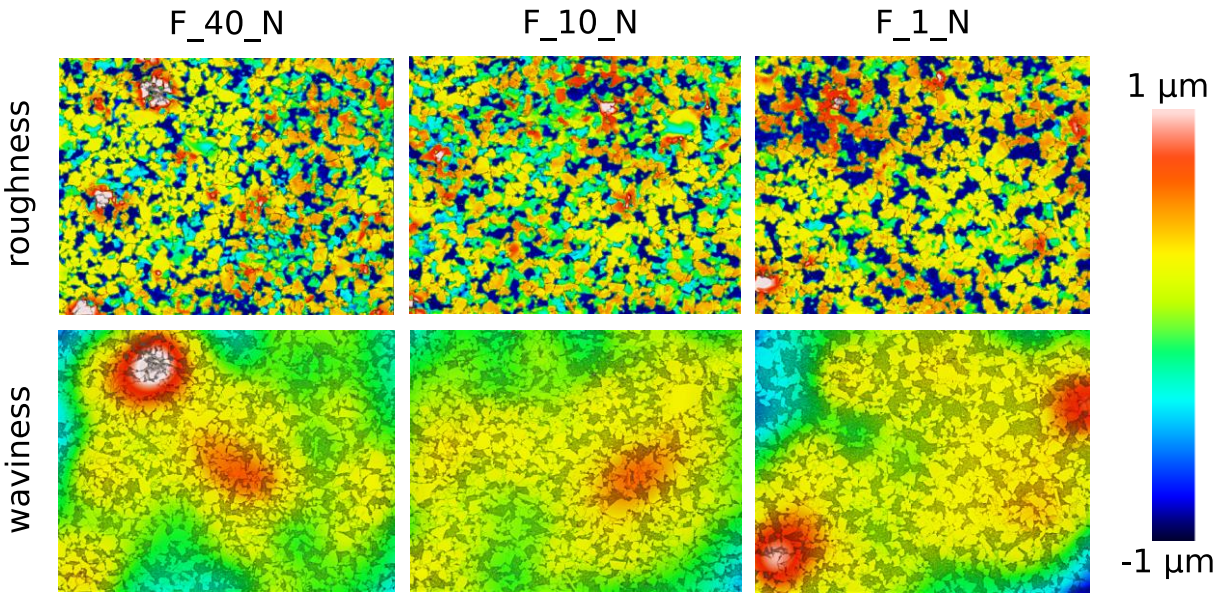

Figure 4.44: Confocal images of samples with film as substrate and different web speeds after printing metallic ink of 40 m/min, 10 m/min and 1 m/min. Image data obtained with a PLu neox are selectively filtered for roughness and waviness. Each image has a size of 260 x 200 µm². Abbreviations and corresponding print parameters are given in Table 4.8. The composition of the images of false color confocal images and black/white light microscopy images is as explained in Section 4.5.2.

For the five samples F_40_N, F_20_N, F_10_N, F_5_N and F_1_N, Sq and Sdq values obtained from topography data filtered for roughness and waviness are plotted against specular gloss measured at 60° in Figure 4.45. In contrast to the samples printed on the laboratory flexo machine on Chromolux paper (see Section 4.5), no clear trend can be identified as the 3D-parameters of the five samples only differ to a small degree. While Sq values of data filtered for roughness tend to increase slightly with rising specular gloss measured at 60°, all other values exhibit a slight decreasing tendency with increasing specular gloss measured at 60°. Sample F_1_N has a greater specular gloss measured at 60° than the other samples but also a greater haze and lower specular gloss measured at 20°. When comparing the Sq and Sdq values obtained from roughness and waviness data with those of the samples of ChromP_VMP_nha (see Section 4.5), it is noticeable that Sdq roughness values of those samples with film as substrate are twice as high. The Sq roughness is a little higher than the roughest sample of ChromP_VMP_nha and the Sq and Sdq values obtained from the data filtered for waviness are about the same.

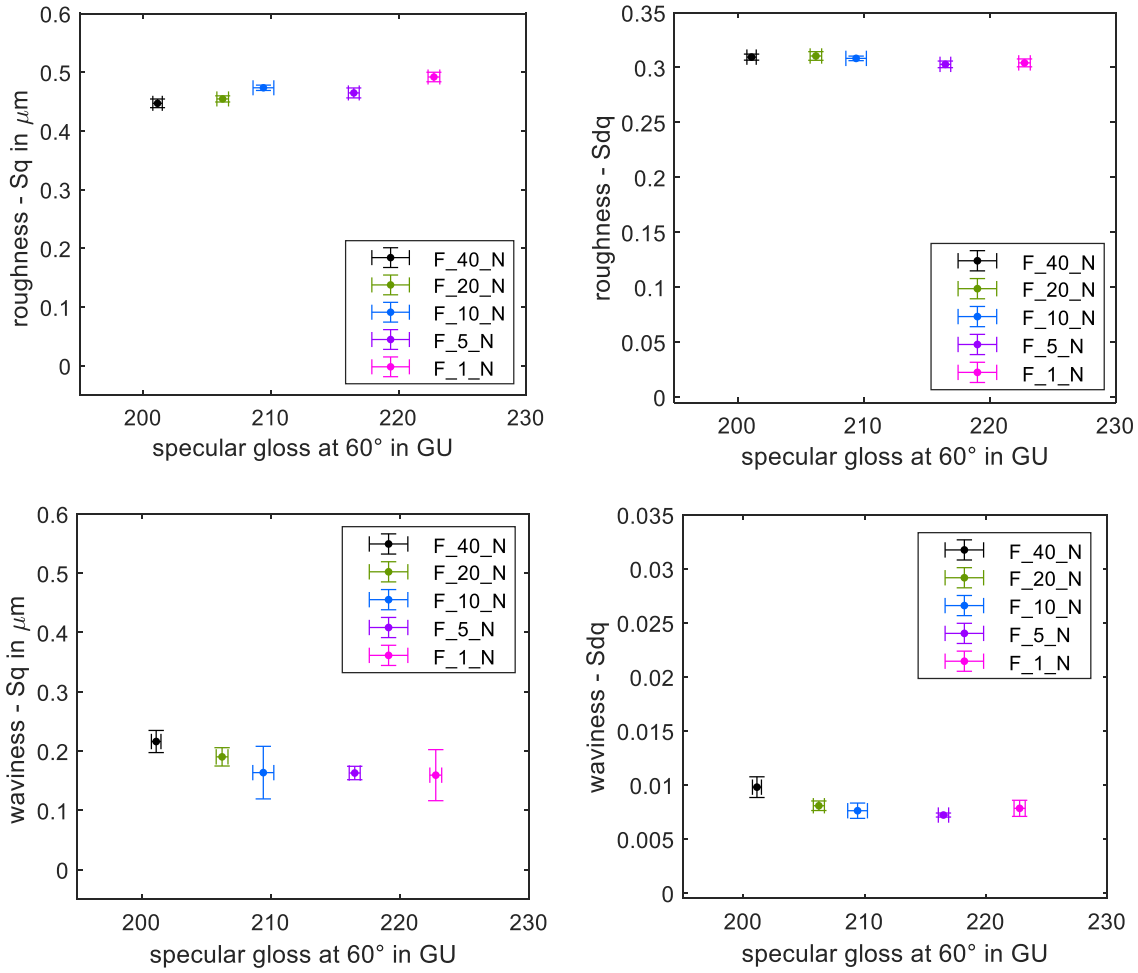

Figure 4.45: Sq and Sdq roughness and waviness data and specular gloss measured at 60° of five samples with film as substrate and different web speeds after printing of the metallic ink. After printing metallic ink, the speed of the web was 40 m/min, 20 m/min, 10 m/min, 5 m/min, and 1 m/min. This web speed is indicated in the sample name. Each data point represents one sample of which ten gloss measurements with the IQ-S gloss meter and five topography measurements were obtained with a PLu Neox confocal microscope. The whiskers around the points show the standard error of the mean. Abbreviations and corresponding print parameters are given in Table 4.8.

Topography data from samples with paper or primed paper substrate

Confocal data filtered for roughness and waviness obtained from the samples P_40_N, P_P5_40_N, and P_P5_1_Y are shown in Figure 4.46. A comparison of the samples P_40_N and P_P5_40_N shows that the pigment layer topography both in terms of waviness and roughness is heavily affected by the use of UV-primer. While for sample P_40_N, for which no primer was applied, small hills and valleys are visible in the roughness data, sample P_P5_40_N shows a more jagged surface topography. Further, waviness on sample

P_P5_40_N seems to be reduced. A comparison of the confocal images obtained from P_P5_40_N and P_P5_1_Y shows that a reduction of the web speed after printing and hot air also influences pigment layer topography. Pigments on P_P5_1_Y seem to align to each other much better than on P_P5_40_N.

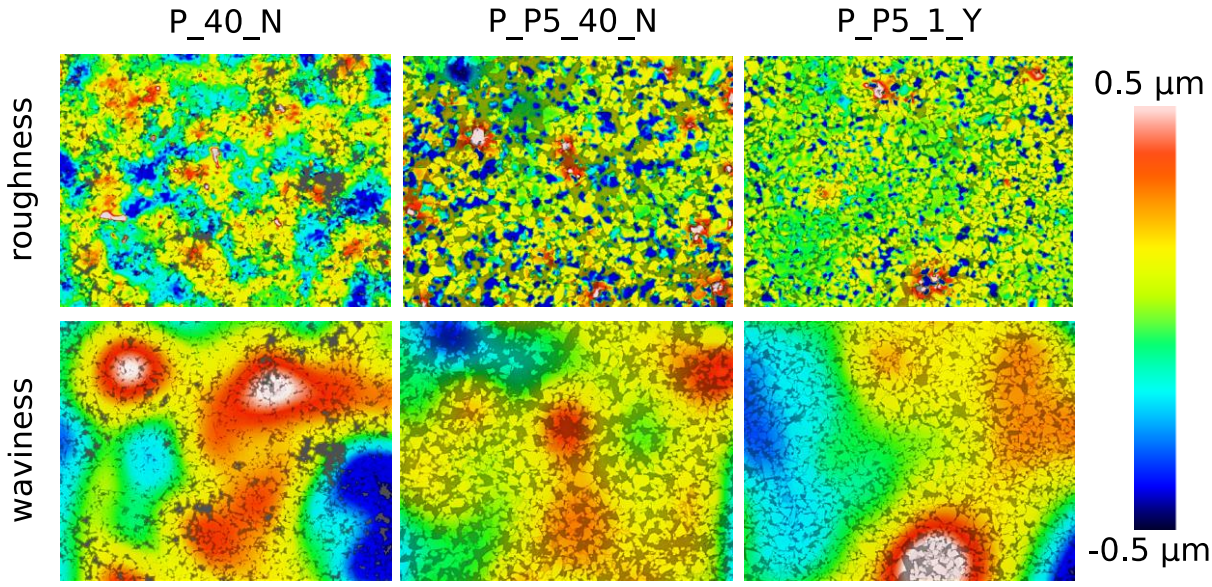

Figure 4.46: Confocal images of samples with paper or primed paper as substrate selectively filtered for roughness and waviness obtained with a PLu neox. Prior to printing metallic ink, no UV*-primer was applied on sample P_40_N, while it was applied for P_P5_40_N and P_P5_1_Y. For sample P_P5_1_Y after printing the metallic ink, the speed of the web was reduced to 1 m/min and hot air was applied. A detailed explanation of the abbreviations is given in Table 4.8. Each image has a size of 260 x 200 µm². The composition of the images of false color confocal images and black/white light microscopy images is as explained in Section 4.5.2.*

For the five samples P_40_N, P_P3_40_N, P_P4_40_N, P_P5_40_N and P_P5_1_Y, Sq and Sdq values of data filtered for roughness and waviness are plotted against specular gloss measured at 60° in Figure 4.47. It can be seen that there is no correlation between specular measured at 60° and the 3D-parameters.

Notably, the difference between the samples printed on primed paper and sample P_40_N for which metallic ink was printed on un-primed paper is most outstanding for the Sdq parameter obtained from topography data filtered for roughness. The comparatively low Sdq value obtained from sample P_40_N indicates that the slopes between the pigments on this sample are the most gradual. One possible reason for this could be that the leafing pigments were unable to partially float to the top of the printed ink due to the substrate's strong ink absorbency. After printing, a portion of the ink binder was absorbed into the

paper, causing the pigments to align themselves more on the paper surface and leading to smaller vertical gaps between the pigments.

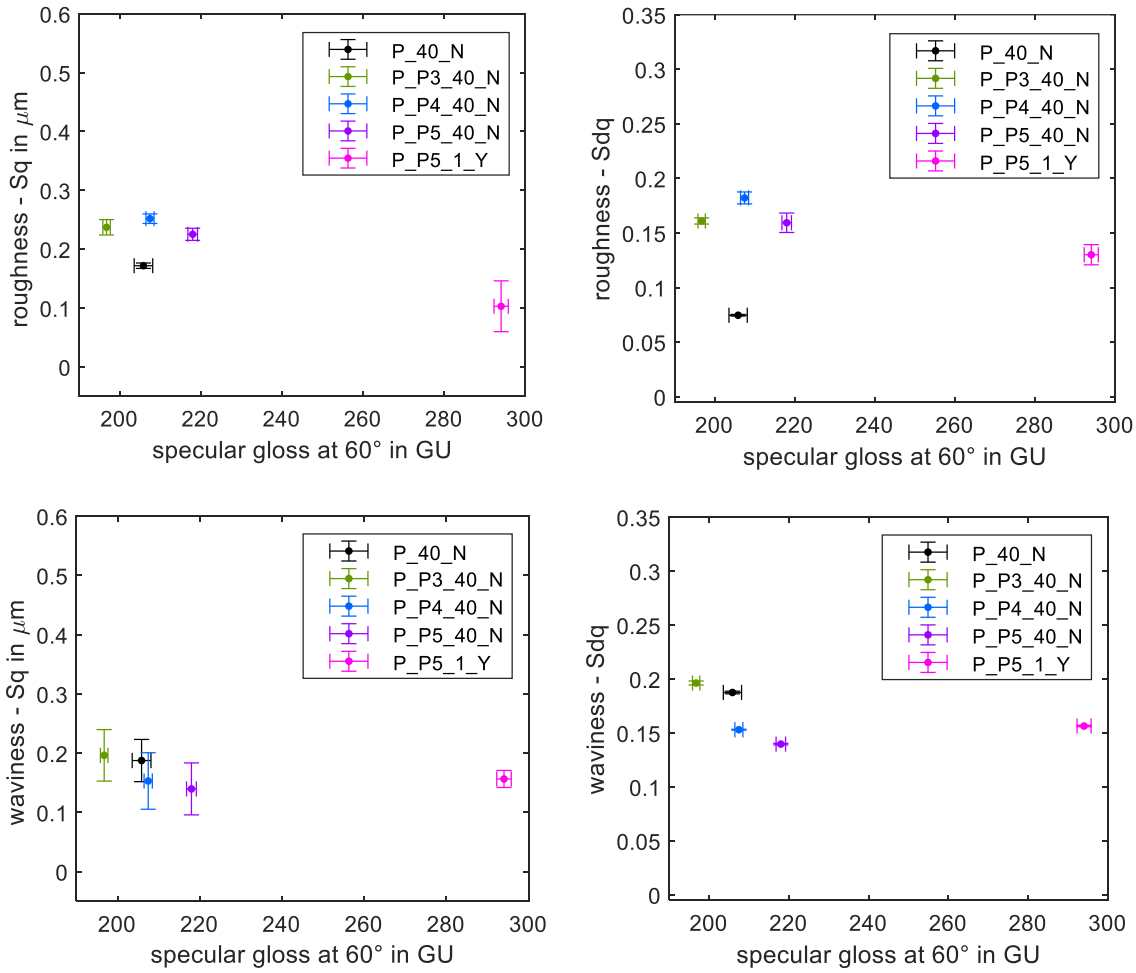

Figure 4.47: Sq and Sdq roughness and waviness data and specular gloss measured at 60° of five samples with paper or primed paper as substrate. Each data point represents one sample of which ten gloss measurements with the IQ-S gloss meter and five topography measurements were obtained with a PLu Neox confocal microscope. The whiskers around the points show the standard error of the mean. Abbreviations and corresponding print parameters are given in Table 4.7.

Only the Sq parameter of the data filtered for roughness gives an indication that sample P_P5_1_Y has a much higher specular gloss measured at 60° than the other four samples. This suggests that the prolonged dwell time and the decreased viscosity of the metallic ink, induced by the application of hot air, allowed more pigments to float to the top of the ink film. Consequently, this results in smaller deviations of the height of these pigments from the mean height and smaller gaps between the pigments.

Compared to sample P_40_N, the Sq and Sdq values obtained from waviness data show only a slight decrease when preprinting a UV-primer under the influence of hot air. When UV-primer is applied without the influence of hot air, as done for sample P_P3_40_N, waviness is not decreased. The reason for this could be the faster filament setting of the printed UV-primer when its viscosity is reduced under the influence of hot air.

To achieve a more robust intercorrelation between 3D-surface parameters and gloss data, additional gloss parameters and 3D-surface parameters should be considered. Moreover, the focus should extend beyond the topography of the pigment layer alone and include the topography of the thin binder layer atop the pigments, which could be measured with a stylus profilometer.

4.6.6 Outcomes

The measurement data and findings in Section 4.6 indicate that the conclusions drawn from the laboratory experiments on the influence of dwell time and hot air in Section 4.5 can only be partially transferred to an experimental setup involving an industrial printing machine. It could be shown that preprinting UV-primer can have a positive influence on the gloss of the printed metallic ink. The finding, that hot air and a longer dwell time can have a positive influence on gloss still holds. The reason for the smaller impact of a prolonged dwell time on gloss in the experiment on the industrial printing machine compared to the laboratory experiments could be that the anilox roller used in the industrial printing machine had a smaller volume, which led to less metallic ink applied onto the substrate.

Additionally it was found that the settings for the UV-primer application influence gloss. Turning on the hot air when printing UV-primer can have a positive influence on gloss. This means for printing practice that for some cases, hot air, if available, could be turned on when printing the primer to increase the gloss of the overprinted metallic ink.

The observation in Section 4.5 that the selected 3D-surface parameters Sq and Sdq, derived from topography data filtered for roughness and waviness, exhibit a negative correlation with specular gloss measured at 60° does not hold true for the samples analyzed in Section 4.6. For the samples printed on film, one possible explanation could be that the gloss differences are not substantial enough to clearly manifest in the 3D-

surface parameters. For the analyzed samples printed on paper and primed paper, the substrate variations among the different samples could be too high.

It should be noted that although an industrial printing machine was used in Section 4.6, the print settings are still very experimental. In printing practice the chosen printing speed would be greater and the distance between a print unit and the next unit, be it a printing unit, a UV-curing unit or a hot air unit would be much smaller.

5 Psychophysical experiment

To address several research questions, a psychophysical study was conducted. The experiment was carried out during the Bachelor thesis of Solangi (2022) and subsequent employment at the IDD, supervised by the author. Parts of the research results were published by Weber et al. (2022c) and Weber et al. (2022b). In this chapter, the experiment is described and the evaluation of the results is further elaborated. In its approach, the experiment was inspired by a study on printed metallic gloss conducted by Rich et al. (2017) and studies by Gigilashvili et al. (2018) and Gigilashvili et al. (2019).

5.1 Research questions and points for consideration

The experiment was designed to give answers to the following questions:

- How do different visual aspects of the appearance of metallic surfaces, such as gloss, sharpness of the reflection, metallicity, and perceived surface roughness, correlate with each other for printed metallized samples?
- How do gloss meter readings correlate with the judgement of samples according to these appearance characteristics made by observers?
- How do observers respond when judging very similar and very different print samples?

The following points for consideration were determined for the experiment:

- Both, a group of experts from the printing industry who regularly assess the quality of print products, as well as a group of amateurs should be involved in the experiment. At the beginning of the experiment, it was not clear how many experts would be able to participate.
- Observers should be restricted as little as possible when viewing the samples. This freedom from restrictions reflects real-world scenarios in which there are no limitations when evaluating print samples in a print shop or when looking at packaging in a supermarket.
- To gain insight into the observers' actions, they were encouraged to elucidate their decisions and choices made during the experiment. Additionally, posing general questions about gloss should provide more knowledge about the observers' understanding of gloss.

5.2 Choice of the method

The first step was to determine the type of psychophysical method that should be employed for the experiments. Suitable scaling methods include ranking, paired comparison, and rating methods (Kingdom and Prins 2016). There are three types of perceptual scales that are highly relevant in psychophysics and can be derived using these methods. These are the ordinal scale, interval scale, and ratio scale (Kingdom and Prins 2016; Engeldrum 2000). In a ranking experiment, observers are assigned with the task of ordering a set of samples according to a specific criterion. This results in an ordinal scale for each observer, which represents a straightforward ranking of the samples based on a particular attribute, without quantifying the degree of difference between samples in that specific attribute. A paired comparison experiment requires observers to compare one pair of samples at a time. For each observer an interval scale can be obtained that includes information about the magnitude of difference between the percepts. The paired comparison method yields very precise data. However, the effort and time needed per observer increases proportionally with the quantity of the samples (Engeldrum 2000; Thurstone 1931). In rating experiments, observers are required to assign a rating of, for instance 1-5, or a binary judgement such as ‘glossy’ or ‘not glossy’. In order to obtain a consistent scale, many repetitions have to be made (Beuckels et al. 2023).

Out of the three scaling methods, the ranking method was chosen. It has the advantage that it reflects real-life situations such as comparing packaging in a supermarket or freshly printed samples during the printing process better than the other two options. Further, as stated by Rounds et al. (1978), most observers prefer ranking methods to paired comparison methods. The latter often lead to many trials and can become boring for observers. This is important to consider since happy observers provide good data (Ferwerda 2008). Due to the relative simplicity of the ranking method and its benefit of being relatively time saving, it is possible to obtain responses to different sets of samples on different perceptual attributes in a reasonable timeframe. Most experiments on gloss perception make use of the paired comparison method or more elaborated forms of comparisons such as the Maximum Likelihood Difference Scaling procedure to obtain very precise scales. However, in this experiment, ranking of many different percepts and asking a multitude of questions in a reasonable amount of time was seen as more important than obtaining very precise scales.

5.3 Samples for the experiment

Out of a collection of about 400 printed metallized samples produced by flexo- and offset printing on sheet-fed and narrow-web printing machines, two sets of samples, each consisting of ten samples were extracted. The samples in these sets had negligibly small chroma but differed in gloss. Different to most psychophysical experiments on gloss, the selection was not based on gloss measurements but on the visual appearance of the samples and visual gloss differences.

In the selection of one set called 'Series A' in the following, care was taken to include both similar and very diverse samples. Series A included a wide range of perceptible difference in gloss and image sharpness, texture and surface roughness. For the production of these samples, both sheet-fed presses and narrow-web printing machines came to use. The samples were printed using different sorts of paper and cardboard. The substrate of one of the samples was an in-mold labeling film. In terms of ink, only UV-inks containing VMPs were used. By incorporating such a diverse variety of samples in Series A, it was aimed at addressing a challenge often encountered in the printing industry: determining which types of samples, produced through various printing methods and with different substrates, have the highest gloss.

A second set, called 'Series B' in the following, consisted of samples with very similar appearance. They were all produced using a XL 75 Anicolor printing machine (Heidelberger Druckmaschinen, Germany) with GD2 cardboard (referred to in Section 3.4) as substrate. The printing ink was the same UV-ink containing VMPs as used for the experiments described in Chapter 4. All of these samples were produced with slight differences in print settings during a single print trial. Series B, comprised of very similar samples, exemplifies the printing industry's challenge of determining which print samples achieve the highest gloss while continuously optimizing printing machine settings and making informed decisions about the best print settings for high gloss. Appendix 3 provides information on the printing machine, the substrate type, rasterization of the print plate, preprint of the samples with black ink or primer and the type of metallic printing ink of the individual samples.

During pretests, different ways of presenting the samples were tested. As visual differences between samples are easier to see if the distance between them is very small, it was tried to find a way that samples could be placed in immediate juxtaposition.

However, no satisfying solution could be found. Finally, it was decided to use black cardboard stencils out of Caribic Schwarz SB with a grammage of 700 g/m² (IGEPA, Germany). The outer size was 120 x 150 mm² and an inner window, which was cut with a laser, had a size of 60 x 60 mm². Samples were glued on the stencils from behind. The design of the stencils was inspired by similar stencils used by Brumm et al. (2017).

By using these stencils, the observer's full attention was directed on the samples in the inner window of the stencil. Furthermore, the black cardboard enabled observers to easily pick up the samples without touching the metallized surface what would result in visible fingerprints. Samples printed on lighter paper were backed with a piece of cardboard. By doing so, it was prevented that observers could differentiate the samples by their weight. A random number was assigned to each sample, and the backside of the samples was labeled with these numbers. Pictures of the front- and backside of some of the samples are shown in Figure 5.1. Figure 5.2 shows images of all samples of both Series A and Series B. All images were captured under the same lightning situation and in the same position. Note that Sample 9 and Sample 10 are used in both series. Hence, in total only 18 different samples were used.

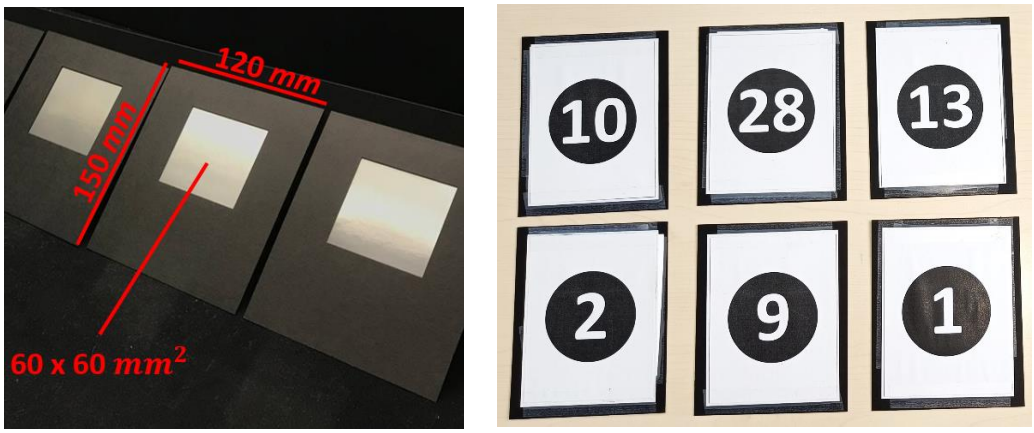

Figure 5.1: Left: samples in cardboard stencils that were used for the ranking experiment. Right: backside of the samples with attributed numbers.

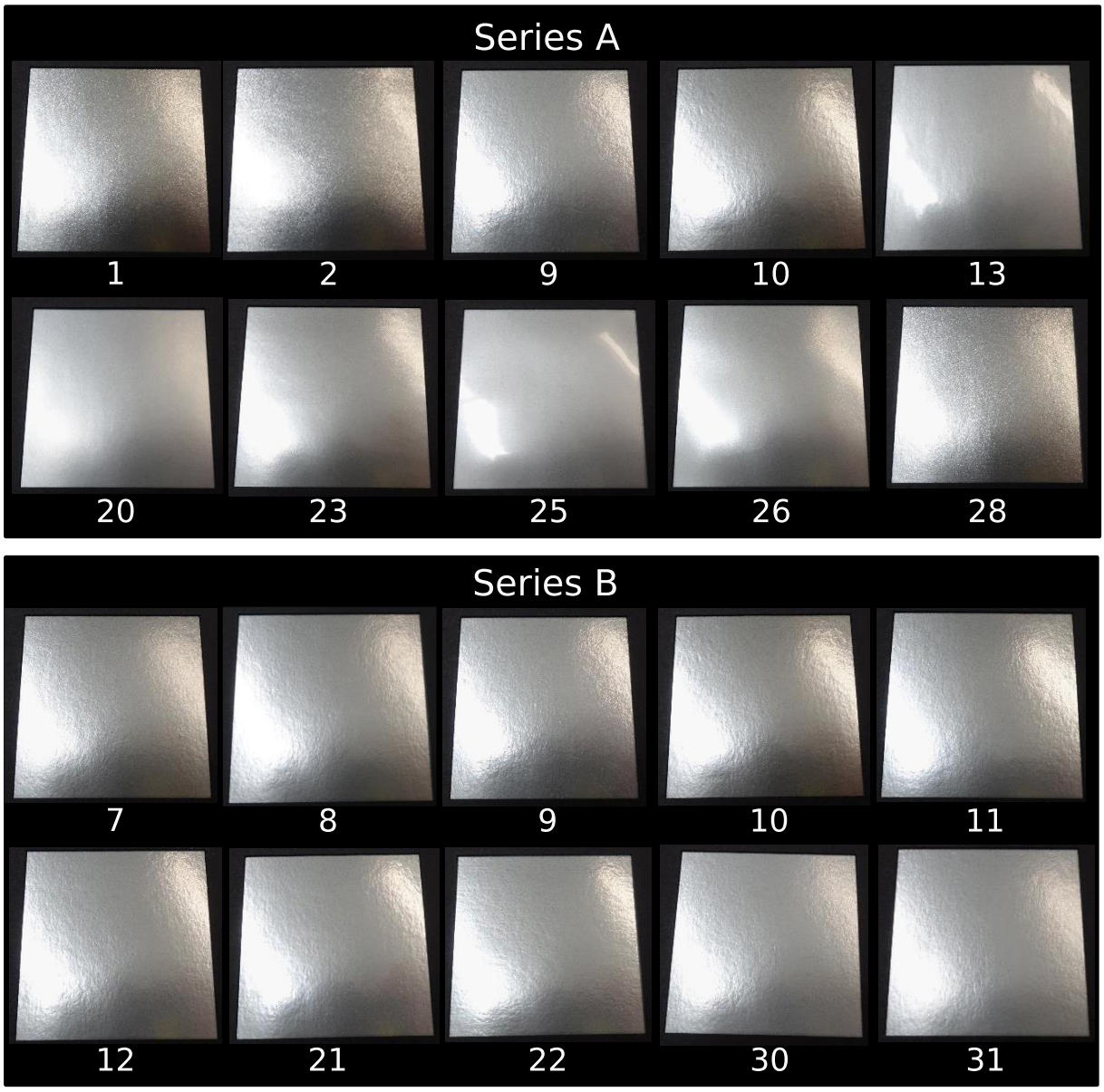

Figure 5.2: Images of the samples used of both Series A and Series B. All images were captured under the same lightning situation and in the same position. The numbers assigned to the samples are the same numbers that were on their backside (see Figure 5.1).

Ten instrumental gloss measurements were made on each sample using the IQ-S gloss meter, following the measurement scheme described in Chapter 3. The mean values of the measurements for both Series A and Series B are presented in Figure 5.3. The exact mean measurement values and standard deviations are shown in Appendix 4. There are only minor differences in the gloss measurement values of Sample 10 and Sample 12 and visible differences are very small.

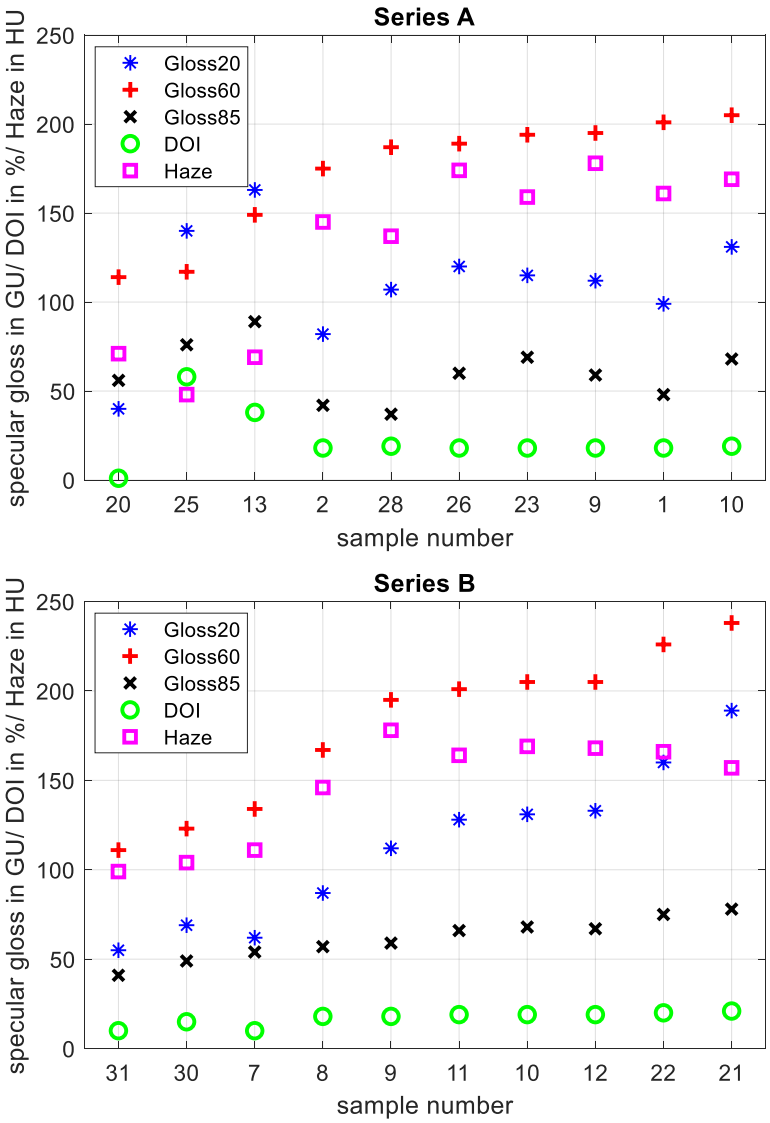

Figure 5.3. Average instrumental gloss measurement results obtained from ten measurements on each of the samples of Series A and Series B using the IQ-S gloss meter. Samples ordered according to the specular gloss measured at 60°. GlossXX denotes specular gloss measured at an angle of XX. The exact mean measurement values and standard deviations are given in Appendix 4.

Table 5.1 shows the correlations between the measured specular gloss values measured on the samples of both series. It can be seen that the correlations between the specular gloss values measured on the samples of Series A are rather small compared to Series B. The reason for this is the similarity of the samples used for Series B and the high variety between the samples used for Series A.

Table 5.1: Pearson's r correlation coefficients of the measured specular gloss values measured on the samples of Series A and Series B. GlossXX denotes specular gloss measured at an angle of XX.

Correlation of	Series A	Series B
Gloss20 with Gloss60	0.17	0.97
Gloss20 with Gloss85	0.64	0.96
Gloss60 with Gloss85	-0.35	0.95

5.4 Experimental setup

A light booth was specifically designed for the experiment, enabling observers to arrange the samples and move along them. Commercial light booths were also available, but their size was considered too small to accommodate all the samples in a single row. In terms of illumination, it was weighted between LEDs and a fluorescent lamp. It was decided to use a fluorescent lamp since it was easier affordable. The choice fell on a D65 fluorescent tube with a length of 1500 mm and 58 W from JUST Normlicht (Germany), with a nominal flux of 3700 lm and a correlated color temperature of 5000 K. In accordance to the standard DIN EN 60081 (reapproved 2019) for double-ended fluorescent lamps, it was used for the experiment after a burn-in time of 100 hours.

The fluorescent tube was enclosed within a frame measuring 1.09 x 0.60 x 1.90 m^3. No diffuser or baffle was installed in front of the fluorescent tube. The fluorescent tube was mounted at a height of 0.6 meters above the tabletop on which the frame was placed on. A white paper screen was affixed to the frame to prevent observer glare. Black cotton canvas (Verhees Textiles, Netherlands, article number: 02900.001) with a grammage of 225 g/m^2 was attached to the sides of the frame and laid on the tabletop where the light booth was positioned, ensuring consistent conditions regardless of the tabletop surface, and minimizing reflections. A vertical elevation was positioned at the rear part of the frame. This elevation, in combination with the white screen ensured that the observers could focus on the samples without feeling observed by the examiner sitting in front of them. At the same time, it allowed the examiner to have a clear view of the area where the samples were sorted and observe the observer's actions. Figure 5.4 depicts the frame with the mounted fluorescent tube, along with the setup involving the white screen and the black canvas on top of the table.

Figure 5.4. Left: frame of the specifically designed light booth with the mounted fluorescent tube. Right: frame with white screen and black canvas seen from the observer's position and the Minilux lux meter on the tabletop where the samples were placed in the experiment.

A Minilux class B lux meter (MX-Electronic, Germany) was used to measure the illuminance at the table height of the light booth. These measurements were taken perpendicular to the tabletop. In total 40 measurement points were recorded. The distribution of the illuminance on the table is shown in Figure 5.5. It can be seen that the illumination directly under the fluorescent tube is the highest. Towards the sides of the table, the illumination decreases strongly. However, the observations and the comparison of the samples mostly took place in the center area of the table where an illumination of 800-1050 lx was measured. The placement of a baffle in front of the fluorescent lamp could have improved the uniformity of illuminance on the tabletop. However, the illuminance measurements were taken after some observers had already participated in the experiment. As a result, no changes to the setup could be implemented at that point.

A NanoCalc-2000-UV/VIS/NIR spectrometer (Mikropack, Germany) was used to characterize the spectrum of the fluorescent tube built into the frame. The measurement was made in the height of the tabletop and perpendicular to it. The recorded spectrum can be seen in Figure 5.6. The influence of the light spectrum on the perception of gloss of metallic samples has not been researched yet.

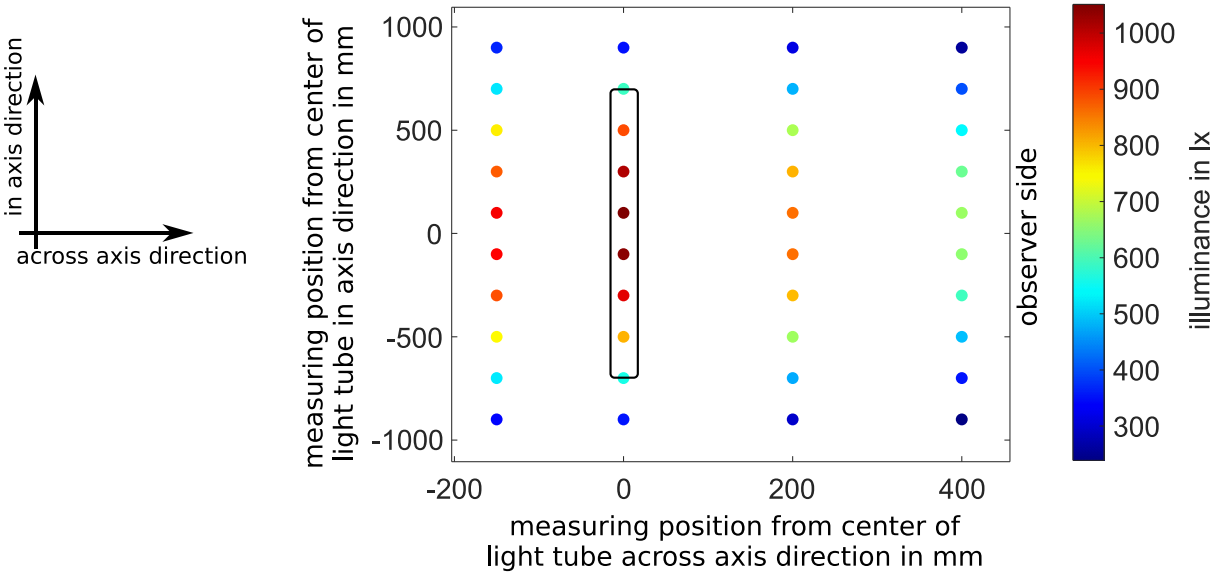

Figure 5.5: Distribution of the illuminance on the table under the fluorescent lamp measured with a MX-Electronic Minilux lux meter. The position of the fluorescent lamp is indicated with a black rectangle inside the graph. The position of the observer in the experiment is on the right side. The 'in axis direction' is the direction along the axis of the tube of the fluorescent lamp. The leftmost row of measurements was taken just before the elevation that prevented observers from seeing the examiner and the rightmost row of measurements was taken just before the edge of the table the light booth was placed on.

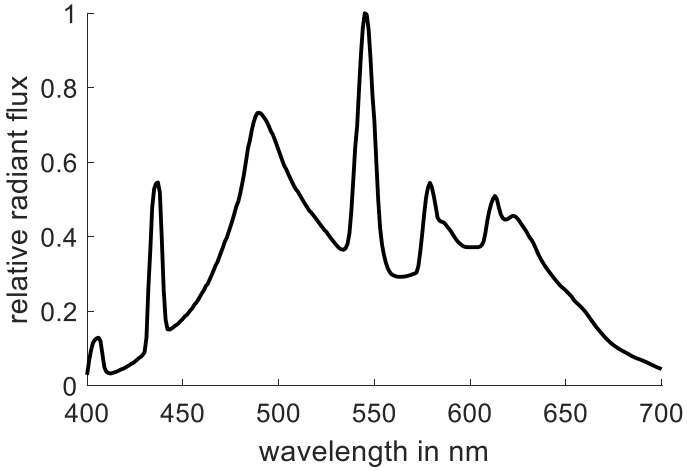

Figure 5.6: Spectrum of the fluorescent tube built into the frame of the specifically designed light booth, measured with a NanoCalc-2000-UV/VIS/NIR spectrometer.

Experimental setups in two different rooms where the experiment was conducted are shown in Figure 5.7. On the left side, the sampling conditions at the IDD, and on the right side, sampling conditions at Heidelberger Druckmaschinen can be seen. In the left image, the position of the observer is on the left side of the light booth. The examiner on the right

side has view on the samples. In the right image the position of observer and examiner are the other way around. The position of a camera that was used to record the position of the samples after each ranking task is encircled.

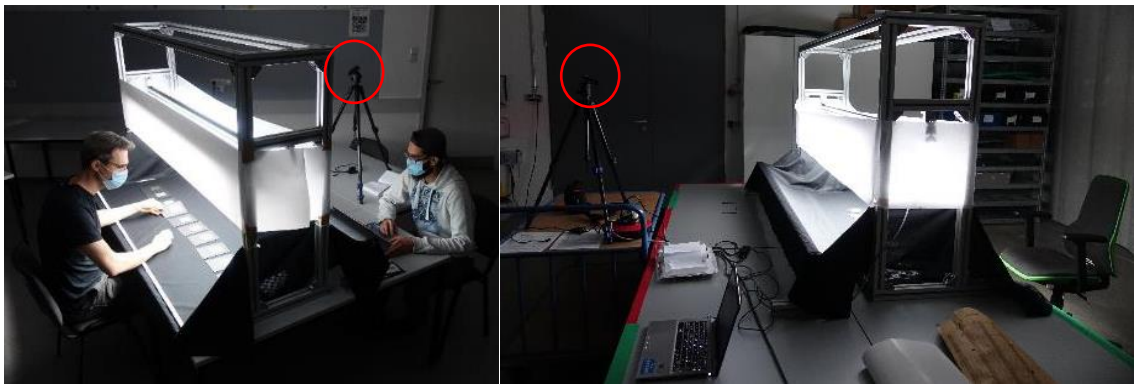

Figure 5.7: Sampling conditions at the IDD (left), TU Darmstadt and at Heidelberger Druckmaschinen (right). The position of a camera used to record the numbers on the backside of the samples (see Figure 5.1) after they were flipped after each finished ranking task is encircled.

Unlike as presented by Weber et al. (2022c), one of the observers could not participate in the experiment in one of these two rooms. Nonetheless, the sampling conditions in the alternative dark room were similar the two shown in Figure 5.7.

5.5 Observers

In total, 27 observers participated in the experiment. 13 of them male and 14 female. All of them spoke German as mother tongue. Ten observers were in the age range of 20 to 30 years, four observers in the age range of 30 to 40 years, three in the age range of 40 to 50 years and ten in the age range of 50 to 60 years. All observers had normal or corrected-to-normal vision. Twelve observers compare and judge printed samples, including metallic ones, on a regular basis in printing press companies. Statements about the frequency ranged from at least five times a week to about once or twice a month. This group of observers is referred to as ‘experts’ in the following. The other group is referred to as ‘amateurs’. Out of this group of amateurs, four observers participated in psychophysical experiments concerning color or roughness of surfaces before. However, they did not judge and compare such kind of samples on a regular basis. 18 observers participated at the experiment at the IDD of whom three belonged to the group of experts. Nine observers participated at Heidelberger Druckmaschinen of whom all belonged to the group of experts.

5.6 Experimental procedure

Prior to the experiment, all observers signed an informed consent form that included information about the observer's rights and the purpose of the experiment. They were also informed that the experiment, described in application EK 55/2021 toward the ethics council of the TU Darmstadt, was considered uncritical. Next, observers generated an individual code word that would both anonymize the data but also allow the possibility to trace the observers if further experiments would follow. The language used in the experiment was German. A single survey for one observer was designed for a duration of 1 to 1.5 hours. The role of the examiner was carried out by L.A. Solangi for all observers who participated in the experiment.

Each observer was provided with three objects that could be used as an aid to assess appearance characteristics. The observers could decide themselves when and how to use these. A reason for providing these aids was the observation that objects mirroring a printed sample can be an aid to assess appearance in printing practice. Two checkerboard patterns were printed on Steinbeis No. 4 paper with a gramature of 80 g/m^2 (Steinbeis Papier, Germany) using a bizhub C258 office printer (Konica Minolta, Japan). The total size of the patterns was about 160 mm^2, with one having a smaller square size of 20 mm^2 and the other a larger square size of 36 mm^2. The printed patterns were backed with black cardboard of Caribic Schwarz SB with a grammage of 700 g/m^2 (IGEPA, Germany). In addition, a pen with a barcode attached to was provided. The variety of objects was given to the observers in order to give them a choice and to learn what kind of object is favored most. The three objects are shown in Figure 5.8.

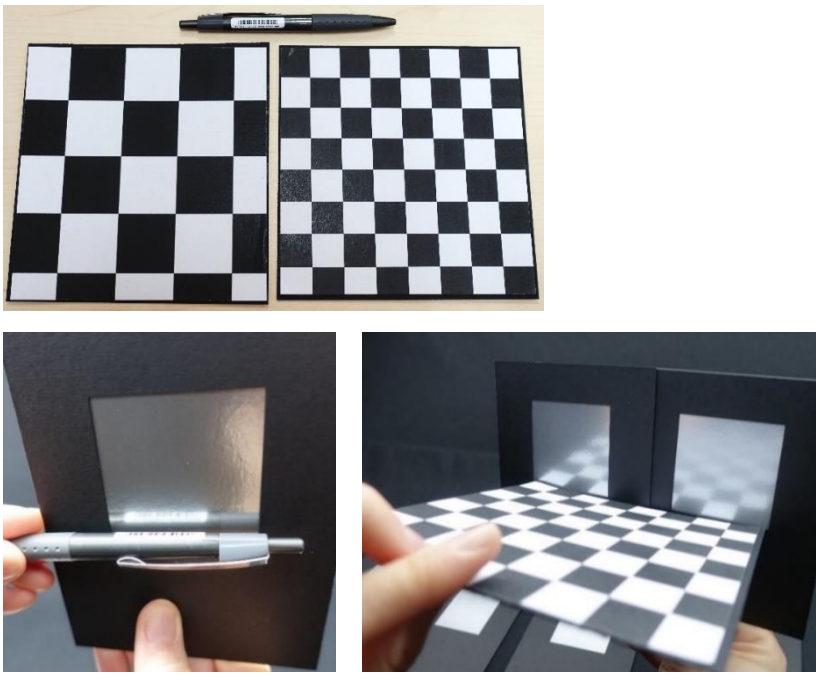

Figure 5.8: Top: Checkerboard patterns and ballpoint pen with barcode used by the observers during the experiments. Bottom: Exemplifications of mirroring the objects in the samples.

Before the experiment, no training of the observers took place and no definition of any of the terms used was given. This was a deliberate decision. In printing practice, people involved also talk directly about gloss or metallicity without exchanging precise definitions.

At the beginning of the experiment, Series A (denotation see Section 5.3) was used and the observers were asked to perform several tasks with it. Afterwards, Series B was used. The samples were given to the observers in a randomized order. Observers were allowed to adjust their viewing angle, stand up and move along the samples and arrange them according to their needs. The different tasks given to the observers are listed in Table 5.2. The exact wording of the tasks is given in German. The purpose of Task 1 was only to ensure that the observers made themselves familiar with the samples of Series A. While performing the tasks, the observers were encouraged to explain their decisions and describe the appearance of the samples. The examiner noted these explanations, as well as the characteristics of the observers' behavior. After the completion of each task, the observers were asked if they were content with their sorting and if they want to make any further changes. To make sure that the order of the samples was noted correctly, it was asked again on which side of the ranking the sample with the strongest and the weakest characteristic of the respective task lies. Subsequently, the observers were instructed to flip the samples over in order to capture a picture of the numerals on the reverse side.

Additionally, the order of the samples was recorded manually in an Excel sheet. Observers were permitted to assign multiple samples to the same rank, if they were determined to be indistinguishable in a specific queried characteristic. This approach aimed at avoiding arbitrary ordering.

Table 5.2: Tasks assigned to the observers regarding the metallized samples in the experiment. The instructions, as originally given in German, are written in italics. Series A and Series B were introduced in Section 5.3

Series	Task number	Denotation	Task
A	**1**	-	Group the sample set by groups of your choice, the size and number of groups is up to you. Explain why you made this grouping. *Gruppieren Sie das Probenset nach Gruppen ihrer Wahl, die Größe und Anzahl der Gruppen steht Ihnen frei. Erläutern Sie, warum Sie diese Gruppierung vornahmen.*
	2	Gloss ranking A1	Place the samples by gloss in order, from highest/strongest to weakest. *Legen Sie die Proben nach Glanz in einer Reihenfolge, vom höchsten/stärksten zum schwächsten.*
	3	Roughness ranking A	Place the samples in order of perceived roughness, from highest/strongest to weakest. *Legen Sie die Proben nach der wahrgenommenen Rauheit in einer Reihenfolge, vom höchsten/stärksten zum schwächsten.*
	4	Sharpness ranking A	Place the samples in order of image sharpness of the reflection, from highest/strongest to weakest. *Legen Sie die Proben nach der Bildschärfe der Spiegelung in einer Reihenfolge, vom höchsten/stärksten zum schwächsten.*
	5	Metallicity ranking A	Place the samples in order of metallic impression, from highest/strongest to weakest. *Legen Sie die Proben nach dem metallischen Eindruck in einer Reihenfolge, vom höchsten/stärksten zum schwächsten.*
	6	Brightness ranking A	Place samples in order of brightness, from highest/strongest to weakest. *Legen Sie die Proben nach der Helligkeit in einer Reihenfolge, vom höchsten/stärksten zum schwächsten.*
	7	Gloss ranking A2	Place the samples again by gloss in an order, from highest/strongest to weakest. *Legen Sie die Proben erneut nach Glanz in einer Reihenfolge, vom höchsten/stärksten zum schwächsten.*
B	**8**	Gloss ranking B	Place the samples by gloss in order, from highest/strongest to weakest. *Legen Sie die Proben nach Glanz in einer Reihenfolge, vom höchsten/stärksten zum schwächsten.*

Upon finishing the first eight tasks, observers were asked several additional questions. These additional questions were slightly adjusted over the course of the experiment. The first 17 observers, of whom two were regarded as experts, were asked the following additional questions. The exact wording used in German is written in italics:

1. What differences do you notice comparing the first sample and the second set?
   Welche Unterschiede fallen Ihnen gegenüber dem ersten Probenset auf?
2. Do you have experience with sampling tests?
   Haben Sie Erfahrung mit Abmusterungsversuchen?
3. How did you feel about the lighting conditions in the room?
   Wie empfanden Sie die Lichtverhältnisse im Raum?
4. What is gloss for you?
   Was ist Glanz für Sie?
5. What three objects from your everyday life do you perceive as glossy?
   Welche drei Objekte aus Ihrem Alltag empfinden Sie als glänzend?

At the beginning of the experiment, it was not known how many experts could be recruited as observers. After the recruitment of further experts, the additional questions were adjusted to the following with the exact wording used in German written in italics:

1. What differences do you notice comparing the first sample and the second set?
   Welche Unterschiede fallen Ihnen gegenüber dem ersten Probenset auf?
2. How many times a week do you assess the quality of print samples?
   Wie oft in der Woche beurteilen sie die Qualität von Druckproben?
3. Have you dealt with the topic of gloss in depth in previous assessments?
   Haben Sie sich im Rahmen vorheriger Beurteilungen vertieft mit dem Thema Glanz beschäftigt?
4. Which gloss parameters and characteristics do you know?
   Welche Glanzmessgrößen und -kennwerte sind Ihnen bekannt?
5. What is gloss for you?
   Was ist Glanz für Sie?
6. How did you feel about the lighting conditions in the room?
   Wie empfanden Sie die Lichtverhältnisse im Raum?

5.7 Results and analysis

In the following, observations on the actions of the observers are provided, and general evaluations of the data are made. Subsequently, the data specifically obtained using Series A are analyzed and interpreted, followed by an investigation of the data specifically obtained using Series B. Afterwards, insights from the additional questions following the ranking tasks are presented.

5.7.1 General evaluations and observations

For the majority of the tasks, most observers chose to order the samples by comparing them in pairs. However, some observers chose to arrange the samples in a row on the table and occasionally switched positions. At least in Task 4 (tasks explained in Table 5.2), in which the sharpness of the reflection was judged, all observers used one of the provided aids. Most observers chose to use one of the two checkerboard patterns, the majority of them used the checkerboard with the smaller squares. Only few observers used the ballpoint pen. To assess the criterion of gloss, some observers, of them mostly experts, used one of the aids. Some bobbed their head and upper body forward and backward to perceive the course of the reflection under different angles. The tasks, for which most observers made a deliberate attempt to not look into the reflection, were those assessing brightness, the perceived roughness, and partly the metallicity. The gloss criterion was primarily evaluated by looking at the direct reflection of the light source. The assessment of brightness was mostly done by stepping far away from the samples and by looking into their diffuse reflection. This position is reproduced in Figure 5.9. Some observers however judged brightness by looking into the direct reflection of the light source. Due to the great difference of these two viewing positions, for brightness, only data of 18 observers who choose to look into the diffuse reflection were considered in further data evaluation.

Figure 5.9: Reproduction of the viewing position that were took up by many observers to judge the brightness of the samples.

To give an impression of the recorded results, Table 5.3 shows an excerpt of five observers who ranked Series A according to gloss. Samples assigned with the rank '1' exhibit the highest level of the assessed attribute. For Observer 4, fractional numbers are used because Sample 2 and Sample 28 as well as Sample 9 and Sample 10 were placed on the same rank. As a result, the distance between 1 and 10 could no longer be divided into integer distances; instead, it had to be divided into slightly larger, non-integer intervals. The amount of observers who chose to place more than one sample on one rank for the specific tasks is shown in Table 5.4. Appendix 5 shows a record of observers' choices regarding the placement of the samples on specific ranks for the individual questions.

Table 5.3: Excerpt of the evaluation of the first ranking of Series A regarding gloss. For Observer 4, fractional numbers are used because samples 2 and 28 as well as samples 9 and 10 were placed on the same rank.

Observer number	Sample number									
	1	**2**	**9**	**10**	**13**	**20**	**23**	**25**	**26**	**28**
4	7.43	8.71	4.86	4.86	2.29	10	6.14	1	3.57	8.71
5	3	5	2	1	7	10	6	9	8	4
6	4	1	2	3	5	10	7	9	8	6
7	3	2	4	5	7	10	6	9	8	1
8	4	5	8	3	1	7	10	2	6	9

Table 5.4: Amount of observers choosing to place more than one sample on one rank for the different tasks. Explanations to the different tasks are given in Table 5.2.

	Series A						Series B
Percept	Gloss ranking A1	Roughness ranking A	Sharpness ranking A	Metallicity ranking A	Brightness ranking A	Gloss ranking A2	Gloss ranking B
Amount of observers	4	3	4	5	0	3	4

To assess the normality of the data, the Shapiro-Wilk test was performed. The results indicated that for a high portion of the observer rankings, it is not reasonable to assume a normal distribution, which is common for data from ranking experiments, as they typically do not follow a normal distribution pattern (Carabante and Prinyawiwatkul 2018). Hence, nonparametric tests were to be used for statistical data analysis.

Kendall's W coefficient was evaluated for the rankings of the different observers regarding the individual tasks. Kendall's W coefficient is a non-parametric measure for the concordance of several ranked lists with a range of zero to one. A value of one means that all lists are ranked the same, a value of zero means that there is no agreement between the lists (Kendall and Gibbons 1990). For the calculation of Kendall's W the Matlab file from Huang (2023) was used. The evaluation is shown in Table 5.5. It can be seen that perceptual terms that encompass a greater level of abstraction, such as 'metallicity' and 'gloss', tend to result in greater disagreement among observers, leading to lower Kendall's W coefficients. Conversely, terms like 'brightness' and 'perceived roughness' exhibit much higher agreement among the observers. Further, it can be seen that the disagreement between the observers in terms of gloss was much smaller for the ranking of the samples of Series B compared to Series A.

Table 5.5: Kendall's W coefficients of the rankings according to the perceptual attributes. For the brightness, only rankings of 18 observers were included. Explanations of the different tasks are given in Table 5.2.

Kendall's W	Series A						Series B
	Gloss ranking A1	Roughness ranking A	Sharpness ranking A	Metallicity ranking A	Brightness ranking A	Gloss ranking A2	Gloss ranking B
Kendall's W amateurs	0.469	0.835	0.764	0.213	0.917	0.429	0.678
Kendall's W experts	0.418	0.788	0.746	0.332	0.978	0.443	0.787
Kendall's W all observers	0.351	0.810	0.742	0.235	0.955	0.356	0.717

Thurstone (1931) mentioned that the rankings obtained in a ranking experiment can be understood as a result of a large number of paired comparisons by the observers as the samples are sorted and compared with each other. As described by Ferwerda (2008), using the ordinal rankings of several observers from a ranking experiment, an interval scale can be obtained by applying Thurstone's law of comparative judgment. By drawing on Thurstone's law of comparative judgment (Thurstone 1927; Torgerson 1958; Rajae-Joordens and Engel 2005) the rank order data was converted into interval scales. To do so, the scheme described by Ferwerda (2008) was followed. Doing so, a Z-score for each sample and each percept was obtained. Z-scores are standardized values that represent the number of standard deviations a score is above the mean if it is positive or below the mean if it is negative. The mean is equal to the value of zero (Kingdom and Prins 2016). For instance, a sample for which a negative Z-score is denoted, the percept is less pronounced than for most of the other samples judged by a group of observers (i.e. it was perceived as less glossy than most other samples).

5.7.2 Evaluation of data obtained with Series A

One of the questions to be addressed was whether there are differences between Gloss ranking A1 and Gloss ranking A2 (denotations explained in Table 5.2). Weber et al. (2022c) presented the Pearson-r coefficients for the comparison for the amateurs ($r = 0.96$), experts ($r = 0.95$) and all observers ($r = 0.98$) and concluded that observers had a high consistency when ranking Series A (series explained in Section 5.3) two separate times according to gloss. However, it was discovered that the assumption of small differences in rankings between Gloss rankings A1 and A2 does not necessarily hold true for individual observers.

Table 5.6 shows the Kendal's τ coefficients (information to Kendal's τ coefficients are given in Section 4.5.2) for each individual observer testing the agreement of the order of Gloss ranking A1 and Gloss ranking A2. A high agreement that is present if Kendal-τ coefficients are higher than 0.75 can only be observed for ten observers. Interestingly, the order of the rankings of some of the observers have nearly no correlation or even a negative correlation. This means that for some observers, the rankings of gloss were heavily influenced by the tasks in between Gloss ranking A1 and Gloss ranking A2. Only one observer, Expert No. 3, maintained the same order. Expert No. 3 stated that he evaluates and compares print samples at least five times a week, with a special focus on printed metallized surfaces. Expert No. 3 was also the observer who conducted the experiment in a different room than all the other observers, as mentioned in Section 5.4.

Table 5.6: Kendal-τ correlation coefficients for Gloss ranking A1 and Gloss ranking A2 (tasks explained in Table 5.6) calculated for every observer individually.

Nr.	1	2	3	4	5	6	7	8	9	10	11	12	13	14	15
Amateurs	0.42	0.30	0.47	0.70	0.96	0.56	0.69	0.11	0.33	0.78	0.80	0.96	0.94	0.78	0.47
Experts	0.42	0.56	1.00	-0.02	-0.16	0.82	0.64	0.64	0.91	0.87	0.29	-0.51			

Figure 5.10 displays intercorrelations of data obtained from Gloss ranking A1 by experts, amateurs, and all observers with specular gloss measured at 20° and 60°. A positive correlation is evident between Gloss ranking A1 judged by experts and specular gloss measured at 20°, but not for Gloss ranking A1 judged by amateurs. Conversely, a positive correlation exists between Gloss ranking A1 judged by amateurs and specular gloss measured at 60°. When intercorrelating data of Gloss ranking A1 judged by all observers, the correlation with specular gloss measurements at 20° or 60° is rather small.

An explanation for this discrepancy between the two groups of observers could be that there were more observers in the group of experts who took the sharpness of the reflected image more into account for ranking gloss than in the group of amateurs. This can be shown by the rank correlation of the Gloss ranking A1 and Sharpness ranking A. While for the group of amateurs this results in a Kendall's τ coefficient of 0.022, for the group of experts a Kendall's τ coefficient of 0.494 was determined. A possible reason for this could be that more observers in the group of experts chose to use one of the checkerboard patterns as and aid to assess gloss. Due to the construction of the gloss meter, this is reflected in the intercorrelation with the specular gloss values measured at 20° and 60°. As shown in Section 2.3.1, the receiver aperture at 20° is smaller than the receiver aperture at 60°. Hence, the specular gloss measurement at 20° is more sensitive to scattered light than the 60° specular gloss measurement and is therefore also more sensitive for the sharpness of the reflection.

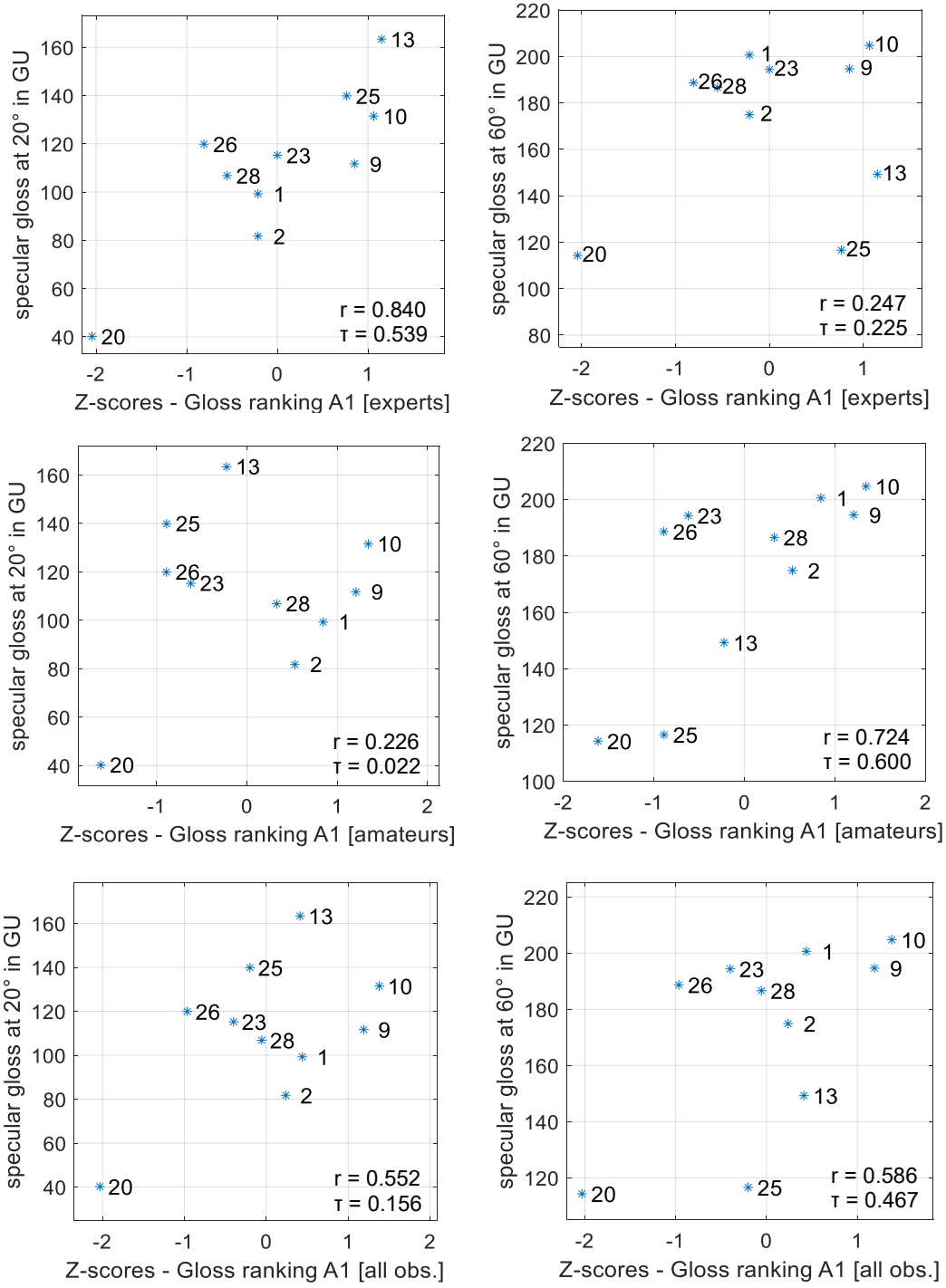

Figure 5.10: Specular gloss at 20° and 60° measured with the IQ-S gloss meter of samples of Series A (shown in Section 5.3) plotted against Gloss ranking A1 (explained in Table 5.2) by the group of amateurs, experts and all observers (obs.). The numbers in the plots are the sample numbers. Pearson's r and Kendal's τ correlation coefficients are given.

Correlations between the measured specular gloss at 20° and 60°, DOI and Rspec with the data from Sharpness ranking A of the group of all observers were evaluated. In Figure 5.11, a positive correlation is evident between Sharpness ranking A and specular gloss

measured at 20°. Interestingly, a slightly negative correlation can observed between data from Sharpness ranking A and specular gloss measured at 60°. For Sample 1, 2, 10, 23, 26, and 28, which have very similar DOI values, discrimination through the DOI values is limited, and they do not exhibit a strong correlation with Sharpness ranking A. Moreover, a positive correlation exists between Rspec values (introduced in Section 3.2) and data from Sharpness ranking A. However, as for DOI, the discrimination through the Rspec values for some of the samples is small.

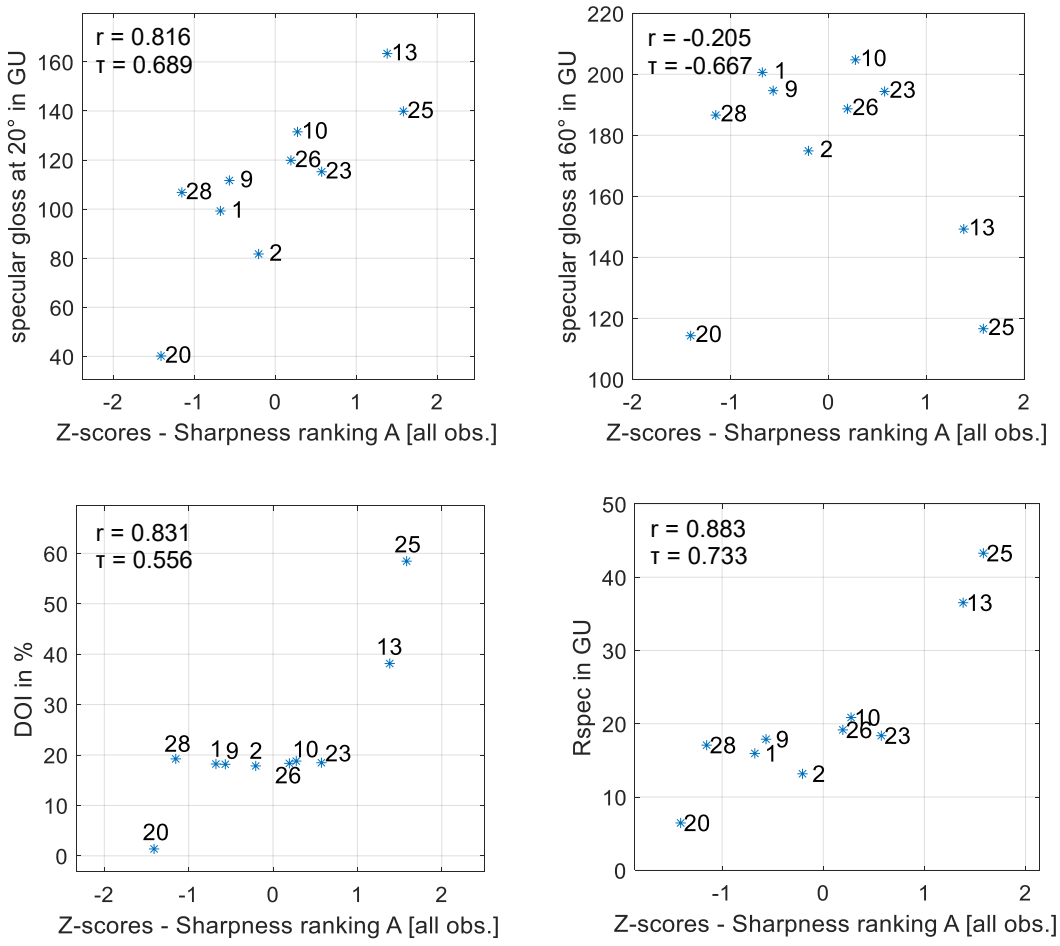

Figure 5.11: Specular gloss at 20° and 60°, DOI, and Rspec measured with the IQ-S gloss meter on samples of Series A (shown in Section 5.3) plotted against Sharpness ranking A1 (explained in Table 5.2) by the group of all observers (obs.). The numbers in the plots are the sample numbers. Pearson's r and Kendal's τ correlation coefficients are given.

Figure 5.12 displays intercorrelations between the rankings of samples according to various perceptual attributes of the group of all observers. In the upper-left, Z-scores obtained from data of Gloss ranking A1 and Sharpness ranking A are plotted against each other. Interestingly, for the group of all observers, there is nearly no correlation between

the rankings for these two perceptual attributes. Other intercorrelations of the perceptual attributes seem to correlate much better.

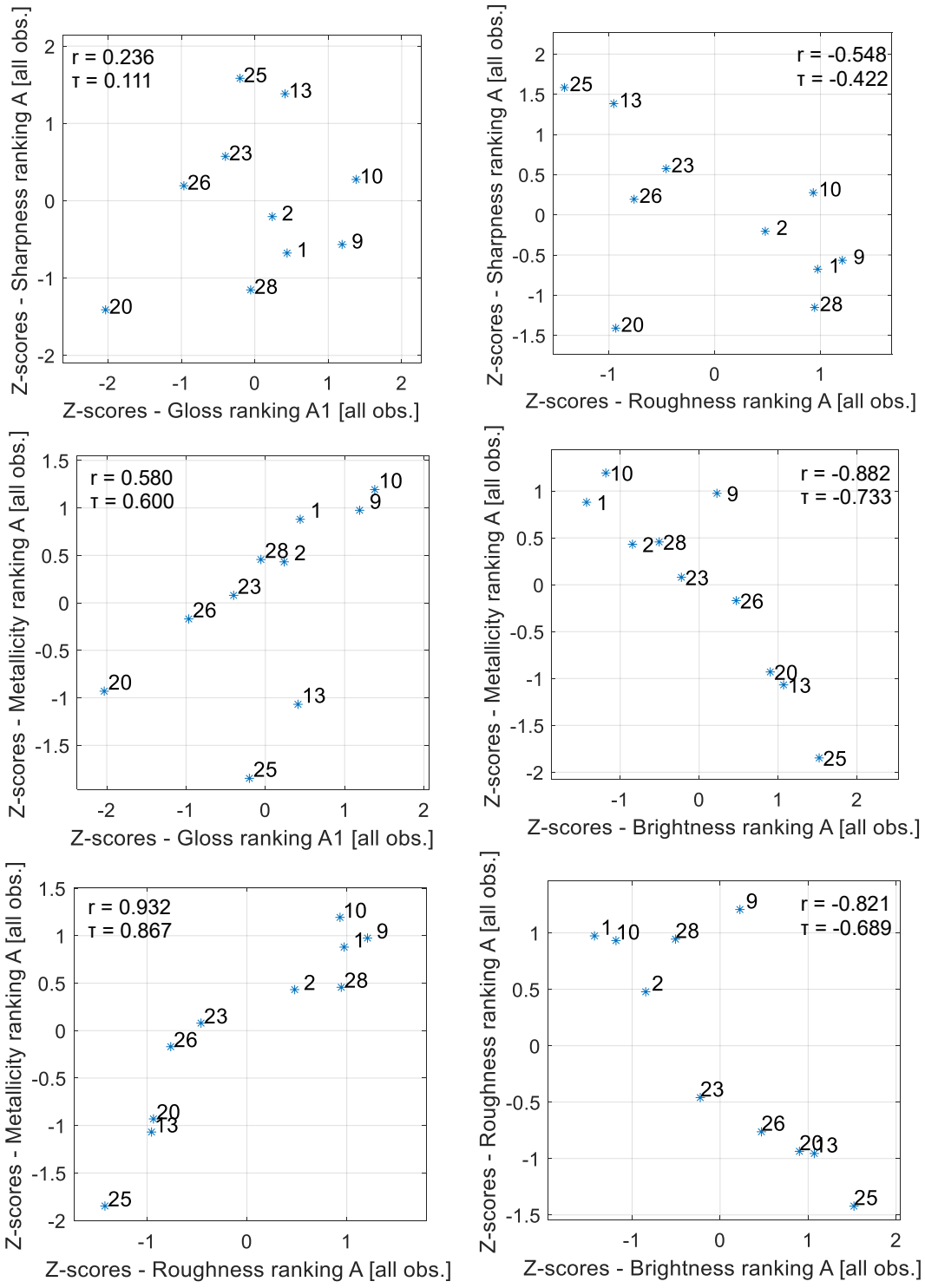

Figure 5.12: Intercorrelations of data obtained from the group of all observers (obs.) obtained from different ranking tasks using the samples of Series A (shown in Section 5.3). The different ranking tasks are explained in Table 5.2. The numbers in the plots are the sample numbers. Pearson's r and Kendal's τ correlation coefficients are given.

In the upper-right plot of Figure 5.12, a strong negative correlation can observed between data from Roughness ranking A and data from Sharpness ranking A, with Sample 20 standing out as an outlier. Sample 20 is metallized by offset printing and printed on illustration printing paper, resulting in lower gloss and image sharpness due to the characteristics of offset printing. Due to the usage of LumiArt paper as substrate, the perceived roughness is also low. Sample 1 and Sample 28 both exhibit low image sharpness and high roughness because they are printed on offset paper, which has a rougher surface and absorbs more binder of the metallic ink, thus reducing image sharpness as elucidated in Chapter 4. Sample 9, printed on GD2 cardboard without primer, has high texture and ink absorptivity, which explains its high perceived roughness and low image sharpness compared to other samples. The difference between Sample 9 and Sample 10 lies in the use of primer and a black preprint on Sample 10, highlighting the influence of primer in terms of slightly reducing perceived roughness and increasing image sharpness. The impact of primer is also evident when comparing Sample 2 and Sample 28; the application of primer on Sample 2 increases perceived image sharpness and decreases perceived roughness.

In the middle-left plot of Figure 5.12, data from Metallicity ranking A are plotted against data from Gloss ranking A1. There is a positive correlation between those two, with the exception of two outliers: Sample 25 and Sample 13. Sample 25 is the only one printed on film, while the printed metallic ink on Sample 13 underwent a special smoothing process, leading to a more plastic-like appearance that does not align with the metallic impression of the other samples.

The middle-right graph in Figure 5.12 reveals a strong negative correlation between Metallicity ranking A and Brightness ranking A, with the outlier Sample 9. Providing a clear explanation for this robust association between brightness and metallicity is a challenge.

Intuitively, one might posit that metallicity primarily relates to gloss and roughness. Gloss plays a role, as metallic surfaces tend to exhibit higher gloss than non-metallic ones, as elucidated in Chapter 2. As illustrated in the bottom-left plot of Figure 5.12, a positive correlation exists between data from Metallicity ranking A and data from Roughness ranking A. This positive correlation may be attributed to the inherent roughness of many metallic surfaces in daily life due to processing marks, weathering, or wear. Additionally, surface texture can contribute to light scattering, generating reflections and shading

typical to such kind of metallic surfaces. Hence, roughness could imply the presence of an authentic metallic surface.

The bottom-right plot shows a negative correlation between Brightness ranking A and Roughness ranking A, which may appear counterintuitive. Typically, one would expect that rougher surfaces, when illuminated at an angle of approximately 0° and viewed from a flat angle, would appear brighter due to increased light scattering. Nevertheless, when observing the samples at a steep angle in the provided light booth, light reflected by the white paper screen could be redirected onto the samples, entering the eyes of the observers. As a result, smoother samples were judged to be brighter. Another factor impacting brightness rankings is the preprint of samples with either 100 % or 50 % black before printing the metallic ink. Samples with a dark preprint tend to be ranked lower in terms of brightness compared to those without a black preprint.

Now an explanation for the pronounced negative correlation between Metallicity ranking A and Brightness ranking A can be derived from the interplay between brightness and perceived roughness, as well as perceived roughness and metallicity. Given the strong negative correlation between data of Brightness ranking A and Roughness ranking A, and the positive correlation between data of Roughness ranking A and Metallicity ranking A, it can be expected that a negative correlation also exists between data from Metallicity ranking A and Brightness ranking A.

5.7.3 Evaluation of data obtained with Series B

As previously mentioned, the divergence between the individual observers in Gloss ranking B was notably smaller compared to Gloss ranking A1 and Gloss ranking A2 (denotations explained in Table 5.2). The correlation between the group of experts and amateurs was strong, with $r = 0.982$ and $\tau = 0.899$. Z-scores were calculated from the rankings of the group of all observers and intercorrelated with the specular gloss measurements at 20° and 60°. The results are presented in Figure 5.13, revealing that both specular gloss measurements at 20° and 60° display robust correlations with data obtained from Gloss ranking B.

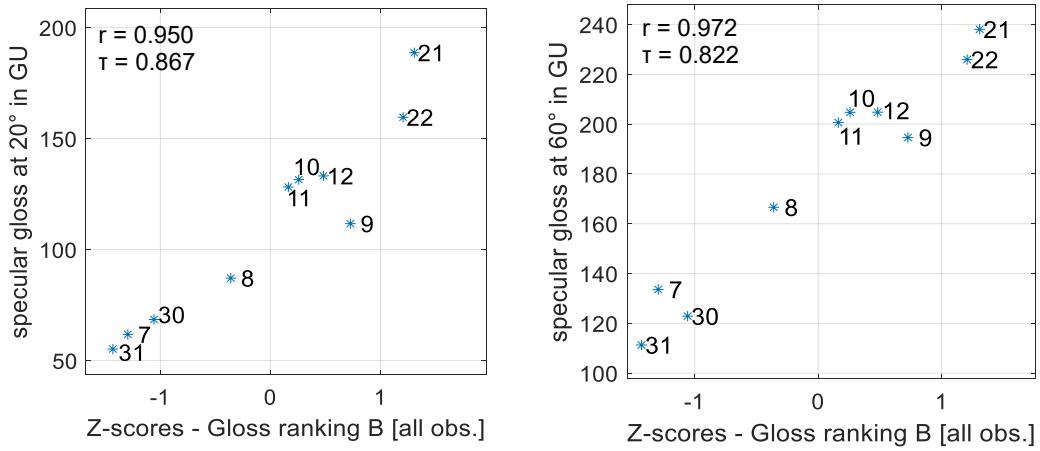

Figure 5.13: Specular gloss measured at 20° and 60° with the IQ-S gloss meter of samples of Series B (shown in Section 5.3) plotted against Gloss ranking B (explained in Table 5.2) by the group of all observers (obs.). The numbers in the plots are the sample numbers. Pearson's r and Kendal's τ correlation coefficients are given.

It remains inconclusive which of these measurement angles for specular gloss is more suitable, as both show high correlations with the gloss rankings. This high correlation to both specular gloss measurements at 20° and 60° can also be attributed to the inherent strong correlation between the specular gloss values measured on samples of Series B.

5.7.4 Evaluation of additional data

After completing the ranking tasks explained in Table 5.2, the first general question raised pertained to the differences between Series A and Series B (shown in Section 5.3). The majority of observers noted that the samples of Series B appeared to have a more metallic appearance compared to those of Series A. It was also observed that the samples within Series B exhibit only small variations, with some observers even suggesting that all samples of Series B looked the same at first glance. Further, some observers mentioned that it would be impossible to group samples of Series B into different categories if that were the task. During ranking the samples of Series B, most observers mentioned that ranking Series B would be more challenging than Series A.

Regarding the light conditions in the room and at the light booth, most observers mentioned that they regarded the light conditions as very comfortable and no disturbance could be perceived. Four observers considered the lighting conditions to be in need of improvement by equalizing the light intensity on the table surface. The overall ambience in the room was perceived as very pleasant and the tasks as interesting, which is also

supported by the fact that some observers were surprised after the experiment that one hour had already passed.

Regarding the question what gloss means, many different explanations were voiced with some observers' statements partially contradicting one another. For example, some suggested that a mirror possesses perfect gloss and that a sharp reflection of images indicates high gloss. Others would not categorize a mirror as having high gloss but rather as having just a reflective surface.

Only some of the experts had worked with gloss meters before, but most of them did not have a deeper understanding of gloss readings or could describe what they mean exactly. When asked to name objects of high gloss from their everyday lives, observers voiced a variety of terms. The stated terms included: watches, automotive paint, silver jewelry, Christmas tree balls, oiled wood, polished metal, piano lacquer, window glass, water tap, mirror, new copper roofing, printed magazines, diamonds, sequins, turned off phone displays, gold jewelry, or tile floors. Also from the mentioned objects, it can be inferred that some observers associate gloss with mirroring objects, while others think of objects with a high luster or sparkle but a limited ability to reflect images sharply

5.8 Comparison to a similar study

The greatest similarities of the psychophysical study made in this dissertation can be found with the study by Rich et al. (2017) named “Modeling the Appearance of Metal-Like Packaging Printing.” In this study, a rank order experiment was conducted with the participation of 20 observers. Their experience in judging the color or metallic appearance of packaging prints varied from none to highly trained and experienced. Two sets, each consisting of nine samples, were used. For the first set, called 'Series A*', nine samples were used that were made on both primed and unprimed paper substrates. For the second set, 'Series B*', nine samples printed on sealed cards were used. The prints were made using inks containing aluminum pigments using laboratory printing equipment. As shown in Chapter 4, using laboratory printing equipment usually facilitates reaching very high gloss levels that would only be attainable with industrial machines when using solvent-based gravure printing, which is rarely used in package printing, because specialized printing machines have to be used. Samples used for the experiment were selected based on the Specular Reflection Index (SPI). This index was calculated by using data measured with a sphere spectrophotometer, capturing the luminous reflectance Y, using the CIE

1931 standard observer (2°) and the CIE illuminant C. A sphere spectrophotometer can measure color values with both the specular component of the reflection in the sphere included (SPIN) and with the specular component excluded (SPEX), which results in two different Y values: Y_{SPIN} and Y_{SPEX}. Using these two values, the SPI can be calculated as shown in Equation 5.1:

$$SPI = 100\ \% \cdot \left(\frac{Y_{SPIN} - Y_{SPEX}}{Y_{SPIN}}\right) \quad 5.1$$

According to Rich et al. (2017), there is historical evidence suggesting that the SPI correlates with the perception of brilliance, as demonstrated in a study by Ji et al. (2006). In the study conducted by Rich et al. (2017), the selection of samples from the two sets aimed to ensure an approximate equidistance of the SPI values. The SPI values of the samples should be close to SPIs of 10, 20, 30, 40, 50, 60, 70, 80 and 90. During the experiment, observers were given no constraints in the viewing position or angle, and it is reported that observers had no difficulty in sorting the samples according to brilliance. The observers ranked the samples in order of their brilliance, for which no definition was given for.

The measurement values and resulting rank orders of Series A* and Series B* were similar. Table 5.7 shows the reported gloss measurement values obtained with the IQ-S, the SPI values and the average rank of the nine samples in Series A*. Data for the calculation of the SPI values were obtained with a SP64 X-rite spectrophotometer (X-rite, US). The Kendall's W coefficient that was calculated for the average ranking was reported to be 0.97, which indicates a very high agreement among the observers.

Rich et al. (2017) demonstrated that when plotting the average ranks obtained with Series A* against the SPI values, the SPI exhibits linearity across the entire range. Specular gloss values measured at 20°, haze and Rspec values however are not linear. As a result it is mentioned that it is somewhat disturbing that the gloss readings are not linear with the average ranks and that it "would be very serendipitous if it were to turn out that metallic brilliance is modeled simply as self-luminous brightness." Further, it was shown that a linear connection between gloss measurements and the results of the visual ranking can be obtained if the natural logarithm of the specular gloss values measured at 20° is employed.

Table 5.7: IQ-S gloss meter measurement values (blue), calculated SPI values (orange) and average rankings of the samples of Series A reported in the study of Rich et al. (2017).*

Sample	A*3	A*8	A*1	A*5	A*7	A*4	A*9	A*2	A*6
Gloss 20 in GU	6.8	19.7	29.9	42.1	51.5	139.1	273.3	483.5	621.8
Gloss 60 in GU	32.0	59.4	154.5	172.3	158.2	365.2	391.3	538.2	578.3
Gloss 85 in GU	59.1	63.1	94.1	80.9	82.1	110.7	107.8	123.7	123.9
Haze in HU	17.5	41.7	68.8	114.4	143.3	214.0	229.9	303.6	279.1
RIQ in %	2.3	1.9	1.7	1.2	1.0	3.0	4.0	7.3	6.1
Rspec in GU	1.2	3.3	5.1	7.5	9.4	23.4	45.2	82.7	105.7
SPI in %	9.9	20.5	26.6	39.7	48.5	59.7	75.8	80.7	88.1
Average rank	**1.02**	**2.04**	**3.06**	**4.15**	**4.79**	**5.96**	**7.19**	**7.94**	**8.85**

One issue of the findings of Rich et al. (2017) is that the samples used have a great range from very dull to highly mirroring. As a result, it poses no challenge for the observers to rank these samples. Based solely on the gloss measurement values, an experienced gloss researcher would have no doubt that the majority of observers would rank Sample A*3, A*8, and A*1 as 1st, 2nd, and 3rd, and Sample A*4, A*9, A*2, and A*2 as 6th, 7th, 8th, and 9th. Some uncertainty might arise with Sample A*5 and A*7, as A*7 has a higher specular gloss measured at 20°, while Sample A*6 has a higher specular gloss measured at 60°. As a result, given that the samples were chosen to have SPI values of near equidistance, it could be foreseeable that a linear relationship can be found between the measured SPI values and the average ranks. An open question is whether the findings of Rich et al. (2017) still hold if the ranked samples were selected without considering the measured gloss or SPI values. This was done in the study of this dissertation. To address this question, the SPI values of the samples of both Series A and Series B (shown in Section 5.3) were computed and plotted against data of Gloss ranking A1, Gloss ranking A2, Metallicity ranking A and Gloss ranking B. It can be assumed that the observers in the study of Rich et al. (2017) understood the term 'brilliance' as something similar to gloss or metallicity.

The SPI values were obtained from measurements of a Ci64 sphere spectrophotometer (X-Rite, US). Three measurements were taken on each of the samples used in the study of this dissertation, and the device internally calculated the mean values of these measurements. Since the variations of these measurements were only small, the SPI values derived are given without specification of the standard deviation in Table 5.8.

Table 5.8: SPI values calculated using Equation 5.1 with data obtained with a Ci64 sphere spectrophotometer from the samples of Series A and Series B from this dissertation (shown in Section 5.3).

Series A	**Sample**	**1**	**2**	**9**	**10**	**13**	**20**	**23**	**25**	**26**	**28**
	SPI in %	35.6	36.5	37.3	43.3	28.8	23.1	39.2	15.5	27.4	30.2
Series B	**Sample**	**7**	**8**	**9**	**10**	**11**	**12**	**21**	**22**	**30**	**31**
	SPI in %	33.7	36.5	37.3	43.3	41.9	39.0	41.5	39.6	26.3	25.6

Figure 5.14 shows the intercorrelations of measured SPI values of Series A and Series B with ranking data from Gloss ranking A1, Gloss ranking A2, Metallicity ranking A, and Gloss ranking B. Surprisingly, it can be seen that there are quite good positive correlations between SPI values measured on Series A and Gloss ranking A1, Gloss ranking A2 and Metallicity ranking A.

The correlation between the SPI values obtained from samples of Series A and data from Gloss ranking A1 and Gloss ranking A2 of the group of all observers is higher than the correlation of the specular gloss measured at 20° or 60° with the gloss rankings of the group of all observers which is shown in Figure 5.10. If neglecting the outlier Sample 25, which is the only sample printed on film instead of paper, the correlation between the SPI values and Gloss ranking A1 becomes $r = 0.780$, $\tau = 0.556$. That means that there is a good linearity between the measured data and ranked data and a moderate correlation of the concordance of the order of the two data sets. In addition, the correlation between the SPI values and the data from Metallicity ranking A is surprisingly high.

For these data, the advantage of specular gloss readings of a gloss meter over SPI readings can only be seen from the comparison of data from Gloss ranking B with the obtained SPI values from Series B. Here, the ranking according to gloss is more congruent with the specular gloss values measured at 20° or 60° than with the SPI values.

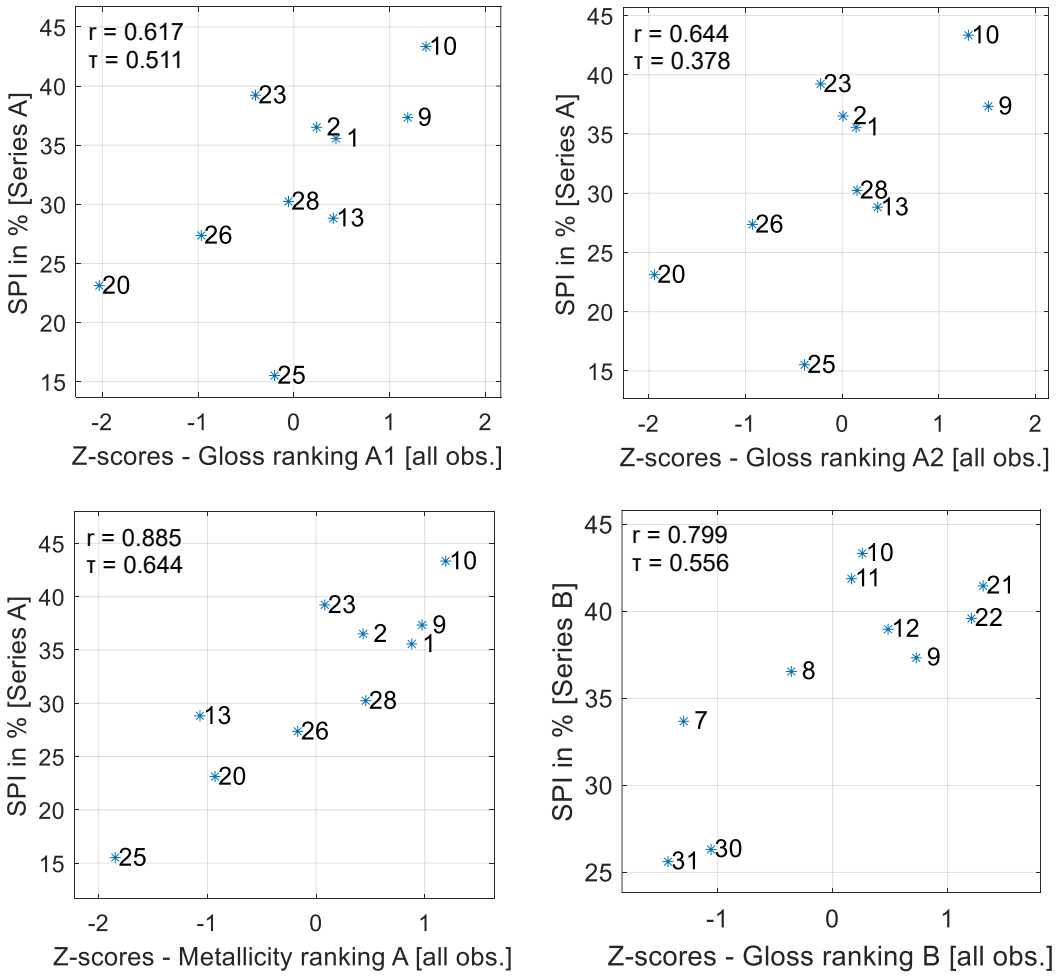

Figure 5.14: SPI values calculated using Equation 5.1 with data obtained with a Ci64 sphere spectrophotometer of samples of Series A and Series B (shown in Section 5.3) plotted against Gloss ranking A1, Gloss ranking A2, Metallicity ranking A and Gloss ranking B (tasks explained in Table 5.2) by the group of all observers (obs.). The numbers in the plots are the sample numbers. Pearson's r and Kendal's τ correlation coefficients are given.

To the author's knowledge, SPI values are not used in the printing industry for gloss assessment. Further research on this topic is necessary to prove a possible advantage of these values over traditional specular gloss measurements.

6 Discussion

In the following, the results and findings from the previous chapters are reflected and discussed.

6.1 Comparison of three gloss meters

In Chapter 3 of this dissertation, criteria on the suitability of gloss meters for the research of this dissertation were listed. In order to select the most suitable gloss meter out of three gloss meters for this research, a comparison between the micro-TRI-gloss, the IQ-S and the SRA was conducted. To give a better understanding of the measurement values that can be obtained using these gloss meters, a first general comparison was made using four different metallized samples from the printing industry. It has been demonstrated that measuring a 1D-BRDF or 2D-BRDF, as with the IQ-S and the SRA, can yield additional data on the measured gloss, including haze, DOI, IC, and other instrument-specific values.

For the reason that it was intended to make continuous gloss measurements in the study on dynamic gloss, the three gloss meters were tested under a continuous measurement condition and the deviations from the measurement target value of specular gloss on the instrument specific calibration tiles were recorded every 100^{th} measurement. The results showed that the micro-TRI-gloss can be expected to be the most reliable out of these three gloss meters under continuous measurement mode.

Considering that printed metallic samples often exhibit a certain texture and that a printing process can introduce irregularities in gloss, the expectation was that the standard deviations of measurements on such samples would be rather high. Accordingly, a measurement scheme was devised specifying five measurements in the print direction and five measurements across the print direction for each sample, totaling ten measurements per sample. This quantity is relatively high compared to many other research studies on gloss.

For the research conducted, it was important to determine the relative standard deviations for gloss measurements that could be expected for measurements on printed metallic samples. Hence, gloss measurements were made on 48 industrially metallized printed samples using the three gloss meters. The analysis primarily focused on specular

gloss values measured at 60°, 20°, and 85°, which are commonly used gloss values in both scientific and industrial applications.

It was shown that there can be high systematic deviations between specular gloss measurements when comparing the IQ-S and the micro-TRI-gloss. For instance, a sample with a specular gloss measured at 20° of 200 GU using the micro-TRI-gloss might would be expected to yield a reading of about 260 GU when measured with the IQ-S. Systematic deviations between the micro-TRI-gloss and the SRA in terms of specular gloss measurements were smaller. Furthermore, it was observed that measurements on samples with higher gloss levels resulted in higher relative standard deviations of specular gloss values measured at 20°. For example, specular gloss measured at 20° on print samples with a mean 20° specular gloss of about 50 GU exhibited relative standard deviations of approximately 5 %, while measurements on print samples with a mean of about 200 GU lead to relative standard deviations of about 10-15 %. Notably, among the three gloss meters, measurements of the micro-TRI-gloss tended to yield the smallest relative standard deviations. This could be attributed to its larger measurement spot size for 20° measurements compared to the IQ-S.

Regarding specular gloss measured at 60° and 85°, there was no correlation between the relative standard deviation and the mean specular gloss values. Haze measurements between the IQ-S and SRA were remarkably similar, despite differences in specular gloss measurements at 20°. Furthermore, comparisons were drawn between the DOI values measured with the IQ-S and the C20 values measured with the SRA. Both DOI and C20 offer insights into the sharpness of a surface's reflection of objects. It was observed that the relative standard deviation of DOI measured with the IQ-S and C20 measured with the SRA exhibited different trends in relation to the overall DOI of a surface. The relative standard deviation of DOI was smaller for prints with high gloss, whereas C20 showed smaller values for prints with low gloss.

In the existing literature, various studies have compared specular gloss measurements obtained from different gloss meters. Discrepancies in the measurement results across these gloss meters were primarily ascribed to differences in their construction, affecting factors such as aperture sizes and measurement spot sizes. Previous comparisons, often focused on specular gloss measured at 60° and were primarily conducted on dielectric surfaces with minimal texture. In this dissertation, however, gloss meter comparisons are based on measurements on printed samples with visible texture and high gloss due to

metallization. As a result, it was demonstrated that, given the anticipated high relative standard deviations in measurements on printed metallized samples, it is crucial to conduct a substantial number of measurements and derive the mean value from these readings. A finding from Chapter 3 was that, among the three gloss meters employed, the IQ-S emerged as the most suitable for non-dynamic gloss measurements for the research of this dissertation. This suitability arises from its capability to measure the 1D-BRDF at 20° and compute gloss values such as DOI, haze, or the device specific value Rspec, in addition to specular gloss. While the micro-TRI-gloss is accepted in both scientific and industrial contexts and is particularly well-suited for continuous measurements, the SRA does not enjoy the same level of acceptance in science and industry. Furthermore, its many device specific measurement values, apart from specular gloss and haze, do not exhibit good comparability with other research studies.

The issue that measurements of appearance measurement instruments of different manufacturers can lead to differing measurement results does not only apply to gloss meters. Perales et al. (2019) conducted a study on the instrumental agreement of spectral and colorimetric data of three different commercial multiangle spectrophotometers. It was found that the measurement geometries of these instruments differ leading to systematic differences in the measurement results. To the authors' knowledge, automotive companies handle this problem by requiring every supplier of appearance critical components to conduct quality assurance only by using the exact instruments specified by the automotive companies. However, such stringent standards are not common in the printing industry, and it is questionable whether the printing industry should adopt such kind of standards from the automotive industry. Nevertheless, it is advisable to communicate gloss measurement values or gloss requirements only with specifying the regarding gloss meter.

6.2 Printing experiments using metallic inks

First, the general procedure of Chapter 4 is described. Then the results of the experiments are discussed in more detail in the following sub-chapters.

6.2.1 General procedure

Multiple printing experiments using UV-inks that contain aluminum pigments revealed several factors that influence gloss. Critical factors that were singled out for investigation in the context of this dissertation was the time between printing and curing, for which the

term ‘dwell time’ was introduced, as well as the influence of hot air on the ink during the dwell time. Another important factor that was addressed was the influence of primer application on a paper substrate prior to printing the metallic inks. The investigation of these factors has been divided into three different scopes. First, an investigation of dynamic gloss was conducted by continuously measuring the gloss of freshly printed UV-ink printed with a flexo print proofer. Second, a similar setup with the same UV-inks and the same flexo print proofer was used to print samples of which the UV-ink was cured at different time intervals after printing. Hot air was applied to some of the samples during the dwell time. This allowed for an investigation of the topographies of the pigment layer, and the relevant topography parameters were then compared to the measured gloss. Third, an industrial printing machine with a flexo printing unit was employed to test the extent to which the results obtained from the experiments using the flexo print proofer could be transferred to a large-scale printing machine.

The application of heat onto the freshly printed ink could also have been possible by infrared radiators or by heating the substrate from the back. However, aluminum has a very high reflection in the infrared range, which means that infrared radiation is not the best method for heating printing ink with aluminum pigments. Heating plates are generally not available in industrial printing presses that was dealt with in course of this dissertation and they would make the heating of the printing ink very dependent from the substrate used.

6.2.2 Experiments on dynamic gloss

Dynamic gloss measurements were conducted using four different substrates and two types of UV-ink, one containing VMPs and the other containing cornflake pigments. The measurement results revealed significant variations in dynamic gloss depending on the ink and substrate used. In general, substrates with low ink absorptivity and small substrate roughness exhibited a consistent, monotonic increase in gloss over the measurement period. Conversely, substrates with higher ink absorptivity can lead to decreasing gloss values. Dynamic gloss measurements using UV-ink containing VMPs generally yielded higher gloss values. In contrast, printed ink layers with cornflake pigments exhibited a more rapid increase in gloss after printing, reaching a stable state earlier with no significant gloss changes later. It was shown that the trend in dynamic gloss can vary depending on the measurement angle. For instance, while specular gloss

measured at 20° might decrease, specular gloss measured at 60° could increase and vice versa.

Interestingly, it was observed that dynamic gloss measurements on Chromolux cardboard and Chromolux paper, of which both have similar smoothness and gloss, differed greatly. The presence and share of mineral particles in the coating of these substrates appeared to influence dynamic gloss development. Chromolux cardboard, whose coating is rich in calcium carbonate, exhibited a sharp increase in specular gloss at 20° and 60° after printing. In contrast, Chromolux paper, with a high content of kaolin in its coating, showed a comparatively slower but steady rise in specular gloss over time. Notably, for Chromolux paper, the specular gloss measured at 20° could initially decrease before increasing after a few seconds post-printing.

The influence of kaolin or calcium carbonate in the paper coating on dynamic gloss was also noticed by Preston et al. (2006). In this study two different paper substrates, one with 100 % kaolin coating and one with 100 % calcium carbonate coating were printed with offset UV-inks. The pigment sort of the printing ink is not known but no metal effect pigments came to use. It was found that while both substrates were very similar in terms of gloss and roughness, the porosity was very different. Pore size, pore volume and pore density were much lower for the kaolin coated paper. Dynamic gloss measurements during the first ten seconds after printing showed that the kaolin coating caused a higher gloss, which continued to rise longer. Conversely, the calcium carbonate caused an initial fast rise in gloss, which was followed by a slow decay in gloss. Long-term measurements conducted over a 20-minute period after printing revealed a decline in the gloss of the ink film printed on the kaolin-coated paper during the initial 5-10 minutes after printing. Subsequently, there was an increase in gloss in the subsequent 10-20 minutes. This was attributed to an initial increase in microroughness, followed by a decrease in macroroughness of the printed ink layers (microroughness and macroroughness were not explained in that study). This was considered a consequence of either the filling of macroroughness features on the paper surface or the continued leveling of the ink. The terms microroughness and macroroughness were not explained in detail in this study. Although the study of Preston et al. (2006) provides some explanation on the different behavior of dynamic gloss measured on Chromolux cardboard and Chromolux paper in this dissertation, there are still open points. First, the coatings of the paper substrates contained a mixture of kaolin and calcium carbonate. It cannot be excluded that such kind

of mixture can lead to different results in dynamic gloss than a coating of 100 % of one of the minerals. This could explain why in the study on dynamic gloss in this dissertation, dynamic gloss measured on Chromolux cardboard with less kaolin was continuously higher than dynamic gloss measured on Chromolux paper although, according to data of Preston et al. (2006) showed that kaolin coating lead to higher gloss. Preston et al. (2006) measured the decrease and subsequent increase on gloss on kaolin coated paper during the first ten minutes after printing. In case of the experiment of this dissertation, this effect was observable during the first few seconds after printing on Chromolux paper. It is possible that this difference can be attributed to the lower viscosity of the flexo printing ink used in the experiment of this dissertation compared to the offset printing ink used by Preston et al. (2006).

Former studies by Preston (2001) and Jeon (2002) on dynamic gloss identified oil-based offset-ink leveling and binder penetration into a paper substrate as most important factors of gloss changes after printing. However, in experiments of this dissertation, additionally the leaving of the aluminum pigments within the printed ink film has to be taken into account. It is an open question what the individual contribution of the different effects is to the change in gloss after printing. One approach to understand dynamic gloss is the mathematical modelling of gloss curves. This could be a helpful tool in future research to compare and classify dynamic gloss curves measured using different kind of substrates, inks and pigments.

After the printing of inks, not only a change in gloss occurs, but there is also a shift in color density. Pawlowski (2010) investigated the influence of filament leveling and its subsequent impact on the on the measured color density. Color densitometry involves determining the thickness of an ink layer by assessing the color density of primary printing colors (cyan, magenta, yellow, and black). Printers employ densitometers to manage the printing process and ensure consistent color reproduction throughout a print job. Pawlowski's study revealed that in continuous color density measurement, the measurement values increase within the first few seconds after printing due to the leveling of the ink film. This phenomenon could be attributed to the decrease of surface roughness or waviness, which influences the proportion of reflected light towards the measurement camera used for color density assessment. Following the initial leveling of the ink filaments, the measured color density gradually decreases due to the ink absorption into the paper. This in return results in an increased roughness of the ink film. The

measurement curves for color density resemble the dynamic gloss curve obtained from measuring specular gloss at a 20° angle on LumiArt paper printed with ink containing VMPs. In this scenario, the measured specular gloss also shows a brief rise immediately after printing, owing to ink film leveling. Subsequently, the specular gloss measured at 20° decreases as the ink is absorbed into the paper.

6.2.3 Pigment layer topography

Since dynamic gloss measurements could not reveal information about changes in the pigment layer topographies within the ink over time and did not allow for an assessment of the impact of heat on gloss after printing, experiments were conducted in which the UV-ink film was cured after varying dwell times. Chromolux paper was chosen as the substrate, since the slowest change in specular gloss were measured on this paper. This makes it a good choice for studying variations in the pigment layer's topography over time. However, it must be kept in mind that the change in pigment layer topography can occur very differently when using other substrates. Results of experiments on the topography and gloss of printed inks containing VMPs have been published by Weber et al. (2023). In that study beneath Chromolux paper, also primed MultiArt gloss paper was used as a substrate that shows a slight decrease of gloss with longer dwell time. Weber et al. (2023) only investigated the gloss and topography of a single print sample for each print setting and the distance between the printed sample and the hot air blower was not constant as the hot air blower was merely held by hand. In addition, the analysis of the topography data only considered the mean square height deviation (Sq). The laboratory printing experiment with different dwell times presented in this dissertation represent an enhancement compared to Weber et al. (2023), regarding the experimental setup and data analysis. This improvement can be attributed to several factors, such as the production and analysis of three prints for each print setting and dwell time, maintaining the hot air blower consistently at a fixed distance from the printed sample, and incorporating the root mean square gradient (Sdq) in the analysis of topography data.

The results showed that when Chromolux paper is printed with UV-ink containing VMPs without hot air during dwell time, there is a consistent increase in gloss over time, visually and in terms of specular gloss, up to a dwell time of 120 seconds. DOI measurements also increased on average up to a dwell time of 90 seconds, while no clear trend was observed for haze measurements. When using the same print settings but with hot air applied for 10 seconds during the dwell time, the measured values for specular gloss, DOI, and haze

reached similar levels to those of samples produced without hot air during the dwell time after 60 seconds. This means that either the leveling of ink filaments, the leafing of the pigments, or probably both is accelerated by the application of hot air. This can be attributed to a reduction in the ink viscosity due to the effect of heat as Equation 2.6 shows an acceleration in filament leveling with lower ink viscosity by a factor of three and as Sauer et al. (2022) showed an acceleration of pigment leafing with reduced ink viscosity by a factor of one. However, as shown by Weber et al. (2023), for a more ink absorptive substrate the application of hot air can have a negative impact on gloss, which can be attributed to binder penetration into the substrate.

The gloss measurements on samples produced with hot air during dwell time using the UV-ink with VMPs also show that after 30 seconds a maximum in terms of specular gloss and DOI is reached. For longer dwell times with a longer application of hot air, the specular gloss does not increase further while the DOI decreases and the haze increases. As the experiments on dynamic gloss already showed, no considerable changes in terms of gloss occur when using the UV-ink containing cornflake pigments. Further, for this ink the application of hot air does not have any significant impact on gloss.

When comparing the 3D surface parameters Sq and Sdq obtained from data filtered for roughness and waviness, along with the specular gloss measured at a 60° angle on samples produced without the use of hot air during the dwell time, a linear relationship becomes apparent. However, for samples produced with hot air during the dwell time, no such linear relationship can be identified, and the topography values fail to explain the variations in gloss among these samples. The same holds true when comparing topography data with specular gloss measured at a 20° angle. This discrepancy could be attributed to the very small topography data captured, which may already approach the resolution limit of the confocal microscope. Alternatively, it is possible that changes in the binder layer atop the pigments occur, but are not adequately captured by the confocal microscope. To capture the topography of the binder layer above the pigments, a tactile profilometer could be employed.

The selected 3D-surface parameters do not explain differences in gloss between samples printed with UV-ink containing VMPs and samples printed with UV-ink containing cornflake pigments. It is possible that an analysis of topography data that has been subjected to a FFT filter as done by Sung et al. (2000) would lead to more substantial results. Also an analysis of the autocorrelation length of the topography data could give

more insight in the relationship between gloss and pigment layer topography as indicated by Järnström et al. (2008). In order to find a general model that describes the relationship between gloss and surface topography for metallized print samples with aluminum pigments, further research is necessary.

6.2.4 Transfer to an industrial printing machine

The transition from the laboratory flexo printing machine to the industrial printing machine Gallus RCS330-HD required the use of a rougher, more ink-absorbent paper compared to Chromolux paper. For most samples, a UV-primer was preprinted to reduce ink absorbency, and printing on film was also performed. It was shown that, as in the laboratory experiments on dynamic gloss and dwell time, a longer dwell time, hot air, and UV-primer have a positive influence on gloss. The positive effect of a longer dwell time on gloss was more pronounced when printing on film as opposed to primed paper. It could be assumed that the rising gloss with longer dwell time on film is also reflected in the topography data. However, as indicated by the measurements, the alterations in topography were only small. In contrast to the samples printed on Chromolux paper without the use of hot air with UV-ink containing VMPs, the topography data did not provide a clear explanation for the observed changes in gloss. Furthermore, the study demonstrated that the type of UV-primer and the method of primer application can influence gloss. The differences in the results of the laboratory experiments and the experiments on the industrial printing machine can also be attributed to the smaller volume of the anilox roller that was used for printing the metallic ink in the experiment on the industrial printing machine.

The experiments on the Gallus RCS330-HD were conducted at a relatively low printing speed of 40 m/min. Typical printing speeds are higher to achieve a high machine utilization and better print quality. Also increasing the length between the flexo printing unit and the hot air blower to 4.6 m to achieve a longer dwell time is unrealistic as in industry on web-fed printing machines many printing units are close to each other and space is most often scarce. However, this study was the first to scientifically demonstrate how the gloss of metallic printing inks can be increased with hot air or an increased dwell time. Print jobs conducted during the author's work on sheet-fed printing machines operating at printing speeds of 8000 sheets/hour demonstrated that a small but noticeable increase in gloss can also be observed when applying heat to the freshly printed UV-inks containing aluminum pigments.

6.3 Psychophysical ranking experiment

For the reason that it is essential for the research and understanding of gloss of metallic surfaces to study the human visual perception, a psychological experiment was conducted. 27 observers ranked one set of metallic printed samples, which differed greatly in their appearance (Series A), according to their gloss, perceived roughness, image clarity, metallicity, brightness and again gloss. A second set (Series B) of samples with very similar appearance was ranked according to their gloss. The results were compared to gloss measurements and the rankings of Series A according to the different percepts were compared with each other. Additionally, the results of the study were compared with a study by Rich et al. (2017).

For the analysis of intercorrelations between the obtained data, statistical measures such as Pearson's r and Kendal's τ were given. For a better statistical analysis, it would have been beneficial to provide additional data on the significance of the correlations such as the p-values. The same also accounts for Chapter 3 and Chapter 4. However, also the plots of the data points give a visual impression on the linearity and spread of the data.

When analyzing the results it was found for Series A that more concrete terms such as 'roughness', 'image sharpness' and 'brightness' yield a higher accordance among the observers (Kendal's $W > 0.7$) than more abstract terms as 'metallicity' and 'gloss' (Kendal's $W < 0.4$). However, the ranking according to gloss of Series B yielded a higher concordance (Kendal's $W = 0.717$) that Series A ranked according to gloss (Kendal's $W \approx 0.35$).

When facing the high discordance of observers ranking Series A according to gloss and metallicity, the question emerges, if 27 observers are enough to yield robust data on the perception of these percepts. Many psychophysical studies in appearance research use around 30 observers or even fewer. In experimental design, when deciding the number of observers to use for a study, it is essential to consider factors such as statistical power and the variability of the effect one aims to detect. However, before conducting the experiment, there was no available data to estimate the required number of observers. While there is a high level of discordance among the observers in the gloss rankings, and some individual observers showed great differences between the two gloss rankings in Series A, the overall group of observers did not exhibit great changes. This is evident from the high correlation between data obtained from all observers from the tasks Gloss ranking A1 and Gloss ranking A2 (tasks described in Section 5.6) with a Pearson correlation coefficient of r =

0.98 and Kendall's tau $\tau = 0.78$. Replicating the experiment with a different and larger group of observers could strengthen the findings. However, the time needed and financial costs of such kind of experiment should not be disregarded, especially as most observers participated during their work time.

The groups of experts and amateurs exhibited differences in their gloss rankings of Series A. The experts' rankings showed a stronger correlation with specular gloss measured at 20°, while the amateurs' rankings were more strongly correlated with specular gloss measured at 60°. One potential explanation for this disparity could be the varying frequency with which the observers used specific aids when assessing gloss. Interestingly, many individuals in both the amateur and expert groups were influenced by the questions asked between the first and second ranking of Series A regarding gloss. Before the experiment, it was assumed that experts would demonstrate greater stability in their gloss rankings. However, it was revealed, through additional questions posed after the ranking tasks, that most experts had never previously encountered the topic of gloss in depth. Nevertheless, this revelation does not fully explain why some experts exhibited such substantial discrepancies in their gloss rankings of the same series, to the extent that negative correlation values were observed between the first and second gloss ranking. It could be argued that the differences in sampling conditions and different locations have an impact. The higher average age of the expert group compared to the amateurs could also be a factor. However, these differences do not provide a conclusive explanation for why the rankings of the expert group differed from those of the group of amateurs. In order to test whether the differences of the group of amateurs and experts are significant, a Kruskal-Wallis test could be employed.

It is also not clear what actually distinguishes, or should distinguish, expert vision from amateur vision when considering gloss. Gegenfurtner et al. (2019) investigated professional vision in terms of the medical domain and states that professional vision has been studied in many different kinds of domains and settings such as classrooms, neurology, dentistry, or primary care. However, to the authors' knowledge there are no studies on professional perception or judgement when it comes to the field of general appearance or gloss perception and judgement. Yet, to the authors experience, printers and people often judging print products are much faster aware of the smallest printing errors or minimal color differences as non-trained observers would be.

Interestingly, for Series A, the gloss meter readings of specular gloss measured at 20° and Rspec correlate better with data obtained from all observers from the task Sharpness ranking A than any other gloss meter reading with judged gloss. For Series B, both specular gloss measured at 20° and 60° correlate well with data obtained from Gloss ranking B. Since for the samples of Series B the specular gloss values correlate strongly with each other, it is not possible to conclude which angle of specular gloss meter measurement is more suited. This is conflicting with the literature, as for example ASTM D523 − 14 (reapproved 2014), which states that the specular gloss measured at 20° should be used for comparing samples with specular gloss higher than 70 GU measured at 60°.

It was found that some of the data obtained from the different tasks of the ranking experiment using Series A have high positive or negative correlations with each other. For instance, data obtained from the group of all observers for the tasks Metallicity ranking A and Brightness ranking A (r = -0.882, τ = -0.733) or data obtained from the tasks Metallicity ranking A and Roughness ranking A (r = -0.932, τ = -0.867). Interestingly, the correlation between data obtained from Gloss ranking A and Sharpness ranking A was found to be very low (r = -0.236, τ = -0.111).

Gemeinhardt (2020) reported on a FOGRA (Germany) research study on the metallicity of metallic printed samples and compared it with the brightness of the samples. The findings revealed a link between measured brightness and perceived metallicity. However, no explanation for this finding could be given. In this study, assessing more visual percepts than Gemeinhardt (2020), a possible explanation for the correlation between metallicity and brightness could be given. This correlation becomes clearer when correlating metallicity with roughness and roughness with brightness. However, experimental conditions and materials in this study differed from the study by Gemeinhardt (2020). In order to ensure the transferability of the explanation, measurements on samples from the study in this dissertation would have to be analyzed using FOGRA's measuring equipment that was used in the study by Gemeinhardt (2020).

The comparison of the gloss judgements in this dissertation with measured SPI values showed that some of the findings by Rich et al. (2017) have to be put into perspective. As a conclusion of their study, it is stated that the “measured index allows converters and designers to select an appearance level and have confidence that the print will provide the desired level of specular reflectivity.” Here, the measured index means the SPI or the natural logarithm of specular gloss measured at 20°. However, if this would be the case, a

good correlation between data obtained from Gloss ranking B and the SPI would have to be expected. Hence, the SPI value cannot be regarded as suitable to compare very similar samples in terms of gloss as indicated by Rich et al. (2017). For an assessment of gloss of similar samples, specular gloss measured at 20° or 60° is much better suited. However, the SPI appears to be a useful tool for estimating the gloss of samples with diverse appearances in Series A. Surprisingly, it can also provide a rough estimate of the judged metallicity for samples in Series A, particularly when considering samples printed on paper substrates. Hence, Rich et al. (2017) might be right in their statement that SPI can be used to estimate the brilliance of printed metallic samples if the term brilliance is understood as metallicity.

A limitation of the results of the psychophysical experiment in this dissertation, concerning their applicability in practice, is that packaging often involves the metallization of only small components, such as logos or fine ornaments. No research has been conducted to determine whether gloss or gloss differences are perceived differently when applied to larger patches as opposed to only small areas and fine lines. In the realm of color research, differences in color perception have been observed when comparing color patches to fine lines. Morovič and Morovič (2022) published a study on perceived line color differences. In an online visual experiment, the perception of color differences between lines with varying thicknesses was examined. The study revealed that, in comparison to color patches, observers were less sensitive to color differences when it came to fine lines. It is possible that such an effect is also noticeable when it comes to gloss. To conduct experiments on the smallest perceptible gloss differences of metallic printed lines or patches using physical samples, the findings from Chapter 4 could be utilized. When printing samples with slightly varying dwell times, the necessary samples with very small variations in gloss could be produced.

Furthermore, it is not known what effect overprinting the metallic samples with color would have on gloss perception. In order to answer this question, metallic samples with overprinted offset colors were produced on an industrial printing machine. The outcomes of this research are subject to future research and cannot be dealt with within the scope of this dissertation.

It is possible that future research on gloss perception of metallic embellishments of packaging will be conducted using virtual samples. The industry is working on various tools for displaying metallic gloss on packaging as the recent launch of the

‘Dreamcomposer’ software by KURZ (Germany) shows. With the advancement of computer screens capable of displaying HDR images with 2000 nits and beyond, along with improvements in rendering realistic gloss on metallic surfaces, research on this subject could shift more towards utilizing virtual samples.

6.3.1 Brightness and lightness

In this dissertation, the German term ‘Helligkeit‘ was translated to ‘brightness‘. The term ‘Helligkeit’ can be translated to both ‘brightness’ and ‘lightness’. CIE S 017/E:2020 (reapproved 2020) defines brightness as the “attribute of a visual perception according to which an area appears to emit, transmit or reflect, more or less light”. Lightness is defined as “brightness of an area judged relative to the brightness of a similarly illuminated area that appears to be white or highly transmitting.” Weber et al. (2022c) translated the term ‘Helligkeit’ to ‘lightness’ when describing the same psychophysical study. The reason for this choice was that ‘brightness’ is often also used for the luminance or luminous flux of emitters, and when viewing the ten samples from a steep angle, they appear as grey patches of differing intensity that are ordered. However, the task assigned to the observers was not to compare the whiteness or blackness of the color samples but rather to assess the amount of light reflected by the samples. The observers’ task was not to compare the brightness of the samples with the brightness of a similarly illuminated white area. Therefore, the term 'brightness' was used in this dissertation as the translation of the term 'Helligkeit'.

7 Summary and outlook

The objective of this dissertation was to deepen the scientific understanding of metallic surface gloss in the context of printing. An extensive literature review was conducted, focusing on gloss perception and measurement, with a particular emphasis on metallic surfaces. Additionally, printing methods employed in the industry for producing metallic embellishments were introduced, with special focus on flexo printing and inks containing aluminum pigments. The literature review revealed the absence of prior research on the dynamic gloss (the change of gloss of printed ink after the printing process) of printing inks containing metal effect pigments, a lack of studies on intentionally influencing metal effect pigment topographies in the printing domain, and scarcity in research addressing the visual perception of gloss of printed metallic samples. The investigations of gloss of printed metallic surfaces encompassed three distinct levels, which were physical gloss measurement, printing of inks that contain aluminum pigments and an investigation on visual perception of printed metallic samples.

Firstly, gloss on metallized print samples was physically measured and three different gloss meters were compared in this course. Deviations in measured gloss values and different performance under continuous measurement were discussed, leading to the selection of two gloss meters for further investigations. The micro-TRI-gloss gloss meter was chosen for its high measurement rate and reliability under continuous measurement conditions, specifically for dynamic gloss assessments. Due to its increased number of measured gloss values, the IQ-S gloss meter was employed for all other non-continuous gloss measurements.

Secondly, the interdependency between the behavior of flexo printed inks with aluminum pigments and the resulting measured gloss was explored. Dynamic gloss measurements were conducted on two UV-inks containing different types of aluminum pigments, printed on four different substrates. Variations in dynamic gloss were analyzed based on the substrate and ink types. Notably, when printing on Chromolux paper, the change of gloss in the uncured UV-ink was found to be slow but steadily rising. This substrate was selected for further small-scale laboratory experiments on the influence of dwell time on gloss and pigment layer topography. The influence of hot air during the dwell time was also investigated. In the course of these experiments, a direct correlation between measured topography parameters and specular gloss at an angle of 60° was identified for

one laboratory experimental series. This series involved UV-inks containing vacuum metallized pigments applied with no use of hot air during the dwell time. Further experiments assessed the transferability of results obtained using the laboratory print proofer to an industrial printing machine. Despite the use of different substrates, positive effects of a longer dwell time, the application of hot air during the dwell time, and preprinted UV-primer on gloss were confirmed in the industrial application. However, for the print samples obtained in this experiment, no clear correlation between measured pigment topography values and specular gloss could be found.

Thirdly, the visual appearance of metallic printed samples underwent assessment in a psychophysical ranking experiment. Two sets of ten samples were examined: the first set, exhibiting great visual differences, was ranked twice based on gloss, metallicity, sharpness of reflected images, perceived roughness, and brightness. The second set, with closely similar appearances, was ranked solely based on gloss. A group of 27 observers, some possessing considerable experience in judging print samples and others with little or negligible experience, participated in this experiment. The findings revealed that, for the set with visually diverse samples, more abstract terms such as 'gloss' or 'metallicity' led to greater deviations in rankings among observers compared to more concrete terms like 'brightness', 'sharpness of reflections', and 'perceived roughness.' Additionally, some observers significantly altered the ranking order when ranking samples regarding gloss for a second time. Only weak correlations were identified for the set with visually different samples between the gloss rankings and measured specular gloss. However, for the set with similar appearances, a robust correlation was observed between the rank data and both specular gloss measured the angles of 60° and 20°.

The investigations conducted in this dissertation make a substantial and distinctive contribution to research on the gloss of printed products, particularly those incorporating metallic inks. They advance the scientific understanding of gloss measurement on printed metallic surfaces, elucidate how the topography of the pigment layer and the gloss of UV-inks containing aluminum pigments can be influenced, and explore how observers assess gloss and other appearance aspects on these surfaces, and how these assessments correlate with gloss measurements.

Future research in the realm of printed metallic gloss could focus more on the development and improvement of methods to simulate the gloss of metallic printed samples. This would enable a more realistic virtual gloss impression of metallic embellishments. By doing so,

the existing soft proofing and design capabilities of the printing industry and available scientific methods for the examination of gloss could be enhanced.

Bibliography

Alexander-Katz, R.; Barrera, R. G. (1998): Surface correlation effects on gloss. In *Journal of Polymer Science: Part B: Polymer Physics* (36), pp. 1321–1334. DOI: 10.1002/(SICI)1099-0488(199806)36:8<1321::AID-POLB7>3.0.CO;2-U.

Alhotary, A. (2022): Untersuchung von dynamischem Glanz und dem Einfluss von Wärme in Druckprozess. Study of dynamic gloss and the influence of heat in the printing process. Bachelor thesis. TU Darmstadt, Darmstadt.

Ariño, I.; Kleist, U.; Mattsson, L.; Rigdahl, M. (2005): On the relation between surface texture and gloss of injection-molded pigmented plastics. In *Polymer Engineering & Science* 45 (10), pp. 1343–1356. DOI: 10.1002/pen.20393.

Arney, J.; Ye, L.; Banach, S. (2006): Interpretation of Gloss Meter Measurements. In *Journal of Imaging Science and Technology* (50), pp. 567–571. DOI: 10.2352/J.ImagingSci.Technol.(2006)50:6(567).

ASTM D4039 − 09 (reapproved 2015): Test Method for Reflection Haze of High-Gloss Surfaces. American Society for Testing and Materials (ASTM). West Conshohocken, PA.

ASTM D523 − 14 (reapproved 2014): Test Method for Specular Gloss. American Society for Testing and Materials (ASTM). West Conshohocken, PA.

ASTM D5767 − 95 (reapproved 2012): Test Methods for Instrumental Measurement of Distinctness-of-Image Gloss of Coating Surfaces. American Society for Testing and Materials (ASTM). West Conshohocken, PA.

ASTM E284 −17 (reapproved 2017): Standard Terminology of Appearance. American Society for Testing and Materials (ASTM). West Conshohocken, PA.

ASTM E430 - 11 (reapproved 2011): Measurement of Gloss of High-Gloss Surfaces by Abridged Goniophotometry. American Society for Testing and Materials (ASTM). West Conshohocken, PA.

Aydemir, C.; Yenidoğan, S.; Karademir, A.; Arman Kandirmaz E. (2018): The examination of vegetable- and mineral oil-based inks' effects on print quality: Green

printing effects with different oils. In *Journal of Applied Biomaterials & Functional Materials* 16(3), pp. 137–143. DOI: 10.1177/2280800018764761.

Bechtold, B. (2016): Violin Plots for Matlab. Github Project. Available online at https://github.com/bastibe/Violinplot-Matlab.

Bergsma, W.; Dassios, A. (2014): A consistent test of independence based on a sign covariance related to Kendall's tau. In *Bernoulli* 20 (2), pp. 1006–1028. DOI: 10.3150/13-BEJ514.

Bertholdt, U.; Müller, A. (2014): Material-, Verfahrens-, Veredelungs- und Klimaeinflüsse auf die Ausprägung von Metallic-Effekten im Druck. Fogra Research Report 50.039. Munich.

Beuckels, S.; Audenaert, J.; Hanselaer, P.; Leloup, F. (2022a): Development of an image-based measurement instrument for gloss characterization. In *Journal of Coatings Technology and Research* (19), pp. 1567–1582. DOI: 10.1007/s11998-022-00630-0.

Beuckels, Stijn; Audenaert, Jan; Leloup, Frederic (2023): Optical characterization of the psychophysical surface gloss space in the presence of surface haze. In *Optics Continuum* 2 (3), pp. 535–553. DOI: 10.1364/OPTCON.480680.

Beuckels, Stijn; Audenaert, Jan; Leloup, Frédéric B.; Hanselaer, Peter (2022b): Contrast gloss evaluation by use of a camera-based gloss meter. In Marc P. Georges, Gabriel Popescu, Nicolas Verrier (Eds.): Unconventional Optical Imaging III. Unconventional Optical Imaging III. Strasbourg, France, 2022: SPIE, p. 80. Available online at https://www.spiedigitallibrary.org/conference-proceedings-of-spie/12136/2621134/Contrast-gloss-evaluation-by-use-of-a-camera-based-gloss/10.1117/12.2621134.full.

Billmeyer, F. W.; O'Donnell, F. X. (1987): Visual gloss scaling and multidimensional scaling analysis of painted specimens. In *Color Research & Application* 12 (6), pp. 315–326. DOI: 10.1002/col.5080120606.

Blechschmidt, J. (Ed.) (2010): Taschenbuch der Papiertechnik. Munich: Fachbuchverlag Leipzig im Carl Hanser Verlag.

Briones, V.; Aguilera, J. M.; Brown, C. (2006): Effect of surface topography on color and gloss of chocolate samples. In *Journal of Food Engineering* 77 (4), pp. 776–783. DOI: 10.1016/j.jfoodeng.2005.08.004.

Brock, T.; Groteklaes, M.; Mischke, P. (2000): Lehrbuch der Lacktechnologie. With assistance of Ulrich Zorll. 2nd ed. Hannover: Vinzentz Network.

Brumm, P.; Dörsam, E.; Nguyen, D. L.; Schmitt-Lewen, M. (2017): Quality control of embossed holograms by measuring gloss and color values. In *Journal of Print and Media Technology Research* 6, pp. 7–18. DOI: 10.14622/JPMTR-1701.

Burrows, T. (2021): gloss measurement instruments. call to C. F. Weber. Darmstadt, 2021.

Byk Gardner (n.d.a): Byk Tri Gloss Betriebsanleitung. Available online at https://www.byk-instruments.com/de/Appearance/micro-gloss-Glanzmessung/Dreiwinkel-Glanzmessger%C3%A4t/c/p-32937, checked on 8/17/2023.

Byk-Gardner (n.d.b): Dreiwinkel-Glanzmessgerät. Available online at https://www.byk-instruments.com/de/Appearance/micro-gloss-Glanzmessung/Dreiwinkel-Glanzmessger%C3%A4t/c/p-32937, checked on 1/24/2023.

Campbell, R. (2023): notBoxPlot. Available online at https://github.com/raacampbell/notBoxPlot, checked on 8/27/2023.

Canon (n.d.): new tool measures 4 surface appearance quality conditions at once. Available online at https://vertassets.blob.core.windows.net/download/6d044d6c/6d044d6c-5c64-4881-8f36-caeedd309226/canon_2_118.pdf, checked on 5/7/2021.

Carabante, K. M.; Prinyawiwatkul, W. (2018): Data analyses of a multiple-samples sensory ranking test and its duplicated test: A review. In *Journal of Sensory Studies* 33 (4), e12435. DOI: 10.1111/joss.12435.

Christie, J. S. (1969): An instrument for the geometric attributes of metallic appearance. In *Applied Optics* 8 (9), pp. 1777–1785. DOI: 10.1364/AO.8.001777.

CIE S 017/E:2020 (reapproved 2020): International Lighting Vocabulary, 2nd Edition. International Commission on Illumination.

Clement, J. (2007): Visual influence on in-store buying decisions: an eye-track experiment on the visual influence of packaging design. In *Journal of Marketing Management* 23 (9-10), pp. 917–928. DOI: 10.1362/026725707X250395.

Croux, C.; Dehon, C. (2010): Influence functions of the Spearman and Kendall correlation measures. In *Statistical Methods & Applications* 19 (4), pp. 497–515. DOI: 10.1007/s10260-010-0142-z.

Czifra, Á.; Barányi, I. (2020): Sdq-Sdr Topological Map of Surface Topographies. In *Frontiers in Mechanical Engineering* 6, Article 50, pp. 1–9. DOI: 10.3389/fmech.2020.00050.

Dalal, E. N.; Natale-Hoffman, K. M. (1999): The effect of gloss on color. In *Color Research & Application* 24 (5), pp. 369–376. DOI: 10.1002/(SICI)1520-6378(199910)24:5<369::AID-COL8>3.0.CO;2-A.

Dekker, N.; Kirchner, E. J. J.; Supèr, R.; van den Kieboom, G. J.; Gottenbos, R. (2011): Total appearance differences for metallic and pearlescent materials: Contributions from color and texture. In *Color Research & Application* 36 (1), pp. 4–14. DOI: 10.1002/col.20586.

Deltombe, R.; Kubiak, K. J.; Bigerelle, M. (2014): How to select the most relevant 3D roughness parameters of a surface. In *Scanning* 36 (1), pp. 150–160. DOI: 10.1002/sca.21113.

Desjumaux, D. M.; Bousfield, D. W.; Glatter, T. P.; Donigian, D. W.; Ishley, J. N.; Wise, K. J. (1998): Influence of Pigment Size on Wet Ink Gloss Development. In *Journal of Pulp and Paper Science* 24 (5), pp. 150–155.

Desjumaux, D. M.; Bousfield, D. W.; Glatter, T. P.; van Gilder, L. (2000): The influence of latex type and concentration on ink gloss dynamics. In *Progress in Organic Coatings* 38 (2), pp. 89–95. DOI: 10.1016/S0300-9440(00)00078-3.

DFTA (1999): Technik des Flexodrucks. With assistance of K. H. Meyer. 4th ed. St Gallen: Coating Fachbücher.

Dietz, C.; Rhopoint Instruments (2023): Rhopoint IQ gloss meters. Email to C. F. Weber, 2023.

DIN EN 60081 (reapproved 2019): Zweiseitig gesockelte Leuchtstofflampen Anforderungen an die Arbeitsweise. Double-capped flourescent lamps - Performance specifications. German Institute for Standardization. Berlin.

DIN EN ISO 13803:2014 (reapproved 2014): Beschichtungsstoffe – Bestimmung des Schleiers von Beschichtungen bei 20°. Paints and varnishes - Determination of haze on paint films at 20°. German Institute for Standardization. Berlin.

DIN EN ISO 25178-2 (reapproved 2012): Geometrische Produktspezifikation (GPS) – Oberflächenbeschaffenheit: Flächenhaft – Teil 2: Begriffe und Oberflächen-Kenngrößen. Geometrical product specifications (GPS) - Surface texture: Areal - Part 2: Terms, definitions and surface texture parameters. German Institute for Standardization. Berlin.

DIN EN ISO 2813:2014 (reapproved 2014): Beschichtungsstoffe – Bestimmung des Glanzwertes unter 20°, 60° und 85°. German Institute for Standardization. Berlin.

DIN EN ISO 535:2014 (reapproved 2014): Bestimmung des Wasserabsorptionsvermögens - Cobb-Verfahren. Determination of water absorptiveness - Cobb method. German Institute for Standardization. Berlin.

DuPont Teijin Films (n.d.): Melinex 339. Available online at https://usa.dupontteijinfilms.com/wp-content/uploads/2017/01/339-Datasheet.pdf, checked on 6/30/2023.

Eckart GmbH (n.d.): Printing the Brilliant Way. An Introduction into Metallic Effect Pigments. Available online at https://eckart.net/de/de/LP-Metallic-Ink-Pigment-Guide, checked on 8/18/2021.

Engeldrum, P. G. (2000): Psychometric scaling. A toolkit for imaging systems development. 1st ed. Winchester, Mass: Imcotek Press.

Enomae, T.; Hayano, S.; Takano, K.; Teramoto, M.; Naito, H.; Kamada, K.; Onabe, F. (2000): Mechanisms of print gloss development. 2000 International Printing and Graphic Arts Conference in Savannah, GA. Savannah, GA, 2000.

Eugene, C. (2008): Measurement of "total visual appearance": a CIE challange of soft metrology. 12th IMEKO TC1 & TC7 Joint Symposium on Man, Science & Measurement. International Commission on Illumination, 2008.

Fensterseifer, F.; Byk Gardner (2021): gloss measurement instruments. phone call to C. F. Weber. Darmstadt, 2021.

Ferwerda, J. A. (2008): Psychophysics 101. In : ACM SIGGRAPH 2008 classes. SIGGRAPH '08: Special Interest Group on Computer Graphics and Interactive Techniques Conference. Los Angeles California, 11 08 2008 15 08 2008. Association for Computing Machinery; ACM Special Interest Group on Computer Graphics and Interactive Techniques. New York, NY: ACM (ACM Conferences), pp. 1–60.

Ferwerda, J. A.; Pellacini, F.; Greenberg, D. P. (2001): Psychophysically based model of surface gloss perception. In *Proceedings of SPIE - The International Society for Optical Engineering* (4299), pp. 291–301. DOI: 10.1117/12.429501.

Fetsko, J. M.; Zettlemoyer, A. C. (1962): Factors Affecting Print Gloss and Uniformity. In *Tappi Journal* (45(8)).

Frankhuizen, N. (2015): A terminology and metrology view on gloss. In *Polymers Paint Colour Journal*, pp. 24–25.

Frankhuizen, N.; Industrial Physics (2023): specular gloss meters. email to C. F. Weber, 2023.

Gayduscheck, M. S. (2019): Rauheitsreduktion lasergesinterter Substrattopographien mittels mehrlagigen Inkjet-Drucks. Dissertation. TU Darmstadt, Darmstadt. Available online at https://tuprints.ulb.tu-darmstadt.de/9629/.

Ged, G.; Rabal-Almazor, A.; Himbert, M. E.; Obein, G. (2020): Assessing gloss under diffuse and specular lighting. In *Color Research & Application* 45 (4), pp. 591–602. DOI: 10.1002/col.22510.

Gegenfurtner, A.; Lehtinen, E.; Helle, L.; Nivala, M.; Svedström, E.; Säljö, R. (2019): Learning to see like an expert: On the practices of professional vision and visual expertise. In *International Journal of Educational Research* 98, pp. 280–291. DOI: 10.1016/j.ijer.2019.09.003.

Gemeinhardt, J. (2020): Kommunikation von messtechnischen Kenngrößen zur Beschreibung des metallischen Aussehens von Drucken. Fogra Research Report 34.021. Munich.

Gibbons, J. D. (1993): Nonparametric measures of association. Newbury Park, Calif.: Sage Publ (Quantitative applications in the social sciences, 91).

Gigilashvili, D.; Thomas, J.; Hardeberg, J. Y.; Pedersen, M. (2018): Behavioral Investigation of Visual Appearance Assessment. Color and Imaging Conference. Society for Imaging Science and Technology. Vancouver, BC, 2018.

Gigilashvili, D.; Thomas, J.; Pedersen, M.; Hardeberg, J. Y. (2019): Perceived Glossiness: Beyond Surface Properties. Color and Imaging Conference. Society for Imaging Science and Technology. Paris, 2019.

Glatter, T.; Bousfield, D. W. (1996): Print Gloss Development on Model Substrates. In *International Printing & Graphic Arts Conference Proceedings* (139).

Glatter, T.; Bousfield, D. W. (1997): Print gloss development on a model substrate. In *Tappi Journal* (80(7)).

Golhin, A. P.; Strandlie, A. (2023): Appearance evaluation of digital materials in material jetting. In *Optics and Lasers in Engineering* 168, p. 107632. DOI: 10.1016/j.optlaseng.2023.107632.

Gruber, D. P.; Buder-Stroisznigg, M.; Wallner, G.; Strauss, B.; Jandel, L.; Lang, R. W. (2008): A novel methodology for the evaluation of distinctness of image of glossy surfaces. In *Progress in Organic Coatings* 63 (4), pp. 377–381. DOI: 10.1016/j.porgcoat.2008.06.008.

Gruber, D. P.; Buder-Stroisznigg, M.; Wallner, G.; Strauß, B.; Jandel, L.; Lang, R. W. (2012): Characterization of gloss properties of differently treated polymer coating

surfaces by surface clarity measurement methodology. In *Applied Optics* 51 (20), pp. 4833–4840. DOI: 10.1364/AO.51.004833.

Haas, M. (2012): Untersuchungen zum Verdrucken von Interferenzeffektfarben im Flexodruckverfahren. Dissertation. TU Darmstadt, Darmstadt. Available online at https://tuprints.ulb.tu-darmstadt.de/3011/, checked on 10/15/2023.

Hanson, A. R. (2006): Good Practice Guide for the Measurement of Gloss. In *Measurement Good Practice Guide* (94).

Harder, L. (2023): The ABC to our cardboard materials: What's behind the shortcuts? Available online at https://www.packaging-warehouse.com/en/magazine/the-abc-to-our-cardboard-materials-whats-behind-the-shortcuts-103.php, checked on 7/31/2023.

Harrison, V. G. W. (1945): Definition and measurement of gloss, a survey of published literature. Cambridge, England: Patra.

Harrison, V. G. W.; Poulter, S. R. C. (1951): Gloss measurement of papers - the effect of luminance factor. In *British Journal of Applied Physics* (2), pp. 92–97.

Hartmann, O.; Haupt, S. (2019): The Power of Print. Creatura - Metaanalyse zur Werbewirkung von Print für Erfolgreich Marketingpraxis - Executive Summary. Zell/Mosel: Fachverband Medienproduktion e.V.

Hébert, M. (2013): Reflection and transmission of light by a flat interface, Fresnel's formulae. Institut d'Optique. Available online at http://paristech.institutoptique.fr/site.php?id=797&fileid=11468, checked on 10/15/2023.

Heinzler, F. A.; Piepenbrink, M.; Doege, T. (2020): Glanzmessung an verchromten Kunststoffbauteilen. In *Journal für Oberflächentechnik* 20 (1), pp. 40–45.

Herranz, A. F. (2014): Perceptual Modeling and Reproduction of Gloss. Dissertation. Rochester Institute of Technology, New York. Available online at https://scholarworks.rit.edu/theses/8525/, checked on 10/15/2023.

Ho, Y.; Landy, M. S.; Maloney, L. T. (2008): Conjoint Measurement of Gloss and Surface Texture. In *Psychological Science* 19 (2), pp. 196–204. DOI: 10.1111/j.1467-9280.2008.02067.x.

Ho, Y.; Maloney, L. T.; Landy, M. S. (2007): The effect of viewpoint on perceived visual roughness. In *Journal of vision* 7 (1), pp. 1–16. DOI: 10.1167/7.1.1.

Huang, S. (2023): Compute the Kendall's coefficient of concordance of the matrix X. MATLAB Central File Exchange. Available online at https://www.mathworks.com/matlabcentral/fileexchange/27833-compute-the-kendall-s-coefficient-of-concordance-of-the-matrix-x, checked on 5/30/2023.

Hunter, R. S. (1937): Methods of determining gloss. In *Journal of Research of the National Bureau of Standards* 18 (1), pp. 19–39.

Hunter, R. S.; Harold, W. H. (1987): The Measurement of Appearance. 2nd edition. New York: John Wiley & Sons, Inc.

Hupp, H. (2008): Qualitäts- und Prozesskontrolle gedruckter Interferenzeffektfarben erster Generation. Dissertation. TU Darmstadt, Darmstadt. Available online at https://tuprints.ulb.tu-darmstadt.de/1016/, checked on 10/16/2023.

Hutchings, J. B. (1999): Food Colour and Appearance. New York, NY: Springer.

Ignell, S.; Kleist, U.; Rigdahl, M. (2009): On the relations between color, gloss, and surface texture in injection-molded plastics. In *Color Research & Application* 34 (4), pp. 291–298. DOI: 10.1002/col.20510.

Inoshita, C.; Hirabayashi, J.; Kato, S.; Kimura, J. (2018): Applications of Material Appearance Technology in CANON INC. In *The Imaging Society of Japan* 57 (2), pp. 225–230.

Inoue, S.; Igarashi, Y.; Hoshi, T.; Tsumura, N. (2022): Measuring BRDF for curved surfaces based on parabolic reflection. In *Optics Continuum* 1 (8), pp. 1637–1651. DOI: 10.1364/OPTCON.453077.

Inoue, S.; Kotori, Y.; Takishiro, M. (2012a): Paper Gloss Analysis by Specular Reflection Point Spread Function (Part I). In *Japan Tappi Journal* 66 (8), pp. 879–886. DOI: 10.2524/jtappij.66.879.

Inoue, S.; Kotori, Y.; Takishiro, M. (2012b): Paper Gloss Analysis by Specular Reflection Point Spread Function (Part II). In *Japan Tappi Journal* 66 (8), pp. 879–886. DOI: 10.2524/jtappij.66.879.

Iyer, R. R.; Bousfield, D. W. (1996): The Leveling of Coating Defects with Shear Thinning Rheology. In *Chemical Engineering Science* 51 (20), 4611-4617. DOI: 10.1016/0009-2509(96)00318-1.

Järnström, J.; Ihalainen, P.; Backfolk, K.; Peltonen, J. (2008): Roughness of pigment coatings and its influence on gloss. In *Applied Surface Science* 254 (18), pp. 5741–5749. DOI: 10.1016/j.apsusc.2008.03.043.

Jenkins, F. A.; White, H. E. (1981): Fundamentals of Optics. 4th ed. New York, NY: Mcgraw-Hill Higher Education.

Jeon, S. J. (2002): Mechanisms of Print Gloss Development with Controlled Coating Structure. Masterthesis. University of Maine, Maine, ME.

Ji, W.; Pointer, M. R.; Luo, R. M.; Dakin J. (2006): Gloss as an aspect of the measurement of appearance. In *Journal of the Optical Society of America* 23 (1), pp. 22–33. DOI: 10.1364/josaa.23.000022.

JIS K 7374:2007 (2007): Plastics - Determination Of Image Clarity. Japanese Standards Association.

Judd, D. B.; Wyszecki, G. (1952): Color in business, Science, and Industry. 2nd ed. New York, NY, London: Wiley and Sons.

Kehren, K. (2013): Optical Properties and Visual Appearance of Printed Special Effect Colors. Dissertation. TU Darmstadt, Darmstadt. Available online at https://tuprints.ulb.tu-darmstadt.de/3503/.

Kendall, M. G.; Gibbons, J. D. (1990): Rank correlation methods. 5. ed. London: Arnold (A Charles Griffin title).

Kettler, W. H.; Richter, G. (1997): Investigation on topology of platelet-like effect-pigments in automotive surface-coatings. In *Progress in Organic Coatings* 31 (4), pp. 297–306. DOI: 10.1016/S0300-9440(97)00087-8.

Kigle-Boeckler, G. (1995): Measurement of Gloss and Reflection Properties of Surfaces. In *Metal Finishing* (93), pp. 28–31.

Kim, H. K.; Kim, J. G.; Hong, J. W. (2002): Determination of key variables affecting surface properties of UV curable coatings using experimental design. In *Polymer Testing* 21 (4), pp. 417–424. DOI: 10.1016/S0142-9418(01)00105-2.

Kingdom, F. A. A.; Prins, N. (2016): Psychophysics. A practical introduction. 2nd ed. Amsterdam: Elsevier/Academic Press.

Kipphan, H. (Ed.) (2000): Handbuch der Printmedien. Technologien und Produktionsverfahren. Berlin, Heidelberg: Springer.

Kirchner, E. (2009): Film shrinkage and flake orientation. In *Progress in Organic Coatings* 65 (3), pp. 333–336. DOI: 10.1016/j.porgcoat.2009.01.006.

Kirchner, E.; Houweling, J. (2009): Measuring flake orientation for metallic coatings. In *Progress in Organic Coatings* 64 (2-3), pp. 287–293. DOI: 10.1016/j.porgcoat.2008.08.023.

Kohlrausch, R. (1854): Theorie des elektrischen Rückstandes in der Leidener Flasche. In *Annalen der Physik* 91 (1), pp. 179–214.

Koivula, H.; Juuti, M.; Bousfield, D.; Preston, J.; Silvennoinen, R.; Peiponen, K-E.; Toivakka, M. (2009): Comparison of dynamic print gloss measurement techniques. In *Tappi Journal* 8 (2), pp. 19–28. DOI: 10.32964/TJ8.2.19.

Konica Minolta (n.d.a): Specifications - IQ-S. Available online at https://www5.konicaminolta.eu/de/messgeraete/produkte/glanz-und-appearance-messung/glanzmessgeraete/rhopoint-iq-s/specifications.html, checked on 8/17/2023.

Konica Minolta (n.d.b): Understanding Gloss with the Rhopoint IQ-S. Konica Minolta. Available online at https://assets.thermofisher.com/TFS-Assets/ANZ/brochures/konica-minolta-understanding-gloss.pdf, checked on 3/27/2021.

Krietsch, B.; Schlenk Metallic Pigments (2021): Metal effect pigments. personal notice to C. F. Weber. Roth, Germany, 2021.

Kurz (2021): Veredelung der nächsten Generation. In *PrePress - World of Print* (10).

Label Pack (2019a): Metallictinten für Inkjetdruck. Edited by Label Pack. Available online at https://www.labelpack.de/metallictinten-fuer-inkjetdruck/, checked on 5/5/2021.

Label Pack (2019b): VFP Ink Technologies Metalleffekt und Relief mit einer Farbe. Available online at https://www.labelpack.de/metalleffekt-und-relief-mit-einer-farbe/, checked on 5/5/2021.

Leach, R. (2011): Optical Measurement of Surface Topography. Berlin, Heidelberg: Springer.

Leach, R. (2013): Characterisation of Areal Surface Texture. Berlin, Heidelberg: Springer.

Leach, R. (2014): Fundamental principles of engineering nanometrology. 2nd ed. Oxford, England: William Andrew (Micro and Nano Technologies Series). Available online at https://ebookcentral.proquest.com/lib/kxp/detail.action?docID=1694272.

Leloup, F. B. (2012): New methods and models improving the prediction of visual gloss perception. Dissertation. KU Leuven, Leuven.

Leloup, F. B.; Audenaert, J.; Obein, G.; Ged, G.; Hanselaer, P. (2016): Repeatability and reproducibility of specular gloss meters in theory and practice. In *Journal of Coatings Technology and Research* 13 (6), pp. 941–951. DOI: 10.1007/s11998-016-9813-5.

Leloup, F. B.; Obein, G.; Pointer, M. R.; Hanselaer, P. (2014): Toward the soft metrology of surface gloss: A review. In *Color Research & Application* 39 (6), pp. 559–570. DOI: 10.1002/col.21846.

Leloup, F. B.; Pointer, M. R.; Dutré, P.; Hanselaer, P. (2010): Geometry of illumination, luminance contrast, and gloss perception. In *Journal of the Optical Society of America* 27 (9), pp. 2046–2054.

Leloup, F. B.; Pointer, M. R.; Dutré, P.; Hanselaer, P. (2012): Overall gloss evaluation in the presence of multiple cues to surface glossiness. In *Journal of the Optical Society of America* 29 (6), pp. 1105–1114.

Levine, S.; Kamen, M. E.; DeFazio, A.; Cueli, P., Revion (1982): Process for making metallic leafing pigments. Patent no. US4321087.

Lohmann, F. (2020): Alternative Metallic-Effekte. In *Deutscher Drucker* (7), pp. 26–28.

Maile, F. J.; Pfaff, G.; Reynders, P. (2005): Effect pigments—past, present and future. In *Progress in Organic Coatings* 54 (3), pp. 150–163. DOI: 10.1016/j.porgcoat.2005.07.003.

MAN Roland Druckmaschinen (2002): In edler Gesellschaft – Druckveredelung in der Praxis. MAN Roland Druckmaschinen. Offenbach/ Main.

Martin, A. (2022): Entwicklung strukturierter Oberflächen zur Verbesserung der Osseointegration von PEEK. Disseration. TU Darmstadt, Darmstadt. Available online at https://tuprints.ulb.tu-darmstadt.de/22557/.

Meert, K.; Pandelaere, M.; Patrick, V. M. (2014): Taking a shine to it: How the preference for glossy stems from an innate need for water. In *Journal of Consumer Psychology* 24 (2), pp. 195–206. DOI: 10.1016/j.jcps.2013.12.005.

Meilgaard, M. C.; Civille, G. V.; Carr, B. T. (2015): Sensory Evaluation Techniques. 5th ed. Boca Raton: CRC Press. Available online at http://gbv.eblib.com/patron/FullRecord.aspx?p=4742816.

Michigan Metrology (n.d.): Root Mean Square Roughness. Available online at https://michmet.com/glossary-term/root-mean-square-roughness/, checked on 10/16/2023.

Mirjalili, F.; Moradian, S.; Ameri, F. (2014): A new approach to investigate relationships between certain instrumentally measured appearance parameters and their visually perceived equivalents in the automotive industry. In *Journal of Coatings Technology and Research* 11 (3), pp. 341–350. DOI: 10.1007/s11998-013-9544-9.

Mirjalili, F.; Moradian, S.; Ameri, F.; Amani Tehran, M. (2016): Quantification and prediction of visually perceived specular gloss at three illumination/viewing geometries. In *Journal of Coatings Technology and Research* 13 (2), pp. 239–256. DOI: 10.1007/s11998-015-9756-2.

Monjardet, B. (1997): Concordance between two linear orders: The Spearman and Kendall coefficients revisited. In *Journal of Classification* 14 (2), pp. 269–295. DOI: 10.1007/s003579900013.

Monro, A. (2014): Papier - wie eine chinesische Erfindung die Welt revolutionierte. 1st ed. Munich: C.Bertelsmann.

Morovič, J.; Morovič, P. (2022): The Perceptibility of Color Differences between Thin Lines and its Application to Printing Imaging Pipelines. In *Color and Imaging Conference* 30, 36 - 41. DOI: 10.2352/CIC.2022.30.1.08.

Nadal, M. E.; Early, E. A.; Thompson, E. A. (2006): NIST Measurement Services: Specular Gloss, pp. 250–270. Available online at https://www.nist.gov/publications/nist-measurement-services-specular-gloss, checked on 10/16/2023.

Nassau, K. (2001): The Physics and Chemistry of Color - The Fifteen Causes of Color. 2nd ed. New York, NY: John Wiley & Sons.

Neumann, J. (2009): Methode zur Volumenstrommessung und zur Viskositätskontrolle von Beschichtungsfluiden der grafischen Industrie. Dissertation. TU Darmstadt, Darmstadt. Available online at https://tuprints.ulb.tu-darmstadt.de/2385/.

Nicodemus, F. E. (1965): Directional Reflectance and Emissivity of an Opaque Surface. In *Applied Optics* 4 (7), pp. 767–775. DOI: 10.21236/AD0463473.

Nicodemus, F. E.; Richmond, J. C.; Hsia, J. J.; Ginsberg, I. W.; Limperis, T. (1977): Geometrical considerations and nomenclature for reflectance. National Bureau of Standards. Gaithersburg, MD.

novasens Sensortechnik (n.d.): Emissionsgradtabelle für die Infrarot Temperaturmessung. Available online at https://www.novasens.de/wp-content/uploads/Emissionsgradtabellenovasens.pdf, checked on 10/30/2023.

Obein, G.; Knoblauch, K.; Viénot, F. (2004): Difference scaling of gloss: nonlinearity, binocularity, and constancy. In *Journal of vision* 4 (9), pp. 711–720. DOI: 10.1167/4.9.4.

Obein, G.; Leroux, T.; Knoblauch, K.; Vienot, F. (2003): Visually relevant gloss parameters. 11th International Metrology Congress. Toulon, 2003.

O'Donnell, F. X. D.; Billmeyer, F. W. (1968): Psychometric Scaling of Gloss. In *Review and Evaluation of Appearance: Measurements and Techniques*, pp. 14–32. DOI: 10.1520/STP18343S.

Orchard, S. E. (1963): On surface leveling in viscous liquids and gels. In *Applied Science Research* (11), pp. 451–464. DOI: 10.1007/BF03184629.

Oxford Learner's Dictionary (n.d.): topology. Available online at https://www.oxfordlearnersdictionaries.com/definition/english/topology?q=topology, checked on 10/16/2023.

Ozcan, A.; Sonmez, S.; Tutak, D. (2022): Effect of coating pigment type on paper printability with water-based inks. In *Journal of Coatings Technology and Research* 19 (4), pp. 1149–1157. DOI: 10.1007/s11998-021-00593-8.

PaperSpecs (n.d.): Chromolux: Making Your Design Shine for 60 Years. Available online at https://www.paperspecs.com/spotlight/chromolux-making-your-design-shine-for-60-years/, checked on 7/31/2023.

Pawlowski, K. (2010): Untersuchungen zur Bestimmung der Farbdichte druckfrischer Offsetfarben mit einem Druckinspektionssystem. Dissertation. TU Darmstadt, Darmstadt. Available online at https://tuprints.ulb.tu-darmstadt.de/2761/.

Perales, E.; Micó-Vicent, B.; Huraibat, K.; Martínez-Verdú, F. M.; Dietz, C.; Yamanoi, Y. (2019): Review of instrumental inter-agreement study of spectral and colorimetric data of commercial multiangle spectrophotometers. In *Color Research & Application* 44 (2), pp. 168–175. DOI: 10.1002/col.22320.

Pfaff, G. (2017): Inorganic Pigments. Berlin, Boston: De Gruyter.

Pfund, A. H. (1930): The Measurement of Gloss. In *Journal of the Optical Society of America* 20 (1), p. 23. DOI: 10.1364/JOSA.20.000023.

Podieh, S. (2021): Hochwertige Bierflaschen-Etiketten mit Metallic-Effekt. Glänzende Lösung ganz ohne „Heavy Metal“. neue verpackung. Available online at https://www.neue-verpackung.de/markt/hochwertige-bierflaschen-etiketten-mit-metallic-effekt-495.html, checked on 10/16/2023.

Pointer, M. R. (2003): Measuring Visual Appearance - A Framework for the Future. Project 2.3 Measurement of Appearance. In *NPL Report: COAM 19*.

Polat, I. (2022): Untersuchung des Glanzes von gedruckten Metallicfarben. Examination of the gloss of printed metallic inks. Bachelor thesis. TU Darmstadt, Darmstadt.

Polyanskiy, M. (2023): Refractive index database. Available online at https://refractiveindex.info/?shelf=main&book=Al&page=Rakic, checked on 7/25/2023.

PremierPaper (2017): LumiArt Data sheet. Available online at https://www.paper.co.uk/PremierPaper/media/Standard/Documents/Lumiart-data-sheet-9-17.pdf, checked on 7/31/2023.

Preston, J. S. (2001): The Influence of Coating Structure on the Print gloss of Coated Paper Surfaces. Dissertation. University of Bristol, Bristol.

Preston, J. S.; Parsons, D. J.: Gate, L. F.; Husband, J. C.; Legrix, A. (2003a): Ink gloss development mechanisms after printing - part 1 - the influence of ink film thickness. In *Journal of Graphic Technology* 1 (2), pp. 29–37.

Preston, J. S.; Rousu, S.; Wygant, R.; Parsons, J.; Heard, P.; Gate, L. (2006): Interactions Between UV Curing Offset Inks And Coated Paper - Part 1. Laboratory Investigations. In *TAGA Journal* (2), pp. 82–98.

Preston, J. S.; Parsons, D. J.; Husband, J. C.; Nutbeem C. (2003b): Ink Gloss Development Mechanisms After Printing Part 2 - The Influence of Substrate. In *8th Advanced Coating Fundamentals Symposium TAPPI*.

Print.de (2023): Metallpigmente erzeugen Spiegeleffekt. Available online at https://www.print.de/allgemein/metallpigmente-erzeugen-spiegeleffekt/?omhide=true&utm_source=ddv_daily_nl&utm_campaign=Metallpigmente_erzeugen_Spiegeleffekt_27072023&utm_medium=email, checked on 7/27/2023.

Radermacher, K. (2016): Ökologisch-ökonomische Entscheidungen in Unternehmen. Auswirkungen auf die Produktqualität am Beispiel der Druck- und Verpackungsindustrie. Berlin: Oekom Verlag (Hochschulschriften zur Nachhaltigkeit, v.71).

Radiation curing. Coatings and printing inks : technical basics, applications and trouble shooting (2008). Hannover: Vincentz Network (European Coatings TECH FILES).

Rajae-Joordens, R.; Engel, J. (2005): Paired comparisons in visual perception studies using small sample sizes. In *Displays* 26 (1), pp. 1–7. DOI: 10.1016/j.displa.2004.09.003.

Ranfeld, C. (2015): Wet etching of printed silver layers using an etch resist structured by flexography. Dissertation. TU Darmstadt, Darmstadt. Available online at https://tuprints.ulb.tu-darmstadt.de/4534/.

Rhopoint Instruments (n.d.): Rhopoint IQ-S Datasheet Konica Minolta. Available online at https://www5.konicaminolta.eu/de/messgeraete/produkte/glanz-und-appearance-messung/glanzmessgeraete/rhopoint-iq-s/einfuehrung.html, checked on 10/16/2023.

Rich, D. C.; Marcus, R.; Lovell, V.; Kreutz, T. (2017): Modeling the appearance of metal-like packaging printing. In *Color Research & Application* 42 (1), pp. 38–49. DOI: 10.1002/col.22035.

Rounds, J. B.; Miller, T. W.; Dawis, R. V. (1978): Comparability of Multiple Rank Order and Paired Comparison Methods. In *Applied Psychological Measurement* 2 (3), pp. 415–422. DOI: 10.1177/014662167800200316.

Rozanski, L.; Majchrowski, R.; Staniek, R. (2014): Choosing of roughness parameters to describe the diffuse reflective and emissive properties of selected dielectrics. DOI: 10.21611/qirt.2014.045.

Samadzadegan, S.; Baar, T.; Urban, P.; Segovia, M. V. O.; Blahová, J. (2015): Controlling colour-printed gloss by varnish-halftones. In O. Segovia, P. Urban, F. H. Imai (Eds.): Measuring, Modeling, and Reproducing Material Appearance.

Šarić, D.; Kraushaar, A.; Mattuschka, M.; Green, P. (2021): Benchmarking modern gloss correlators with established ISO 2813 standard and visual judgment of gloss. In *Color and Imaging Conference* 29, pp. 306–310. DOI: 10.2352/issn.2169-2629.2021.29.306.

Sauer, H. M.; Braig, F.; Dörsam, E. (2021): Leveling and Drying Dynamics of Printed Liquid Films of Organic Semiconductor Solutions in OLED/OPV Applications. In *Advanced Materials Technologies* 6 (2), Article 2000160. DOI: 10.1002/admt.202000160.

Sauer, H. M.; Weber, C. F.; Dörsam, E. (2022): Glossy Surfaces: Metal Flake Alignment in Printed Liquid Films. 36th European Colloid & Interface Society Conference. Chania, Crete, 2022.

Seubert, C. M.; Nichols, M. E.; Frey, J.; Shtein, M.; Thouless, M. D. (2015): The characterization and effects of microstructure on the appearance of platelet–polymer composite coatings. In *Journal of Materials Science* 51 (5), pp. 2259–2273. DOI: 10.1007/s10853-015-9528-5.

Seubert, C. M.; Nichols, M. E.; Kappauf, C.; Ellwood, K.; Shtein, M.; Thouless, M. D. (2018): A hybrid ray-wave optics model to study the scattering behavior of silver metallic paint systems. In *Journal of Coatings Technology and Research* 15 (3), pp. 471–480. DOI: 10.1007/s11998-017-0028-1.

Sève, R. (1993): Problems connected with the concept of gloss. In *Color Research & Application* 18 (4), pp. 241–252. DOI: 10.1002/col.5080180407.

Shin, J. Y.; Bousfield, D. (2009): The leveling of surface irregularities in pigment coatings on porous substrates. In *Appita : Technology, Innovation, Manufacturing, Environment* (4), pp. 279–284.

Silvennoinen, R.; Juuti, M.; Koivula, H.; Toivakka, M.; Peiponen, K-E. (2008a): Diffractive glossmeter for measurement of dynamic gloss of prints. In *TAGA Journal* (4), pp. 59–71.

Silvennoinen, R.; Peiponen, K-E.; Myller, K. (2008b): Specular gloss. 1st ed. Amsterdam, Oxford: Elsevier.

Simonot, L.; Elias, M. (2003): Color change due to surface state modification. In *Color Research & Application* 28 (1), pp. 45–49. DOI: 10.1002/col.10113.

Smith, K. B. (1999): Measuring the perception of glossy surfaces. In *Pigment & Resin Technology* 28 (4), pp. 217–222. DOI: 10.1108/03699429910280738.

Smith, T. (1983): Aluminium Pigments. In *Pigment & Resin Technology* 12 (12), pp. 9–14. DOI: 10.1108/eb041970.

Solangi, L. A. (2022): Untersuchung des Glanzes von metallisierten Oberflächen unter Anwendung Psychophysikalischer Methoden. Investigation of the gloss of metallized surfaces using psychophysical methods. Bachelor thesis. TU Darmstadt, Darmstadt.

Sung, L.; Nadal, M. E.; McKnight, M. E. (2000): Characterizing the appearance and its related microstructure of metallic flaked coatings. 3rd International Conference on the Coatings for Plastics Symposium. National Institute of Standards and Technology, 2000.

Sung, L.; Nadal, M. E.; McKnight, M. E.; Marx E., Laurenti, B. (2002): Optical reflectance of metallic coatings: Effect of aluminum flake orientation. In *Journal of Coatings Technology* 74 (932), pp. 55–63. DOI: 10.1007/BF02697975.

Tego Journal (2007): EVONIK Tego Chemie Service GmbH. 3rd ed. Essen.

Teschner, H. (2017): Druck- und Medientechnik. Informationen gestalten, produzieren, verarbeiten. 14th ed. Konstanz: Dr.-Ing. Paul Christiani GmbH & Co. KG.

Testo (n.d.): Emissionsgrade der wichtigsten Materialien. Available online at https://www.testo.com/de-DE/services/wissensdatenbank-thermografie-emissionsgradtabelle, checked on 10/30/2023.

Thurstone, L. L. (1927): A law of comparative judgement. In *Psychology Review* 34, pp. 273–286.

Thurstone, L. L. (1931): Rank order as a psychophysical method. In *Journal of Experimental Psychology*, pp. 187–201.

Todd, J. T.; Norman, J. F. (2018): The visual perception of metal. In *Journal of vision* 18 (3), pp. 1–17. DOI: 10.1167/18.3.9.

Toivakka, M.; Kokko, A.; Akademi, Å.; Salminen, P; Urscheler, R.; Bousfield, D. W. (2001): Leveling of surface defects in thin films of pigmented coatings. In *Nordic Pulp and Paper Research Journal* 16 (3), pp. 246–250.

Torgerson, W. S. (1958): Theory and methods of scaling. 1st ed. New York, NY, London, Sydney: John Wiley & Sons.

UPM (n.d.): UPM Digi Finesse gloss. Available online at https://www.upmpaper.com/de/products/paper-catalogue/categories/digitaldruckpapiere/upm-digi-finesse-gloss2/, checked on 6/30/2023.

Vangorp, P.; Barla, P.; Fleming, R. W. (2017): The perception of hazy gloss. In *Journal of vision* 17 (5), p. 19. DOI: 10.1167/17.5.19.

Vazquez, A. T.; Šarić, D.; Klein, S.; Parraman, C. (2021): Influence of procedural noise on the glossiness of 2.5D printed patches. Color and Imaging Conference. Society for Imaging Science and Technology. Online, 2021.

Vessot, K.; Messier, P.; Hyde, J. M.; Brown, C. A. (2015): Correlation between gloss reflectance and surface texture in photographic paper. In *Scanning* 37 (3), pp. 204–217. DOI: 10.1002/sca.21201.

Wang, Y. (2021): Softwarebasierte Auswertung von Mikroskopaufnahmen und Druckparametern zur Analyse von gedrucktem metallischem Glanz. Software-based evaluation of microscope images and printing parameters for the analysis of printed metallic gloss. Master thesis. TU Darmstadt, Darmstadt.

Wang, Z.; Xu, L.; Hu, Y.; Mirjalili, F.; Luo, M. R. (2017): Gloss evaluation from soft and hard metrologies. In *Journal of the Optical Society of America* 34 (9), pp. 1679–1686. DOI: 10.1364/JOSAA.34.001679.

Weber, C. F.; Dörsam, E. (2021): Untersuchungen am Glanz von gedruckten metallisierten Oberflächen. Deutsche farbwissenschaftliche Gesellschaft. Kerpen-Horrem (DfwG Annual Meeting 2021).

Weber, C. F.; Polat, I.; Sauer, H. M.; Dörsam, E.; Schmitt-Lewen, M. (2023): Influence of dwell time and temperature on the measured gloss of printed UV-inks containing aluminum pigments. In *Journal of Coatings Technology and Research*. DOI: 10.1007/s11998-023-00820-4.

Weber, C. F.; Sauer, H. M.; Dörsam, E. (2022a): Modeling and investigating the dynamic gloss of flexo printed UV-inks containing aluminum pigments. In *Advances in Printing and Media Technology*, pp. 2–11. DOI: 10.14622/Advances_48_2022_01.

Weber, C. F.; Solangi, L. A.; Sauer, H. M.; Dörsam, E.; Schmitt-Lewen, M. (2022b): Erkenntnisse von Psychophysikalischen Untersuchungen an durch Drucken metallisierten Oberflächen. Deutsche farbwissenschaftliche Gesellschaft. Stuttgart (DfwG Annual Meeting 2022).

Weber, C. F.; Solangi, L. A.; Sauer, H. M.; Dörsam, E.; Schmitt-Lewen, M. (2022c): Perception of the appearance of metal-like package printing. In *Color and Imaging Conference* 30, pp. 258–263. DOI: 10.2352/CIC.2022.30.1.45.

Weber, C. F.; Spiehl, D.; Dörsam, E. (2021a): Comparing gloss meters for gloss measurements on metallic embellishments from the printing industry. In A. E. Politis (Ed.): iarigai Athens 2021 Conference proceedings. 47th annual conference if iarigai "Printing in the Digital Era". Athens. iarigai print and media research, pp. 189–199.

Weber, C. F.; Spiehl, D.; Dörsam, E. (2021b): Comparing measurement principles of three gloss meters and using them for measuring gloss on metallic embellishments produced by the printing industry. In : Lux junior 2021: 15. Internationales Forum für den lichttechnischen Nachwuchs, 04. – 06. Juni 2021, Ilmenau : Tagungsband. With assistance of Thüringer Universitäts- und Landesbibliothek Jena, pp. 327–341.

Weber, C. F.; Spiehl, D.; Dörsam, E. (2022d): Printing methods used in the label and package printing industry for the production metallic embellishments with a focus on metal effect pigments. In *Journal of Print Media Technology Research* 11 (1), pp. 29–45. DOI: 10.14622/JPMTR-2118.

Westlund, H. B.; Meyer, G. W. (2001): Applying Appearance Standards to Light Reflection Models. In *Proceedings of ACM SIGGRAPH,NewYork, E. Fiume, Ed., Computer Graphics Proceedings, AnnualConference Series*, pp. 501–510. DOI: 10.1145/383259.383318.

Wheeler, I. (1999): Metallic Pigments in Polymers. Shawbury, U.K: Rapra Technology Ltd. Available online at http://site.ebrary.com/lib/academiccompletetitles/home.action.

Wißling, P. (Ed.) (2013): Metalleffekt-Pigmente. 2nd ed. Hannover: Vincentz Network (Farbe-und-Lack-Edition).

Wu, M.; Xu, H.; Wang, Z.; Li, H. (2016): Towards a practical metric of surface gloss for metallic coatings from automotive industry. In *Journal of Coatings Technology and Research* 13 (3), pp. 469–477. DOI: 10.1007/s11998-015-9771-3.

Yang, S.; Huang, J.; Chen, J.; Noël, J. J.; Barker, I.; Henderson, J. D. et al. (2022): A Comparative Study on the Anti-Corrosive Performance of Zinc Phosphate in Powder Coatings. In *Coatings* 12 (2), p. 217. DOI: 10.3390/coatings12020217.

Yong, Q.; Chang, J.; Liu, Q.; Jiang, F.; Wei, D.; Li, H. (2020): Matt Polyurethane Coating: Correlation of Surface Roughness on Measurement Length and Gloss. In *Polymers* 12 (2). DOI: 10.3390/polym12020326.

Zwinkels, C. J.; Côté, É.; Morgan, J. (2018): Investigation of converging and collimated beam instrument geometry on specular gloss measurements. In *Journal of Physics: Conference Series* 972, p. 12025. DOI: 10.1088/1742-6596/972/1/012025.

In the course of the literature research, mainly Google Scholar was used. ChatGPT 3.5 and DeepL were occasionally used for linguistic improvements in the writing process. After using these tools/services, the author reviewed and edited the content as needed and takes full responsibility for the content of the publication.

Own and contributed publications

Weber, C. F.; Spiehl D.; Dörsam E. (2021): Comparing measurement principles of three gloss meters and using them for measuring gloss on metallic embellishments produced by the printing industry. In *Lux junior 2021: 15. Internationales Forum für den lichttechnischen Nachwuchs*, Ilmenau, Germany, June 2021, pp. 327-342. DOI: 10.22032/dbt.48427

Weber, C. F.; Spiehl D.; Dörsam E. (2021): Comparing gloss meters for gloss measurements on metallic embellishments from the printing industry. In *Advances in Printing and Media Technology Proceedings of the 47th International Research Conference of IARIGAI,* Athens, Greece, October 2021 (47), pp. 155-164. DOI: 10.14622/Advances_47_2021

Weber, C. F.; Dörsam E. (2021): Untersuchungen am Glanz von gedruckten metallisierten Oberflächen. DfwG Jahrestagung, Köln, Germany, October 2021.

Weber, C. F.; Spiehl D.; Dörsam E. (2022): Printing methods used in the label and package printing industry for the production of metallic embellishments with a focus on metal effect pigments in ink – a review. In *Journal of Print and Media Technology Research* 11 (3), pp 29-45. DOI: 10.14622/JPMTR-2118

Weber, C. F.; Sauer, H. M.; Dörsam E. (2022): Modeling and investigating the dynamic gloss of flexo printed UV-inks containing aluminum pigments. In *Advances in Printing and Media Technology Proceedings of the 48th International Research Conference of IARIGAI,* Greenville (SC), US, October 2022 (48), pp. 2-11. DOI: 10.14622/Advances_48_2022_01

Sauer, H.M.; Weber, C. F.; Dörsam E. (2022): Glossy Surfaces: Metal Flake Alignment in Printed Liquid Films. In *European Colloid Interface Society Conference*. Chania (Crete), Greece, September 2022 (36).

Weber, C. F.; Solangi, L. A.; Sauer, H. M.; Dörsam Edgar; Schmitt-Lewen, M. (2022): Psychophysikalische Untersuchungen an metallisierten gedruckten Oberflächen. DfwG Jahrestagung Stuttgart, Germany 2022.

Weber, C. F.; Solangi, L. A.; Sauer, H. M.; Dörsam, E.; Schmitt-Lewen, M. (2022): Perception of the appearance of metal-like package printing. In *Color and Imaging Conference* 30, pp. 258–263. DOI: 10.2352/CIC.2022.30.1.45.

Weber, C. F.; Polat, I.; Sauer, H. M.; Dörsam, E.; Schmitt-Lewen, M. (2023): Influence of dwell time and temperature on the measured gloss of printed UV-inks containing aluminum pigments. In *Journal of Coatings Technology and Research*. DOI: 10.1007/s11998-023-00820-4

Weber, C. F.; Sauer, H. M.; Dörsam E.; Schmitt-Lewen, M. (2023): Einfluss von Zeit und Temperatur auf den gemessenen Glanz von gedruckten UV-Farben mit Aluminiumpigmenten. DfwG Jahrestagung Potsdam, Germany 2023.

Supervised student works

Wang, Y.: Softwarebasierte Auswertung von Mikroskopaufnahmen und Druckparametern zur Analyse von gedrucktem metallischem Glanz. *Engl.: Software-based evaluation of microscope images and printing parameters for the analysis of printed metallic gloss.* Submission: February 2021, Master thesis, Supervisor: Weber, C. F.

Kumar, S.: Verwendung von Software zur Darstellung und Analyse von Glanz. *Engl.: Use of software for the display and analysis of gloss.* Submission: May 2021, Bachelor thesis, Supervisor: Weber, C. F.

Meise, F.; Bialek, F.; Windolf, H.; Niemöckl, J.; Pflüger, K.; Bückner, M.: Entwicklung einer Vorrichtung zur frühzeitigen Erkennung des Ablösens von gedruckten Bauteilen im 3D Druck. *Engl.: Development of a device for early detection of detachment of printed components in 3D printing.* Submission: July 2021, Advanced Design Project, Supervisors: Weber, C. F.; Laumann, D.

Zeithammer, M.; Sauer, S.; Rahman, S.; Kraus, S. O.: Erstellung eines Konzepts zur Abmusterung von metallischem Glanz. *Engl.: Creation of a concept for the sampling of metallic gloss.* Submission: July 2021, Advanced Design Project, Supervisor: Weber, C. F.

Polat, I.: Untersuchung des Glanzes von gedruckten Metallicfarben. *Engl.: Examination of the gloss of printed metallic inks.* Submission: March 2022, Bachelor thesis, Supervisor: Weber, C. F.

Solangi, L. A.: Untersuchung des Glanzes von metallisierten Oberflächen unter Anwendung Psychophysikalischer Methoden. *Engl.: Investigation of the gloss of metallized surfaces using psychophysical methods.* Submission: April 2022, Bachelor thesis, Supervisor: Weber, C. F.

Ahmad, S.: Untersuchung von Konzepten für ein neuartiges Druckverfahren. *Engl.: Investigation of concepts for a novel printing process.* Submission: August 2022, Bachelor thesis, Supervisor: Weber, C. F.

Hamarash, K.: Untersuchung der Rheologie von Metallicfarben. *Engl.: Investigation of the rheology of metallic inks.* Submission: September 2022, Bachelor thesis, Supervisor: Weber, C. F.

Tharmakulanathan, R.: Vergleich von Messung, Charakterisierung und Wahrnehmung von Farbe und Glanz. *Engl.: Comparison of measurement, characterization and perception of color and gloss.* Submission: September 2022, Bachelor thesis, Supervisor: Weber, C. F.

Alhotary, A.: Untersuchung von dynamischem Glanz und dem Einfluss von Wärme im Druckprozess. *Engl.: Study of dynamic gloss and the influence of heat in the printing process.* Submission: October 2022, Bachelor thesis, Supervisor: Weber, C. F.

El Araibi, A.; Breburda, V.; Elbæk, E.; Hendlich, S.: Entwicklung, Bau und Test eines Demonstrators für ein neuartiges Druckverfahren. *Engl.: Development, construction and testing of a demonstrator for a novel printing process.* Submission: October 2022, Advanced Design Project, Supervisor: Weber, C. F.

Kiefer, B.; Postina, L.; Reutzel, L.; Schrimpl, T.; Vogel, C.: Weiterentwicklung eines Demonstrators für ein neuartiges Druckverfahren. *Engl.: Further development of a demonstrator for a novel printing process.* Submission: February 2023, Advanced Design Project, Supervisor: Weber, C. F.

Appendix

Appendix I

This graph provides additional information for Section 3.4. It displays the spectrum of the LED at 20° of the SRA. It was measured with a CAS140CT spectrometer (Instrument Systems, Germany) with an integration time of 1000 ms at the Institute of Adaptive Lighting Systems and Visual Processing of the TU Darmstadt.

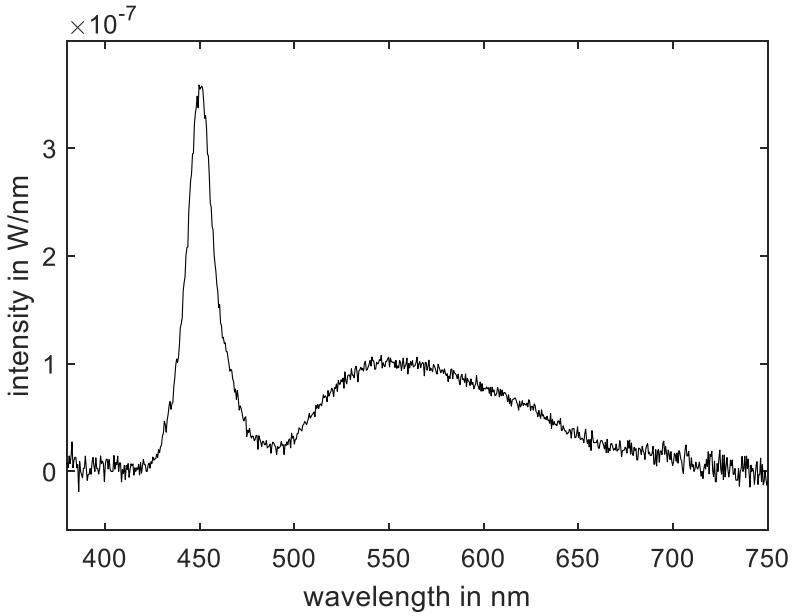

Appendix 2

This table offers supplementary information for Section 4.5.1., giving an overview on the mean standard deviations of the gloss measurements made on various substrate-ink-hot air combinations which are ChromP_VMP_nha, ChromP_VMP_ha, ChromP_corn_nha, and ChromP_corn_ha (abbreviations explained in Table 4.6). The mean inter-sample standard deviation represents the average of the standard deviations from ten gloss measurements on each sample. The mean between-sample standard deviation represents the average standard deviation of the mean values from three samples consistently printed with the same settings. It gives the average variability among three identically printed samples.

		ChromP_VMP_nha	**ChromP_VMP_ha**	**ChromP_corn_nha**	**ChromP_corn_ha**
Mean of inter-sample standard deviation	Gloss20	28.7 GU	67.1 GU	3.0 GU	5.0 GU
	Gloss60	10.0 GU	8.9 GU	1.9 GU	1.8 GU
	DOI	5.0 %	5.6 %	5.2 %	5.9 %
	haze	11.5 HU	16.2 HU	1.9 HU	1.9 HU
Mean of between-sample standard deviation	Gloss20	19.2 GU	21.4 GU	2.2 GU	2.7 GU
	Gloss60	10.3 GU	5.7 GU	1.8 GU	1.0 GU
	DOI	1.5 %	2.6 %	1.3 %	1.6 %
	haze	10.9 HU	11.0 HU	0.8 HU	1.1 HU

Appendix 3

This table offers additional information for Section 5.3. For each of the 18 samples used in the psychophysical experiment, details on the printing machine, type of printing unit, rasterization of the printing plate, substrate type, primer preprint, and the ink with aluminum pigments are provided. The sample numbers and series designations correspond to those in Figure 5.2. The series designations were introduced in Section 5.3.

Sample number	Series	Description
1	A	• Printed on Gallus RCS330-HD (Gallus, Switzerland) on flexo printing unit, no rasterization on flexo plate • Substrate: offset paper (comparable to book paper) with UV-primer • Black preprint • UV-ink with VMP pigments
2	A	• Printed on Gallus RCS330-HD (Gallus, Switzerland) on flexo printing unit, no rasterization on flexo plate • Substrate: offset paper (comparable to book paper) with UV-primer • UV-ink with VMP pigments
7	B	• Printed on XL 75 Anicolor (Heidelberger Druckmaschinen, Germany) on flexo printing unit, 90% rasterization on flexo plate for printing metallic ink • Substrate: cardboard • Black preprint • UV-ink with VMP pigments
8	B	• Printed on XL 75 Anicolor (Heidelberger Druckmaschinen, Germany) on flexo printing unit, 90% rasterization on flexo plate for printing metallic ink • Substrate: cardboard • 50% black preprint • UV-ink with VMP pigments
9	A & B	• Printed on XL 75 Anicolor (Heidelberger Druckmaschinen, Germany) on flexo printing unit, 90% rasterization on flexo plate for printing metallic ink • Substrate: cardboard • UV-ink with VMP pigments
10	A & B	• Printed on XL 75 Anicolor (Heidelberger Druckmaschinen, Germany) on flexo printing unit, 90% rasterization on flexo plate for printing metallic ink • Substrate: cardboard with UV-primer • 100% black preprint • UV-ink with VMP pigments
11	B	• Printed on XL 75 Anicolor (Heidelberger Druckmaschinen, Germany) on flexo printing unit, 90% rasterization on flexo plate for printing metallic ink • Substrate: cardboard with UV-primer • 50% black preprint • UV-ink with VMP pigments

Sample number	Series	Description
12	B	• Printed on XL 75 Anicolor (Heidelberger Druckmaschinen, Germany) on flexo printing unit, 90% rasterization on flexo plate for printing metallic ink • Substrate: cardboard with UV-primer • UV-ink with VMP pigments
13	A	• Printed on Label printing machine Labelfire (Gallus, Swizerland), on flexo printing unit, no rasterization on flexo plate • Substrate: Digi Finesse (illustration printing paper) with UV-primer • UV-ink with VMP pigments. After application the metallic ink layer was specially smoothed in a special process
20	A	• Printed on XL 75 Anicolor (Heidelberger Druckmaschinen, Germany) on offset printing unit, no rasterization on offset plate for printing metallic ink • Substrate: LumiArt (illustration printing paper) • UV-ink with VMP pigments
21	B	• Printed on XL 75 Anicolor (Heidelberger Druckmaschinen, Germany) on flexo printing unit, no rasterization on flexo plate for printing metallic ink • Substrate: cardboard with UV-primer • UV-ink with VMP pigments
22	B	• Printed on XL 75 Anicolor (Heidelberger Druckmaschinen, Germany) on flexo printing unit, no rasterization on flexo plate for printing metallic ink • Substrate: cardboard with UV-primer • UV-ink with VMP pigments
23	A	• Printed on XL 75 Anicolor (Heidelberger Druckmaschinen, Germany) on flexo printing unit, no rasterization on flexo plate for printing metallic ink • Substrate: LumiArt (illustration printing paper) • 50% black preprint • UV-ink with VMP pigments
25	A	• Printed on Label printing machine Labelfire (Gallus, Swizerland), on flexo printing unit, no rasterization on flexo plate • Substrate: IML film • UV-ink with VMP pigments
26	A	• Printed on Label printing machine Labelfire (Gallus, Swizerland), on flexo printing unit, no rasterization on flexo plate • Substrate: Digi Finesse (illustration printing paper) with UV-primer • UV-ink with VMP pigments
28	A	• Printed on Gallus RCS330-HD (Gallus, Switzerland) on flexo printing unit, no rasterization on flexo plate • Substrate: offset paper (comparable to book paper) • UV-ink with VMP pigments
30	B	• Printed on XL 75 Anicolor (Heidelberger Druckmaschinen, Germany) on flexo printing unit, no rasterization on flexo plate for printing metallic ink • Substrate: cardboard with UV-primer • UV-ink with VMP pigments

Sample number	Series	Description
31	B	• Printed on XL 75 Anicolor (Heidelberger Druckmaschinen, Germany) on flexo printing unit, 90% rasterization on flexo plate for printing metallic ink • Substrate: cardboard with UV-primer • UV-ink with VMP pigments

Appendix 4

The following tables provide additional information for Figure 5.3 in Section 5.3. The sample numbers and series designations correspond to those in Figure 5.2, with series designations introduced in Section 5.3. These tables display the gloss measurement values obtained from the samples used in the psychophysical experiment and the standard deviations of the ten gloss measurements per sample. An IQ-S gloss meter was used for the measurements. GlossXX denotes specular gloss measured at an angle of XX.

Series A	Sample									
	1	2	9	10	13	20	23	25	26	28
Gloss20 in GU	99 ± 5	82 ± 2	112 ± 13	131 ± 9	163 ± 14	40 ± 1	115 ± 7	140 ± 12	120 ± 6	107 ± 9
Gloss60 in GU	201 ± 6	175 ± 5	195 ± 17	205 ± 8	149 ± 5	114 ± 2	194 ± 4	117 ± 1	189 ± 3	187 ± 10
Gloss85 in GU	48 ± 3	42 ± 1	59 ± 4	68 ± 2	89 ± 4	56 ± 1	69 ± 1	76 ± 9	60 ± 7	37 ± 4
DOI in %	18 ± 1	18 ± 1	18 ± 0	19 ± 1	38 ± 6	1 ± 0	18 ± 0	58 ± 4	18 ± 1	19 ± 1
Haze in HU	161 ± 4	145 ± 3	178 ± 9	169 ± 5	69 ± 3	71 ± 1	159 ± 6	48 ± 3	174 ± 8	137 ± 4

Series B	Sample									
	7	8	9	10	11	12	21	22	30	31
Gloss20 in GU	62 ± 4	87 ± 6	112 ± 13	131 ± 9	128 ± 10	133 ± 13	189 ± 17	160 ± 18	69 ± 3	55 ± 3
Gloss60 in GU	134 ± 8	167 ± 8	195 ± 17	205 ± 8	201 ± 5	205 ± 8	238 ± 5	226 ± 8	123 ± 4	111 ± 3
Gloss85 in GU	54 ± 3	57 ± 3	59 ± 4	68 ± 2	66 ± 3	67 ± 3	78 ± 2	75 ± 3	49 ± 2	41 ± 1
DOI in %	10 ± 1	18 ± 0	18 ± 0	19 ± 1	19 ± 0	19 ± 1	21 ± 1	20 ± 1	15 ± 3	10 ± 0
Haze in HU	111 ± 5	146 ± 5	178 ± 9	169 ± 5	164 ± 3	168 ± 5	157 ± 14	166 ± 13	104 ± 2	99 ± 4

Appendix 5

The following tables provide additional information for Section 5.7. For each of the seven ranking tasks explained in Table 5.2, the number of observers who chose to assign a specific rank to each sample is shown. As described in Section 5.7, some observers opted to assign more than one sample to a specific rank, resulting in fractional rank numbers. For the presentation of the data in the following tables, these fractional rank numbers were rounded to the nearest integer. The order of the samples is based on the average ranking order, with the leftmost sample ranked highest in the specific percept, and the rightmost sample ranked lowest. For example, in the task Gloss ranking A1, nine observers chose to assign Sample 10 to the highest rank, while five observers assigned it the second rank.

Gloss ranking A1		Sample									
		10	**9**	**1**	**13**	**2**	**28**	**25**	**23**	**26**	**20**
Ranks	**1**	9	9	1	5	1	1	3	0	0	0
	2	5	7	1	3	2	1	4	2	0	1
	3	5	0	9	3	2	4	1	2	2	0
	4	2	3	4	2	3	5	3	2	3	0
	5	3	4	3	1	11	3	0	0	0	0
	6	1	0	2	2	3	2	3	9	3	2
	7	0	0	4	8	2	4	1	4	3	1
	8	1	2	2	1	1	2	4	5	8	0
	9	0	1	1	1	2	5	5	2	6	5
	10	1	1	0	1	0	0	3	1	2	18

Roughness ranking A		Sample									
		9	**1**	**28**	**10**	**2**	**23**	**26**	**20**	**13**	**25**
Ranks	**1**	12	6	6	5	0	0	0	0	0	0
	2	6	3	6	9	2	0	0	0	0	0
	3	4	11	3	2	5	0	0	0	0	0
	4	3	5	8	5	5	0	1	0	0	0
	5	1	0	4	5	15	0	0	0	1	0
	6	1	2	0	1	0	14	5	1	4	1
	7	0	0	0	0	0	8	8	4	6	1
	8	0	0	0	0	0	2	5	15	1	1
	9	0	0	0	0	0	3	5	5	9	6
	10	1	1	0	1	0	0	3	1	2	18

Sharpness ranking A		Sample									
		25	13	23	10	26	2	9	1	28	20
Ranks	1	17	9	0	1	0	0	0	0	0	0
	2	8	15	1	0	2	0	0	0	0	0
	3	2	1	9	9	3	1	0	0	0	1
	4	0	0	10	4	7	4	2	0	0	0
	5	0	1	3	5	7	4	1	2	0	1
	6	0	1	2	2	1	6	9	4	1	2
	7	0	0	1	2	3	8	5	7	3	0
	8	0	0	1	1	3	1	4	11	4	0
	9	0	0	0	3	1	3	3	3	17	1
	10	0	0	0	0	0	0	3	0	2	22

Metallicity ranking A		Sample									
		10	9	1	28	2	23	26	20	13	25
Ranks	1	8	9	2	3	2	1	1	3	1	1
	2	6	3	5	2	4	2	1	0	1	0
	3	1	2	6	6	3	3	5	2	1	0
	4	3	3	3	5	0	4	3	1	1	1
	5	3	0	4	1	8	1	0	0	2	3
	6	0	2	3	2	5	6	5	4	4	1
	7	1	2	2	3	1	5	3	1	4	2
	8	3	5	0	0	2	4	5	7	1	1
	9	1	0	1	3	1	1	4	2	7	4
	10	1	1	1	2	1	0	0	7	5	14

Brightness ranking A		Sample									
		25	13	20	26	9	23	28	2	10	1
Ranks	1	18	0	0	0	0	0	0	0	0	0
	2	0	14	3	1	0	0	0	0	0	0
	3	0	3	15	0	0	0	0	0	0	0
	4	0	0	0	13	4	1	0	0	0	0
	5	0	1	0	4	13	0	0	0	0	0
	6	0	0	0	0	1	14	2	1	0	0
	7	0	0	0	0	0	1	14	2	1	0
	8	0	0	0	0	0	2	2	12	1	1
	9	0	0	0	0	0	0	0	2	13	3
	10	0	0	0	0	0	0	0	1	3	14

Gloss ranking A2		Sample									
		9	**10**	**13**	**28**	**1**	**2**	**23**	**25**	**26**	**20**
Ranks	**1**	11	7	4	2	0	0	0	4	0	1
	2	6	9	4	0	3	0	1	2	1	0
	3	3	2	1	5	8	2	2	3	1	1
	4	0	3	3	6	3	7	2	1	3	0
	5	4	1	3	3	1	8	5	0	0	0
	6	1	2	2	3	2	3	9	2	4	0
	7	1	2	6	1	4	4	3	2	3	1
	8	1	0	2	4	3	1	3	4	4	3
	9	0	1	2	3	1	1	2	3	11	3
	10	0	0	0	0	2	1	0	6	0	18

Gloss ranking B		Sample									
		21	**22**	**9**	**12**	**10**	**11**	**8**	**30**	**7**	**31**
Ranks	**1**	16	7	3	0	1	0	0	0	0	0
	2	5	13	2	2	1	2	0	1	0	0
	3	2	1	9	6	3	3	1	1	0	0
	4	0	4	6	9	5	4	1	0	0	0
	5	2	0	4	4	8	6	2	0	0	0
	6	0	1	2	4	6	7	6	0	0	1
	7	1	1	0	2	1	3	13	3	1	2
	8	0	0	0	0	1	2	4	7	9	2
	9	1	0	1	0	1	0	0	8	9	6
	10	0	0	0	0	0	0	0	7	8	16